

Magnetic Locomotion for In-Pipe Inspection Robots



George Henry Jackson-Mills

University of Leeds

School of Mechanical Engineering

Submitted in accordance with the requirements for the degree of

Doctor of Philosophy

June, 2020

This thesis is dedicated to my wife, Cass.
I couldn't have done it without you.

Intellectual Property Statement

The candidate confirms that the work submitted is his own and that appropriate credit has been given where reference has been made to the work of others.

This work was supported by National Grid Gas Transmission (NGGT) and its project partners Synthotech, Premtech, and Pipeline Integrity Engineers as part of Project GRAID: Gas Robotic Agile Inspection Device. ESPRC Grant Number: 1657711

The work in Chapter 2 of this thesis has appeared in the following publication: **G. H. Mills, A. E. Jackson, and R. C. Richardson**, *Advances in the inspection of unpiggable pipelines*, Robotics, vol. 6, no. 4, p. 36, 2017.

The work in Chapter 6 of this thesis has appeared in the following publication: **Mills, G. H., Liu, J. H., Kaddouh, B. Y., Jackson, A. E., & Richardson, R. C.** (2018, September). *Miniature Magnetic Robots For In-Pipe Locomotion*. In *Memorias de Congresos UTP* (pp. 289-300)

In the mentioned publications the candidate was responsible for the collection, review, data analysis, and writing of material. The remaining authors contributed guidance and proof reading.

This copy has been supplied on the understanding that it is copyright material and that no quotation from the thesis may be published without proper acknowledgement.

The right of George Henry Jackson-Mills to be identified as Author of this

work has been asserted by him in accordance with the Copyright, Designs and Patents Act 1988.

© 2020 The University of Leeds and George Henry Jackson-Mills.

Acknowledgements

I would like to thank my supervisors, Professor Robert Richardson, and Dr Andrew Jackson for all of their support, guidance, and encouragement throughout the research and preparation of this thesis.

To my funders, National Grid Gas Transmission who made this work possible. Furthermore, thank you to the GRAID project partners, and especially Synthotech for their invaluable industry knowledge and guidance.

Thanks to everyone in the *Library Study Group* for all the laughs. Our time in the Library was well spent even if the research sometimes got a bit messy. Also to my friends in the lab, and particularly Dom Jones who convinced me to keep going when I felt like quitting to become a landscape gardener, I think I'll save it for retirement.

To my family back in Manchester; Mum, Dad, Elliott, Lucie, and Suzie. For always being there when I needed them, and a perfect retreat to forget all the thesis based troubles here in Leeds.

Finally to Cassie. During the *short* time it's taken me to finish this thesis we moved in together, got engaged in Paris, got two cats (Salem and Diego), got married, got pregnant, bought our first house (you did all the work), and had our beautiful boy Jasper. I love you both so much and I don't know what I'd do without you.

Cheers.

Abstract

Pipeline Inspection Gauge's, (PIGs) currently inspect 95.4% of the United Kingdom's National Transmission System (NTS) for the transportation of natural gas. The remaining 4.6% found in Above Ground Installations (AGIs) is deemed "unpiggable" due to its complex geometry. Current robotic technology entering these pipelines requires expensive modifications to the pipeline to gain inspection access. A system that can bypass modifying the pipe and complete a condition inspection could generate a minimum saving of £60 million and 2145 tonnes of CO_2 over a 20 year period.

This thesis explores new approaches towards the robotic inspection of ferrous pipeline systems with the design and development of a wheeled magnetic robot for sub 100mm pipelines. The work begins with a thorough literature review surrounding the field of in-pipe robotics. The target environment is analysed and the requirements and specification of the robot are generated. Methods of creating magnetic traction wheels are explored and a rubber coated flux plate magnetic array wheel is developed and tested experimentally. The developed flux plate array wheels were found to channel the power of 6 rare-earth magnets into a single wheel contact point and created a force equal to that of the 6 magnets (83N) combined at the cost of a 90% reduced field depth. The application of rubber coating increased the frictional co-efficient μ_s of the wheels from 0.27 to 0.71, at the cost of halving the contact force to a mean of 41N. A high level LabVIEW control system was developed to communicate with the robot's micro-controller over wireless Bluetooth using a custom serial protocol to minimise the message size for speed. Conceptual mechanical designs were conceived and two systems chosen to suit requirements for a 2-inch (50.8mm) pipeline, and a 4-inch (101.6mm) pipeline were developed further. A robust prototype of the 4-inch robot was fabricated using 3D printing techniques, the design was preferred for its curved wheelbase geometry, allowing it to negotiate convex and concave corner cases. Unlike current magnetic systems of its size the robot was found to complete all orientations of descending convex cases as well as all corner case angles of 115° or greater.

CONTENTS

1	Introduction	1
1.1	Research background	2
1.1.1	National Grid Gas Transmission System	2
1.1.2	Premature Asset Replacement	3
1.1.3	Robotic Pipe Inspection	3
1.1.4	Project GRAID	4
1.2	Motivation for research	4
1.3	Scope of the research	5
1.4	Research aims and objectives	5
1.4.1	Objectives	5
1.5	Contributions of the thesis	6
1.5.1	Published work (Appendix A/B)	6
1.6	Outline of thesis	7
2	Literature Review	9
2.1	Pipe network environment	10
2.1.1	Pipe Bends and Joints	11
2.1.2	Methods of pipe inspection in operation	12
2.1.3	Locomotion Categories	12
2.1.4	Traction Generation	14
2.2	Robotic locomotion categories	16
2.2.1	Pipeline Inspection Gauges	17
2.2.2	Wheeled Locomotion	18
2.2.3	Track Locomotion	23

2.2.4	Screw Locomotion	28
2.2.5	Snake Locomotion	30
2.2.6	Inchworm Locomotion	34
2.2.7	Fluid Locomotion	36
2.2.8	Walking Locomotion	37
2.3	Magnetic traction locomotion	38
2.4	NTS environment	39
2.4.1	Pipeline infrastructure	40
2.4.2	Natural gas	44
2.4.3	Environment summary specification	45
2.5	Literature summary	45
2.6	Literature discussion	48
2.7	Literature conclusion	52
3	Robot Requirements Analysis	54
3.1	Introduction	55
3.2	Locomotion and traction method requirements	55
3.2.1	Traction requirement criteria and selection	57
3.2.2	Locomotion requirement criteria and selection	59
3.3	Robot Specification	62
3.4	Discussion and conclusion	64
4	Design of Magnetic Traction Wheels	66
4.1	Introduction	67
4.1.1	Simplifying in-pipe geometry problems	67
4.2	Methods of designing a magnetic traction robot	68
4.2.1	Magnetic wheel design	68
4.2.2	Chassis traction design	70
4.3	Magnetic wheel requirements and specification	71
4.4	Design and assembly of the magnetic wheel	71
4.5	Magnetic wheel experimentation	73
4.5.1	Normal force	73
4.5.2	Increasing friction	80
4.6	Discussion and conclusion	83

5	Embedded System and Software Design	86
5.1	Introduction	87
5.1.1	System requirements	87
5.2	Hardware	90
5.2.1	Robot Micro-Controller	91
5.2.2	Communication	91
5.2.3	Actuation and Power	92
5.2.4	Circuit Integration	92
5.3	Open loop control system	96
5.3.1	High level control: LabVIEW	96
5.3.2	Low level control: micro-controller	102
5.4	Discussion and conclusions	103
6	Mechanical and Conceptual Design of Magnetic Robots	105
6.1	Introduction	106
6.1.1	Conceptual Design Process	106
6.1.2	Prototype Design Requirements	107
6.2	Mechanical power transmission and layout	108
6.2.1	Transmission design and motor layout	108
6.3	Concept designs for a 2-inch pipeline	113
6.3.1	Concept 1: planetary spherical parallel axis	114
6.3.2	Concept 2: co-axial coupled drive and steering	115
6.3.3	Concept 3: bevel spur gear parallel axis	118
6.3.4	Prototype development	120
6.4	Concept and prototype for step case obstacles	125
6.4.1	Optimal curvature	126
6.4.2	Concept 4: bevel with rear wheelbase	130
6.5	Discussion and conclusion	133
7	Robot Obstacle Statics, Experimentation and Evaluation	135
7.1	Introduction	136
7.2	Overcoming step-case obstacles	136
7.2.1	Concave case	138
7.2.2	Convex case	144

7.3	Experimental testing	148
7.3.1	Concave cases	148
7.3.2	Convex cases	151
7.4	Real in-pipe operation	155
7.4.1	Contact loss in-pipe	156
7.5	Discussion and conclusions	158
8	Conclusions and Future Work	160
8.1	Assessment of research objectives	161
8.2	Conclusions	162
8.2.1	Magnetic traction wheels	162
8.2.2	Embedded system and software design	163
8.2.3	Magnetic in-pipe robot for step-case negotiation	164
8.2.4	Conclusion summary	164
8.3	Future work	164
8.3.1	Magnetic traction wheels	165
8.3.2	Embedded System and Software Design	165
8.3.3	Magnetic in-pipe robot for step-case negotiation	165
	References	168
8.4	Appendix A: Published Work "Advances in the Inspection of Unpiggable Pipelines"	182
8.5	Appendix B: Published Work "Miniature Magnetic Robots For In-Pipe Locomotion"	196

LIST OF FIGURES

2.1	The most commonly encountered in-pipe bends and joints in networks A-G.	11
2.2	The eight main elements of in-pipe robotic locomotion A-F.	13
2.3	Four most common traction systems used in-pipe. A. Gravity, B. Wall-Press, C. Adhesion, D. Fluid-Flow. Where A-C rely on wall-contact to move, and D - fluid-flow systems use the wall to slow down, or not at all in the case of free-flowing passive systems.	14
2.4	Typical planar wall-press designs; A: 2, B: 3, and C: 4 arm designs.	15
2.5	Parallelogram and pantograph centralised adaptability mechanisms.	15
2.6	Motion singularity problem in a T-section [1].	16
2.7	Self-driving PIG [2].	17
2.8	Kurt II, an autonomous wheeled in-pipe robot [3].	19
2.9	MRINSPECT IV +; the latest instalment in an in-pipe robot series designed and developed at Sungkyunkwan University [4].	20
2.10	The Adaptable Quad Arm Mechanism AQAM: a wheeled wall-pressing robot for 260mm - 300mm pipes [5].	21
2.11	Hanyang Universities two-plane in-pipe robot [6].	22
2.12	Osaka Gas Company, magnetic in-pipe robot [7].	22
2.13	MagneBike developed by Autonomous Systems Lab, ALSTOM uses wheeled magnetic wheels with actuated lateral leverl arms to overcome magnetic contact forces [8].	24
2.14	Sewage cleaning robot [9].	25
2.15	FAMPER CAD model and assembled robot [10].	26
2.16	Hanyang's two module caterpillar wall-pressing robot [11].	27

2.17 PAROYS-II an articulated caterpillar pipe robot [12].	28
2.18 Heli-Pipe screw wall-press system [13].	30
2.19 Osaka University’s SPRING pipe robot [14].	31
2.20 Pipetel’s Explorer [15].	32
2.21 Kangawa Snake Robot [16].	33
2.22 PIRATE, gas network autonomous inspection robot [17].	34
2.23 3SPR Parallel Manipulator inchworm pipe robot [18].	35
2.24 CMMWorm, continuous-wave peristalsis pipe robot [19].	35
2.25 MORITZ pipe inspection robot [20].	37
2.26 OmniClimbers: Omni-directional magnetic wheeled climbing robot [21].	39
2.27 M-Blocks, magnetic robots that use angular momentum to break mag- netic bonds and solve both concave and convex step cases [22].	40
2.28 The growth of the bulk of National Transmission System between its inception in 1966 and 1983 [23].	41
2.29 Construction and installation of an underground pipe network being lay down before burial. [24].	41
2.30 PIG grate entrance from a main PIG launch vessel onto an AGI site [24], a type of interior T-Section to from the main.	42
2.31 Render of underground pipe network on an AGI, 2-inch risers can be seen entering the network from above ground access points [24].	43
2.32 Render of the GRAID robot within a concept launch vessel that would be fitted to the AGI due for inspection [24]. The launch vessel floods the robot from ATM (atmospheric pressure) to full pressure with nitrogen to remove oxygen before entry.	44
2.33 History of In-Pipe Robotic Locomotion [25].	46
4.1 Simplification of in-pipe obstacles, reducing the problem to two dimen- sional step-cases.	68
4.2 Types of magnetic wheel design; standard ring magnet (A), outer magnet placement wheel (B), shielded magnet array (C), and magnetised chassis (D).	69
4.3 Different possible magnetic skeleton chassis frames for in-pipe magnetic robots.	70

LIST OF FIGURES

4.4	Different design for the mountable wheel hub built into the magnetic flux plates. A: D-Shaft. B: Hex. C: Multiple D-Shaft. D: Key. E: Nucleus. F: Triangular.	73
4.5	Components of the magnetic wheels ready to be assembled for a 5mm flux plate, 6mm length x 6mm diameter x 6 magnet array.	74
4.6	Diagram of the magnetic wheel test rig set-up.	75
4.7	Standard magnet pull test over a 5mm range for both a regular N42 disc magnet, and a magnet wheel array.	76
4.8	Mean force for various wheel configurations (force +/- SD)	77
4.9	Comparison of the effect of wheel magnet array rotation angle on the peak force produced by the wheel for both a three and six wheel array.	78
4.10	Graph of the force to pull a free rotating magnetic wheel from a right angle concave case where the wheel is in double contact.	79
4.11	Graph of the force to pull a free rotating magnetic wheel from a 90° wall up to a convex corner case, and then detach from the corner case.	80
4.12	Graph showing the force to pull a rotation locked uncoated magnetic wheel across a steel contact.	81
4.13	Bar chart showing the average pull force for a 665A wheel at four different points around the wheel in both aligned and misaligned conditions.	82
4.14	Graph of the force required to pull the rubber coated magnet up the steel block with the axle locked in contact at the 180° mark in 4.13.	83
4.15	Wear of the rubber coating showing after five repetitions of friction testing on the linear force tester.	84
5.1	A: Laptop PC with Bluetooth built-in. B: USB Xbox controller receiver. C: Xbox 360 wireless controller. D: 300W power pack. E: Robot electronics prototype breadboard.	90
5.2	Diagram of the integrated circuit.	94
5.3	Diagram of the assembled robot hardware circuit to be embedded in a mechanical system.	96
5.4	Diagram of the high level control system used to develop the robot software.	97
5.5	Overall system architecture including simplified LabVIEW and micro-controller programs.	98

LIST OF FIGURES

5.6	LabVIEW method to convert user control inputs to condensed serial commands to be transmitted to the micro-controller.	101
5.7	Arduino method to convert condensed LabVIEW serial commands to use-able micro-controller instructions to be passed to components. . . .	103
6.1	Flow diagram showing the conceptual design process used in this chapter.	107
6.2	Robotic Concept 1: Spherical planetary design based on layout 42 in Table 6.2.	114
6.3	Robotic Concept 2: Based on layout 12 in Table 6.2, where the drive and steering are linked and then mirrored.	116
6.4	Robotic Concept 2: Based on layout 12 in Table 6.2, with an combined spur gear transmission axle.	120
6.5	Exploded view of concept 3 early wheel design.	122
6.6	In-pipe design of the 2-inch concept, avoiding double wheel contact with both walls.	124
6.7	In-pipe design of the 2-inch concept, avoiding double wheel contact with both walls.	125
6.8	Chassis interaction with a convex curve case. Robot A: standard chassis design. Robot B: estimated clearance design. Robot C: optimally generated clearance curve.	127
6.9	Minimal contact curve generation for convex step-case, example using a 32mm front wheel, 10mm rear, and 65mm wheelbase.	128
6.10	Change in curve generation with an increase in the wheelbase of the robot.	129
6.11	Schematic diagram of the robot dual bevel robot with rear magnetic wheel.	130
6.12	Schematic diagram of the robot dual bevel robot with rear magnetic wheel.	133
7.1	Concave case section one: robot approaches the wall.	139
7.2	Concave case section two: robot is in double contact case with the step at wheel one.	141
7.3	Concave case section three: robot has overcome double contact and rotation about the corner has begun.	142
7.4	Concave case section four: robot is in double contact case with the step at wheel two.	143

7.5 Convex case section one: robot angle is at 90° , ready to start rotation about the corner. 145

7.6 Convex case section two: robot has begun rotation around the corner and is the weakest magnetic contact case for wheel one. 146

7.7 Convex case section three: wheel one has passed the corner and is now attempting to pull the rear passive wheel around the corner. 147

7.8 Convex case section four: wheel two is in the weakest magnetic case. . . 148

7.9 Test rig used to evaluate the robots performance on both concave and convex step cases at varying angles. 149

7.10 Concave case performed on the test rig. A: approaching the corner case. B: Double contact, the motor ramps up to overcome the unwanted contact force. C: The robot rotates around the concave corner after detachment. D: The completion of the concave corner case. 151

7.11 Graph showing the effect of an increase in wheel friction co-efficient on the contact forces at w_1c_1 and w_1c_2 for drive wheels with a pull strength of 9.5N. 152

7.12 Robot attempting the convex corner case. A: Approaching the step case. B: The point of weakest contact for the magnetic wheel. C: Rotation of the robot around the convex corner. D: The robot can go no further as the passive rear wheel halts movement. 153

7.13 Robot completing the convex corner case. A: Approaching the step case. B: The point of weakest contact for the magnetic wheel. C: Rotation of the robot around the convex corner. D: The robot completes the case. . 153

7.14 Robot completing the convex corner case. A: Approaching the step case in reverse. B: The back wheels lose contact at the convex weak corner point. C: The chassis rotates about the wheel axis. D: The robot crashes. 154

7.15 The difference in angle between a 4-inch pipe connection with a 48-inch pipe, and a 4-inch pipe with a 12-inch pipe. 155

7.16 Graph of the change in approach angle with different size pipe connection fittings and different size target pipe inspection diameters. 155

LIST OF FIGURES

7.17 Pictures from the real world tests on a decommissioned 1016mm natural gas pipeline. A: Driving vertically. B: Inverted. C: On the outer side of the pipe. D: Iron particles and scales that "clogged" the wheel flux. E: Full shot view of the pipe size versus the robot size. 157

LIST OF TABLES

2.1	National Transmission System (NTS) possible path variables, obstacles, and environmental (Env) conditions. [26]	45
2.2	In-pipe environment, conditions, and pathways, categorised by robotic challenge level as shown by in-pipe robots reviewed in literature.	48
2.3	A summary of the most relevant robotics systems reviewed in this chapter. X (horizontal), Y (vertical), L (elbow), T (T-section), V (valves), - (unknown).	49
2.4	A summary of the various environments and conditions found within the National Transmission System (NTS) that should be considered in this research.	50
3.1	Requirements for an ideal robotic locomotion system within the National Transmission System AGI environment.	56
3.2	In-pipe robot, traction selection criteria to be analysed against possible traction methods.	58
3.3	In-pipe robot traction selection matrix based on the criteria defined in Table 3.2.	59
3.4	In-pipe robot locomotion selection criteria and definitions of relative low (0), medium (3), and high (5) scores. Criteria are categorised by pipe path (Path), obstacles (Obs), general robot attributes (Att), and environment conditions (Env).	60
3.5	In-pipe robot locomotion selection matrix based on the criteria defined in Table 3.4. Criteria are categorised by pipe path (Path), obstacles (Obs), general robot attributes (Att), and environment conditions (Env).	61

3.6	Complete in-pipe robot specification based on the NTS environment analysis and locomotion and traction methods explored in this chapter. . .	63
4.1	Requirements for the robots magnetic wheel design.	72
4.2	Test program used in the Mecmesin tensile tester to produce normal force results.	76
4.3	Test program used in the Mecmesin tensile tester to produce concave results.	79
4.4	Test program used in the Mecmesin tensile tester to produce convex results.	80
4.5	Test program used in the Mecmesin tensile tester to produce concave results.	81
5.1	Major requirements of the software control features	88
5.2	Major requirements of the hardware system	89
5.3	Micro-controller options considered for robot development comparison table	91
5.4	Comparison table of bluetooth vs wifi	92
5.5	Micro Metal Gearmotor selection table: High-power 6V precious metal brushed [27]. All gear ratios are created to 1.6 Amp stall current and No-load current of 0.07 Amps.	93
5.6	Cluster array elements that store each individual robots data and configuration settings.	99
6.1	The currently defined requirements and parameters for use in concept generation and design.	108
6.2	Selection Table of Motor Layout against Transmission Design	110
6.3	Selection criteria used in the transmission decision matrix, Table 6.4 to choose optimal an design solution from Table 6.2.	111
6.4	The decision matrix of used to select an ideal transmission design in conjunction with the criteria presented in Table 6.3, as well as the designs of the layouts 11 - 72 in Table 6.2.	112
6.5	Key design features in the spherical concept in Figure 6.2.	115
6.6	Key design features in the coupled drive and steering design in Figure 6.6.	117
6.7	Key features in concept 3, bevel spur gear parallel axis design in Figures 6.4 and 6.5	121

LIST OF TABLES

6.8	Selection criteria to choose concept to carry to prototype development .	123
6.9	Dimensions of the CH12 approximate volume.	124
6.10	Final Concept: Bill of Materials	126
6.11	Design of concept 4: a dual bevel connection robot with a rear magnetic wheelbase and curve for convex case locomotion.	132
7.1	Description of parameters used within the free body diagrams in the concave and convex cases.	138
7.2	Step-case rig: robot experimental results for concave testing at different angles.	150
7.3	Step-case rig: robot experimental results for convex testing at different angles.	154

Abbreviations

AGI	Above Ground Network	ATEX	ATmosphères EXplosives
ATM	Atmospheric Pressure	BPS	Bits Per Second
BW	Butt Welding	C	Centigrade; Celsius
CA	Corrosion Allowance	CAD	Computer Aided Design
CG	Centre of Gravity	CIPS	Cathodic Interval Protection Survey
CO ₂	Carbon Dioxide	COM	Serial Communication Port
CR	Carriage Return	CW	Continuous Welding
DC	Direct Current	DN	Nominal Diameter
EC	Eddy Current Testing	ECDS	External Corrosion Direct Assessment
EFW	Electric Fusion Welding	EMI	Electromagnetic Inspection
FPV	First Person View	FW	Field Welding
GRAID	Gas Robotic Agile Inspection Device	GUI	Graphical User Interface
ID	Inner Diameter	IDE	Integrated Development Environment
IMU	Inertial Measurement Unit	ISO	Isometric
LED	Light Emitting Diode	LiPo	Lithium Polymer
MFL	Magnetic Flux Leakage	MOP	Maximum Operating Pressure
NDT	Non-Destructive Testing	NGGT	National Grid Gas Transmission
NTS	National Transmission System	OD	Outer Diameter
PIE	Pipeline Integrity Engineers	PIG	Pipeline Inspection Gauge
PWM	Pulse Width Modulation	RPM	Revolutions Per Minute
SD	Standard Deviation	SW	Socket Welding
TRL	Technology Readiness Level	WB	Wheel Base

CHAPTER 1

Introduction

1.1 Research background

Across the globe, pipeline networks have been constructed for efficient transportation of fluids, whether they contain gas, oil, or water. Many of these networks are now reaching the end of their design lives and are due for replacement, however with the condition of their interior walls unknown it is impossible to tell which pipes should take priority. Main transmission lines; large straight pipelines which connect key stations around the world, are easily inspected using a Pipeline Inspection Gauge (PIG). These cylindrical devices are uncontrollable after insertion, relying only on the in-pipe fluid flow to move. The problem lies within pipe networks that consist of more than just straight sections; those that contain complex bends, junctions and highly varying fluid flow velocities. These installations are impossible to inspect using an uncontrollable PIG and hence the focus of this thesis will be the robotic inspection of these unpiggable pipelines.

1.1.1 National Grid Gas Transmission System

The United Kingdom's National Transmission System (NTS) is comprised of a 7,600km network of welded steel pipeline for the transportation of high pressure natural gas at a Maximum Operating Pressure (MOP) of 97 bar in main branches. Most of this system was constructed during the 1970's and 1980's and was built with a 40 year design life in mind, this period is now coming to an end [23]. In order to keep the network in safe working condition these assets must be inspected to determine the amount of damage they have sustained over their years in service. Damage can be caused through methods such as corrosion, creep, degradation, constant temperature change and can result in the erosion of the inner pipe wall as well as other defects. Currently 95.4% of the NTS can be evaluated in-line; through pigging. The remaining 4.6% (350km) of the NTS is considered unpiggable, and consists of Above Ground Installations (AGIs) of which there are over 200 scattered across the country [26]. These relatively small sections of pipe network are deemed unpiggable and are present in any pipe network: the in-line assessment of unpiggable pipelines is therefore a global problem.

Despite the name most of the pipework found in an above ground installation is buried, with only a small portion available for visual analysis. The interior condition of the buried pipework has not been seen since the installations took place, however the networks are known to be in safe condition thanks to large safety margins used

for initial design. These protective measures include: thicker pipes than necessary, use of external protective coatings, and employing cathodic protection to reduce corrosion [28].

1.1.2 Premature Asset Replacement

Currently if any corrosion issues are suspected then the underground pipe network is excavated for closer inspection at reduced flow, sometimes this requires shutting down the site completely. In high pressure installations such as these pipelines can reach up to 95% Corrosion Allowance (CA) before failure occurs, because of this many of these excavations are considered premature. Roughly thirty of these replacements are currently undertaken each year, this method is expensive, damaging to the environment, and causes disruption to customers and the running of the network. During the replacement of pipework and one valve on a small AGI the environmental cost of carbon released into atmosphere was estimated at 700 tonnes. Considering that the typical western home will produce 5 tonnes of carbon emissions a year this is equal to running 140 households.

1.1.3 Robotic Pipe Inspection

Robotic inspection of the interior condition of the network will eliminate the risk of replacing these assets prematurely, and hence stop the needless excavation of the site. A robotic solution will not require excavation of a site, needing access to only pre-existing pipework the system could enter and survey the network from an above ground entrance point. The successful development of a robotic platform with the ability to safely and accurately determine the condition of the unpiggable high pressure pipework, will enable pipe maintenance to be completed using a risk based replacement methodology. The rewards for achieving this goal are great; avoidance of disruption caused by excavations, unnecessary asset replacement, and unplanned shut downs, will result in a minimum saving of £60 million and 2145 tonnes of CO_2 over a 20 year period [24].

Research into in-pipe robots began in the mid 1980's, from this point onwards the field of in-pipe robotics inspection only grew. The research area became popular due to the unique shape of the environment (encompassing walls) and the prevalence of pipes in the modern world. Many robotic systems have been created for the inspection

of large bore straight pipes, however unpiggable pipelines remain a challenge. The primary difficulty in unpiggable sections is the inspection of large ranges of pipeline diameters. Although many attempts have been made over the years to create systems with extremely adaptive diameters no robot has been created that can inspect every pipe size present on an unpiggable network such as an AGI. Solving this problem would require the development of a small system capable of scaling the walls of the pipe, or a sophisticated articulated system that could re-form into larger configurations. These are substantial robotic challenges and ones that so far have not been solved.

1.1.4 Project GRAID

In order to tackle the issue of unpiggable AGI's in the NTS a funded research project was launched in 2015. Project GRAID (Gas Robotic Agile Inspection Device) aims to design and build a robotic inspection device that determines the true condition of pipeline assets in below-ground high pressure gas installations. National Grid Gas Transmission (NGGT) initiated Project GRAID with £5.7m of Ofgem funding for the inspection of unpiggable pipelines. Together with three SME's; Synthotech, Premtech, and Pipeline Integrity Engineers (PIE), NGGT should see the project's completion by 2018. The project as a whole will be managed by PIE, Premtech will design the robots launch and retrieval facilities as well as use point-to-point cloud mapping to create a 3D model of the AGI sites. Synthotech will design and develop the in-pipe robotic platform, which is currently scoped to inspect 750mm - 900mm Nominal Diameter (DN) pipes and will be able to travel up to 100 metres around two bends. The work presented in this thesis shares the same overarching aim as Project GRAID [26].

1.2 Motivation for research

The motivation for this research is to create a robotic inspection device capable of locomotion within existing pipeline infrastructure. By inspecting the interior network pipe assets before hitting the end of their design life their true condition can be assessed and unnecessary excavations will be avoided. By accessing pipelines through entrances that already exist, the environmental costs for creating new connection points on natural gas pipelines can be mitigated. This thesis explores the problems faced when using robots to inspect unpiggable pipeline networks and the route which has been taken to

solve these issues. This thesis will present the theory, design, and analysis of proposed robotic devices capable of inspecting ferrous unpiggable pipelines such as AGIs found on the NTS. There are few examples of magnetic inspection robots within the field of in-pipe robotics that are also capable of exploring small diameter pipelines. The robotic solution proposed will bring cost effective inspection of ferrous unpiggable pipelines one step closer.

1.3 Scope of the research

The research carried out in this thesis focuses on the robotic locomotion method used to traverse the National Transmission System and related AGI networks. The scope of this work has been narrowed to solve specific locomotion issues regarding small wall-climbing robots, and specifically locomotion of tight spaces with minimal actuators. The work does not include methods of localisation in-pipe, optimisation of distances travelled and hence battery life. The robot intends to tackle in-pipe path problems (as in joints and connections) rather than obstacles (such as pipe damage, grease and contaminants, and weld beads).

1.4 Research aims and objectives

The aim of this project is to design and develop a miniature magnetic robot capable of inspecting high pressure unpiggable pipelines using low diameter access points. Through negotiation of simplified convex and concave obstacles complex in-pipe geometry paths will be overcome and large bore pipes will become accessible for inspection. The robot will be designed such that manufacture and assembly is simple and small batch productions can be rapidly fabricated. This will be achieved through 3D printing, and the robots miniature size.

1.4.1 Objectives

The major objectives to achieve this aim were:

1. **Review current literature** to better understand and critically assess existing literature surrounding state-of-the-art in-pipe robotics and to evaluate the

performance of current locomotion methods used to negotiate complex pipe geometries.

2. **Understand the in-pipe environment** by assessing the national grid gas network and developing a robotic specification and set of requirements to **choose the correct traction and locomotion methods**.
3. **Design a detailed locomotion system for the robot** and use this as a foundation to create a platform on which the robot can be built.
4. **Design and develop a software system** to communicate with an embedded robot micro-controller.
5. **Generate detailed conceptual designs** based upon the robot requirements and specification, the locomotion system, and the electronics package. **Fabricate a working prototype** using rapid techniques.
6. **Assess the performance of the robot** in a range of step-cases simulating complex in-pipe geometry.

1.5 Contributions of the thesis

The original work completed during this research has contributed to knowledge in the following main areas:

1. A novel magnetic robot to overcome ferrous convex and concave corner cases of steel structures in 4-inch (101.6mm) pipelines.
2. A novel magnetic wheeled robot capable of ferrous in-pipe exploration within a 2-inch (50.8mm) diameter pipeline. (Published Paper 1).
3. A novel LabVIEW program and integrated micro-controller system allowing control of multiple wireless robots over serial communication.

1.5.1 Published work (Appendix A/B)

1. **G. H. Mills, A. E. Jackson, and R. C. Richardson**, *Advances in the inspection of unpiggable pipelines*, Robotics, vol. 6, no. 4, p. 36, 2017.

1. Mills, G. H., Liu, J. H., Kaddouh, B. Y., Jackson, A. E., & Richardson, R. C. (2018, September). *Miniature Magnetic Robots For In-Pipe Locomotion*. In *Memorias de Congresos UTP* (pp. 289-300)

1.6 Outline of thesis

This thesis will consist of eight chapters in the following structure:

Chapter 2: Literature Review

A review of the current state-of-the-art in-pipe and out-pipe robotic systems relevant to the work presented in the thesis. The review focuses on the locomotion and traction methods used by these robots and their individual abilities in overcome in-pipe obstacles.

Chapter 3: Robot Requirements Analysis

A detailed specification for the robotic system that is to be deployed within the ferrous natural gas pipeline. The aim of this chapter is to create the specific requirements needed to generate a robotic solution from the data gathered about the in-pipe environment.

Chapter 4: Design of Magnetic Traction Wheels

An overview will be given surrounding the magnetic traction, the methods utilised, and the optimisation of magnetic forces in order to produce a combined magnetic traction and locomotion method.

Chapter 5: Embedded System and Software Design

Work surrounding the design of the electrical systems to meet the robot specification criteria. The chapter will explore the use of actuators and control methods to drive the magnetic adhesion wheels. The wireless communication method between a high level and low level robot controller will be defined, and an optimised command protocol will be developed.

Chapter 6: Mechanical and Conceptual Design of Magnetic Robots

A detailed view into the design methods of magnetic robots, it will cover an overview of

the robots capabilities, mechanical design, and power transmission. This chapter will incorporate the previously explored magnetic design, the electronic design as well as the control system and manufacture method. The chapter will start with basic mechanical concepts that were explored to find a suitable magnetic locomotion method for restricted space in-pipe applications.

Chapter 7: Robot Obstacle Statics, Experimentation and Evaluation

This chapter brings together the work from preceding chapters and combines the knowledge gained into one functional prototype. This final prototype is mathematically analysed in static and dynamic conditions attempting step-case problems. The robot is tested experimentally to determine the limits of its functionality when moving around concave or convex cases in different orientations. After assessment the robot is deployed into real world in-pipe environments.

Chapter 8: Conclusions and Future Work

This chapter details the conclusions that have been drawn from the work in previous chapters before summarising the research and its findings. The benefits of using the proposed systems are discussed and recommendations are made for further research.

CHAPTER 2

Literature Review

This chapter presents a review of the current state-of-the-art in-pipe and out-pipe robotic systems relevant to the work presented in the thesis. The review focuses on the locomotion and traction methods used by these robots and their individual abilities to overcome in-pipe obstacles. The review will cover a large number of systems so that the general trends and overall capabilities of different in-pipe robot types can be assessed. The resultant overview of the research field will highlight gaps in knowledge that will formulate the basis for research carried out in this thesis.

Pipeline networks transport fluids such as oil, gas, water, and sewage between key locations through an estimated total of 2.5 million km (2.2 million miles) of global infrastructure [26]. Failure to adequately inspect and replace pipes results in pipe failure and subsequent loss of fluid transport, environmental damage, large excavations resulting in transport delays and air pollution. Most of the worlds pipelines are relatively easily inspected using advanced Pipeline Inspection Gauges or "PIG's"; passive devices placed into the pipe and driven by the flow of the transported fluid (type A in Figure 2.2). However, PIG's are uncontrollable and unable to adapt to sharp changes in pipe direction and diameter, making complex pipe infrastructure impossible to inspect. It is estimated that just 0.5% of pipe networks are inaccessible to conventional "PIGGING" technology, the remaining 99.5% generally consisting of large bore, straight piggable lines. Whilst this proportion may seem low, the remaining 12,500 km represents the most valuable pipes in the network; Above Ground Installations (AGI's). Many of these unpiggable networks are now reaching the end of their design lives and are due for replacement, however with the condition of their interior walls unknown it is impossible to tell which pipes should take replacement priority. It has been estimated that through the use of advanced inspection techniques, savings made from unnecessary pipeline replacement could be equivalent to £14,000 per km a year.

2.1 Pipe network environment

This section will cover the topic of in-pipe robotic locomotion methods for Unpiggable pipelines. Figure 2.2 provides a visual summary of the eight types of in-pipe locomotion used in modern pipe robotics. These elements cover the primary methods of movement in the pipe be it passive, or active. These primary elements can be combined with

other elements as well as different traction methods to create a diverse array of in-pipe robotic systems.

2.1.1 Pipe Bends and Joints

Unpiggable pipe networks vary in diameter range, material, and fluid type and can be joined in various methods and configurations. Categorized pipe joint configurations are shown in Figure 2.1. Horizontal sections (2.1.A) are considered the baseline for in-pipe complexity, any in-pipe robot should be able to navigate these. Configurations B-G are more complex, passing through them requires advanced motion planning techniques.

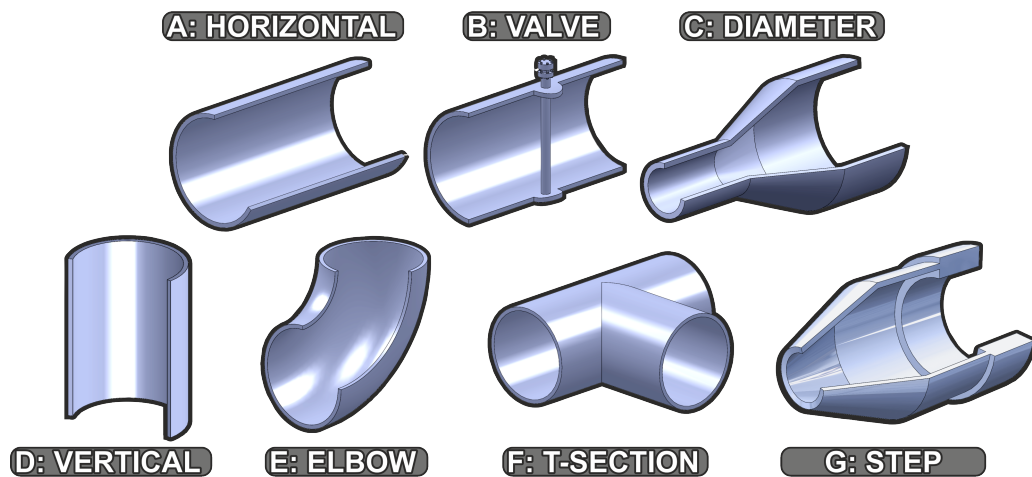


Figure 2.1: The most commonly encountered in-pipe bends and joints in networks A-G.

Valves, are particularly difficult, designs such as plug valves (2.1.B) can split the cross-section in two which can hinder full bore robots. Changes in diameter (2.1.C) are a common occurrence in unpiggable systems, many robots take measures to prepare for this obstacle specifically. Vertical sections (2.1.D) require a traction method that must also overcome gravity. Elbows (2.1.E) are very commonly encountered and are often described in terms of their bend radius; lower radius bends are tighter harder to navigate. T-Sections (2.1.F) are extremely challenging obstacles due to their lack of wall support; only sophisticated robotic platforms can navigate these. Each of these in-pipe obstacles can be found in any orientation and possibly even back-to-back e.g.

encountering two consecutive bends. Step cases (2.1.G), can occur at a flange face or large valve connection where the pipe diameter may differ slightly, resulting in a small step up or down in diameter around the entire circumference of the pipe. Developing a single robot to solve all of these problems in a wide range of diameters is currently unheard of and often requires a fleet of multiple systems in different class sizes. In this review significant robots that have furthered the research field will be presented. Current state-of-the-art methods of in-pipe travel and inspection are discussed as well as the future abilities of in-pipe robots. By analysing the barriers facing current technology and the methods being employed to overcome them, breakthroughs can be made towards universal in-pipe inspection. This review addresses in particular the problems surrounding shape adaptability, fleets, and system classes and their role in universal pipe inspection.

2.1.2 Methods of pipe inspection in operation

Pipeline inspection gauges are used worldwide to inspect consistent diameter pipelines for large and fast inspections, usually via Magnetic Flux Leakage (MFL) Non-Destructive Testing (NDT) modules built into the pigging device [29]. Work has been done on optimising PIG's for many years, however there is little novelty in these devices besides control aspects such as speed and flow rate by braking [30], [31], [32], or optimisation of travel through curved pipe sections [33]. Currently the most effective method for analysing the condition of unpiggable pipe assets is through Close Interval Protection Surveys (CIPS) [28]. Although other test methods exist such as EC (Eddy Current Testing), Electro-Magnetic Inspection (EMI), and ECDS (External Corrosion Direct Assessment). By providing a detailed profile of the potential difference between the pipeline and the soil CIPS can be interpreted to evaluate the condition of the pipe coatings and assess whether the cathodic protection is working or is compromised. CIPS is flawed in that it can only detect the presence of corrosion and cannot identify the scale of the problem, it can also be affected by external factors which may cause a false alarm; detecting a problem where there is none [34].

2.1.3 Locomotion Categories

In-pipe inspection robots have the potential to inspect the condition of these vital assets. Many potential robotic solutions have been proposed to inspect these "unpig-

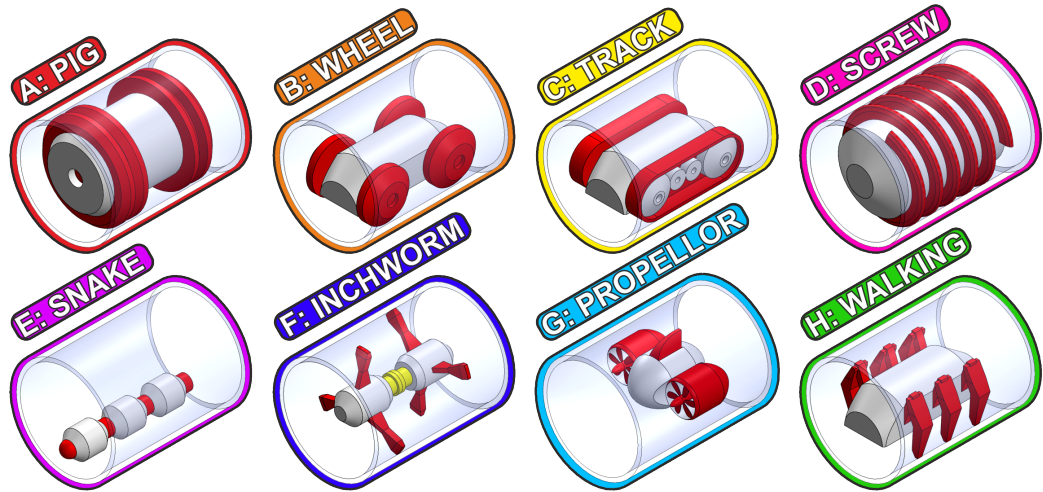


Figure 2.2: The eight main elements of in-pipe robotic locomotion A-F.

gable” pipelines that are classified by their locomotion mechanism into eight types in Figure 2.2. PIGs (2.2.A) are transport fluid driven devices, although very effective in horizontal pipes they cannot be controlled in complex networks. Wheeled robots (2.2.B) are the simplest method of in-pipe locomotion and can be used in combination with many other element types. Tracked robots (2.2.C), also known as caterpillars, are used as an alternative to wheeled systems, their large surface contact area generates high friction and reduces the chance of losing wall contact. Screw robots (2.2.D) use a spiral inspection path, they perform well in vertical sections and are resistant to slip due to their angled approach, even against an in-pipe flow. Snake robots (2.2.E) take advantage of the length of the pipe, they are generally modular and adaptable to many in-pipe environments. Inchworm robots (2.2.F) are slower than other types but can generally carry higher payloads due to their need for high wall-traction forces, useful in industrial transport tasks where speed is unimportant. Propeller based robots (2.2.G) use transported fluid medium to navigate pipelines and have the advantage of not relying on walls for any movement, however they cannot move in offline systems without fluid. Walking robots (2.2.H) use legs with multiple degrees of freedom (D.O.F) to move, their end effectors have low surface areas, useful in cutting through in-pipe wall contaminants.

2.1.4 Traction Generation

Not only do in-pipe robots use unique locomotion methods, their traction methods, presented in 2.3, also differ depending on the application. These traction methods are; Gravity (2.3.A), reliance on gravity alone restricts vehicles to only horizontal and lightly inclined pipes. Wall-Pressing (2.3.B), using the reaction force from the enclosed walls, usually in combination with diametric adaptation mechanisms. Adhesion (2.3.C), refers to methods that allow climbing of walls by adhering to the surface, this could be mechanical climbing using spines, chemical glues, or magnetic adhesion by utilising ferrous materials to produce a reaction force. Fluid Flow (2.3.D), utilising the transport medium to move usually in combination with a passive or propeller device. Through the combination of these traction methods and the locomotion elements presented in 2.2 specialised hybrid in-pipe systems can be created.

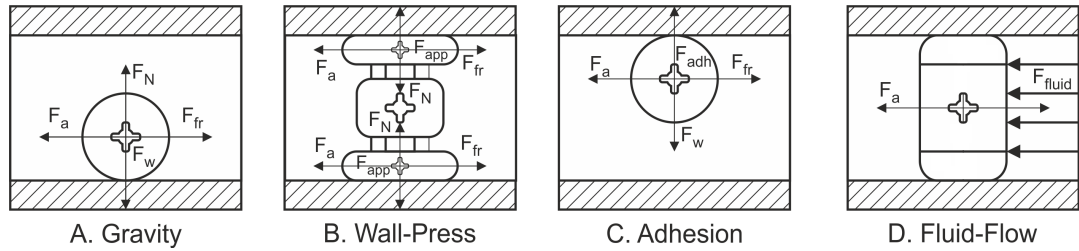


Figure 2.3: Four most common traction systems used in-pipe. A. Gravity, B. Wall-Press, C. Adhesion, D. Fluid-Flow. Where A-C rely on wall-contact to move, and D - fluid-flow systems use the wall to slow down, or not at all in the case of free-flowing passive systems.

Initially when issues surrounding in-line inspection of unpiggable pipelines became apparent, traditional gravity based exploration robots were re-purposed for the task. These robots were generally track or wheel based and built to handle rough terrain, they were not well suited to the pipeline environment and could explore only horizontal sections and gentle inclines. Although these systems performed adequately in large bore sewage and water based networks. It wasn't until robotic systems developed methods of in-pipe traction such as wall-pressing, magnetics, and fluid flow that the more complex pipeline configurations could be explored.

Wall-pressing is the most popular method of generating in-pipe traction, these sys-

2.1 Pipe network environment

tems mostly consist of a chassis that is kept concentric with pipe using some form of locomotion method or "plane" of contact with the wall. These planes are normally tracks or wheel subsystems that are mounted perpendicular to the chassis. Wall-press designs using varying numbers of planes, each with set-up having their own advantages and disadvantages.

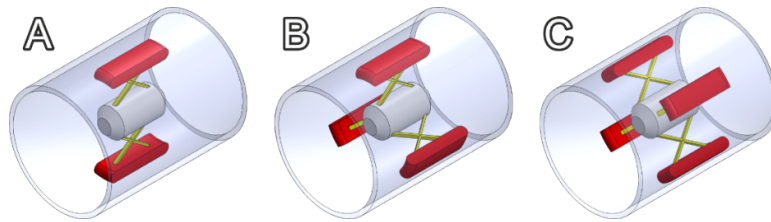


Figure 2.4: Typical planar wall-press designs; A: 2, B: 3, and C: 4 arm designs.

A great advantage of having a concentric chassis is the distance to each contact plane is constant and methods of adaptability to pipe diameter changes can be centrally located. The parallelogram mechanism and pantograph scissor mechanisms are among the most commonly used in wall-pressing in-pipe robotics. These mechanisms work well because the planes of the tracks, or wheels remain parallel with the chassis of the robot and if centred properly, parallel with the inner wall of the pipe. Although they have many variations, basic versions of these mechanisms based on lead screw rotation are shown in Figure 2.5.

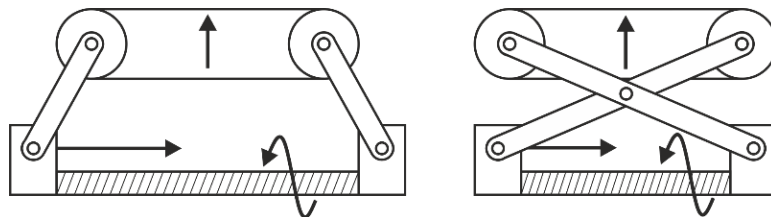


Figure 2.5: Parallelogram and pantograph centralised adaptability mechanisms.

With these benefits come disadvantages; Wall-press traction has limited adaptability when it comes to changing pipe diameters. Extension of the mechanism in Figure 2.5 are limited to by the factors of robot length and target pipe width, with decreasing pipe size and increasing length robots become less manoeuvrable through any geometry besides horizontal sections in Figure 2.1. The issue is that wall-pressing in-pipe robots must maintain constant contact with the inner walls of the pipe, in certain cases contact

becomes impossible for planar designs. The loss of contact occurs namely in T-Section junctions (Figure 2.1.F) where a section of the normally encompassing wall is removed, Figure 2.6.

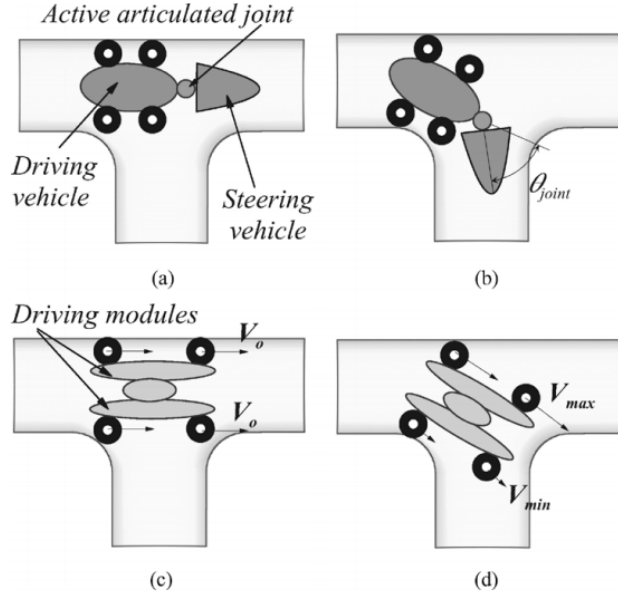


Figure 2.6: Motion singularity problem in a T-section [1].

2.2 Robotic locomotion categories

Using a database of in-pipe research robots ranked by quality and novelty the key systems that have influenced the field have been selected and reviewed. These robotic platforms have been categorised in terms of their primary locomotion method, traction system, and their specified pipe diameter range. There have been many in-pipe robot literature reviews carried out in previous researchers work for use in industrial power plants [35], water mains [36], hybridised locomotion methods [37], [38] including specific focus on wall-press systems [39], or general in-pipe reviews [40]. The general consensus in these reviews is to categorise the robots in terms of the most common combined methods e.g. "Wall-press" which can actually be a combination of different locomotion methods with wall-press being the traction method. In order to complete a more in depth review, section 2.2 will look at robots from each of the eight in-pipe locomotion categories in detail. The strengths, weaknesses, and research direction of each element

type will be presented and discussed.

2.2.1 Pipeline Inspection Gauges

PIG's may be simple devices but they are still the most efficient method of inspecting straight pipelines with a constant bore, Figure 2.7. New methods of pigging pipelines are still being developed, for example in 2005 the University of Durham developed a new form of "PIG" [2] which incorporates a propeller, driven by the fluid flowing in the pipe as a mobile power source. The turbine rotates a double threaded screw shaft upon which a nut sits. The double thread transforms the rotary motion into a reciprocating movement through the rotation of the nut on the shaft, this in turn causes the attached brushes to reciprocate. The Brushes embedded in the chassis will only allow movement in a single direction depending on which way they are facing, this results in a steady motion either upstream or downstream. The design of the self-driving PIG has been verified experimentally to crawl both up and downstream and the in-pipe turbine based propulsion was found to be a reliable source of power. Another example of modern PIG is the fluid driven robot for high flow liquid pipes developed at the Massachusetts Institute of Technology. The robot relies on fluid flow as all PIG's do, however this system has a novel magnetic brake to control the speed of the chassis [41]. This braking system consist of a three axis wall-press mount with a rotatable inner section, when rotated the magnets align normal force is increased at the wall-pressing feet.

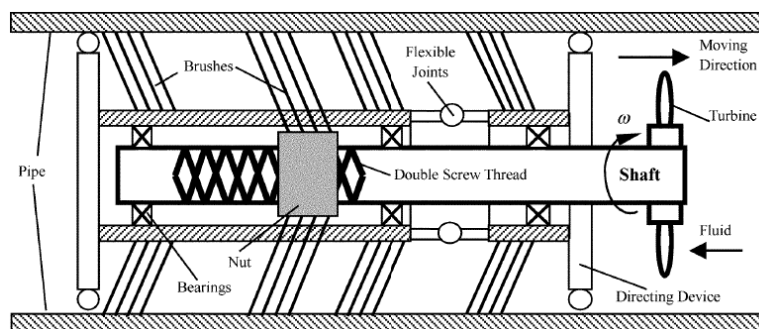


Figure 2.7: Self-driving PIG [2].

PIG's are currently the most efficient method of pipe inspection, were it not for their inability to move independently of the gas flow they would be used everywhere.

Unfortunately the passive design makes them unable to manoeuvre anything other than a straight pipe section. This is why robotic platforms must instead be designed in order to inspect Unpiggable pipelines. Selection of the base element type for these platforms is heavily influenced by the obstacles that the robot is specified to encounter, these obstacles can be typically broken down into a number of complex pipe geometry problems.

2.2.2 Wheeled Locomotion

Classified by the use of wheels as a main locomotion method, these systems can be combined with any of the four traction methods. When combined with wall-press and magnetic traction methods simple wheel based systems become efficient in-pipe robots. Shows wheeled systems (orange) are the most prevalent method of in-pipe locomotion, being used in 43% of all systems. This is due to their adaptability and ease of combination with other locomotion types excluding tracks to create hybrid in-pipe systems. Wheeled systems are predominantly used with wall press traction methods, 49% of all wall pressing robots using wheel locomotion.

Early in-pipe robots were simply basic adaptations of gravity based wheeled systems before they evolved to hybridised locomotion [42]. The KURT series of robots was developed at Technical University Graz in conjunction with GMD Autonomous Intelligent Systems, Germany. The robot series ran from 1996 starting with KURT and then later KURT II in 1999 shown in Figure 2.8, the robots were the first wheeled inspection devices for in-pipe sewer applications. Wheels alone were suitable for this task as sewage pipes rarely feature any complex geometry besides low radius elbows and low inclines. The purpose of KURT was not focused on locomotion but rather the autonomous assessment of in-pipe objects such as grid covers and inlets. The robots featured stereo cameras for this a purpose and successfully detected objects within the pipe albeit with a very poor resolution [3].

MOGRER, an in-pipe robot developed by Niigata University circa 1987 was one of the first wall-pressing systems [43]. It was created for the purpose of industrial pipe inspection tasks and set out to solve the biggest problem at the time; climbing angled pipes against gravity. MOGRER was an improvement on an even earlier wall-press design FERRET-1 which introduced a three wheeled adaptable robot with passive configuration using a spring system [44]. MOGRER further improved the spring system



Figure 2.8: Kurt II, an autonomous wheeled in-pipe robot [3].

forming a scissor structure similar to a pantograph mechanism, a popular choice for diametric change methods in the future. Simple wheeled wall-press systems like are the common in-pipe movement method and are present in many robotic systems. Many use a passive spring design, like the adaptable wheel wall-press system for 140mm - 200mm diameter pipelines [45]. Kanagawa University, Yokohama Japan created a wheeled wallpress system for 125mm - 180mm pipes uses a central worm gear with three linkage connectors with active drive wheels to press into the pipe rather than the more common lead screw method [46]. This direct gear method is useful for smaller diameter pipe robots where space is at a premium. Shanghai Jiaotong University, China, used a three planed wheeled wallpress vehicle with a lead screw based linkage design to increase or decrease the adaptive pipe range of the robot [47].

MRINSPECT is a series of advanced wall-pressing wheeled in-pipe robot series designed and developed at Sungkyunkwan University, which have been in development for over a decade [4], [48], [49], [50]. The robot, presented in Figure 2.9, is capable of performing all types of geometry manoeuvres besides valves and has a 50mm adaptability range from 130mm - 180mm. MRINSPECT uses a multi-axial differential gear system to control each of its four wheeled legs angles through active bevel drive connections. The body frame of the robot consists of a spring loaded central rod which supports two sets of linkages either end, the springs force the linkages to adapt to any diametric changes in-pipe. The active wheeled driving modules are connected to the linkages at both ends allowing them to be in contact at different heights depending

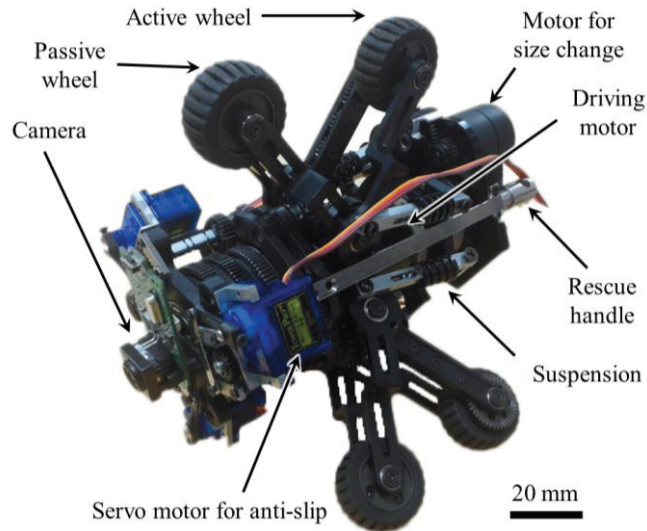


Figure 2.9: MRINSPECT IV +; the latest instalment in an in-pipe robot series designed and developed at Sungkyunkwan University [4].

on the in-pipe geometry [51]. MIT developed a similar wheeled wall-press system for leak detection in the for 100mm pipelines for in-pipe leak detection. The robot has a small compliant spring in each wall-press wheel to account for slight defects or welds in the pipe [52]. Large robots can also be built with the wheeled wall-press design, DEWALOP is a cleaning in-pipe robot for 800mm - 1000mm pipes [53]. The robot uses linear actuators rather than linkages to achieve sufficient normal force on the pipe walls, this would be viable for a robot this large but not for smaller systems.

Shenyang Institute of Automation have proposed a system which allows different robots to be created from the same platform. Although based around the same class size and pipe diameter of 200mm three different systems were developed from one, MMU [54]. These wheeled wall-pressing systems performed different functions; MMU1 could adapt to slight changes in pipe diameter, MMU2 was focused on detecting defects, MMU3 added a propeller function for fluid travel. The use of one common skeleton allowed these systems to be created from one design with relative ease compared a complete re-design.

In 2012, YonSei University developed an advanced wheeled system that can adapt to vertical pipe sections, elbows, and even T-Sections. The Adaptable Quad Arm Mechanism (AQAM), presented in Figure 2.10 is a wheeled wall-pressing robot for

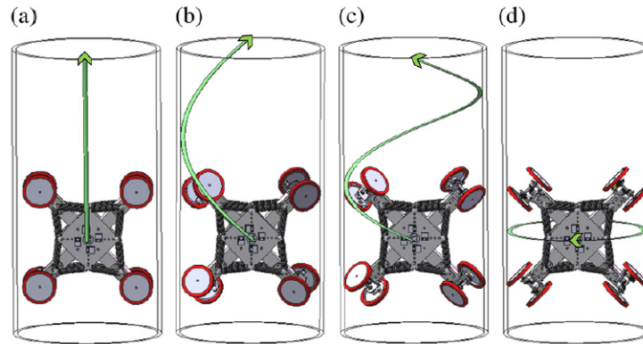


Figure 2.10: The Adaptable Quad Arm Mechanism AQAM: a wheeled wall-pressing robot for 260mm - 300mm pipes [5].

260mm - 300mm pipes, consisting of four arm mounted wheels in a single plane [5]. The robot has impressive manoeuvrability due to its four controllable arms and swivel mechanism to angle the wheels and hence rotate the robot in-pipe. This design allows the robot move through extremely complex in-pipe geometry such as T-Sections into a reduced vertical pipe section. AQAM shares its single plane design with Hanyang University's single-plane wheeled system [6].

These two systems have an advantage over multi-plane wall-pressing robots, by rotating in the pipe they can always maintains contact with the pipe walls in most complex obstacles. The problem faced with single plane contact is stability, any loss of wall contact in these designs will de-centralise the robot and make recovery extremely difficult. This is especially restrictive for the system developed at Hanyang University, shown in Figure 2.11, as the robot was capable of 80mm - 100mm diameter pipes and hence only has a 20mm adaptability range [55]. Larger robots can also cover a wide range of diameters, Shanghai developed a large 3 planed wheeled system with a parallelogram mechanism that allowed adaptation from 400mm - 650mm pipelines. Hanyang University also take a novel approach to wall-pressing using a wheeled clutch system that overpowers the wall-press active wheels. This clutch system allows for emergency retrieval of the robot form 100mm pipelines [56].

Through the addition of magnetic materials, wheeled in-pipe robots can capitalise on the ferrous properties of certain pipelines. Magnetic wheeled robots allow the operator to scale walls and maintain normal force without the need for wall-pressing

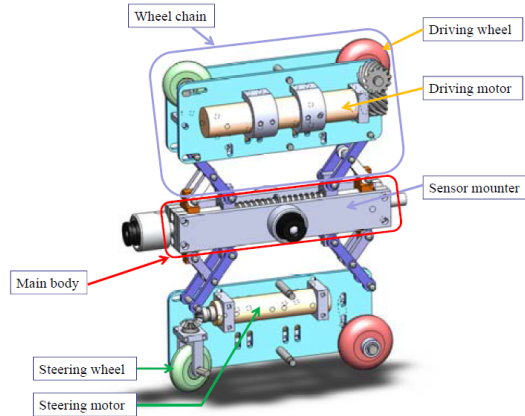


Figure 2.11: Hanyang Universities two-plane in-pipe robot [6].

functions. The first magnetic in-pipe robot was developed by the Osaka Gas Company in 1995, the system was a dual wheeled magnetic concept for the inspection 150mm - 600mm iron pipelines [7]. The concept was designed specifically to solve the T-section geometry problem without the need for a wall press robot, as these generally struggle with in-pipe valves and other sharp obstacle negotiation.

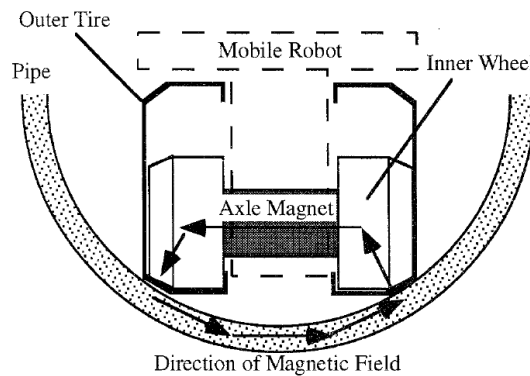


Figure 2.12: Osaka Gas Company, magnetic in-pipe robot [7].

MagneBike, presented in Figure 2.13, is an advanced example of a wheeled in-pipe robot using magnetic traction that can steer in a large range of in-pipe diameters developed by Autonomous Systems Lab, ALSTOM. Not only this but in-pipe obstacles such as T-Sections become trivial [8]. MagneBike could inspect a maximum pipeline diameter of 300mm and was designed for industrial applications inspecting

power plants. MagneBike's use of wall adhesion in-pipe reduces all complex in-pipe obstacles to either convex or concave corners which it must overcome. The robot can complete convex and concave bends in any orientation with or against gravity because of its dual active drive magnetic wheels [57], [58], [59]. The system has 5 degrees of freedom each with an actuator, 2 for drive, two for lifting, one for steering. The two lateral lever arms integrated into the same rotational axis of the wheels allow the robot lift the wheels off in concave corner case thus allowing the robot to continue up the step without becoming stuck in double contact. This mechanism can also be used to stabilise the wheels by essentially giving four extra points of contact and potentially avoid the magnets clipping off at an angle [60]. The simplified concave and convex problem for magnetic robots is also outlined in work from ALSTOM systems, such as in their wheeled mobile magnetic robots, such as the hexagonal climbing robot [61]. Magne-bike has advanced to 3D in-pipe visualisation of the robot in order for a remote user to drive the vehicle effectively in complex spaces based on odometry and a three-axis accelerometer [62]. University Tenga National built a micro magnetic wheeled robot for the inspection of 80mm - 180mm pipelines [63]. Their magnetic wheel traction consists of neodymium magnetic discs surrounded by a low carbon steel 1018 ferromagnetic housing, the configuration is much like a pot magnet with attached gears.

Wheeled systems are even used in conjunction with PIG-like locomotion; using the fluid force to accelerate. Kantaro a wheeled wall-pressing in-pipe robot for sewage pipe applications developed at Kyushu Institute of Technology, Japan takes a different approach to wall-pressing by combining it with a fluid driven locomotion [64]. Relying simply on pipe geometry to sit in the pipe, whilst it also has adaptability built in to move from 200mm - 300mm diameters. Fully autonomous with passive damping springs and no tether, the system was ambitious, boasting the ability to manoeuvre through pipe bends without the need for a controller.

2.2.3 Track Locomotion

Track, or caterpillar based locomotion can be used in the place of wheels, they hold the advantage when generating friction. The large contact surface area makes these systems more stable but also generally larger than their wheeled counterparts. Caterpillar tracks have been used in 11% of in-pipe systems and are growing in popularity in research robotics, Figure 2.1. Tracked systems are also predominantly wall-pressing with 75% of



Figure 2.13: MagneBike developed by Autonomous Systems Lab, ALSTOM uses wheeled magnetic wheels with actuated lateral lever arms to overcome magnetic contact forces [8].

all caterpillar robots using the traction method, the remaining 25% relying on gravity alone. In situations where smooth terrain is not guaranteed high contact area caterpillar tank tracks are considered superior as opposed to the point contacts on wheel systems. They excel at moving over obstacles and rough terrain and are often used in cleaning applications.

Pure track systems have been developed in recent years such as the in-pipe cleaning robot developed in 2011 by the University of Technical Education in Viet Nam shown in Figure 2.14. The robot is tasked with cleaning the inner surface of sewage pipes where many contaminants, greases, and oils are likely to be present. In this case the increased surface area in contact with the interior of the pipeline is ideal for generating high tractive effort and reducing slippage. The robot is specified to enter 300 - 600mm pipes, because it does not rely on wall press it needs no function for changing diameter so could potentially enter very large pipes. However the robot is equipped with a 300mm bore cleaning device to remove debris and residue from the sewage pipes and hence is only really effective in its specified range. For the function of this design perhaps a wall press system would have been better suited, especially as the cleaning tool could be kept in line with the pipes central axis [9]. The sewage robot is similar in structure to the

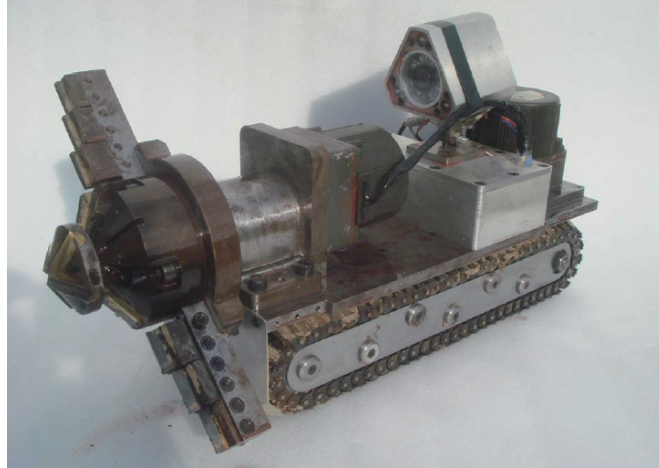


Figure 2.14: Sewage cleaning robot [9].

250mm - 500mm bore pipe inspection crawler (PIC), a heavy duty tethered wall-press caterpillar system [65]. The system is outfitted with an ultrasonic sensor and camera but is held back due to the limitations of tethered design [66]. Likewise the University of Technical Education, Viet Nam also created a sewage pipe-cleaning tracked robot for 300mm - 600mm diameter bores. The robot uses a large rotating cutting plate like a drill to remove sludge and other contaminants [67].

Massachusetts Institute of Technology also developed a omni-wheel based caterpillar robot that has been dubbed OmniTracks. The omnidirectional cylindrical tracks allow the robot mobility forwards, backwards and sideways without need for rotation of the body [68]. AGH University of Science and Technology produced a pure caterpillar track system with a reconfigurable track arrangement. The robot can extend the tracks from a 210mm diameter up to a 350mm pipe, and can even rotate the tracks to drive in rectangular ducts [69].

FAMPER was developed as a fully autonomous mobile pipeline exploration robot at Seoul National University [10], it was a track/caterpillar robot using wall-pressing traction with four-planes. Designed for 6-inch sewage pipes; Famper uses a passive method of wall-pressing to attain normal force against the pipe using compression springs and coupled with a slider linkage mechanism. The four separate caterpillar tracks can be actuated independently allowing the robot to differentially drive through elbows and other obstacles where varied speed is required. Famper performs well in 6-inch pipes and claims to be capable of T-Sections but has only been proven to complete

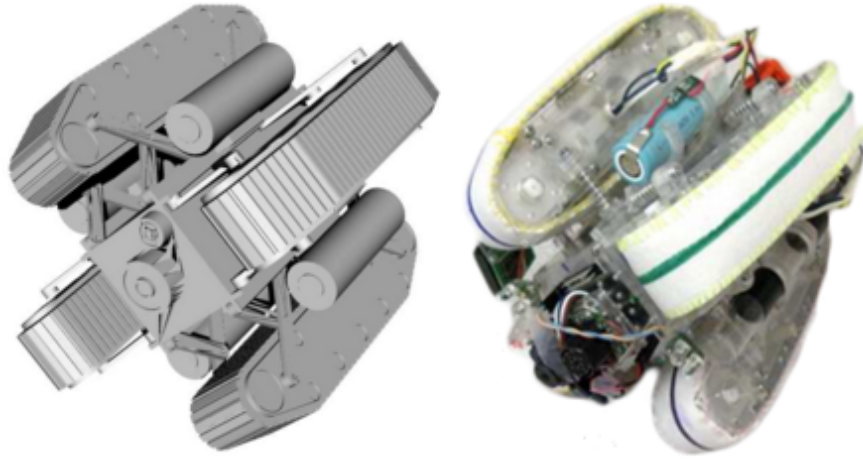


Figure 2.15: FAMPER CAD model and assembled robot [10].

vertical T-sections from a horizontal down, utilising gravity in its favour during the contact-loss phase of the manoeuvre. The full-bore design of Famper leaves little room for shape adaptability, with a full range of just 127mm - 157mm, the purpose of which is mainly for obstacle negotiation. The lack of adaptability makes Famper unsuitable for any situation other than 6-Inch pipelines [70]. This is a common occurrence with passive adaptability even in larger robots, systems such as AQAM which are exceptionally mobile and adaptable to changes in pipe geometry [5].

Caterpillar Wall-press systems are one of the most adaptive types of system in terms of shape adaptability. Tarbiat Modares University used active parallelogram adaption in a three-planed caterpillar wall-press system which could adapt from 250mm - 350mm, however this could be increased by altering the length of the linkages [71]. The lead screw used to alter the height of the tracks keeps all three planes extended at the same rate and hence keeps the chassis central in the pipe. Nigata University's tracked robot uses an adapted scissor mechanism can passively adapt from 140mm - 210mm [72].

Hanyang University developed a two module caterpillar wall-pressing robot using differential steering and a passive adaptability module using a four bar mechanism to produce the required normal force on the tracks. This system could handle 80mm - 100mm pipes and can tackle many difficult in-pipe obstacles using the two-module design [11]. The separate tracked modules were connected via a tension spring which would drag the rear or front module through an obstacle, removing the need for both



Figure 2.16: Hanyang's two module caterpillar wall-pressing robot [11].

modules to steer.

AGH University have prototyped a large in-pipe robot for the inspection of 200mm pipelines that uses caterpillar tracks on a linkage which can alter their effective diameter [73]. This allows the robot to travel horizontally in a range of pipes from 201mm - 235mm. Although vertical travel is possible, this is only the case when the tracks are fully extended essentially making vertical travel possible only in a 235mm pipe.

AGH's systems low adaptability range is in stark contrast with Ritsumeikan University's parallelogram crawler; a caterpillar wall-press system with an impressive adaptive diameter of 136mm - 226mm almost double its own length [74]. Ritsumeikan have in fact developed multiple version of the system and has another under-actuated parallelogram robot with modular style caterpillar tracks [75].

PAROYS-II uses an actively controlled pantograph mechanism with a partially passive spring mechanism, this allows large changes to be controlled and small obstacles to be ignored [12]. Its use of a second set of articulated caterpillar tracks allows a huge adaptive range of 400mm - 700mm. The tracks are actively adaptable as the front and rear tracks are connected via an active joint [76]. The joint contains structural compliance and can passively maintain wall contact and normal force with the use of forces sensing control algorithms. PAROYS has been used in conjunction with advanced control simulations to determine a case to complete T-sections while avoiding contact loss at the pipe junction. With this model the curve trajectory needed for motion

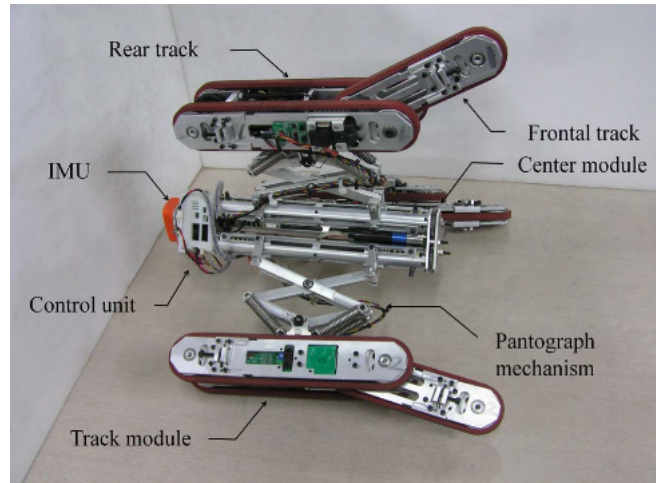


Figure 2.17: PAROYS-II an articulated caterpillar pipe robot [12].

planning of the robot through a branched section can be determined, however it has only been shown to complete these cases in simulations [77], [78].

Similarly Pukyong National University's tracked in-pipe robot uses modules with both passive and active adaptability mechanisms [79]. The shape adaptability is controlled using a driven threaded shaft lead screw and allows for transitions between 300mm - 500mm effective diameter by altering the position of a four bar linkage. The second module replaces the lead screw with a compression spring allowing for both passive and active diametric adaptations. Gunma university produced a magnetic caterpillar track robot capable of inspection pipelines with a diameter of 150mm and above, the robot has been shown to be capable of negotiating T-sections. The track locomotion allows a detachment from one of the two driving spurs in the case of non-continuous surfaces [80].

2.2.4 Screw Locomotion

Screw systems are defined by the method of locomotion in-pipe, using a rotary motion to drive themselves forward using a spiral track, to move through the pipe in a pitched circle. These systems are always wall-pressing as they rely on the inner walls in order to thread through the pipes, this allows them to climb vertical pipelines with ease. Screw locomotion robots are generally very difficult to back-drive due to their angled wheels or tracks, making them effective in high flow networks. Screw systems have stayed

relatively steady in terms of growth in Figure 2.33 although the element is only used in 9% of research systems.

Heli-Pipe a screw wall-press system has a diametric adaptive ability of just 10mm, as a result four different prototypes were made, ranging from 170mm - 40mm. The largest of the systems having a range of 10mm and the smallest 5mm [13]. Emerging methods of in-pipe adaptability show the possibility of continuously deforming systems with many degrees of freedom. This sprung wall-press screw design is quite common to in-pipe robotics, and is used again by Ritsumeikan University, Japan to create a screw drive robot capable of completing T-sections. The Ritsumeikan robot is unique in that it has an active link between two of its drive modules that allows it to select a direction at a pipe junction. Like other spring press designs this robot has limited pipe diametric adaptability and is only suit to 109mm - 129mm pipelines. Tokyo Institute of Technology created a small diameter screw style system an order of magnitude smaller, for just 10mm - 20mm pipelines. At this scale motion is very limited and so the robot takes inspiration from the way helical bacteria produce movement using flagellum. The robots mechanical actuation consist of just four wires running down the body which contract in different modes to rotate the flexible body [81]. An similarly interesting and novel micro screw robot has been developed by the Tokyo Institute of Technology, Yokohama, a robot that consists of just three intertwined hollow tubes. The hollow tubes can be inflated to force the twisted bundle of tubes into a helical formation, by inflating each of the three tubes intermittently the robot can screw its way through a pipe of just 8mm - 20mm [82].

SPRING is a screw type wall-press robot developed at Osaka University, although it relies on full wall traction it is unlike traditional full-bore wall-press systems which keep their chassis centralised in the pipe [14]. The design consists of many connected modules which form a continuous tight spiral some of which contain wheels allowing the robot to move in a spiral motion. When faced with a sharp change in diameter the robot can stretch this spiral increasing its pitch and therefore decreasing its diameter to less than half its optimal width of 150mm pipelines. This function is entirely possible because of the lack of a centralised chassis, making the robot very adaptable when faced with obstacles such as valves. Current issues include the complexity of the design, optimal redesign of the robot is very difficult due to the amount of parameters involved and so a simulation tool had been created to aid in this. Shenyang Institute of Automation



Figure 2.18: Heli-Pipe screw wall-press system [13].

produced a much simpler robot, also for 150mm pipelines that is actuated using just one DC motor to turn the body of the robot. The wheeled-screw system was quite complex and featured no diametric adaptation method which caused it to become stuck in the pipe often. Their solution was to create a "lock up" control mechanism which activates when stuck allowing the robot to reverse and escape the locked contact point [83].

Shenyang University created a wall-press robot based on helix movement in-pipe, capable of 250mm - 300mm pipeline exploration using a passively adaptive four bar linkage [84]. The robot can complete complex manoeuvres such as T-Sections using its active drive module to steer the course.

Screw robots have also been combined with magnetic [85] and is quite a popular method of locomotion in-pipe for medical applications. An external field is not use-able for underground in-pipe applications, the field would need to be extremely strong, and the location of the robot would need to be known which is not the case.

2.2.5 Snake Locomotion

In-pipe snake robots are typically feature articulated joints in a modular design paired with wheels or tracks for locomotion. The articulation allows many degrees of freedom within a single system making them very versatile in their approach to obstacles. In the last 15 years, in-pipe snake robots have become the preferred method of commercial



Figure 2.19: Osaka University's SPRING pipe robot [14].

pipeline inspection and account for 13% of in-pipe robotic research.

The PipeTron series developed by HiBot, Tokyo is a multitude of robotic in-pipe exploration snake robots. Predominantly designed for tight bend systems such as refineries and chemical plants, the system is tethered for instant retrieval and consists of passively articulated wheels connected in a series [86]. The passive torsion springs in each module joint allow the robot to bend and alter shape depending on the problem encountered and the width of the pipe without requiring further actuators. Due to relatively low range of passive adaptability multiple platforms have been created for each commonly encountered pipe diameter: 75mm, 100mm and 150mm.

The Explorer series is a prime example of the amount of effort going into translation of robots for different size pipelines, initially developed at Carnegie Mellon University [15]. This large snake robot is designed for the inspection of live gas networks under operating conditions, however it requires a full bore to operate with little adaptability ranging from just 150mm - 200mm. Multiple systems have now been developed for operations in larger than specified networks [87]. PIBOT is a 350mm - 400mm snake robot system similar in its modular style to the explorer series, its focus is the delivery of its NDT module into unpiggable natural gas pipelines. The drive modules on-board use wall-pressing wheel traction to position the magnetic flux leakage (MFL) module, the MFL system is then deployed via a pantograph mechanism [88]. Natural gas snake robots have also been developed at Sungkyunkwan University for use with NDT MFL



Figure 2.20: Pipetel's Explorer [15].

equipment [89]. The robot is a standard articulated snake structure with two active drive modules, two controls, and other modules with tethered power. The novel work in the robot is the Double Active Universal Joint (DAUJ) which is present between the modules. This was developed for routing a snake vehicle through the tight bends and enables control of the joint compliance. The National Energy Technology Laboratory of the US Department of Energy have created a wall-press wheeled snake robot for unpiggable pipelines to carry MFL modules through the pipe. The tethered robot "RoboScan" uses compliant wall-pressing drive modules to maintain traction in-pipe [90].

Kanagawa University, presented an unusual and interesting method for coping with various pipe diameters. The robot is a hybrid of caterpillar and snake components, built from modular units each containing a driving caterpillar track [16]. Connecting three or more units allows the robot to drive in-pipe, should a larger diameter need to be traversed the number of driving units can be increased. Promising results were shown in experimental pipes of 100mm - 300mm, an exceptional range for a robot with modules of just 50mm. A similar method of this dimateric adaptation in snake robots has been explored by Applied Cybernetics, Norway. The snake robot they created for 250mm - 300mm pipelines. The robot can span the pipe with active joints between its wheeled drive modules, although the active joint range is not as large as Kangawa's system [91].

Czech Technical University, Prague have developed a snake robot with the purpose of identifying new methods of generating pipe contact without relying on traditional wall-press mechanisms such as pantographs and parallelogram linkages [92]. The modular snake robot consists of many segments each of which contain both rotary and

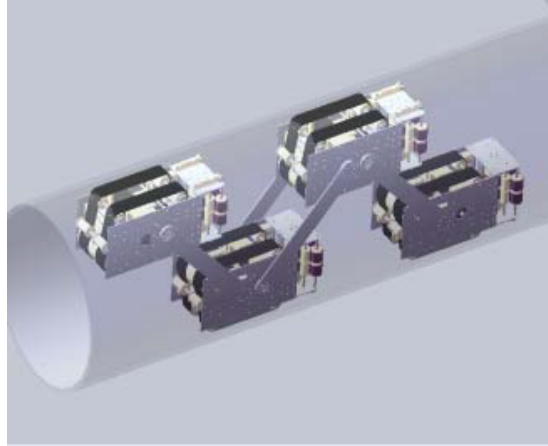


Figure 2.21: Kangawa Snake Robot [16].

translational actuators, this allows the snake to form structures much more complex than full bore robots. The shape adaptability of 100mm is already greater than twice the length of the body segments which measure just 50mm, with greater numbers of segments this robot may even be able to handle a wider range of diameters.

PIRATE was an in-pipe robot with the intended purpose of autonomous inspection of the gas distribution network in the Netherlands [17]. The robot is snake-like, and modular in nature featuring articulated clamping modules that can actively change the height of the robot to adapt to changes in pipe diameter. The design of the clamping modules was somewhat similar to the first proposal for a passively adaptive three wheeled inspection robot, [44]. However unlike passive systems the active articulated joints allow for an efficient change in pipe diameters, stretching to twice its original inspection diameter from 125mm - 63mm [93].

Snake robot's can also be used out-pipe, and generally grip and wrap themselves around pipe obstacles, such as Carnegie Mellon University's unified snake robot for 50mm pipe climbing using shape memory alloys (SMA's) [94]. While out-pipe snake methods are not generally applicable to in-pipe locomotion the general actuation of the robots still applies. This is also true of OC Robotics, snake-arm system which is highly flexible and dynamic for movement in close range tethered areas of a minimum 100mm pipeline. The snake-arm can enter a hole and search for a defect using the robots base as stabilisation [95]. This is currently used in the aerospace industry but could be applied to an in-pipe robot to search pipe branches at a reduced range.

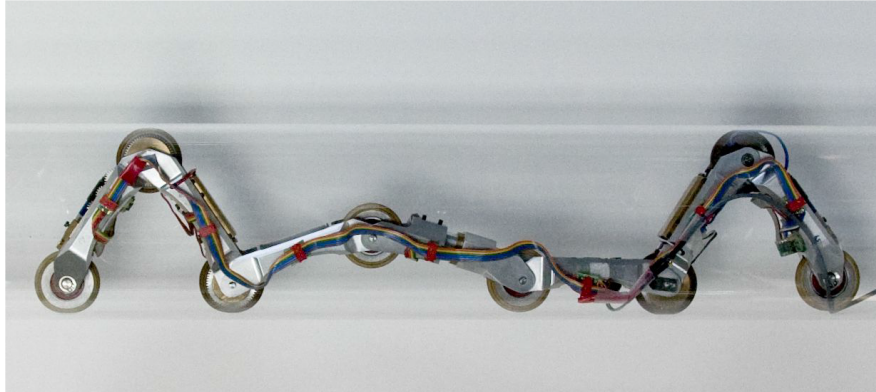


Figure 2.22: PIRATE, gas network autonomous inspection robot [17].

2.2.6 Inchworm Locomotion

In-pipe inchworms are currently only wall-pressing, they generate traction through large normal force applied at the front or back module whilst a central module contracts and extends in sequence. The high normal forces needed to support the robot during contraction makes these systems generally well suited for carrying high payloads. The use of point contact in inchworms and the removal of wheels or tracks makes them much more stable than other designs. Inchworms are also generally less prone to slip due to contaminants in-pipe as they can "cut" through the grease. Use of inchworms is quite widespread in the field, 11% of systems were found to use this technique in the study.

A highly mobile inchworm inspection robot based on a parallel manipulator, developed at YonSei University. This wall-press inspection device can handle 205mm - 305mm pipes the large inspection range coupled with its ability to traverse T-Sections makes up for the slow inspection speed [96].

These platforms have shown promise in industrial networks and have inspired the further exploration of large inchworm systems such as the 3SPR parallel manipulator under development at Yanshan University. This is a large two-module in-pipe inchworm robot, although currently in a theoretical state is intended to have large load carrying capacity for industrial applications [18].

Industrial pipeline networks often contain large amounts of oil and grease traces; it is these applications where wall-pressing systems such as these excel due to their low contact area end effectors. Case Western Reserve University have developed a

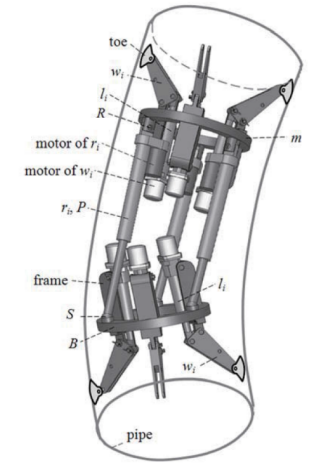


Figure 2.23: 3SPR Parallel Manipulator inchworm pipe robot [18].

new method of in-pipe robotic locomotion using continuous-wave peristalsis, the same mechanism employed by earthworms [19]. The robot, named CMMWorm, is composed of many interlinked joints forming a mesh like structure that can deform in the presence of an environmental change. The braided mesh can currently smoothly expand and contract from 220mm - 180mm and although currently unable to steer through in-pipe obstacles the mechanism shows great promise in shape adaptability research. These robots can potentially alter their effective diameters in-pipe in any section of their body.



Figure 2.24: CMMWorm, continuous-wave peristalsis pipe robot [19].

On the smaller end of the scale, a micro inch-worm robot for 17mm - 10mm pipelines has been developed at the National University of Defense Technology, Changsha, China. The robot has a unique self-locking mechanism that allows it to drastically increase normal force in a single module allowing inchworm movement at the second

module by contraction. The locking mechanism is a three footed folding linkage with a lead screw based actuator [97].

The flexible squirm pipe robot developed at the Automation School, Beijing University is another example of a novel adaptation of an inchworm device. The inchworm configuration of the robot is a standard two part lead screw design, interestingly though this robot is designed to utilise the pressure of the pipe fluid to move much like a PIG, and is equipped with a nozzle tip that helps guide it through bends and T-sections [98].

A novel bristle mechanism based inchworm design has been developed by Dailan University of Technology, China. Similar to the University of Durhams bristle based PIG [2] this robot uses many bristles as points of contact and relies on bending force of each strand to produce movement [99]. The robot is asupported in-pipe by passive wall-press modules that ensure the system remains concentric with the pipeline.

2.2.7 Fluid Locomotion

Propeller based locomotion is quite unusual in pipe inspection, used in combination with mainly fluid flow in water pipes this niche application featured in only 3% of reviewed systems. These water pipe inspection robots have the opportunity to utilise the fluid and develop swimming robots for use in leak detection. The main advantage of propeller systems is removing the need for wall contact altogether.

A swimming in pipe robot was developed at the Massachusetts Institute of Technology as a solution to the challenges faced by robots relying on wall contact in water transport networks. The robot, MIT-MRL contains a chassis with housed electronics and two propellers for propulsion, the swimming nature of the robot allows exploration of pipes 100mm and above autonomously [100].

The University of Sheffield took a different approach to swimming, developing a modular robot which can manipulate the fluid in order to generate propulsion in a certain direction by combining their chassis to form complex shapes. Each of the modules in this system form a section of a hydraulic system which when connected to another module forms a flowing network [101].

Although primarily a caterpillar track type robot, the Multifunctional Mobile Unit, MMU3 [54] also utilised a propeller in a version specified for fluid travel.

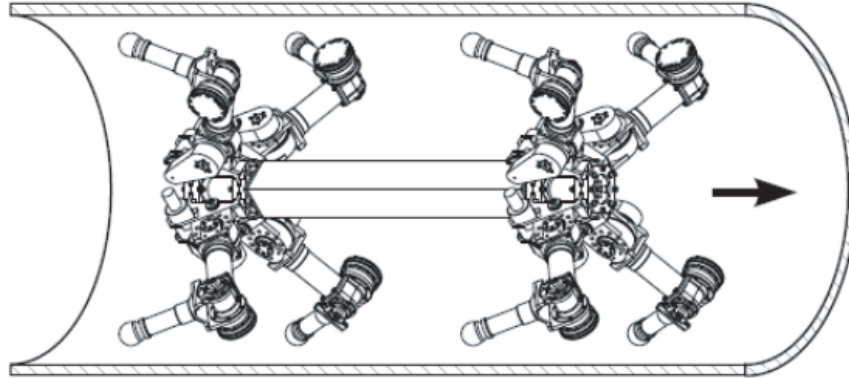


Figure 2.25: MORITZ pipe inspection robot [20].

2.2.8 Walking Locomotion

Walking type in-pipe robots use multi D.O.F. legs to move around the pipe, these are generally complex and quite large due to the number of actuators involved. Walking types which incorporate wall-pressing functions sacrifice mobility for increased stability, these are generally slower in-pipe. As a trade-off, the application of active wall pressing mechanisms give them a great amount of control over the applied normal force in pipe and they can deliver heavier payloads. Walking systems are somewhat uncommon with only 7% of research robots using the technique although they have been appearing more often in recent years, seen in FIGURE 2.1.

MORITZ, a pipe inspection robot built at the Technical University of Munich was one of the first walking style robots to be developed [20]. Using 2 modules with a total of eight legs with 2 actuators each, a bending joint, and a rotation joint this complex system had a large number of degrees of freedom for an in-pipe robot. MORITZ was capable of travelling through 600mm - 700mm diameter pipes thanks to the highly variable actuated legs, each with 2 degrees of freedom, extension of these legs allowed normal force to be controlled and frictional forces strong enough to hold up to 20kg payloads. The high amounts of control and increased carrying capabilities compared to passive systems make robots such as MORITZ ideal for industrial inspection of power plants, where safety is a priority over speed of inspection and power requirements.

2.3 Magnetic traction locomotion

Magnetic traction is used in many areas such as ship hull inspection, tank inspection and cleaning, and medical applications. Reviews of magnetic wall-climbing devices have previously been performed [102], this literature search will focus on key robots as well as the current state-of-the-art for wall-climbing magnetic systems. Some of these robots would work quite well in-pipe such as a caterpillar magnetic robot that can complete concave cases from 10° to 90° approach angles. The robot uses a magnetic track with alternate facing poles at each track point, its configuration is a triangular track to avoid double contact cases on approach [103]. A downside of this system is that double contact can still be made if the target angle is equal to the track angle. This robot could be adapted to in-pipe work but is only capable of concave cases. The caterpillar robot had magnetised tracks with direct contact of the magnets at the wall, a different approach to creating a magnetic wheel is to create a magnetic chassis with a regular wheel that puts traction through the axle. A novel magnetic wheel of this design was developed which sported a symmetrically centralised unit [104]. The wheel is a standard rubber tire with a large magnetic skirt that envelopes the wheel. This configuration allows magnetic forces to still adhere the wheel even in a pipe like curvature. A magnetic cleaning robot from Zhejiang University also uses this design method to spray down dirt using a water jet in a tank. Its magnetic structure is held within the chassis and not the wheel themselves, this means the robots chassis distance to the pipe must be maintained at the correct point, and that a stronger magnet must be used to produce the same magnetic force relative to magnets that may be used within the wheels instead [105]. In some cases direct wheel contact is not even needed, like the magnetic in-pipe actuated device has been developed at Tohoku Gakuin University for 33mm - 40mm inspections. The robot uses a shape memory alloy shield to wall-press, and then uses magnetic vibration actuators to move through the pipe [106].

Other magnetic traction system locomotion methods that could be adapted in-pipe include Omni-Climber, shown in Figure 2.26. This multi-directional magnetic wheeled robot has built in chassis compliance which allows it to adapt to a wide range of pipe diameters [21]. This could be adapted to in-pipe scenarios allowing a small robot to explore pipes which are respectively large in diameter. In a similar weight class but completely different approach is HyReCRo (Hybrid Redundant Climbing Robot), is

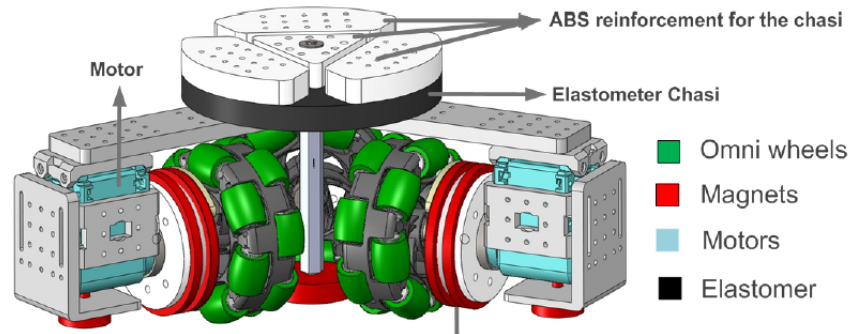


Figure 2.26: OmniClimbers: Omni-directional magnetic wheeled climbing robot [21].

a walking robot developed from climbing three dimensional magnetic structures. It uses switchable permanent magnets which can be turned on and off but do not need constant energy supply like electro-magnets. The robot prototype based on a walking 3RPR style parallel robot has been shown to be able to climb convex cases but not convex [107].

Magnetics have been used to create reconfigurable robots, for instance magnetic modular robots developed at MIT Science and Artificial Intelligence Lab. M-Blocks are magnetic self-assembling cuboid that can reconfigure around each other, these systems use a flywheel to store angular momentum inside the robot and then by rapidly braking the flywheel the angular momentum transferred to the body can be used to move around concave and convex corners. The robots themselves are attached at the corners by permanent magnets, the momentum from the flywheel is strong enough to break the bonds of the permanent magnet when needed [22].

2.4 NTS environment

This section will explore the general environment, conditions, paths, and obstacles, that may be encountered within the National Transmission System. The robots aim to complete the inspection of Above Ground Installations (AGI's), an AGI consists many functional mechanical components and there are a wide range of different obstacles and potential opportunities for robotic inspection. This section will explore known and expected environmental conditions on an unpiggable AGI site.

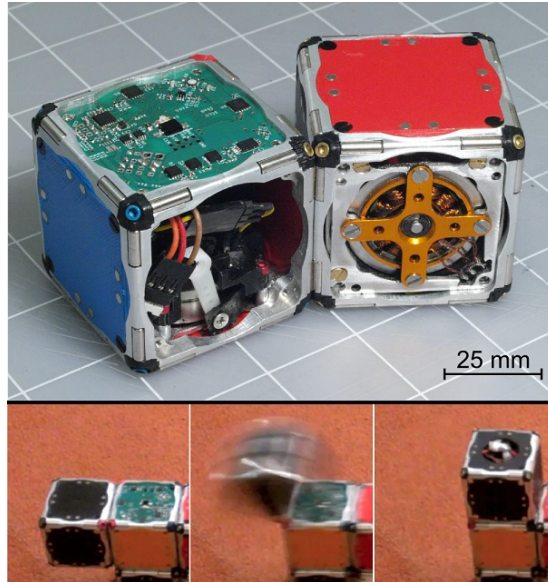


Figure 2.27: M-Blocks, magnetic robots that use angular momentum to break magnetic bonds and solve both concave and convex step cases [22].

2.4.1 Pipeline infrastructure

After the discovery of natural gas along the UK's continental shelf in 1965, the first 18-inch gas feeder lines were built just two years later in 1967 [108]. From this point onwards the network rapidly expanded and most of the network was constructed between 1966 - 1983 [23]. Within this time frame 5150km of the total 7600km of pipeline had been built, the specific growth of the NTS in this time period is shown in Figure 2.28.

As the gas travels from the North Sea the pressure in the pipes drops and the gas must be re-pressurised in a AGI compressor station using gas driven turbines. There are 25 compressor AGIs across the network compressing the gas from 48 bar to 65 bar [109]. The construction material of the NTS pipelines consisted completely of welded low carbon steel most of which was buried within on site of the AGI compressor stations shown in Figure 2.29. Most NTS infrastructure initially had a 40-year design life and the earlier sections are now due for replacement including these now buried pipelines.

Obstacles vary AGI's, there will however be common obstacles present. T-Sections such as those seen in 2.1.F will occur between small diameter pipelines and the larger pipes. Vertical sections will occur when heading below ground and high and low radius bends will be present everywhere. Valves will be present in many different forms and

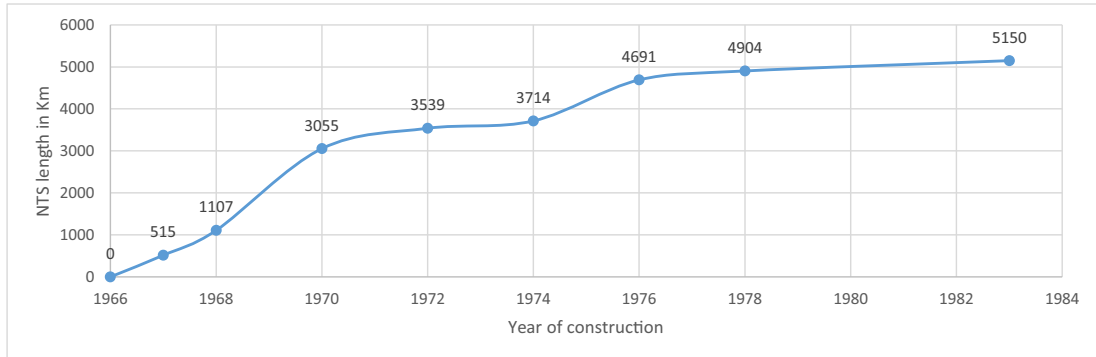


Figure 2.28: The growth of the bulk of National Transmission System between its inception in 1966 and 1983 [23].



Figure 2.29: Construction and installation of an underground pipe network being lay down before burial. [24].

diametric changes will be found at many connection points. All of these features and obstacles can be seen in Figure [24].

Existing access points

Existing access points were first reviewed and it was found that two methods would make access possible, these are the PIG gate, and the 2-inch risers. The PIG gate, seen in Figure 2.30 exists as a barrier between the AGI's main transmission line and the entrance point of the gas to the AGI. The gate forces the PIG to continue down the main transmission path and away from the unpiggable AGI, but it also provides a

possible entrance to the system. The barriers purpose is to stop PIG's crashing into the T-section connection point. Each AGI site has a PIG launch point to launch PIG's from one site down the main transmission lines to another site, the connection to the AGI is also along this line. The grate is necessary because PIG's are inherently simple fluid driven sensors and cannot be controlled, when they pass the T-section they can potentially crash and become stuck. Most of the largest diameter sections (40-inch, 1016mm+) connect directly to the cross-country grid network and anything beyond the PIG grate is inspect-able through pigging.

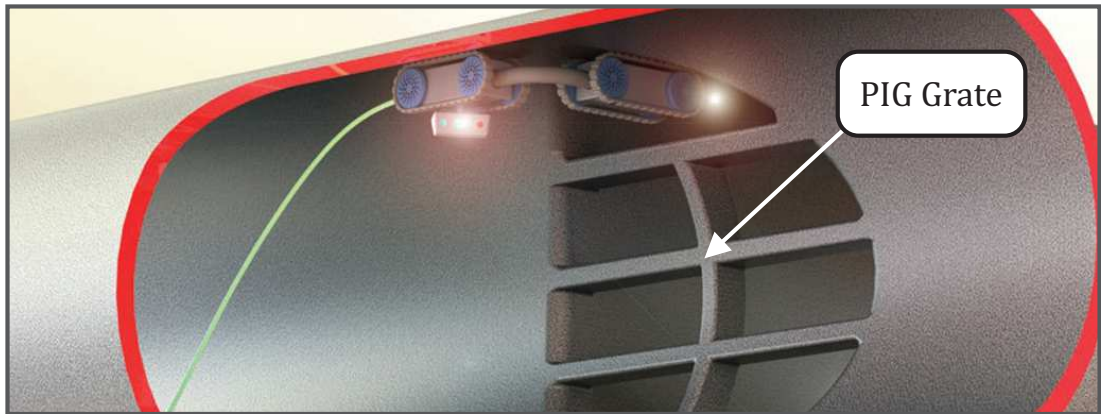


Figure 2.30: PIG grate entrance from a main PIG launch vessel onto an AGI site [24], a type of interior T-Section to from the main.

GRAID is a large magnetic robot specified for mid range diameter of 750mm - 900mm and used a large custom launch vessel to access the network. This is the diameter range chosen to be inspected to cover the most of the AGIs infrastructure with a single robot as this is the most common pipeline range that can cover the most asset volume [24]. These access points still remain unused for robotic inspection.

Launching and retrieving robots

When using a robotic inspection device the first problem faced is the method of entrance to the pipeline. The actual bulk of the pipework within the AGIs is mostly buried under the site and hence inaccessible to humans as seen in Figure 2.29. To enter a robot such as the into the national grid gas transmission system a launch vessel must be used. It is critical no oxygen is present inside the gas pipeline, combined with a spark this could cause an explosive catastrophe. The vessel acts as an airlock of sorts between the

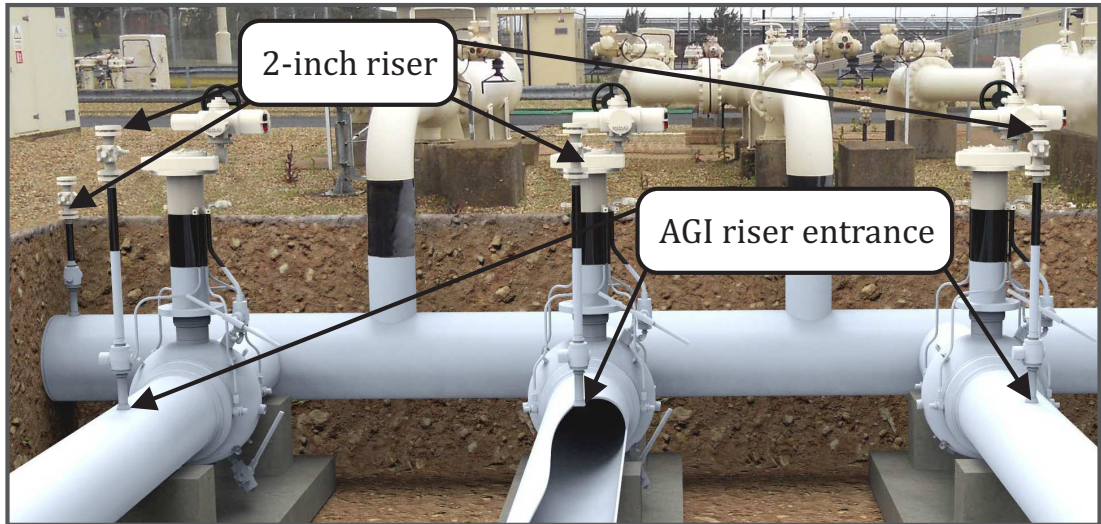


Figure 2.31: Render of underground pipe network on an AGI, 2-inch risers can be seen entering the network from above ground access points [24].

atmosphere and the natural gas pipeline. The robot is sealed inside the launch vessel and is then flooded with nitrogen to remove all trace of oxygen from the system, only then is the pipe flooded with pressurised natural gas and the valve opened. The launch vessel shown in Figure 2.32 can be fitted to the existing above ground network using a hot-tap procedure and can then be driven into the underground network. These procedures are used to fit custom pipework however these procedures can be quite costly and price increases with an increase in robot diameter (and hence launch vessel diameter) [110].

The NTS is a highly valuable system, a robot which is stuck or lost in a live pipe will require a shut-down to retrieve and possibly even an excavation. The robot must be retrievable before being granted access to pipeline assets. This can be achieved with the use of a tether to wind a potentially broken down robot back to the launch vessel so that it can be retrieved. Large modifications must be made to the existing pipe network to fit the launch vessel in Figure 2.32, it would be much simpler to use existing access points. Using existing pipelines the flooding procedure would remain the same however the hot-tap procedure would not be required.

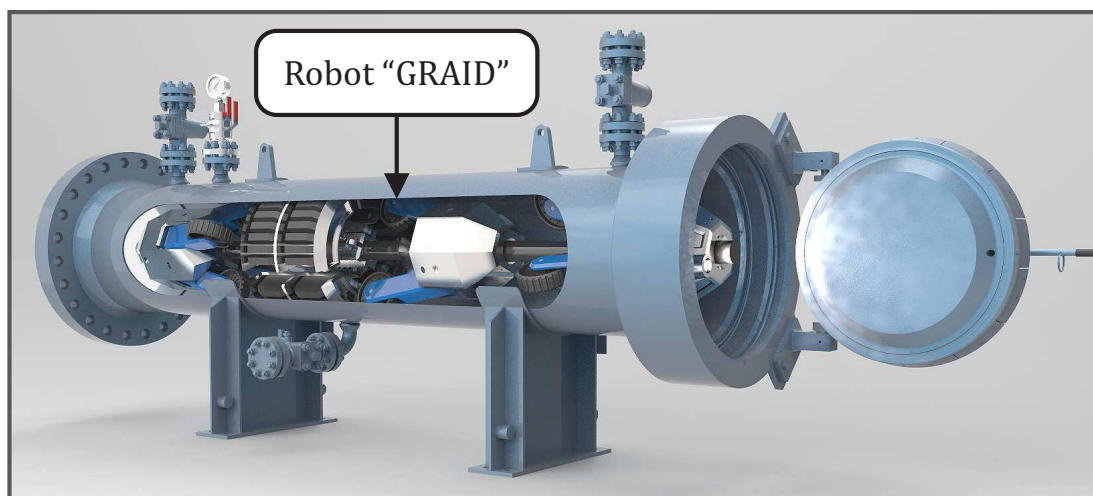


Figure 2.32: Render of the GRAID robot within a concept launch vessel that would be fitted to the AGI due for inspection [24]. The launch vessel floods the robot from ATM (atmospheric pressure) to full pressure with nitrogen to remove oxygen before entry.

2.4.2 Natural gas

When inspecting a natural gas pipeline with any kind of device, procedure states that the pipeline section be shut off and that the natural gas is flooded into the atmosphere. This shut-down is not only costly to the consumer, it is also costly to the environment. This is why Project GRAID aims to Inspect the underground network under live gas conditions, this will be done by venting only a small section of pipeline, entering the robot into this section, and then flooding the section with Nitrogen to purge any oxygen within. By doing this the losses caused through inspection based gas venting can be largely negated. Anything entering the AGI network including robots must also be ATEX rated and pressure tested according to the strict explosion safety regulations [111]. It is vital that no oxygen enters the NTS as when mixed with natural gas and any ignition source an explosion can readily occur.

Flow rate within the NTS across the main pipelines can move at speeds of up to 11 m/s in the main lines and around 5 m/s in an AGI. Pressure in an AGI can be between 48 bar to 65 bar [109], however the pressure in a main line can be anything up to 96 bar. The internal walls can contain contaminants present in-pipe (e.g. grease, oil), the condition of specific pipelines is not currently known.

2.4.3 Environment summary specification

The above ground installations in-pipe and out-pipe environment can be summarised in Table 2.1. This environment specification determined the most appropriate method to inspect the system as well as the locomotion and traction methods.

Table 2.1: National Transmission System (NTS) possible path variables, obstacles, and environmental (Env) conditions. [26]

Path: pipeline entrance points	2-inch risers either side of main valves (50.8mm). 48-inch PIG traps (1219.2mm) through grate.
Path: pipeline diametric range	Range is 2"- 48" or 50.8mm - 1219.2mm, with the most common range being 750mm - 900mm in an AGI.
Path: in-pipe joints present	T-sections, high and low radius bends, angled pipes including verticals.
Path: joint Orientation	Obstacles can be present in all orientations but are usually at right angles with mitred connections.
Path: typical lengths on an AGI	valves, T-sections (1m), straight (10m-40m), vertical (1m-5m), diameter reduction (1m-3m), elbow (1m-6m).
Obstacle: in-pipe features	Weld beads, valves.
Env: pipeline material	Mild Steel (Ferrous)
Env: gas composition	Natural gas.
Env: gas flow speed	0 - 5m/s
Env: gas flow pressure	0 - 94barg
Env: contaminants	Grease, oil, residue, iron scales.

2.5 Literature summary

An in-depth analysis of in-pipe robot publications over the last 30 years is presented in Figure 2.33.C Categorised by locomotion type and year published it gives a high level overview of the trends in the development of in-pipe inspection robots based on 234 published systems. The literature search was performed using the keywords; in-

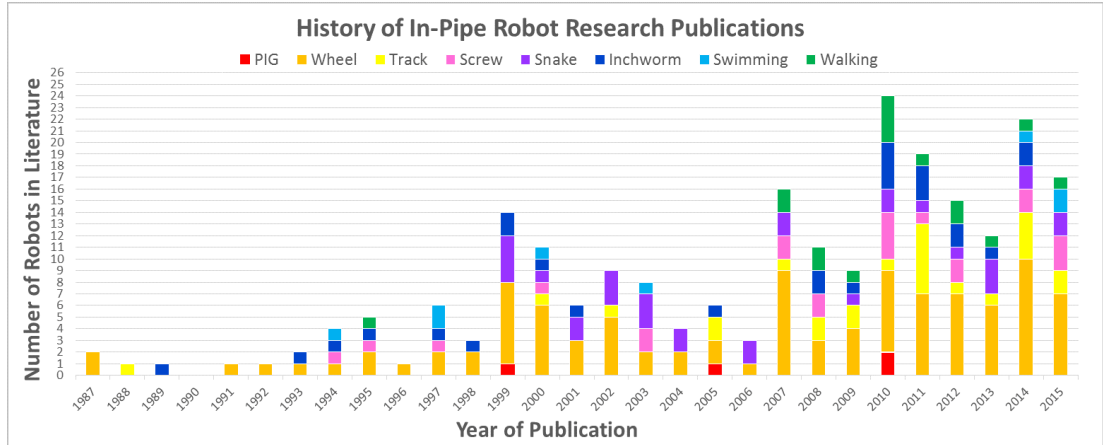


Figure 2.33: History of In-Pipe Robotic Locomotion [25].

pipe, pipe, tube, system, robot, platform, in combination with locomotion and traction methods across multiple publishers. The volume of research robots being produced was found to steadily increase with time as the field has grown, this reflects on the necessity of pipe inspection as more networks become out-dated around the globe.

Chapter 2 explored the literature surrounding the relevant subject areas of in-pipe research, and the many methods currently in use to solve these inspection problems. The key points of in-pipe inspection such as the sizes of these pipelines and networks access points will be broken down into smaller manageable problems and then simplified to find the most elegant solution. By creating a detailed specification based on these simplified problems the proposed robot will contain the tools necessary to complete the aims and objectives set out in this work.

Table 2.3 provides a summary of robots reviewed in this section, where in-pipe geometry obstacles have been simplified to X (horizontal), Y (vertical), L (elbow), T (T-section), V (valves). The capability of the robot to traverse these obstacles is denoted by (✓) when capable, (✗) when incapable, and (-) when a possibility in future versions of the system. Table 2.4 summarises the characteristics of the various environments and conditions that will be considered in this research. The environment conditions within the NTS can vary greatly depending on the section of pipe being inspected. The work of this thesis will focus primarily on the problem of AGI's; unpiggable pipelines with greatest environmental variance. The difficulty or challenge level of a particular section of pipe will be determined entirely by the robot that is attempting to traverse

it.

The gas filled environment can consist of varying speeds and pressure when live, these provide challenges in terms of robot corrosion, power requirements and pressure sealing. In a dry pipe (gas turned off) these challenges can be ignored, however even without gas the in-pipe environment on the NTS proposes a significant challenge to robotic design. The in-pipe environment, conditions, and pathway hazards that can possibly be encountered have been categorised by robotic challenge level in Table 2.2.

For pipe pathway obstacles such as the various bends and joints present, the difficulty of each of these can be inferred from the literature search, and which robots were able to complete them in Table 2.3. In this table all robots could complete the horizontal path (X) making this an easy in terms of robotic design, it is the bare minimum required. Vertical (Y) sections were mostly completed, with only 3 of the studied robots failing. Elbows (L) were completed by all but 1 system, T-sections (T) were completed by only 14 robots, this is unsurprising as it is considered a great challenge and the topic of many in-pipe robotics papers. Valves, especially straight plug valves would be the most difficult obstacle to the reviewed robots, mainly due to many of these robots using full-bore to design the robot making the obstacle unavoidable. Sudden step changes may also be considered threatening obstacles to robot locomotion as many operate under the assumption of smooth diameter transitions. This is specially true of passively adaptive wall-press systems which cannot choose to adapt accordingly. PIG grate meshes are a specialised and rare obstacle, they are extremely challenging as they are specifically designed to stop PIG devices from entering a pipe branch.

Other conditions that provide a challenge for robotic system present in the NTS include grease, oil, residue, and iron and rust flake particles on the pipe walls. These are difficult environment challenges that all affect the traction that can be generated by a robot, hindering its movement, or in the case of fluid-driven systems the ability to slow down. To counter this the robot will need to generate a strong normal force at the pipe wall contact, on the more extreme end of this condition a robot will possibly even need a self-cleaning device to remove the friction reducing residue from the locomotion system. Weld beads are physical steel obstacles formed through joining of pipelines, they are the leftover ridges from various welding forms used in the network manufacture and connection via Continuous Welding (CW), Electric Fusion Welding (EFW), Field Welding (FW), Socket Welding (SW), or Butt Welding (BW) of pipelines.

Table 2.2: In-pipe environment, conditions, and pathways, categorised by robotic challenge level as shown by in-pipe robots reviewed in literature.

Hazard Category	Minor Robotic Challenge	Major Robotic Challenge
Environment	Gas flow < 1m/s	Gas flows > 1m/s
	Pressure < 2 bar	Pressure > 2 bar
	No gas present	Gas present - corrosion
Pathways and Obstacles	Horizontal section	Vertical section
	Elbow	T-section
	Gradual diameter change	Plug valve
	Weld beads	Step diameter change
	Pipe defects, imperfections	PIG grate
Interior Conditions	Oil / grease on walls	Oil / grease pools
	Iron flakes / rust on walls	Large rust corrosion bubbles
	Minor damage (cracked pipe)	Major damage (deformed pipe)

2.6 Literature discussion

Since the development of the first wall-pressing in-pipe robot in 1987 the technique has become the most popular method of generating traction in the field with over 23% of robots applying it in some way in Figure 2.33. The popularity of wall-pressing systems stems from their ability to take advantage of the encompassing walls to generate traction. This feature is guaranteed in pipe networks and allows robots to easily move horizontally and even vertically thanks to the ability to generate friction in any orientation. Issues arise with wall-pressing robots when obstacles such as T-Sections present themselves and there is a possibility for contact loss. Systems were shown to have varying abilities depending on the number of points of contact with the wall varying between two, three or four planes of contact, examples of which are shown in Figure

2.6 Literature discussion

Table 2.3: A summary of the most relevant robotics systems reviewed in this chapter. X (horizontal), Y (vertical), L (elbow), T (T-section), V (valves), - (unknown).

In-Pipe Robot Summary Table										
Robot Name	Ref	Locomotion	Traction	Min	Max	X	Y	L	T	V
Fluid Modules	[101]	Modular	Swimming	125	∞	✓	✓	✓	✓	✓
MagneBike	[8]	Magnetic	Wheel	250	∞	✓	✓	✓	✓	-
MIT-MRL	[100]	Swimming	Swimming	100	∞	✓	✓	✓	✓	✓
Osaka Robot	[7]	Magnetic	Wheel	150	600	✓	✓	✓	✓	-
PAROYS-II	[12]	Caterpillar	Wallpress	400	700	✓	✓	✓	✓	✗
MOGRER	[43]	Wheel	Wallpress	520	800	✓	✓	✓	✗	✗
Pukyong Robot	[79]	Wheel	Wallpress	300	500	✓	✓	✓	-	✗
HELI-PIPE Series	[13]	Screw	Wheel	40	173	✓	✓	✓	✗	✗
KANTARO	[64]	Wheel	Wallpress	200	300	✓	✗	✓	✓	✗
MORITZ	[20]	Walking	Wallpress	600	700	✓	✓	-	-	✗
Tarbiat Robot	[71]	Caterpillar	Wallpress	250	350	✓	✓	✓	-	✗
YonSei Robot	[96]	Inchworm	Inchworm	205	305	✓	✓	✓	-	✗
PIRATE	[17]	Wheel	Wallpress	41	125	✓	✓	✓	-	✗
PIPETRON I - VII	[86]	Snake	Wheel	75	150	✓	✓	✓	✓	✗
EXPLORER II	[87]	Snake	Wallpress	150	200	✓	✓	✓	✓	✓
MRINSPECT VI+	[4]	Wheel	Wallpress	130	180	✓	✓	✓	✓	✗
Shenyang Robot	[54]	Wheel	Wallpress	250	300	✓	✓	✓	-	✗
AQAM	[5]	Wheel	Wallpress	259	305	✓	✓	✓	✓	✗
CMMWorm	[19]	Inchworm	Inchworm	180	220	✓	-	✓	-	✗
FAMPER	[10]	Caterpillar	Wallpress	127	157	✓	✓	✓	✓	✗
FERRET-1	[44]	Wheel	Wallpress	90	120	✓	✓	✓	✗	✗
Two-Plane Robot	[6]	Wheel	Wallpress	80	100	✓	✗	✓	✓	✗
AGH Robot	[69]	Caterpillar	Wallpress	210	210	✓	✗	✓	✗	✗
Kangawa Robot	[16]	Caterpillar	Snake	300	300	✓	✓	✓	✓	-
LOCOSNAKE	[92]	Snake	Snake	120	120	✓	✓	✓	✓	-
SPRING	[14]	Screw	Wallpress	150	150	✓	✓	✓	-	✗

Table 2.4: A summary of the various environments and conditions found within the National Transmission System (NTS) that should be considered in this research.

Environment	Conditions and characteristic features
All natural gas pipeline interiors	Weld beads
	Oil and grease present on wall
	Iron and rust flakes present on wall
	Corrosive natural gas present when live
	Pressures up to 97 bar
Piggable Pipelines (Distribution mains)	Accounts for 95.4% (7250km) of NTS
	Large diameter 18+ inches
	Highest gas flow and pressure
	Grated pipe junctions (prevent PIG's entering)
Unpiggable Pipelines (Above Ground Installations)	Accounts for 4.6% (350km) of NTS
	Varying pipe diameters and junctions
	Varying flow rates
	Pipelines diameters 2 - 18+ inches
	Valves of assorted types (e.g Butterfly, stop)
	Sudden diameter changes (steps)
	Risers either side of valves
	PIG trap collection and entrance
	Many pipe junctions (Elbows, T-Sections)
	Oil and grease collections at junctions
	Turbulent gas flows

2.2.

The field of in-pipe robotics research is heavily invested in the use of these classic wall-pressing systems, many of which have low diameter adaptability ranges. These systems are stable and efficient in their specified diameter range but none of the traditional systems reviewed showed the capability adapt to large changes. Systems such as AGH Universities 200mm robot with only a 34mm adaptability range would not be able to cope with even a $\times 1.5$ increase in pipe diameter and would lose the ability to climb angled pipe sections. In some cases, such as Hanyangs flat pipeline inspection robot a change over 20mm would cause it to become completely unstable and unable to perform even basic locomotion tasks. Many of these robots would be deemed unsuitable for inspection of AGI networks. Some of these designs are simply too constrained by size due to their reliance on a chassis that is always concentric with the pipe. While the central mount provides a good base for adaptability mechanism control it does not benefit transformation range. This limitation means that pipe networks with large varying diameters cannot be inspected without an entire fleet of different class wall-press systems. Assuming a medium size wall-press robot with 100mm adaptability range, a network with pipes ranging from 200mm - 1000mm diameters would require eight separate robots to inspect. Entering 8 different size systems into one network may require multiple access points on the pipe into the correct bore diameter and would need to be repeated across the AGI until the inspection is complete. The use of snake wall-pressing robots overcomes the limitations of traditional wall-pressing systems with multiple planar contact. Snake robots with wall-pressing capabilities can utilise articulated limbs to increase their effective diameter well over the range of parallelogram and pantograph mechanisms. For instance Kangawa University's snake system has an adaptability range of 100mm - 300mm [16]. Snake systems hold a great advantage over full-bore designs as they can be entered into smaller pipes as an access point into larger networks. This non full-bore design also allows them to pass through tricky obstacles such as valves which would stop most traditional wall-press systems in their tracks.

Lateral rotation around the inside of the pipe walls without the need to rotate the body relative to the pipe axis provides a large advantage to long robots in a relatively small diameter pipe. Omnidirectional wheels such as those in MIT's OmniTracks [68], are ideal for cases such as these. Tracked systems are very popular for industrial cleaning purposes, this makes sense as they have the highest gravity based traction,

which is all that is needed for sewage pipelines where verticals are not really used for transportation. Caterpillar tracks can be bulky and heavy but in most applications they are chosen for this bulk and extra weight gives the robot an advantage in gaining traction in an very low friction sewage or contaminant filled pipe. Snake robots can be very articulate if a low diameter than the intended pipe bore and in this case can overcome difficult obstacles such as plug valves which sit central in the pipe that would be impossible for a full bore system [112]. However trends for in-pipe snake robots point tend to use full bore systems in well established diameter pipelines where diametric very rare. Snake robots that can use both wall-press to complete vertical sections and also avoid sub-full bore obstacles are very rare. Non-traditional methods of in-pipe traction generation such as vacuum powered wall-climbing and van der waals forces are not really applicable to in-pipe robotics work as they generally require ideal conditions which are not present in-pipe. For instance vacuum robots would need to conform to many different diameters [113], and van der waals force requires perfect contact and zero contaminants [114].

2.7 Literature conclusion

This review has presented an in-depth analysis of literature surrounding the project, a historical overview of the field, as well as displaying the current trends of in-pipe technology, with a specific emphasis on the locomotion methods used. In-pipe robots are incredibly diverse and many different hybrid systems have been developed, some of which have fulfilled specific niches of pipe inspection. However, the inspection of highly varying diameter networks is an area that has not been fully explored. Tackling this problem would require a method of locomotion that is not constrained by pipe size. This is a complex issue and one that cannot be solved using full bore wall-pressing robots due to the limitations inherent in their diametric adaptability mechanisms. Snake style locomotion methods have been shown capable of spanning pipe bores with complex articulated systems, however neither wall-press or snake systems are close to exploring the entire specified 50.8mm - 1016mm range within the NTS. The only systems capable of this are wall-climbing robots that do not rely on pressing contact with the pipe at all times. A gap in the research has been revealed for a small (<2 inch) in-pipe robotic system that can scale inner pipe walls. There is currently no in-pipe wall climbing robot at this scale, and by filling this gap in the knowledge there is the potential to

inspect the entire pipe range within an AGI.

As the pipes on the NTS are predominantly ferrous steel an ideal traction method would be magnetic adhesion, other wall-climbing methods will not be viable in-pipe. The grand challenge for magnetic robots is to overcome complex 3D geometry in every orientation, these problems are often represented as concave and convex steps the robots must tackle. Many magnetic robots appear capable of vertical sections, and commonly concave steps, but completion of convex steps appear rare for in-pipe robots. The most capable and applicable in-pipe magnetic robots that have been reviewed and are capable of both convex and concave step cases are generally large (<200mm) due to a high number of actuators required to overcome these problems. Completing both step cases with a small magnetic robotic system would require a minimal number of actuators. Solving this problem would allow access to larger underground pipe networks through smaller existing pipeline connections.

CHAPTER 3

Robot Requirements Analysis

This Chapter develops a detailed specification for the robotic system that is to be deployed within the ferrous natural gas pipeline. The aim of this chapter is to create the specific requirements needed to generate a robotic solution from the data gathered about the in-pipe environment.

3.1 Introduction

Chapter 2 explored the various traction and locomotion techniques for use in the field of in-pipe robotics. This chapter will cover requirements of the robot and the subsequent specification. The environment of the National Grid Network will be defined and aspects such as pipe diameter ranges and the likely size of entrance points on the system will be explored. The completed specification and requirements analysis will ultimately decide on key factors such as the robots traction and locomotion methods. In order to be operational in the environment defined in Chapter 2 the robot will need to meet the requirements in Table 3.1.

3.2 Locomotion and traction method requirements

Using a decision matrix the traction and locomotion methods will be scored against the criteria found by reviewing the target inspection composition, environment, and obstacles present in Table 2.1. The decision matrix will give each possible solution for a criteria a score in terms of suitability. Each solution will be scored either: 1 (low), 3 (medium), or 5 (high) in Tables 3.3, and 3.5. The scoring system is based on the literature read and reviewed in Chapter 2. The scores reflect the requirements that need to be fulfilled in order to use that traction or locomotion method. For example in the case of a PIG based on the literature research these are generally fast and efficient devices for inspecting long straight pipelines, and so will score highly on speed and range. However these devices are also generally uncontrollable and difficult to manoeuvre, and hence will be scored low areas such as path navigation of elbows and T-sections.

By generalising the locomotion and traction methods capabilities based on the tasks they can complete and the specific cases they are used in within publications, the strongest methods for use in the national transmission system should become apparent. The table scoring system cannot account for every individual robot reviewed as there

3.2 Locomotion and traction method requirements

Table 3.1: Requirements for an ideal robotic locomotion system within the National Transmission System AGI environment.

Requirement	Description
Robot can enter through existing features	Robot should fit within a common existing connection on an AGI (e.g 2-inch or 4-inch riser)
Robot can move through all pipe junctions	Robot needs to be able to overcome all path in-pipe obstacles it faces.
Robot can move vertically	There are vertical sections present in the pipe - the robot will need to be able to scale them.
Robot can be controlled remotely	Robot will need to be driven on-site by an operator to complete the inspection.
Robot can handle all in-pipe diameters	Robot should be able to inspect the entire range of pipe diameters on site from 2 - 48 inch.

3.2 Locomotion and traction method requirements

are unique cases for each style of locomotion and traction that may go against the general use. Using the completed decision matrix each of the traction and locomotion methods will be queried on each criteria, the score will be applied and then summed to give the most suitable option which will be taken into account when selecting the in-pipe robots traction and locomotion methods.

3.2.1 Traction requirement criteria and selection

When considering the traction requirements of the robot in Table 3.2 the selection criteria are based on paths, obstacles, or environment conditions that may adversely affect traction designs. These criteria include gas flow reliance, (does the traction method need fluid flow force to move, e.g. a PIG). Wall condition reliance, (does the traction need high friction co-efficient at the walls). Pipe orientation reliance, (does the traction method require ideal horizontal pipelines, is it possible to complete vertical sections). Diameter reliance, (can the traction method be used in constantly changing pipeline diameters). Weight reliance, (does the robot require extremely light or heavy design weight to generate traction). Design space refers to the cross-section of the pipe that needs to be used for the particular traction method e.g a fluid flow needs to cover most of the cross-section to generate the fluid pressure behind it, and hence requires a large design space.

Table 3.3 considers the four previously defined traction methods; gravity, wall-press, adhesion, and fluid-flow. Now that the environment conditions have been defined adhesion will be refined to "magnetic adhesion", this is most reasonable method of adhesion in a ferrous environment. The four traction methods will be scored against the criteria in Table 3.2 and the totals will be calculated to indicate the correct solution.

From the applied scores and total points for each traction method in Table 3.3 we can deduce that the most advantageous traction method is magnetic adhesion. Fluid-flow scored the lowest which is to be expected as flow is unreliable and requires a full-bore design unless it is liquid. Gravity traction only works in constant horizontal pipelines with just shallow (<30%) inclines. Wall-press scored second highest, this is unsurprising given that it is the most popular in-pipe traction method in industry and research, it is more reliable than gas flow and can overcome verticals unlike gravity based traction. Magnetic adhesion is the highest scoring and should be used over the other methods. This method has all the advantages of wall-press but without the need

Table 3.2: In-pipe robot, traction selection criteria to be analysed against possible traction methods.

Traction Selection Criteria	Score		
	1 - Low	3 - Medium	5 - High
Gas flow reliance	Requires high gas flow speed	Some gas flow required	No requirements for flow
Wall condition reliance	Requires clean wall conditions (no sludge)	Requires relatively clean surface	Requires no ideal conditions
Pipe orientation reliance	Requires horizontal pipelines	Requires no more than shallow gradients	No requirements, can do all orientations
Diameter reliance	Requires constant diameter	Requires small amounts of diametric change	Can complete a large range of diameters
Weight reliance	Requires specific robot weight and balance (heavy or light)	Requires some weight consideration	Does not require a high or low weight
Design space	Requires a lot of design pace and work	Requires some extra design space	Requires little design space

3.2 Locomotion and traction method requirements

Table 3.3: In-pipe robot traction selection matrix based on the criteria defined in Table 3.2.

Traction Selection Criteria	Traction Method Score			
	Gravity	Wall-Press	Magnetic Adhesion	Fluid-Flow
Gas flow reliance	5	5	5	1
Wall condition reliance	3	5	1	5
Pipe orientation reliance	1	5	5	5
Diameter reliance	5	3	5	1
Weight reliance	1	3	3	5
Design space	5	1	5	1
TOTAL	20	22	24	18

for full-bore designs or adaptability, small adhesion traction robots in large pipes can also make obstacles such as T-sections trivial compared to a wall-press in the same pipeline. Some methods of adhesion are tricky to apply as the material of the pipeline makes a large difference. In the case of the NTS all of the pipework is steel and so magnetic adhesion will work reliably, and hence can be chosen over wall-press. The conclusion from an analysis of the traction requirements is that magnetic adhesion will be used as the traction method in the specification for the robot.

3.2.2 Locomotion requirement criteria and selection

The locomotion selection criteria in Table 3.4 look at all possible environment pipeline paths (Path) and unexpected obstacles (Obs) that could be encountered. In this table a high score is given to the path or obstacle and it is then categorised into a low, medium, or high category. Attributes which give the locomotion method an advantage are given a high score, and locomotion methods at a disadvantage for the path or obstacle are given a low score. When the scores are applied in Table 3.5 the highest total will determine the most generally suitable locomotion method in the overall environment. Attributes (Att) generally associated with specific locomotion methods as well as environment (Env) conditions are also considered in Table 3.4.

From the applied scores in the locomotion selection matrix in Table 3.5 we can

3.2 Locomotion and traction method requirements

Table 3.4: In-pipe robot locomotion selection criteria and definitions of relative low (0), medium (3), and high (5) scores. Criteria are categorised by pipe path (Path), obstacles (Obs), general robot attributes (Att), and environment conditions (Env).

Locomotion Selection Criteria	Score		
	1 - Low	3 - Medium	5 - High
Path: 2-inch pipe	Unlikely to fit 2-inch	Could possibly fit 2-inch	Likely to fit 2-inch
Path: T-section	Unlikely to complete obstacle	Could possibly complete obstacle	Likely to complete obstacle
Obs: valve	Unlikely to complete obstacle	Could possibly complete obstacle	Likely to complete obstacle
Path: elbow	Only high radius bend	Medium radius bend	Low radius bend
Path: diametric change	Unlikely to complete obstacle	Could possibly complete obstacle	Likely to complete obstacle
Path: vertical	Unlikely to complete obstacle	Could possibly complete obstacle	Likely to complete obstacle
Path: horizontal	Unlikely to complete obstacle	Could possibly complete obstacle	Likely to complete obstacle
Att: control	Complex to control	Intermediate to control	Simple to control
Att: power consumption	High power consumption	Medium power consumption	Low power consumption
Att: speed	Fast in-pipe travel speed	Medium in-pipe travel speed	High in-pipe travel speed
Att: range	Generally low range	Generally medium range	Generally long range
Att: design volume	Requires a large workspace	Requires a medium workspace	Requires a small workspace
Env: pressure	Complex to make resistant	Intermediate to make resistant	Simple to make resistant
Env: gas flow	Massively hindered by gas flow	Somewhat hindered by gas flow	Barely hindered by gas flow
Env: wall condition	Requires clean pipe walls	Requires relatively clean pipe	Requires no ideal conditions

Table 3.5: In-pipe robot locomotion selection matrix based on the criteria defined in Table 3.4. Criteria are categorised by pipe path (Path), obstacles (Obs), general robot attributes (Att), and environment conditions (Env).

Locomotion Selection Criteria	Locomotion Method Score							
	P.I.G.	Wheel	Caterpillar	Screw	Snake	Inchworm	Propeller	Walking
Path: 2-inch pipe	5	5	3	5	5	5	1	1
Path: T-section	1	3	3	3	3	3	3	3
Obs: valve	1	3	3	3	3	3	1	1
Path: elbow	1	5	3	3	5	3	3	3
Path: diametric change	1	5	5	5	5	5	5	5
Path: vertical	3	5	5	5	5	5	5	5
Path: horizontal	5	5	5	5	5	5	5	5
Att: control	5	5	5	5	1	3	1	1
Att: power consumption	5	3	3	3	1	3	3	1
Att: speed	5	3	3	3	3	1	3	1
Att: range in-pipe	5	5	5	3	3	1	1	1
Att: design volume	3	3	3	3	5	3	3	5
Env: pressure	5	3	3	3	5	3	1	3
Env: gas flow	5	3	3	3	3	5	1	5
Env: wall condition	5	1	1	1	1	1	5	3
TOTAL	55	57	53	53	53	49	41	43

see the predictions for the best performing in-pipe locomotion method. PIG scores very highly in the matrix however this method is unusable in unpiggable pipelines, it's high score is a testament to how effective this method is in the larger bore, straight pipelines. Wheeled is the highest scoring method as it completes the widest range of obstacles with the greatest efficiency. Caterpillar tracks are generally high traction compared to wheels and avoid slip, they scored on par with both screw and snake locomotion. Screw is generally useful for slow high traction movement and is coupled well with wall-press or fluid flow traction, it would not pose much of an advantage with an adhesive traction method. Snake in-pipe robots are often wall-press, but they can use wall-press whilst avoiding mid-pipe obstacles. This method scores highly as the snake robots can adapt to obstacles such as plug valves. Inchworms score low because versus the other methods due to the slow speed, generally this would be a slow wall-press system, it does not hold much of an advantage when coupled with an adhesive traction method. Propeller locomotion scores the lowest because of its reliance on the pipe fluid contents, in a water fluid pipeline this method may be feasible however in a gas line prop locomotion would have to be based on flight of a drone style system. The drone would have to constantly fly in to the flow to avoid being blown away, this would not be efficient or feasible. Walking robots are slow systems that provide little benefit versus other methods, within the literature the biggest advantage of a walking robot is the relatively high payloads they can carry. The high payload systems are generally wall-press [18], and would not be suited to adhesion methods.

3.3 Robot Specification

The list of robot requirements can be narrowed further to identify the the essential problems. Abstraction of the requirements moves the focus of the problem from many particular and small issues to the general and essential in order to lead directly to the crux of the problem [115]. Defining the key problems ensures that the core functions required of robotic concepts will become clear. By using the tables generated from both the environmental specifications in Table 2.1, and the locomotion and traction method Tables 3.4, 3.2 the robot requirements can now be refined.

To properly refine the specification the crux of the design will be the reduction of size, and power consumption of the robot. This will take precedent over the technical function (obstacle navigation and locomotion), and other focuses such as manufactur-

3.3 Robot Specification

ing, cost, and safety (retrievable design). This is the correct focus as the aim is to enter the small pipelines to enter the larger bores, this will emphasises simple designs with minimal actuators. The robot will enter 2-inch (50.8mm) pipe risers to access large pipelines (50.8mm - 1016mm). The robot could also enter by using the PIG launcher as an entrance to the network, the robot can then enter through the PIG grate and into the AGI.

Table 3.6: Complete in-pipe robot specification based on the NTS environment analysis and locomotion and traction methods explored in this chapter.

Robot Consideration	Specification
Geometry	Cross-section <101.6mm
Locomotion Method	Wheeled (from Table 3.5)
Traction Method	Magnetic Adhesion (from Table 3.3)
Navigation and Planning	IMU on-board for robot orientation
Control	Simple control scheme (standard joystick). Method of steering.
Range	>5m (cover distance between riser entrance points)
Speed	>1 robot length a second
Operation Time	>20 minutes for short operation
Communications	Low power Bluetooth or Wi-Fi. Untethered due to capstan effect of tethers around pipe corners [116].
Electronics and Power	<100mAh average current draw to conserve battery life. Rechargeable
Endurance	Constructed of strong plastic, ABS. Resistant to falls and crashes
Environment Resistance	Gas flow and pressure resistance to be developed at higher TRL
Inspection	On board camera, with headlights for visual inspection

3.4 Discussion and conclusion

Detailed environmental information is very important when planning a robotic inspection tool. The information around current AGIs is limited as the nature of the problem requires assessment of the in-pipe environment and condition as it is currently unknown. The current knowledge has been gathered from visits to AGIs, visual inspection on NGGT sites, and reports from project GRAID which involved a portion of site mapping [24]. The information is presented in section 2.4 and is then summarised in Table 2.1. From this research, small 2-Inch access points seem to be the most efficient access point due to their common presence on the network and the fact that they can be accessed above ground. There is the possibility of using a larger robot such as GRAID and hot-tapping a custom connection point but a hot tap procedure will incur a high cost which increases with diameter of connection.

Section 3.2 explores the use different locomotion and traction methods for robotic movement in the pipe environment. The traction method selected was magnetic adhesion, and the locomotion method was wheeled. The justification for this is that wheeled magnetic robot will be able to explore ferrous pipelines limited only by the smallest rated diameter pipes it can explore. The robot may not be as effective as a large robot in terms of speed, it could be possible to use the systems in a swarm style to inspect the large pipes with many small robots at once. A drawback of focusing the design on magnetic adhesion is that it will only be applicable in ferrous pipelines. Lower tier pipelines such as household level gas mains (tier 1) are currently being replaced with PVC. These new non-ferrous replaced pipelines will not be inspect-able with a magnetic robot in the future.

When deciding on the using wireless or tethered communication the pros and cons of each were assessed against the chosen robot specification. Advantages of using a tether include; the reliability of the communication, removal of a large portion of electronic control, and indefinite battery life. An issue with tether-less systems is the lack of a reliable method of retrieval assuming system failure, the robot will likely have a relatively small battery life so range may become a problem. A disadvantage is that the tether will be connected to a computer and battery at the launch end and a custom vessel would be needed to do this as a tether cannot be breaching the AGI into open atmosphere to reach the operator. As well as this, the weight of the tether will likely reduce the small robots range as it has to drag an increasing mass, and any corners

3.4 Discussion and conclusion

in-pipe will incur, which is why even large tethered systems such as GRAID are only specified to negotiate two 90° bends [116], [26]. The defined robot specification can now be taken forward into the next stages of development in 4 where the design of the magnetic adhesion traction system and the wheeled locomotion system will be explored.

CHAPTER 4

Design of Magnetic Traction Wheels

In this chapter an overview will be given surrounding the magnetic traction to be used in the wheels, the methods utilised, and the optimisation of magnetic forces in order to produce a combined magnetic traction and locomotion method. The developed magnetic wheel will be tested and analysed to determine the most efficient configuration to maximise magnetic force.

4.1 Introduction

Magnetic traction is one of only a few traction methods capable of allowing a robot to travel normal to surfaces in any orientation in reference to gravity. Others may include glue [117], Van der Waals force [114], or vacuum suction [118]. Like these other methods, in order for locomotion with these methods to work, contact with the surface must be maintained. The major advantage of magnetic traction over these other adhesion methods in a ferrous pipeline is the reliability and simplicity as determined in Chapter 2. Magnets can be introduced into many locomotion methods such as caterpillar, screw, mecanum wheels, and legged devices. The locomotion method defined by the requirements for the robot is a wheeled system. In this chapter the wheeled locomotion will be combined with the traction method form a magnetic wheel design.

4.1.1 Simplifying in-pipe geometry problems

To understand the requirements needed of the magnetic wheel, the defined in-pipe obstacles problems are reviewed with this traction method in mind. Many of the in-pipe problems can be simplified as wall-press, and hence full bore robots are no longer needed to generate movement. Plans to tackle obstacles such as T-Sections have been shown to require advanced motion planning for robots when using traction methods such as wall-press [1]. When tackled using small magnetic traction robots these problems can be simplified to just two extreme cases; concave and convex. The simplification of standard in-pipe geometry to these convex and concave step cases is presented in Figure 4.1. By completing these two problems without detaching the magnetic wheel base the majority of in-pipe obstacles can be overcome.

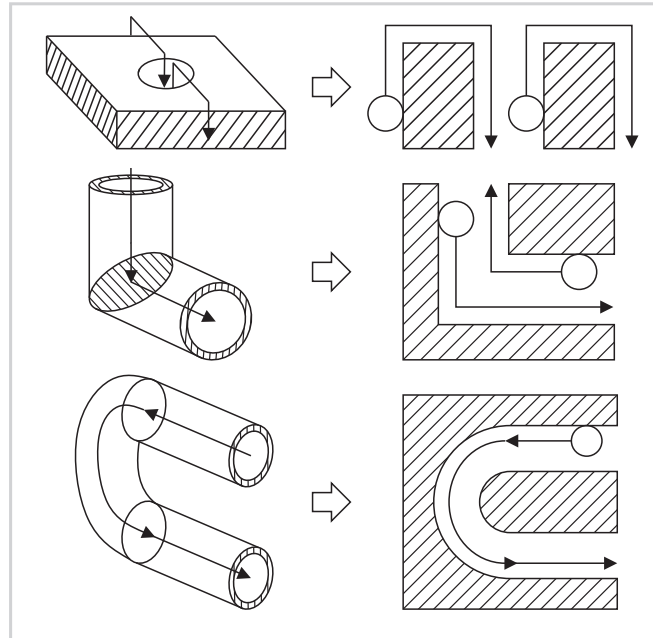


Figure 4.1: Simplification of in-pipe obstacles, reducing the problem to two dimensional step-cases.

4.2 Methods of designing a magnetic traction robot

When designing a magnetic robot there are a number of different approaches to consider, these include the method of generating traction, e.g. should the wheel be magnetic or the robot body? How many magnetic contact points should be used? Will the robot be stable? What type of locomotion should be used? In this section standard methods of magnetic wheel design as well as chassis stabilisation methods will be explored.

4.2.1 Magnetic wheel design

There are four different types of standard magnet wheel configuration as seen in the literature. As shown in Figure 4.2, these are the standard ring magnet (A), outer magnet placement wheel (B), shielded magnet array (C), and magnetised chassis (D). Of all of these methods, method A is the least common in the reviewed literature, designs B - D have multiple examples of use with slightly different methods however the principle is the same. Method B has been used to create wheels with magnets placed on the outer tread rather than the dual flux plate design to inspect vessels [119]. The

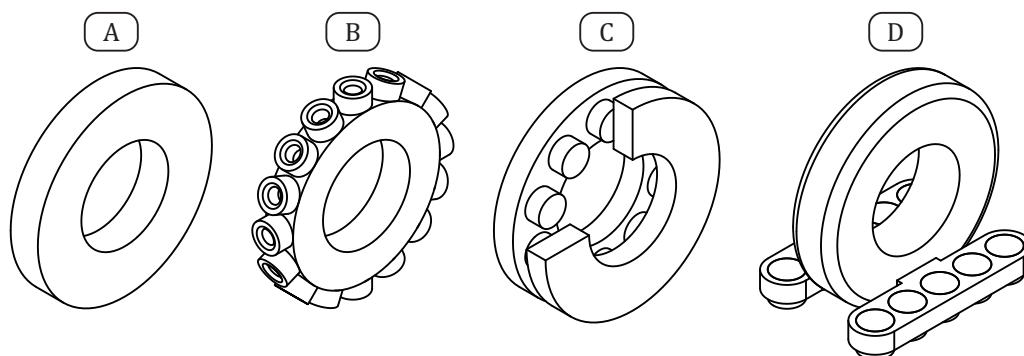


Figure 4.2: Types of magnetic wheel design; standard ring magnet (A), outer magnet placement wheel (B), shielded magnet array (C), and magnetised chassis (D).

dual plate design (C) with an interior ring magnet has been used to create a robot that climbs walls and ceilings [120]. Multiples of this style of magnet wheel have been placed in parallel to make a large wheel unit for adhesion with only thin ferrous wall thickness [121]. This design has even been used with removable shielding pins to create novel wheels that allow easier detachment of high magnetic forces. [122]. This configuration is extremely similar to a common pot magnet, which are commonly created and sold to increase the strength of magnet without increasing the size and cost of the magnet itself. The non-magnetised wheel design (D) uses magnets in the surrounding (and non-rotating) chassis to generate traction at the wheel by applying pressure through the chassis attachment point to the wheel. This method has previously been used with rubber wheels with external magnetic platform surrounding it [104] and also for a water-jet cleaning robot [105].

An advantage of using magnetic traction is that wall-press methods do not need to be used. This means that a magnetic robot does not need to be the size of the full pipe bore and can actually be many times smaller than the pipes diameter and still be able to freely move in any orientation. Being many times smaller than the pipeline gives the robot a great advantage in that in-pipe geometry problems such as those in Figure 2.1 can be simplified greatly, an example of how different problems can be simplified is given in Figure 4.1.

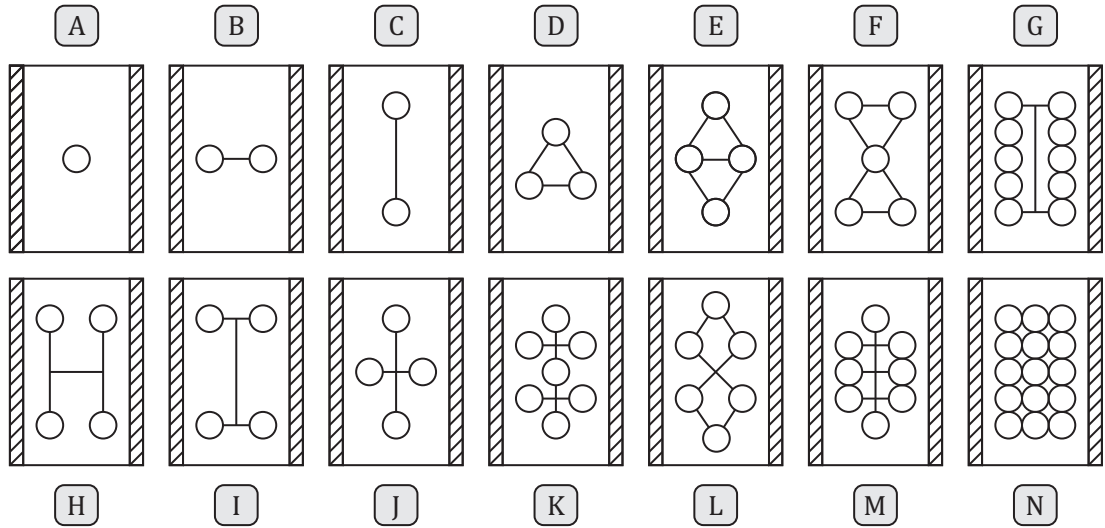


Figure 4.3: Different possible magnetic skeleton chassis frames for in-pipe magnetic robots.

4.2.2 Chassis traction design

Figure 4.1 also show the robots climbing around step cases in different orientations both against and with gravity and even upside down. The robot will have to remain stable in all of these configurations to safely complete an inspection without becoming immobile. In order to complete the step cases in any orientation, the robot magnetic attachment points should be considered, more magnetic points will make the robot stable but also harder to move and less manoeuvrable. Some possible magnetic chassis skeletons for in-pipe robots are presented in Figure 4.3. These attachment points are not necessarily actuated wheels, as some will just provide extra stability in the case of the robot being held in orientations against its own weight in any reference plane. Non-actuated contact points can be free rolling bearing wheels, or even ball bearings.

The simplest skeleton is presented in Figure 4.3.A, with just one point of contact the robot would be unstable in all directions. Magnetic frame B and C are stable when vertically travelling up a wall however when driving on a 90° wall horizontally will fall as they are free to rotate around the tow points of contact axis. D with three points of contact is the minimum to become stable in-pipe. Common four-wheeled vehicles tend to use the magnetic wheels as the traction frame and hence would use H and I style. Caterpillar systems with multiple points of magnetic contact would use styles M or G.

4.3 Magnetic wheel requirements and specification

As more magnetic attachment points are added to the base frame manual detachment of the robot from an inspection point may become a concern. Typically a launch pad must be used to transfer a large magnetic robot from one point to another [26]. Detachment is not a concern for a robot at this specified size of sub 100mm, the robot can simply drive onto a carrier plate in the launcher.

4.3 Magnetic wheel requirements and specification

Based on previous in-pipe and out-pipe magnetic research and robotic examples the requirements for the robot have been defined. Important factors for magnetic wheels on a small in-pipe robot are presented in Table 4.1 as desired features with accompanying descriptions and associated design requirements.

4.4 Design and assembly of the magnetic wheel

To fit the requirements, the overall design of the wheel will follow the shielded magnet array design outlined in Figure 4.2.C. Permanent rare-earth neodymium magnets are currently the strongest permanent magnets in terms of magnetic field intensity (Gauss) available [124]. Neodymium magnets are ranked in strength by their maximum energy product from grade N35 to N52 where the number after "N" represents the strength with the highest value relating to the strongest magnet. The grade used in the wheel design is N42 which is the most widely available, N52 magnets are stronger but not widely available in many sizes.

To direct the strength of all magnets into the wheel contact area they will be held between two steel plates that redirect the flux to the wheels contact point. The array configuration will also protect the magnets as they are susceptible to corrosion, and their increasing brittleness with increasing strength grade.

The shape is circular, this is the most common magnet shape and allows for dense packing of magnets in the array. The wheel flux plate radius is 16mm for a total of 32mm diameter and the inner mountable area radius is 7.5mm. This restriction comes from the workspace available in a 50.8mm pipeline and leaves 8.5mm of space for each magnet. The diameter of the magnets is 6mm allowing 1mm clearance from the outer wheel contact area to the spacer, and allowing 1.5mm for the spacer. The rated pulls of the 2mm, 4mm, and 6mm length magnets used in the wheel have respective pull

4.4 Design and assembly of the magnetic wheel

Table 4.1: Requirements for the robots magnetic wheel design.

Desired feature	Description	Design requiriment
Protected from impact	Rare earth magnets are brittle and prone to shatter on direct contact.	Magnets should not come in direct contact with steel pipe
Uniform contact force at all points	Force should be the same at all points for completing concave and convex cases no matter the wheel angle.	Magnetic force should be stable throughout rotation
Mountable axis geometry	Wheel needs to be mounted easily onto a shaft.	Non-circular shaft mount geometry.
Thin profile	Wheel should be as compact as possbile to fit in the pipeline.	No unnecessary extremities.
High wheel magnetic force density	Wheels force should be greater the robot total weight in a compact space.	High-force density magnets. Such as rare-earth magnets.
Shielded from corrosion	Rare earth magnets are brittle and prone to shatter on direct contact [123]	Protective casing or coating.
High friction	Magnets need a high friction co-efficient to to generate traction of smooth steel surfaces.	Rubber material coating.
Balanced magnetic force and wheel torque	Magnetic force of the wheel must be balanced with the motor torque so not to stall in the worst case (double contact).	Rubber coating must reduce wheel magnetic force to overcome right angle double contact.

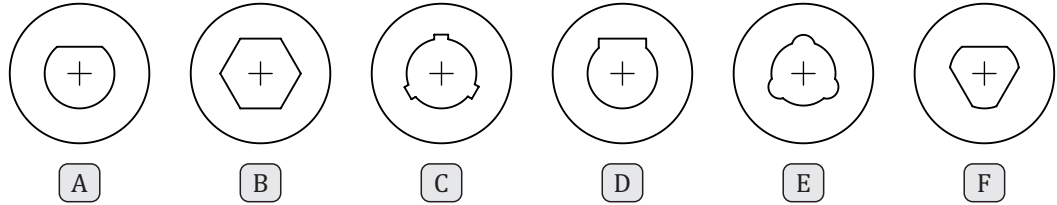


Figure 4.4: Different design for the mountable wheel hub built into the magnetic flux plates. A: D-Shaft. B: Hex. C: Multiple D-Shaft. D: Key. E: Nucleus. F: Triangular.

strengths of 0.73kg, 1.1kg, and 1.4kg, as stated by the manufacturer [125]. The height of the magnets is variable to allow for modifying the wheel strength. The hub design for mounting the magnets is the triangular method shown in Figure 4.4.F, the advantage of this design is the subtle transition from circular to triangular, maximising space for magnets on the array.

The number in an array is variable, the maximum number of 6mm diameter magnets that could possibly fit in the 32mm wheel is 12 but for the purpose of allowing structural support in the magnet spacer and stop magnet movement during wheel use the number of magnets in the array will be set to 6. An example of a two magnet wheels using 5mm flux plates is shown in Figure 4.5, one with an array of 6 magnets, and the other with an array of 3.

4.5 Magnetic wheel experimentation

All magnetic wheel experimentation has been completed with the Mecmesin tensile testing machine with a 1000N load cell of model: "MultiTest 5-i - Intelligent Loadcell ILC-S" [126]. The load cell has an accuracy of 0.1% full scale (1N). The diagram in Figure 4.6 shows the complete set-up used. The data for each type of experiment was logged directly from the load cell to the computer and then analysed in MATLAB. For each experiment the input program written to perform it is presented in a table within each subsection.

4.5.1 Normal force

The normal force is the reactive force caused by the attraction of the magnet to the steel, this force is highest when the wheel is in direct contact with the steel. To test

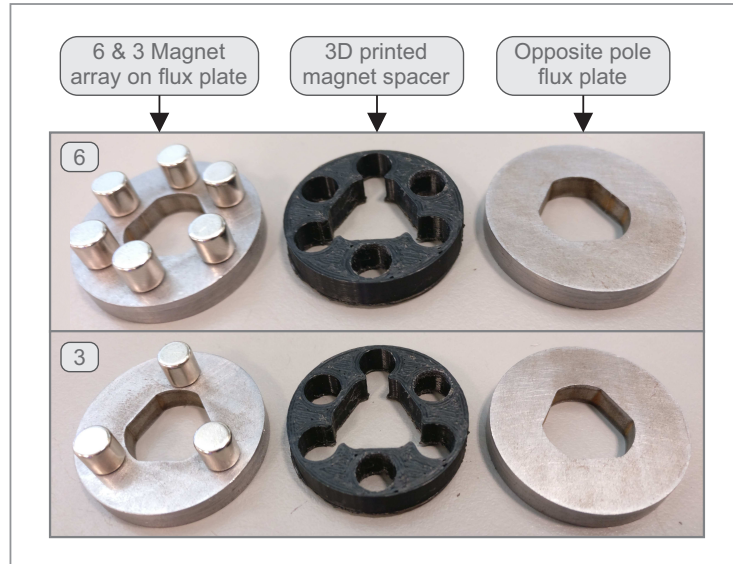


Figure 4.5: Components of the magnetic wheels ready to be assembled for a 5mm flux plate, 6mm length x 6mm diameter x 6 magnet array.

the peak normal force at this point the wheel is loaded into the custom rig and locked in position on the wheels drive shaft. The drive-shaft consist of a 3D printed profile that matches the triangle profile of the wheel in Figure 4.4.F. The shaft houses two bearings which sit on a 5mm stainless steel non-ferrous rod. The rotation of the wheel is locked in place with a grub screw inside a shaft collar which is embedded in one side of the shaft. For tests where rotation is necessary the grub screw can be loosened allowing free rotation on the bearings about the central steel shaft. The test program parameters for the normal force wheel experiments are presented in Table 4.2

Flat plate

The pull force of the wheel peaks around 82N in Figure 4.7, just before contact is made, as the wheel is pulled back it loses half of its force in around 0.06mm. When compared to a regular N42 disc magnet which is unshielded by flux plates and open to the air the pull force is halved around 0.7mm.

Figure 4.8 shows an increase in peak force for magnetic wheel arrays when the flux plate thickness is increased. An increase in plate thickness increases the maximum amount of magnetic flux that can be channelled from the array to the contact point.

4.5 Magnetic wheel experimentation

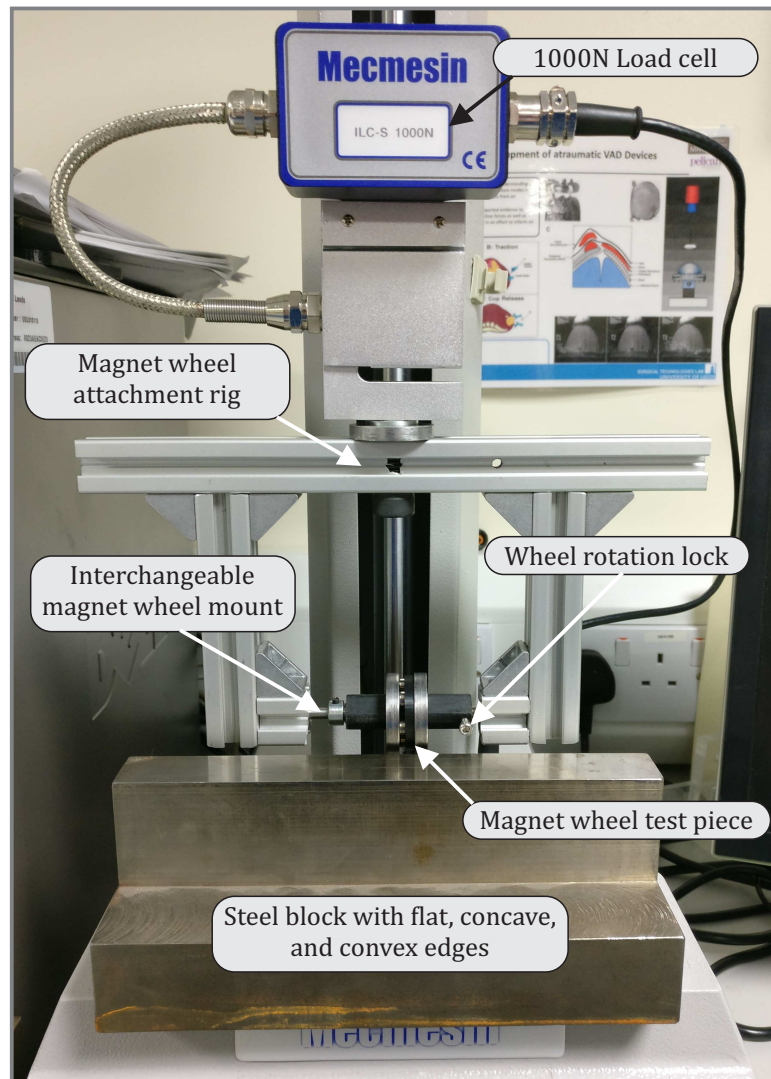


Figure 4.6: Diagram of the magnetic wheel test rig set-up.

4.5 Magnetic wheel experimentation

Table 4.2: Test program used in the Mecmesin tensile tester to produce normal force results.

Command	Linear stage speed (mm/min)	Target Value	Target Unit
RUN	-6.00	0.00	Load (N)
ZERO DISPLACEMENT	0.00	N/A	
CLEAR DATA	0.00	N/A	
RUN	30.00	5.00	Displacement (mm)
RUN	-30.00	0.00	Displacement (mm)
CYCLE X5	6.00	2.00	Displacement (mm)
	-6.00	0.00	Displacement (mm)
END			

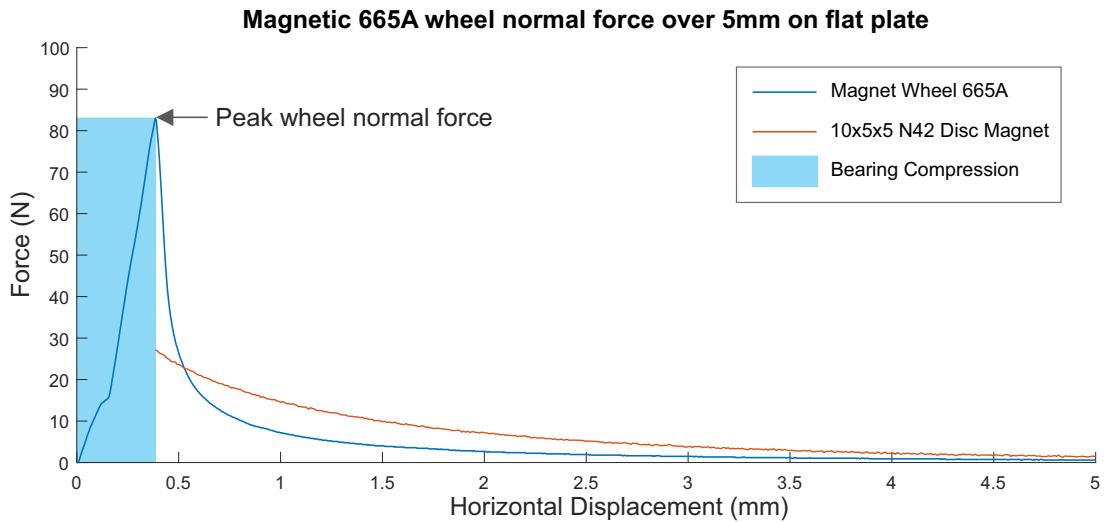


Figure 4.7: Standard magnet pull test over a 5mm range for both a regular N42 disc magnet, and a magnet wheel array.

4.5 Magnetic wheel experimentation

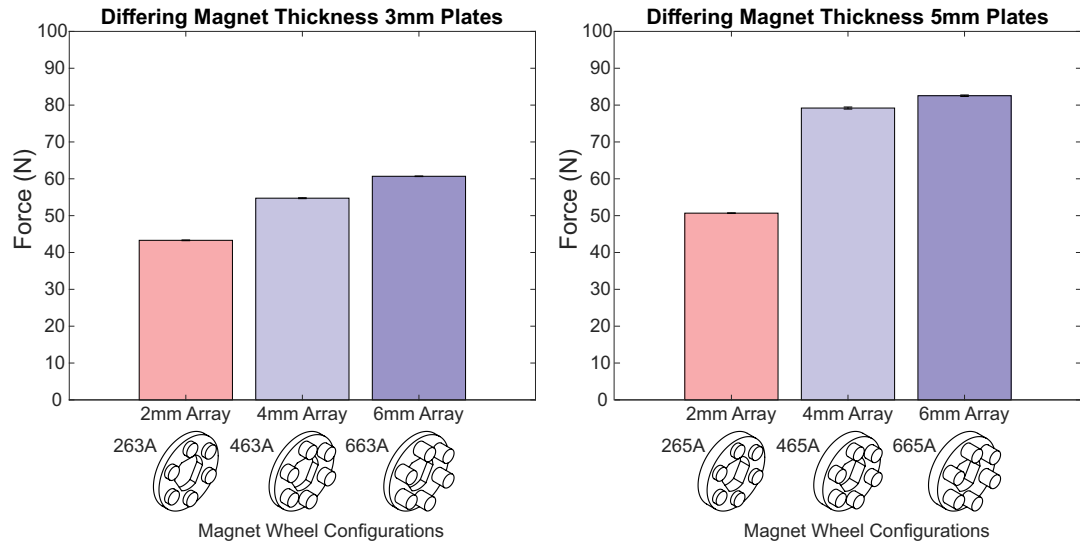


Figure 4.8: Mean force for various wheel configurations (force \pm SD)

For smaller force magnets such as the 2mm array the maximum flux output from the magnets is already being held by the steel plate and so the force will no longer increase with an increase in steel thickness. Tests using the 6mm magnets with 5mm plates and a 6 magnet array (665) will be used to ensure the maximum wheel load is used in the tests to use the most range on the 1000N load cell.

Magnet array alignment

For robot operation when traversing concave and convex step cases the magnetic force at points along the wheels circumference should be as uniform as possible. A uniform field allows the wheel to be predictable in its behaviour, for each case. A non-uniform wheel may be harder or easier to move from a double contact concave case depending on the specific point in contact, this could change for each obstacle. To investigate the possibility of the gaps between the magnets in the array causing force changes two wheel configurations were tested with an array of 6 and an array of 3 magnets. Figure 4.9 shows the results of the alignment test. The misaligned six magnet array (665A) wheel configuration showed a drop of 0.3N from 82.9N, a 0.4% drop in force. The misaligned three magnet array (635A) dropped in force from 44.2N to 42.5N resulting in a 3.8% drop in force.

4.5 Magnetic wheel experimentation

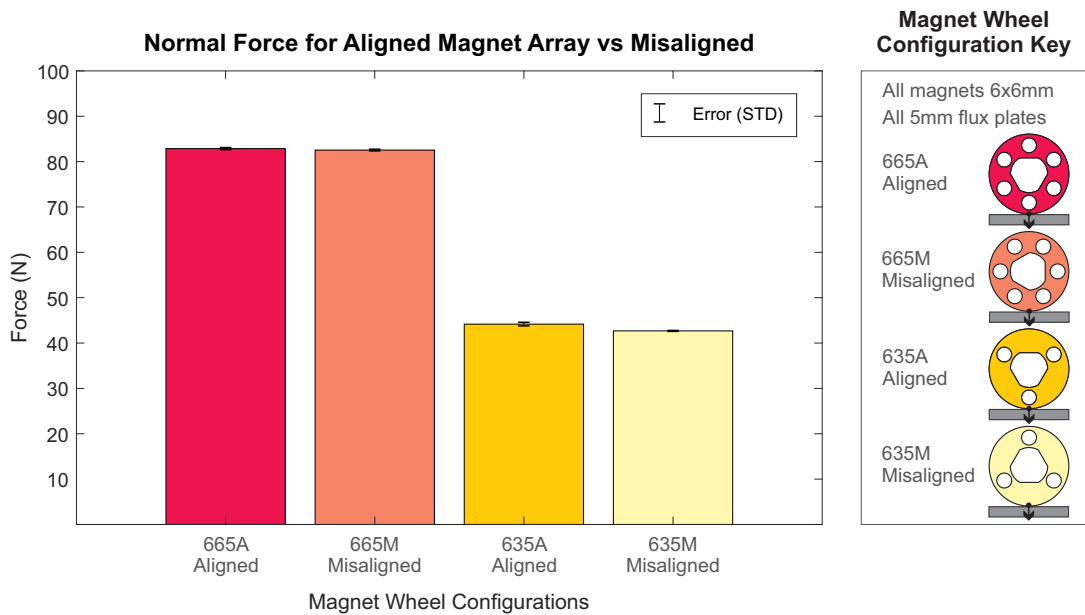


Figure 4.9: Comparison of the effect of wheel magnet array rotation angle on the peak force produced by the wheel for both a three and six wheel array.

Concave case

The concave pull case takes place in free rotation to simulate the robot overcoming the concave case where the peak force occurs just after the double contact case has been broken. The parameters used in this test are present in Table 4.3. The peak force of this case is around 56N, compared to the peak force of 83N that the 665A wheel seen on a standard flat plate. The graph 4.10 shows that in double contact the force of the wheel at both contact points drops to 67% of the peak force on a flat plate.

4.5 Magnetic wheel experimentation

Table 4.3: Test program used in the Mecmesin tensile tester to produce concave results.

Command	Linear stage speed (mm/min)	Target value	Target unit
RUN	-6.00	0.00	Load (N)
ZERO DISPLACEMENT	0.00	N/A	N/A
CYCLE X5	6.00	3.00	Displacement (mm)
	-6.00	0.00	Displacement (mm)
END			

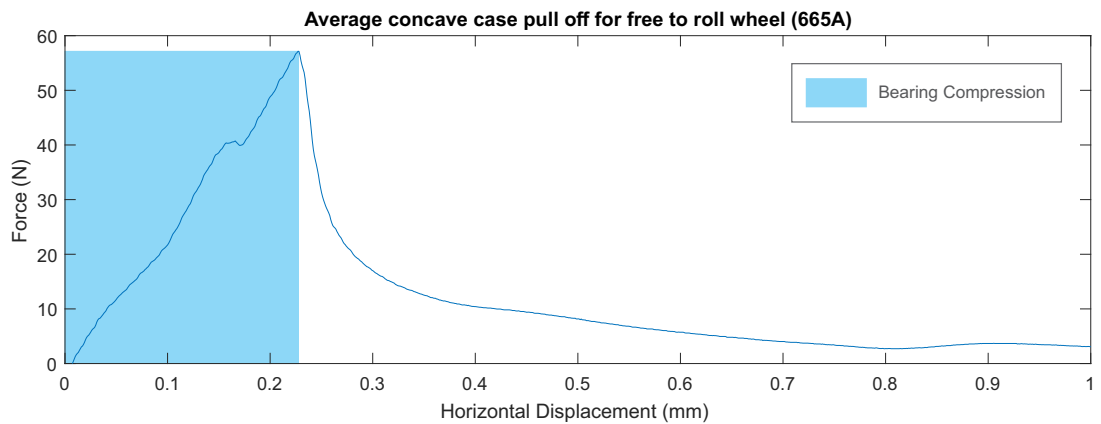


Figure 4.10: Graph of the force to pull a free rotating magnetic wheel from a right angle concave case where the wheel is in double contact.

Convex case

Graph 4.11 shows the averaged force over five reps for a wheel in free rotation moving from a flat 90° wall up to a 90° corner case. The red highlighted area represents the wheels approach up to the corner case. During this section the wheel is rolling with peaks and troughs caused by impurities in the steel plate. The force increases as it approaches the corner section, this is because the magnetic force is acting towards the full contact steel area. The force decreases to a minimum as it reaches 45° to the corner, and then increase as it is pulled from the steel up to the point of corner contact break where the force drop drastically back to open air levels and then tapers to negligible

4.5 Magnetic wheel experimentation

levels.

Table 4.4: Test program used in the Mecmesin tensile tester to produce convex results.

Command	Linear stage speed (mm/min)	Target value	Target unit
RUN	30.00	0.00	Load (N)
RUN	-30.00	15.00	Displacement (mm)
ZERO DISPLACEMENT	0.00	N/A	N/A
CYCLE X5	30.00	15.00	Displacement (mm)
	-30.00	0.00	Displacement (mm)
END			

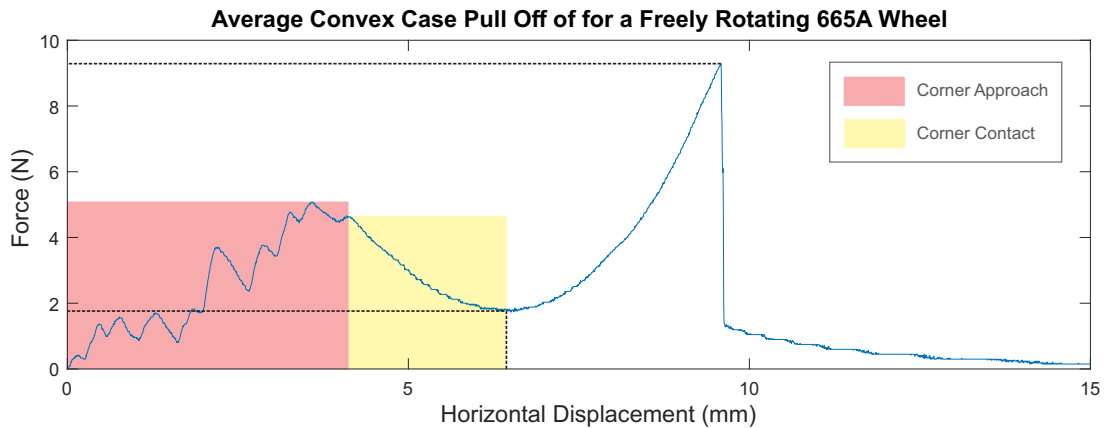


Figure 4.11: Graph of the force to pull a free rotating magnetic wheel from a 90° wall up to a convex corner case, and then detach from the corner case.

4.5.2 Increasing friction

To assess the maximum traction that can be generated by the wheel the wheel was locked in place to stop rotation and dragged along the steel surface. From the peak drag force and the known normal force the co-efficient of friction can be calculated and applied to wheels of other normal force values.

Figure 4.12 shows 4 reps of pulling the magnetic wheel in steel flux plate on steel

4.5 Magnetic wheel experimentation

Table 4.5: Test program used in the Mecmesin tensile tester to produce concave results.

Command	Linear stage speed (mm/min)	Target value	Target unit
RUN	-6.00	0.00	Load (N)
ZERO DISPLACEMENT	0.00	N/A	N/A
CYCLE X5	6.00	3.00	Displacement (mm)
	-6.00	0.00	Displacement (mm)
END			

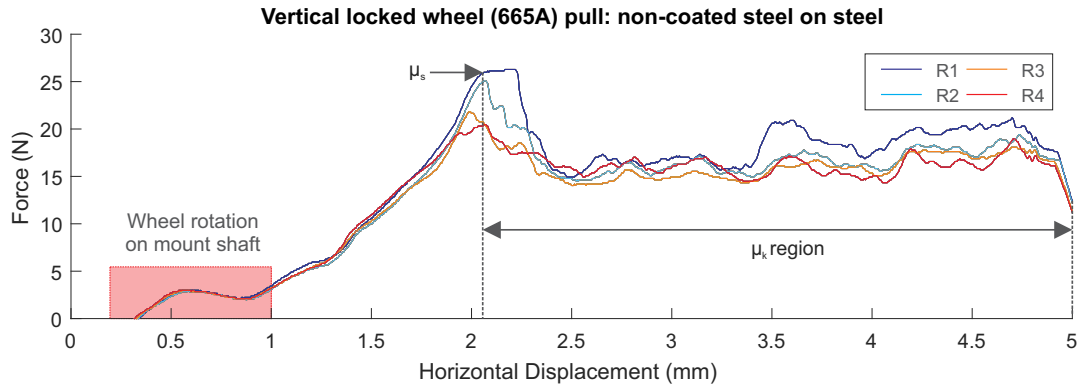


Figure 4.12: Graph showing the force to pull a rotation locked uncoated magnetic wheel across a steel contact.

plate contact The highlighted curved movement at the start of loading is caused by slack in the shaft allowing the wheel to rotate slightly before being pulled completely. The mean average of the pull test peaks in 4.12 is 22.6N, using this as the frictional force the co-efficient of friction in equation 4.3.

$$F_f = \mu_s \cdot N \quad (4.1)$$

$$\frac{F_f}{N} = \mu_s \quad (4.2)$$

$$\frac{22.6}{82.9} = 0.27 \quad (4.3)$$

The rubber material used is "Plasti-dip: Plastic/Rubber Paint", this material is painted onto the wheels as a liquid, it contracts as it dries forming a tight rubber

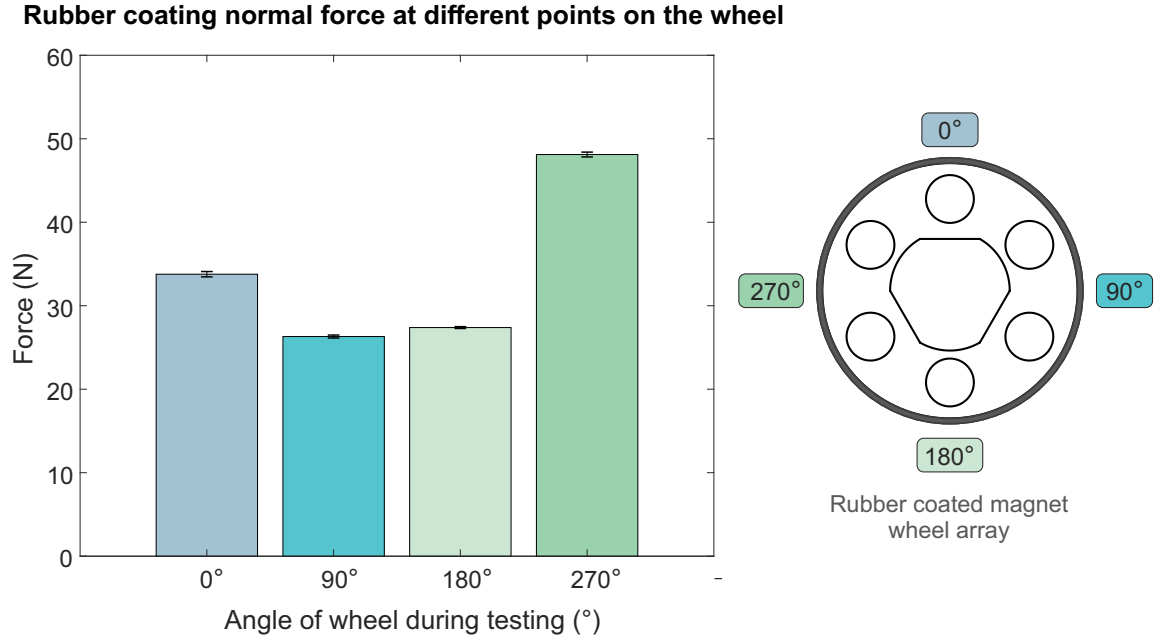


Figure 4.13: Bar chart showing the average pull force for a 665A wheel at four different points around the wheel in both aligned and misaligned conditions.

seal. The rubber seal increases the friction co-efficient of the wheel as it acts as a tire between the magnet and the steel contact point, there is also the added benefit of sealing the rare-earth magnets from corrosion. Because of the small distance at which the wheels magnetic force is affected any frictional material application should be considered against the maximum normal force. The peak force of the wheel with its applied rubber coating was experimentally tested at four different points around the wheel, the results are displayed in Figure 4.13, the mean force of the contact points around the wheel is 51.9N.

The rubber coated wheel was tested in the same way as it was before coating. The force increases until the wheel begins to move, it then steadily rises under static movement, this is likely due to slight temperature increases in the wheel as it is undergoing sliding friction. Each subsequent test the force of the wheel increases slightly, this is because the rubber material wears after each test as seen in Figure 4.15. The force of the first pull test before wear is used to calculate the frictional co-efficient (19.4N).

$$\mu_s - rubber \frac{19.4}{27.4} = 0.71N \quad (4.4)$$

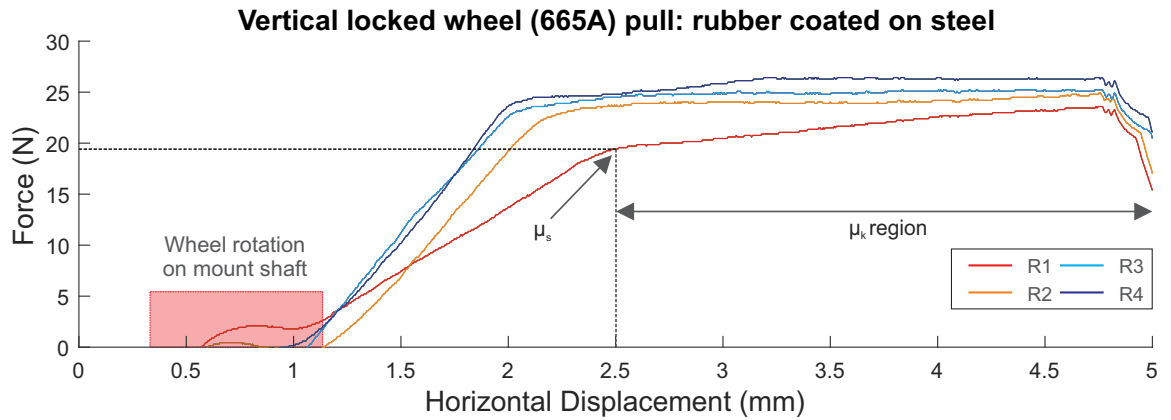


Figure 4.14: Graph of the force required to pull the rubber coated magnet up the steel block with the axle locked in contact at the 180° mark in 4.13.

4.6 Discussion and conclusion

This section will review the chosen design of the magnetic wheel against the initial requirements put forward in the beginning of the chapter.

The flux plate magnet array configuration can produce contact forces equal or greater than the sum of the magnet arrays combined pull force under normal circumstances the wheel produced maximum pull forces of 82.9N whereas the manufacturers rated pull force of the 6x6mm N42 magnets produce 13.73N each, six of these should produce a pull force of 82.38N. To review the uniformity of the magnetic force of the array wheel an experiment was conducted in which the alignment of the array was altered. When a magnet wheel is uncoated and the contact is steel on steel there is a minor change in contact force when the wheel magnets are directly aligned vs when they are misaligned. The drop in force is small enough to be negligible when the magnets are misaligned with the contact point, however it is more pronounced when the array is spaced further apart. For robotic traction the rubber coating has a larger effect on the wheel contact uniformity than alignment, even a small thickness difference in a thin coating of 0.06mm can cause the maximum force to drop to half of the top rated pull force so minor thickness differences in the outer rubber coating will effect the wheel more than the 0.4 - 3.8% drop in force observed in the experiment. Figure 4.7 showed that the designed magnet wheels have a concentrated but shallow magnetic field around the contact area of the wheel. The larger reaching field of the disc magnet

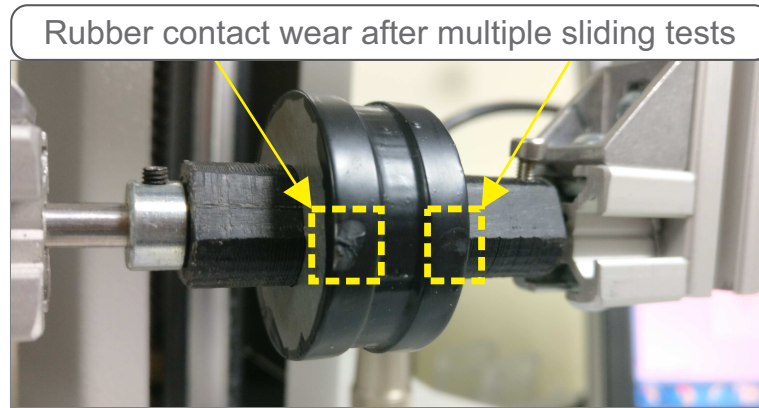


Figure 4.15: Wear of the rubber coating showing after five repetitions of friction testing on the linear force tester.

took over 10 times the displacement to reach 50% of its maximum pull force. This means higher force of the array design can be negated in a very small distance during concave cases allowing simple detachment of the wheel in double contact. A negative of this is that very small amounts of high frictional coating will cause the wheel traction to fall quickly versus a standard magnet design. This means an array configuration wheel needs a higher starting design force to reach the same coated normal force value as a standard magnet.

To create a thin profile wheel to entire pipelines the flux plate and magnet array profile has been chosen. Other options included chassis magnet arrays which were large and not viable for corner cases. The number of magnets in the array can be increased by optimising the 3D-printed spacer, more magnets in the array will give the same force for a smaller profile. The thin profile of the wheel will be combined with a transmission method on the main shaft whether it is a direct drive or a geared connection. The drive transmission method will require mountable geometry, the chosen axis geometry is triangular to reduce the loss of plate material, and to allow 3D printing of shafts without the need for sharp edges.

The flux plates shield the magnets both from impact and potential corrosion. The rubber track coating of "Plasti-dip" further increases protection of the magnets from corrosion by sealing the gap between the 3D printed magnet array spacer and the inner flux plate magnet contact point. The frictional co-efficient has been increased with the use of the applied rubber coating, the frictional co-efficient μ_s increased from 0.27

to 0.71. The force frictional forces need to move both the steel and rubber wheels were very similar in terms of traction however the rubber wheel is far superior as it provides a reduced detachment force needed in a concave double contact case. This lower detachment force requires lower motor torque to overcome and hence smaller motors on the robot. The wheel coating takes four hours to dry in total so replacement of wheel tread after inspection use is not an issue, multiples should be made beforehand to replace during deployments.

The wheels designed in this chapter will be used in the further design and development of the magnetic robot in Chapter 6.

CHAPTER 5

Embedded System and Software Design

This chapter looks at the electrical systems to meet the robot specification criteria laid down in Chapter 3. The chapter will explore the use of actuators and control methods to drive the magnetic adhesion wheels designed in Chapter 4. The wireless communication method between a high level and low level robot controller will be defined, and an optimised command protocol will be developed.

5.1 Introduction

The work in this chapter is focused on the development of a complete open-loop control program that interacts with a robot micro-controller. The specifications and requirements for the desired features of the control program are set out for both the hardware and software.

5.1.1 System requirements

The system requirements for the robotic control software are defined in Table 5.1 and requirements for the robots hardware design are presented in Table 5.2.

Table 5.1: Major requirements of the software control features

Desired control feature	Description	Software requirement
Highly controllable	Robot should capable of forward, reverse, turn on spot, turn slowly to adjust wheel contact in a corner.	An input control method that maps pilots actions to motor control messages.
Simple operation	The robot software should be simple to use and the robots actions should be predictable based on inputs.	Intuitive control scheme, that allows control over the robot with minimal training.
Wireless communication	The robot has been specified to operate without a tether.	Message output from control PC that can be read and executed by robot software (two programs)
Low latency between input and execution	For smooth control of the robot low ping between the controller pilot and the micro-controller is required.	Minimal message package size between communicating systems. Optimised send/receive speed.

Table 5.2: Major requirements of the hardware system

Desired hardware feature	Description	Hardware requirement
Small physical package	The electronic hardware should be as small as possible to fit the robot pipe entrance requirements.	Advanced micro-controllers and control boards with minimal breakout pins, stacked to minimise volume.
Wireless communication	The robot has been specified to operate without a tether.	Integrated robot controller and wireless communication device.
Skid steering	Robot will use skid steering to simplify locomotion and reduce design volume.	Dual-motor drive system able to perceive commands from the micro-controller.
Low power consumption	The robot will require a battery (wireless) and hence power consumption should be kept minimal to increase battery life.	Power consumption of components should be considered when selecting hardware.
User control of hardware	The user should be able to control the robotic hardware with minimal training using simple controls.	Standard joystick such as Xbox 360 controller which is widely used.

To achieve these requirements, the specific objectives are:

- Define the hardware to be used in the system to be embedded within the micro-controller robot.
- Develop an open-loop control program to communicate with a wireless micro-controller.
- Develop a slave micro-controller program to receive information from the main program and react accordingly

- Assess the open-loop system against the requirements.

5.2 Hardware

The high level hardware used is presented in Figure 5.1. A laptop PC, runs the main program and is also used to communicate with the robot hardware over Bluetooth. The graphical user interface runs on PC to pilot the robot, using a Microsoft Xbox 360 controller (wired or wireless). The PC communicates with the robotic micro-controller using wireless transmission over Bluetooth. The main program is built using LabVIEW developed by National Instruments. LabVIEW was chosen as the programming language due to it's simple methods of hardware interface. The micro-controller robots are programmed using the arduino IDE, the language is predominantly C, and C++. A breadboard for the development of the prototype robot circuit is powered via a 300W power supply.

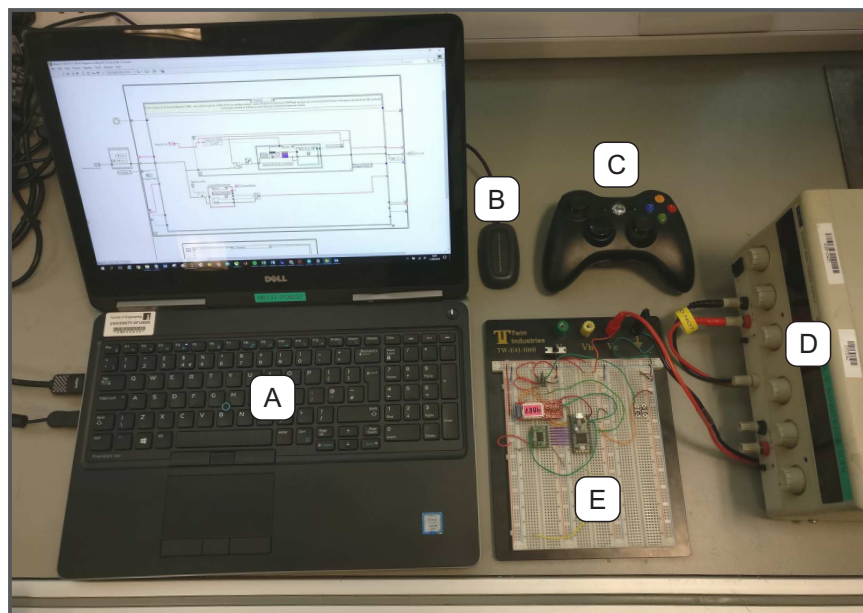


Figure 5.1: A: Laptop PC with Bluetooth built-in. B: USB Xbox controller receiver. C: Xbox 360 wireless controller. D: 300W power pack. E: Robot electronics prototype breadboard.

5.2.1 Robot Micro-Controller

The most popular micro-controllers for sub 100mm robots are summarised in 5.3. The Arduino Pro Mini series is a condensed version of the 328 chip from an Arduino UNO minus the unnecessary peripherals, they are a well supported device with many libraries which helps development speed. The Teensy 3.2 has the disadvantage of requiring a voltage regulator to function. This is because the 2 cell lithium polymer (LiPo) battery required to power the 6V motors runs at 8.4 volts at its highest charge and the Teensy 3.2 is only 6V tolerant. Compared to the Arduino Pro Mini which can take a maximum of 12V board supply it only offers a mild inconvenience vs the the speed which is up to 12 times faster in the 3.3V version, and 6 times as fast as the 5V board. The ESP and the Teensy 3.6 are both simply too large to warrant development despite the faster speed processing. Based on this, the Teensy 3.2 is the most suitable selection for final development.

Table 5.3: Micro-controller options considered for robot development comparison table

Micro-controller	Voltage	Clock Speed (MHz)	Size (mm)	
			x	y
Arduino Pro Mini	3.3	8	33.00	18.00
Arduino Pro Mini	5	16	33.00	18.00
Teensy 3.2	3.3	96	35.00	18.00
ESP32	3.3	160	55.00	28.00
Teensy 3.6	3.3	180	62.30	18.00

5.2.2 Communication

Communication will be wireless, the most commonly used Bluetooth and Wi-Fi modules were compared in Table 5.4. The power draw stated is the consumption during constant communication, as this communication line is intended for piloting it will be constantly open and hence near this maximum value throughout the robots deployment. The Bluetooth model was chosen rather than Wi-Fi despite its larger size due to the lower power consumption for similar in maximum baud rate. Battery size is limited, so reduction of power consumption will ultimately increase inspection time. The Bluetooth

SMIRF Gold module is rated for transmission distances up to 100m.

Table 5.4: Comparison table of bluetooth vs wifi

Wireless module	Input voltage (V)	Power draw (mA)	Baud rate max (bps)	Size (mm)	
				x	y
Bluetooth Smirf Gold	3.3 - 6.0	40	115200	45.0	17.0
Wifi Module ESP8266	3.0 - 3.6	215	115200	25.0	14.5

5.2.3 Actuation and Power

DC motors are the most suitable actuators to drive the robots wheels as they are simple to control versus stepper motors and do not have limited range of servos. The DC motor used is the 6V (*Micro Metal Gearmotor*) manufactured by Pololu, these are driven by a Pololu TB6612FNG dual motor driver with a Pulse Width Modulation (PWM) signal from the micro-controller. There low and medium voltage versions of these motors in both 12V and 6V, however the power rating for each is the same. The 12V require a 3S LiPo (11.1V) battery increasing the size.

The selection of these motors was based on the price and versatility, there are many different motor gear ratios which produce different torque values, as shown in Table 5.5. The motors, including the gearboxes are all the exact same dimension size (10mm x 12mm square face) except for the 1000:1 motor which has an extended gearbox. The uniform dimensions make the motors switch-able between prototype versions depending on required torque and speed. Motor selection has the greatest subsequent effect on battery selection. The battery is required to supply 6V, through a 2S Lithium Polymer (LiPo). The 2S LiPo was selected to be a Turnigy nano-tech 2S 260mah battery. These run at 7.4V but can be modulated to 6V with PWM.

5.2.4 Circuit Integration

The components are integrated into the development breadboard and wired into a complete circuit. In Figure 5.2 the complete circuit on intended for embedding into the

Table 5.5: Micro Metal Gearmotor selection table: High-power 6V precious metal brushed [27]. All gear ratios are rated to 1.6 Amp stall current and No-load current of 0.07 Amps.

No-load speed (RPM)	Stall torque (kg/cm)	Max power (W)	Gear Ratio
6000	0.11	-	5:1
3000	0.22	1.6	10:1
1000	0.57	1.5	30:1
590	0.86	1.3	50:1
410	1.3	1.4	75:1
310	1.7	1.3	100:1
210	2.4	1.2	150:1
150	3.0	1.1	210:1
120	3.4	1.1	250:1
100	4.0	1.1	298:1
84	5.5	1.1	380:1
31	12	-	1000:1

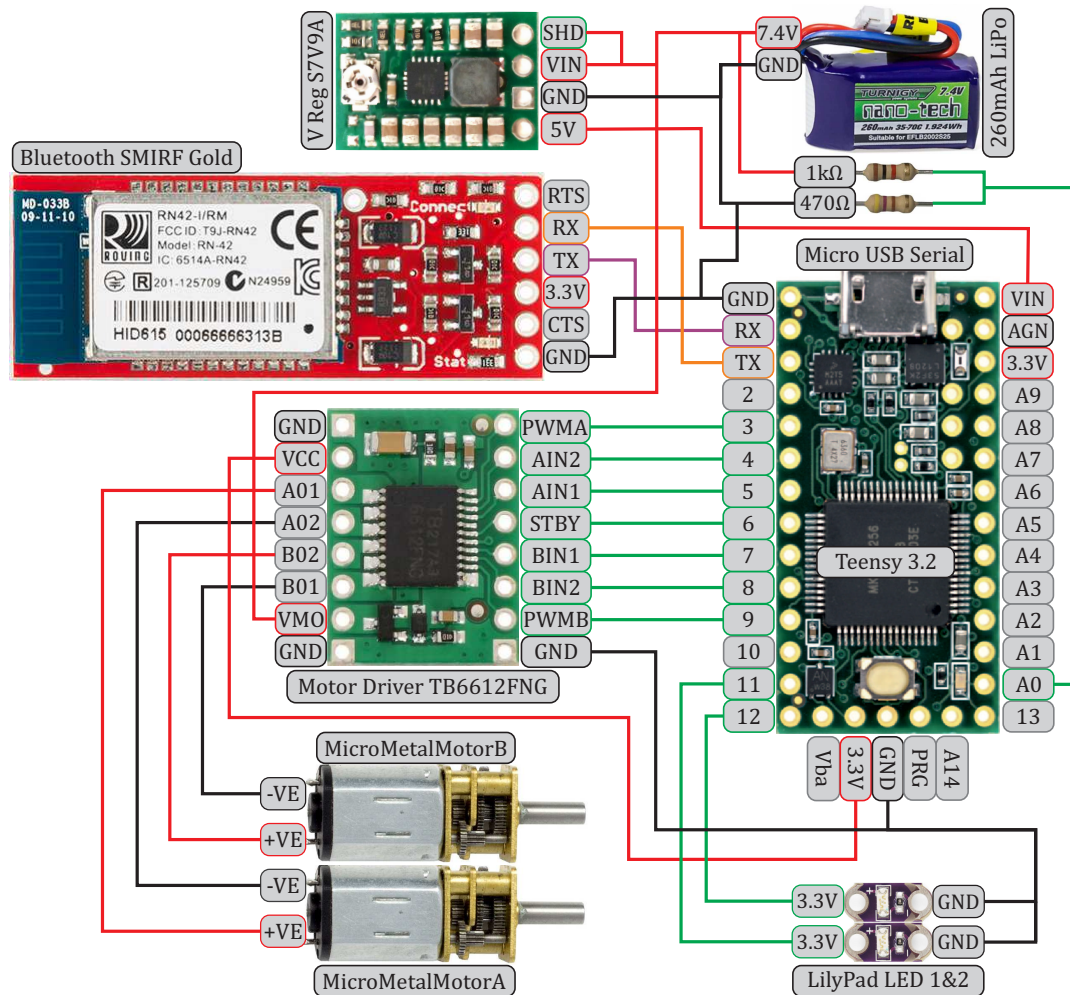


Figure 5.2: Diagram of the integrated circuit.

robot is presented. This circuit contains features such as the LiPo battery pack which replaces the bench power supply.

Not shown in the diagram is a separate first person view (FPV) camera circuit mounted on the robot. This camera is separate due to its requirement of 3.3 volt power with high current draw that cannot be provided by a Teensy output. The two resistors in the circuit in Figure 5.2 form a potential divider. The divider reduces the 8.4 volts supplied by the battery down to a range that is sub 3.3 volts that can be read by the logic pin (A0) on the Teensy. The equation used to choose the potential divider resistor values is given in equation 5.1.

$$V_{out} = \frac{V_s \cdot R_2}{(R_1 + R_2)} \quad (5.1)$$

Where: V_s = Voltage source (V)
 R_1 = Resistor value 1 (Ω)
 R_2 = Resistor value 2 (Ω)
 V_{out} = Voltage out (V)

$$V_{PinBatteryMax} = \frac{8.4 \cdot 470}{(1000 + 470)} = 2.686 \quad (5.2)$$

$$V_{PinBatteryMin} = \frac{6.6 \cdot 470}{(1000 + 470)} = 2.11 \quad (5.3)$$

The power going through the resistor voltage divider is calculated in equation 5.7, the result of 32mW through 1k Ω resistor is safe as it is below the standard safety rating for a $\frac{1}{16}$ Watt (62.5mW) power rated resistor. The power through the 470 Ω is even less.

$$\frac{V}{R_{sum}} = I \quad (5.4)$$

$$\frac{8.4}{1470} = 0.00571A = 5.71mA \quad (5.5)$$

$$I^2 \cdot R = P \quad (5.6)$$

$$0.00571^2 * 1000 = 0.032W = 32mW \quad (5.7)$$

The maximum input voltage that is required to be read is 8.4V, which is reduced to 2.686V (5.2) on the analogue pin through the potential divider. The minimum voltage at which it is safe to re-charge a LiPo is at 3.0V per cell, beyond this point the battery must be disposed of as battery integrity is compromised.

This must be prevented as a battery failure will cause the robot to shut-down and become uncontrollable in an inaccessible location. To prevent the charge from dropping to this minimal value a battery warning system is in place should to indicate when the battery reaches un-safe levels, it is set to 3.3V per cell (6.6V total). This value is shown to be at 2.11V on the analog pin (5.3). The completed hardware package embedded in the robot is shown in Figure 5.3. This completed hardware stack is just 45mm x 18mm x 14mm (excluding motors LEDs and battery).

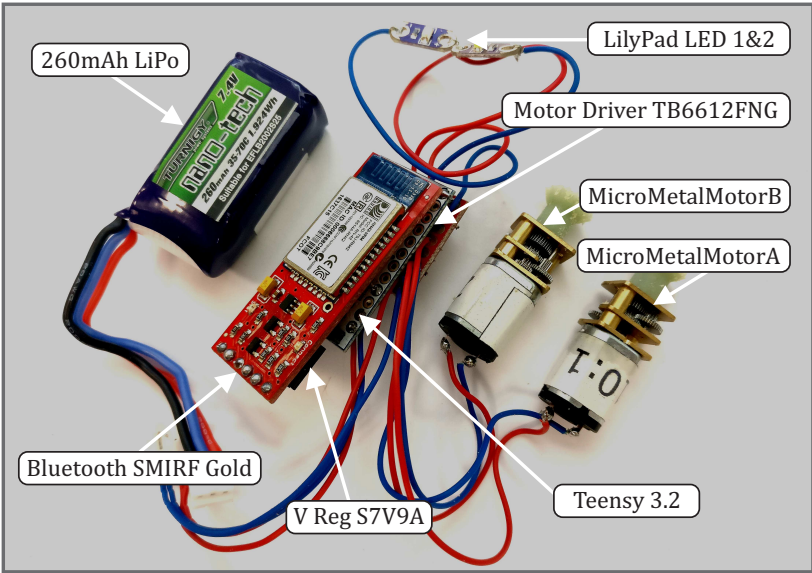


Figure 5.3: Diagram of the assembled robot hardware circuit to be embedded in a mechanical system.

5.3 Open loop control system

The open loop control software developed in this section is designed to interface with the hardware circuit to produce robot motion from user inputs. The high level overview of the control system used is presented in Figure 5.4. The intended close loop condition is for the human driving the robot to make changes based on their visual feedback. The visual feedback will be provided either by line of sight or by the first person view camera on the separate control circuit.

This section will explain the software system architecture in greater detail. A graphical representation of the system architecture and brief overview of how the two individual programs is shown in Figure 5.5. In this set-up the LabVIEW program acts as the higher level controller, sending user driven commands to the lower level robot micro-controller.

5.3.1 High level control: LabVIEW

LabVIEW is the chosen high level programming language because it excels in hardware integration. This allows easy access of multiple input devices for human use such as COM Port integration, keyboard and gamepad input devices, and PC Bluetooth

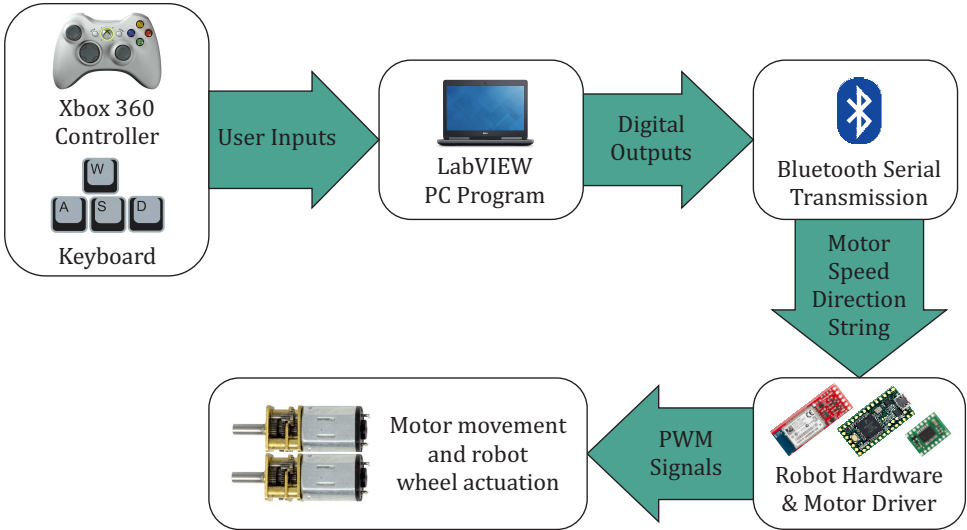


Figure 5.4: Diagram of the high level control system used to develop the robot software.

integration. LabVIEW also makes the creation of functional GUI’s simple to integrate into a program, this is advantageous when using human pilots that require visual feedback. The developed LabVIEW program uses state machine architecture with four main states; initialise, write, read, and shut-down. The LabVIEW program has four states in which the program operates, these run one at a time, at the end of each state a decision is made on which state to progress to.

Initialisation and stop states

The first state initialises the program, this is completed through user input. The user inputs commands into the GUI that are then loaded into the programs main data cluster, the parameters available to alter are presented in Table 5.6. The robot cluster array functions as the spine of the program and provides a constant data stream from which information is pulled, altered, and loaded. The robot cluster array is constantly updated throughout each section of the program loop. Disabling features such as ”Serial Read?” are used to decrease program load when many robots are connected as the read function takes up the most time within the program.

The program then connects to the robot Bluetooth radio, Bluetooth SMIRF radio devices have two COM ports, one for sending and one receiving. Only one COM port is required on the LabVIEW end in order for bi-directional transmission to work though,

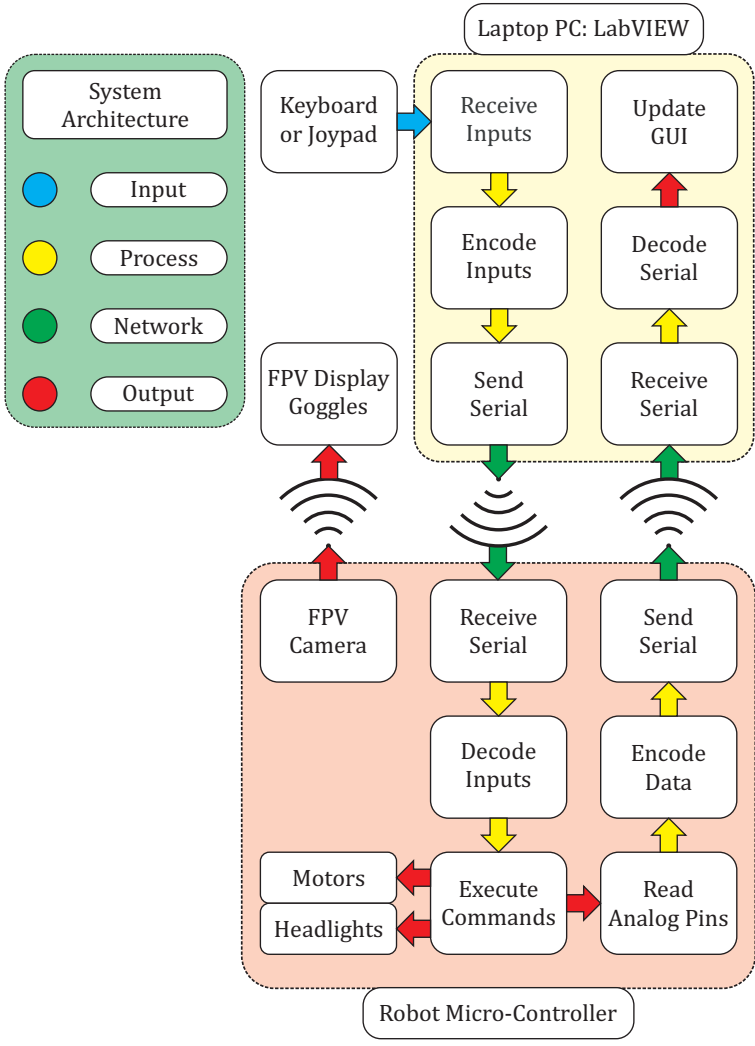


Figure 5.5: Overall system architecture including simplified LabVIEW and micro-controller programs.

5.3 Open loop control system

Table 5.6: Cluster array elements that store each individual robots data and configuration settings.

Cluster Array Item	Cluster data type	Typical Value	User Initialise	Item Description
COM Port	Integer	0 - 255	INPUT	Radio COM port to connect to
Radio COM Status	Boolean	0 - 1	INPUT	Radio connected or not?
Radio I.D.	String	7BA5	INPUT	Define radio I.D. to connect (4 characters)
Radio Connect	Boolean	0 - 1	OUTPUT	Was radio connection successful?
Serial Write?	Boolean	0 - 1	INPUT	Write commands to this radio?
Serial Sent	Character	[20]	OUTPUT	Serial sent by LabVIEW
Serial Read?	Boolean	0 - 1	INPUT	Read data from this radio?
Serial Received	Character	[20]	OUTPUT	Serial received by LabVIEW
Baud Rate	Integer	9600+	INPUT	User defined baud rate from 9600 to 115200 (BPS)
COM Speed	Integer	0 - 60+	OUTPUT	Calculated robot COM speed (Hz)
Bits Recieved	Integer	0+	OUTPUT	Counts the bits received total (to calculate baud rate)
Number of Robots	Integer	1 -10+	INPUT	Input number robots to attempt connection with

the "OUTGOING" port is the correct connection in LabVIEW. In order to prevent a false positive connection message due to an incomplete COM port close procedure, the next step is to check the connection of each robot with a small serial handshake. A simple carriage return (CR) is sent as a message to do this. LabVIEW waits to see if the robot replies and if so, confirms that connection to that robot has been established. The handshake is repeated for each robot that is flagged for connection attempts in the GUI. Each unique robot's information is kept within a data cluster which also holds all the users initialise variable inputs. Cluster information defined as an "INPUT" must be set by the user before running the program to enable the feature.

After the initialisation state LabVIEW enters the main program loop states. The user is able to activate the shut-down state at any time after this by pressing the stop button on the GUI. The shut-down state will proceed to close all COMS one at a time in the reverse operation of the initialisation state. The shut-down state allows safe closing of all COM ports for immediate reconnection.

Write and read states

The second state, "write" and the third "read" form the main program loop, the program will cycle through these two states until the user activates shut-down. When a human is operating a robot the primary send data is converted from human input into the send commands. When considering human operation, an appropriate control scheme needed to be created and be as simple as possible to use. To accompany different preferred control styles different control schemes within the master program are available in the program. A game-pad or a keyboard are available for use, they preferred option is specified in the settings before running the program. The control scheme mapped to the input devices is common for remote control or simulated vehicles and have been designed to be simple to use. The messages sent through the keyboard are slightly different as there are no analog inputs, therefore the PWM range must be preset. The LabVIEW user input and serial communication method is described in detail in Figure 5.6.

5.3 Open loop control system

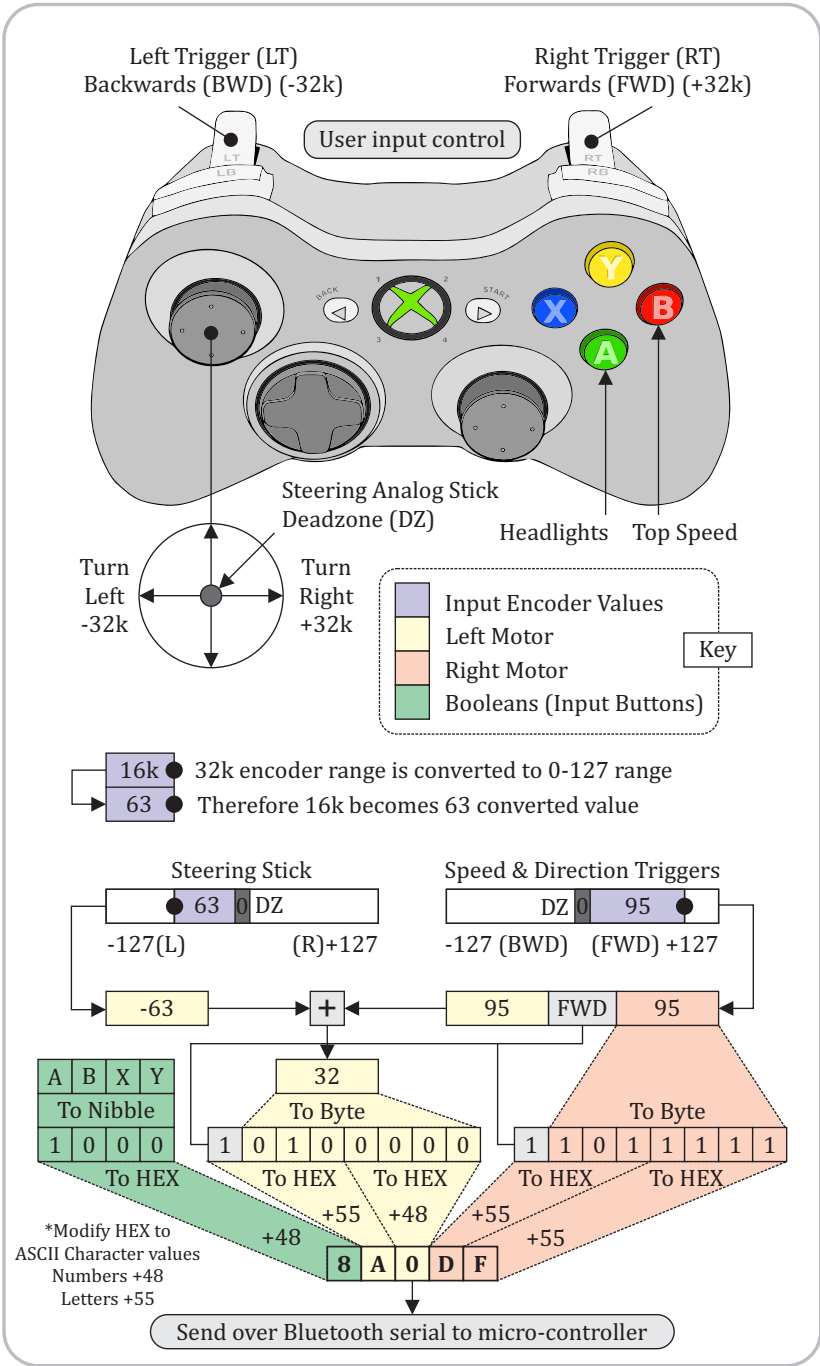


Figure 5.6: LabVIEW method to convert user control inputs to condensed serial commands to be transmitted to the micro-controller.

Once the user inputs have been encoded to the serial character message in LabVIEW

they are sent over Bluetooth to the robot micro-controller. Due to the limitations of ASCII serial only a limited number of characters exist without double-meaning. For instance, not shown in the serial message is the last character of the message which marks the end of a message, this is the carriage return "CR" which has the decimal value 13 and acts as a new line in standard protocol. If a nibble (a package of 4-bits) of decimal value 13 is sent to the micro-controller it will be read as a "CR" new line and ruin the message. ASCII decimal values have different double meanings from values 0 to 31, therefore these values are un-usable in communication. To avoid this LabVIEW takes the controller inputs and converts them to HEX, the HEX values are sent through to the the robot as ASCII characters. For instance a nibble value of 13 which would normally be interpreted as a carriage return is written as its HEX value "D". The ASCII character D has a decimal value of 68 so to convert 13 to 68 an addition of 55 is made. The micro-controller receives "D" (68) removes 55 to convert back to the original nibble value. The modifier value is constant, and is 48 for numbers, and 55 for letters according to the standard ASCII Table [127].

The read state of the program receives messages back from the micro-controller and decodes them using the same method as the low level micro-controller, shown in 5.7.

5.3.2 Low level control: micro-controller

The low level control system receives the serial messages from LabVIEW and coverters them back to useable motor bytes as shown in 5.7. Once this serial ASCII decoding is complete the robot micro-controller combines the character bytes to return the full motor command and the button array. The motors commands are decoded and applied to the motor driver and the button array is treated as a set of boolean switches to perform tasks such as turning the headlights on and off. Other button functions include changing the top speed by editing the PWM multiplier, e.g. 0.5 = Slow (63), 1 = Medium (127), 2 = Fast (255). This is very useful for slow driving in tight areas which require slow manoeuvres.

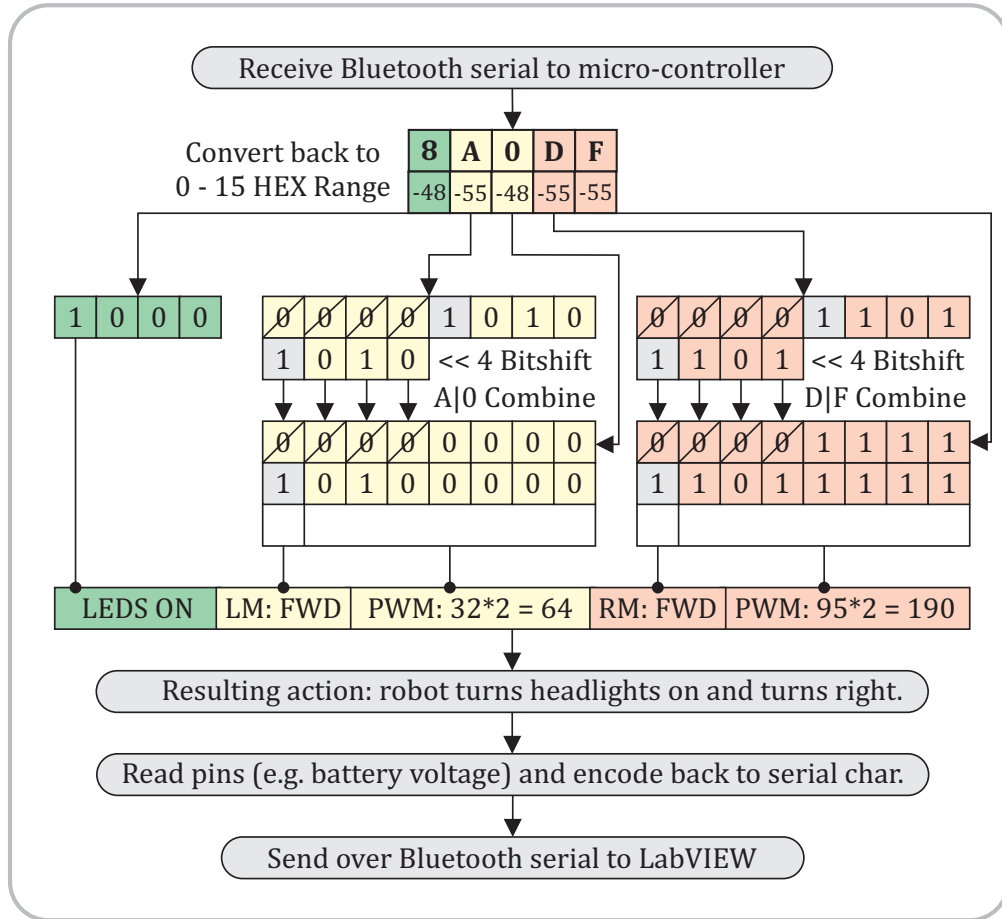


Figure 5.7: Arduino method to convert condensed LabVIEW serial commands to useable micro-controller instructions to be passed to components.

5.4 Discussion and conclusions

The software requirements set out in 5.1 have been fulfilled with the development of the LabVIEW high level control program, and the accompanying low level micro-controller program. The robot is highly controllable and performs a full range of motor movements including forward, reverse, and slow turns. The method for inputting the commands uses a simple controller based system that is easy to learn with minimal practice. The robot high level program communicates over wireless Bluetooth radio and has built in architecture to allow multiple Bluetooth robots to be connected at the same time. To fulfil the software requirement of low latency in Table 5.1, the serial messages have

been optimised to just reduce the length of the message that needs to be sent. The process has been optimised down to 5 character messages over serial. In order to do this one each motors command data is stored in a single byte, with the highest bit being direction and the remaining 7 controlling PWM speed. In use this gives half the resolution for resulting speed commands with only 128 values in the full 256 PWM range. This loss in resolution does not detrimentally affect the user piloting the robot as the end wheel speed of the robot is low due to high torque requirements from the magnets.

The hardware requirements for the robotic platforms set out in 5.2 have been achieved. To create a small physical package or "stack" size the components were selected with volume reduction as a top priority. Smaller micro-controllers have been used instead of larger more powerful models, two motors were used within the same size range as the controller. Limiting the motor number to two fulfils both the small physical package size requirement and the simple skid-steering requirement. The circuit design went through many iterations and it should be noted that the Teensy micro-controller is easily interchangeable with Arduino Pro-Mini 3.3V or 5V boards which were used in early hardware prototypes. The previous Arduino Pro Mini design has been completely replaced with the faster Teensy 3.2 with no adverse effects and the program structure, language, and IDE remain the same. The Bluetooth radio hardware allows wireless communication across a serial TX/RX pipe channel from the low level micro-controller to the high level LabVIEW program. The Bluetooth design choice also greatly contributed the optimisation of the circuit for low power consumption. The secondary option of a Wi-Fi ESP8266 module is half the size, however it consumes over 5 times the power draw under constant communication with no increase in communication speed as both baud rates cap at 115200 BPS.

Both the software and hardware systems developed meet their requirements as set out at the start of this chapter. Now that the system architecture is in place and a electronic circuit stack is produced it is used as a basis for the conceptual design and prototyping of magnetic in-pipe robots in.

CHAPTER 6

Mechanical and Conceptual Design of Magnetic
Robots

This Chapter presents a detailed view into the design methods of magnetic robots, it will cover an overview of the robots capabilities, mechanical design, and power transmission. This chapter will incorporate the previously explored magnetic design, the electronic design as well as the control system and manufacture method. The chapter will start with basic mechanical concepts that were explored to find a suitable magnetic locomotion method for restricted space in-pipe applications.

6.1 Introduction

In Chapter 3 the challenges faced in the in-pipe environment were defined as requirements. It was determined a magnetic robot was most suited as a result of the decision matrix 3.5, and the optimal way to employ magnetic properties into a wheel design were explored in Chapter 4. With the groundwork complete for the necessary circuit design from Chapter 5 the electrical system can be built into prototype robot. The selection of prototypes to take forward will be those that make it through the initial concept design stages and into full test models. In Chapter 5, a preliminary selection of was made regarding suitable DC motors for the in-pipe robot. The motor was selected due to it's capability for interchangeable design and has been used as the model in the preliminary mechanical concept designs. Once the decision has been made to select one of the generated solutions a mathematical model will be produced. The model will focus on finding the required minimum force generated by the magnetic wheels and the torque required by the motors to turn the wheels at a minimum and to overcome the step cases as defined in the geometry requirements. A suitable gear ratio from the interchangeable motor designs can then be selected.

6.1.1 Conceptual Design Process

This chapter aims to integrate the previously designed wheel, and electronic systems into mechanical design concepts. To achieve this, many concepts with the potential to be brought into a further development stage are generated. During this chapter designs that either cannot complete the requirements, or those that do not provide a significant advantage over a preferable design will be systematically ruled out.

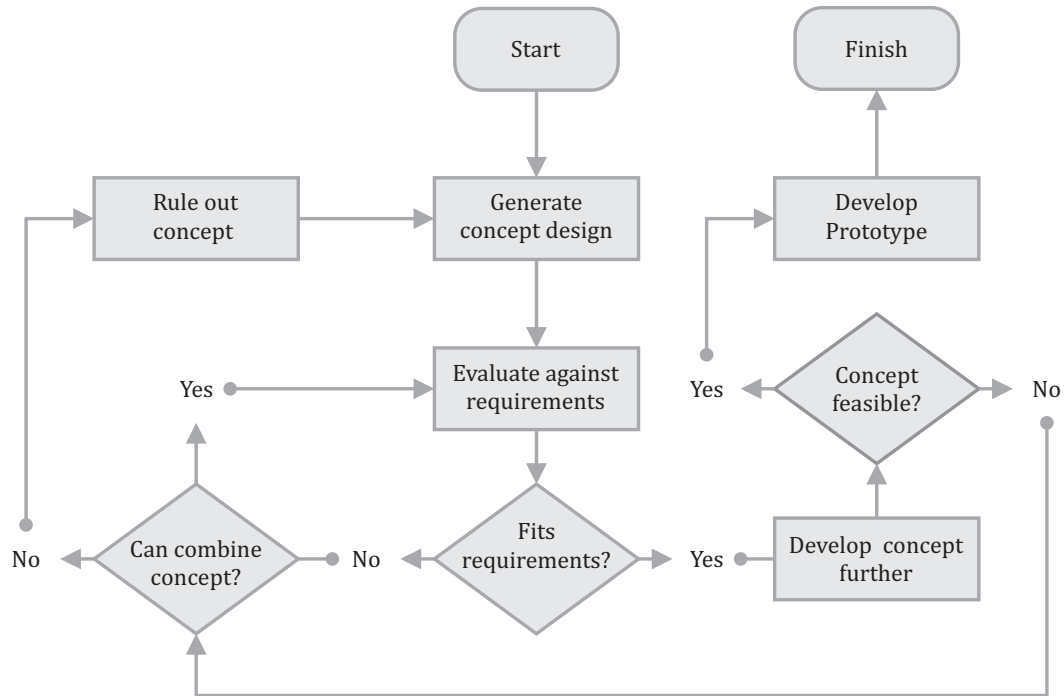


Figure 6.1: Flow diagram showing the conceptual design process used in this chapter.

6.1.2 Prototype Design Requirements

The robots volume must be used efficiently for navigation in the smaller 2-inch pipelines as defined and selected in Chapter 3. The aim of the concept designs should be minimise volume of mechanical components and therefore reduce complexity in the drive transmission system. The robot should also be able to complete concave and convex step-cases, the ability of concepts to perform these tasks will be reviewed after each design stage. The base components that form the robot communication and computation systems have been previously selected. These base components will form a significant portion of the robots total volume so for design flexibility the battery size will remain undefined. This will allow the battery to be reduced in size to create room for slightly larger transmission designs, providing they hold advantages over other more compact methods. Table 6.1 contains the currently defined information that will be used in the generation of concepts throughout this section. This will narrow the scope and allow the generation of concepts to be specific to the problem specification.

6.2 Mechanical power transmission and layout

Table 6.1: The currently defined requirements and parameters for use in concept generation and design.

Requirements	Defined in	Value/Notes
Function	Chapter 3	Enter a 2-inch pipeline, complete step-cases.
Steering capabilities	Chapter 3	Simple skid or tank steering, as well as reversing functionality.
Wheel design	Chapter 4	Two flux plate design with interior magnet array, diameter is variable.
Electronic stack design	Chapter 5	Volume of stack is defined, orientation of components flexible.
Motor number	Chapter 5	Two motors (minimum to fulfil skid steering requirement)
Software design	Chapter 5	LabVIEW control over Bluetooth serial.
Motor layout	Chapter 6	To be defined in current chapter
Transmission method	Chapter 6	To be defined in current chapter
Chassis design	Chapter 6	To be defined in current chapter
Battery size	Chapter 6	To be defined in current chapter

6.2 Mechanical power transmission and layout

6.2.1 Transmission design and motor layout

There are many methods of mechanical power transmission, in order to determine those that propose suitable solutions the methods must first be gathered. Considering power transmission methods, the most common methods selected are presented in Table 6.2. The table explores the layout combinations and the space efficiency in a particular pipe axis in all possible combinations of layout and transmission. The methods of power transmission are systematically combined with motor layouts in order to eliminate principles that are unsuitable for the final robot. The process of elimination will be defined first by functionality, and then by volume efficiency of the assembly in Table 6.3. There are methods that were considered but not included such as crown gears and

6.2 Mechanical power transmission and layout

helical gears as these mechanisms are nearly identical in terms of layout to spur and bevel/worm gears respectively and differ in only functionality.

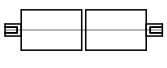
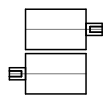
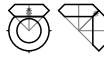
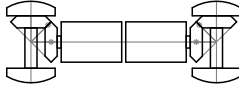
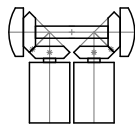
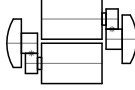
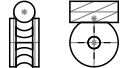
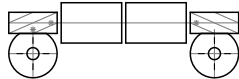
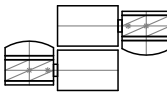
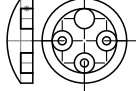
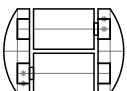
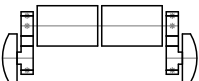
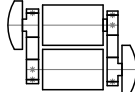
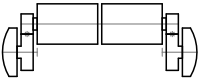
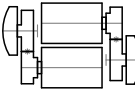
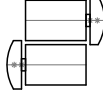
Transmission methods 1 to 4 use traditional mechanical gearing methods. Bevel gears can transmit torque at an angle but also produce thrust force along the rotation axis and therefore require a stopping mechanism such as a shaft collar. Spur gears produce no lateral thrust and are the simplest method of power transmission. Worm gears generally have high gear ratios and are difficult to back-drive which is useful for holding a magnetic robot when climbing vertically. Planetary gears are a combination of multiple small gears supporting a larger gear that acts as the wheel. One of the smaller spur gears is the drive from the motor, the remaining spur gears are idle and simply support the planetary wheel. Belt transmission is a combination of spur gears supporting a belt at each end with one of the gears being the driven pinion. Belt transmission (method 5) has the advantage of transferring torque over long distances without requiring a large gear train, its disadvantage is that it may require tensioning. Friction drive (method 6) is essentially the same as bevel or spur gear transmission except instead of gear teeth the contact point at the mesh, the force is transmitted through the friction of the materials on the belt faces. This has the benefit of providing slip at the gears in high torque circumstances, potentially saving gear teeth from shredding. Damage to the motor can also be prevented if the maximum torque transmission on the friction drive is balanced just below the maximum torque output of the motor. Slip can shorten the lifespan of the drives as the material wears, it also requires tightening which is a major downside in terms of space efficiency (requires a slot), they are also hard to manufacture relative to traditional gears. Direct drive is the simplest method of transmission as it only requires a mount to the motor shaft, the disadvantage is that the motor orientation dictates the layout of the robot. The transmission methods designed in Table 6.2 are intentionally simplistic and do not cover the possibilities of using combined transmission methods. The possibility of using combined systems will be explored if there appears to be a significant advantage.

Each possible transmission combination has been explored in Table 6.2, the criteria for success of the transmission design can be applied. The criteria are presented in Table 6.3 where they are given weighted score values depending on the performances of each design.

The criteria cover factors such as the overall size of the transmission assembly vs

6.2 Mechanical power transmission and layout

Table 6.2: Selection Table of Motor Layout against Transmission Design

Motor Layout Transmission Method	1 Co-Axial 	2 Parallel Axis 
1 Bevel Gear 	11 	12 
2 Spur Gear 	21 	22 
3 Worm Gear 	31 	32 
4 Planetary Gear 	41 	42 
5 Belt Drive 	51 	52 
6 Friction Drive 	61 	62 
7 Direct Drive 	71 	72 

6.2 Mechanical power transmission and layout

Table 6.3: Selection criteria used in the transmission decision matrix, Table 6.4 to choose optimal an design solution from Table 6.2.

Transmission design criteria	Score		
	1 - Low	3 - Medium	5 - High
Size vs motor	Greater than 100% motor	Neither small nor large	Less than 100% motor
Steering capability	Cannot steer (wheels in-line)	Large turning radius	Low turning radius
Min in-pipe radius	Large sub-optimal minimum radius	Neither small nor large	Small optimal pipe radius
Ease of manufacture	Difficult to produce	Neither difficult nor simple	Simple to produce
Step case negotiation	Impossible to climb	Neither difficult nor simple	Simple to climb

the motor size (It is required to be compact). Steering capability is required to move in the pipe so it is weighted accordingly. Minimum in-pipe radius refers to the driving direction of the robot, e.g. if the robot is long (co-axial design) the drive wheels can also be co-axial (design 21 in Table 6.2) or perpendicular (design 11). The minimum pipe radius of design 11 is half that of design 21. Design 11 has perpendicular wheels to its drive axle and can drive lengthways down the pipe with the width of just over one motor. Whereas design 21 has wheels with a n axle parallel to the motors axis and must drive head on with a width of over two motors (double the minimum in-pipe radius of design 11). Ease of manufacture refers to how simple this design is to produce, the components for this robot will be small and making bespoke belts and friction drives will be difficult. Some of these belt like drives such as those used in designs 51, 52, 61, and 62. These designs will also require belt tensioners to be built into the design and will take a considerable amount of volume within the robot assembly. Step-case negotiation ability is ideal and must also be considered at this stage, the transmission designs will be judged on how simple it will be to modify to overcome these obstacles. Generally designs need to have the capability to make wheel contact with walls at the central axis of the robot (so that corner cases do not cause a rotation of the robot).

6.2 Mechanical power transmission and layout

This is untrue for designs with one such as designs 22, 52, 62, and 72, with have wheels with a different offset axis. These robots would require large wheels such as designs 41, and 42 to make symmetrical wall contact and therefore make these designs redundant vs the planetary gear system. The values for each of these designs when compared against the criteria were scored in Table 6.4, the scores were then totalled in order to find the best suited designs to take forward into conceptual design.

Table 6.4: The decision matrix of used to select an ideal transmission design in conjunction with the criteria presented in Table 6.3, as well as the designs of the layouts 11 - 72 in Table 6.2.

	11	12	21	22	31	32	41	42	51	52	61	62	71	72
Size vs motor	1	3	3	3	3	3	1	1	3	3	3	3	5	5
Steering capability	1	3	3	5	1	1	5	5	3	3	3	3	3	3
Min in-pipe radius	5	5	1	3	5	5	1	3	1	3	1	3	1	3
Ease of manufacture	5	5	5	5	3	3	5	5	1	1	1	1	5	5
Step case negotitaion	5	5	3	1	5	5	3	5	3	1	2	1	3	1
TOTAL	17	21	15	17	17	17	15	19	11	11	10	11	17	17

From Table 6.4, the most suitable designs with the highest total points are designs 12 (score of 21), and 42 (score of 19). Many of the other designs averaged at a score of 17. Because of it's potential in a straight pipeline, design 11 will be chosen to go forward from the number of robots scoring 17. These transmission designs will form the basis of the concept designs taken forward in section 6.3:

- Design 11: bevel co-axial
- Design 12: bevel parallel axis
- Design 42: planetary parallel axis

6.3 Concept designs for a 2-inch pipeline

In this section concept designs will be created from previously selected transmission designs, electronic components, and custom designed chassis models. After systematic elimination of unsuitable principles via the decision matrix in section 6.2 three different transmission designs were developed further. These transmission designs are developed into a conceptual design with a focus on designs that will work in a 2-inch pipeline. The main focus of this first concept investigation is to enter the robot into a 50mm pipeline. For this purpose the robot will be designed with effective use of space as the main selection parameter, and with step-case negotiation taking a lower priority. The focus on 2-inch pipelines allows for initial concepts to solve basic design problems such as fitting the robot components within a 2-inch cross section. The first problem to focus on will be, fitting within a 2-inch pipeline. Each concept is designed in SOLIDWORKS as a master sketch base drawing. This typically involves drawing one sketch on each plane and drawing the intersections of motors and gear meshes. Modelling the prototypes in this way ensures that components fit. Placement of components quickly can be done using "blocks" within SOLIDWORKS. This function is useful as it creates an individual object from each sketch that can interact allowing you to create mechanisms and linkage design. The design process for creating these robot models using the transmission method as a base is as follows:

- Draw in the wheel rotation axis on a plane intersecting with the origin.
- Draw in transmission method e.g. bevel gear connection. Including Bearing seating and mechanical components such as shaft collars.
- Draw in wheel design this is done relative to target pipe size to maximise the magnetic force allowed through wheel volume without contacting the pipe boundary.
- Draw in motor placement.
- Draw in electronic stack from the wireless micro-controller circuit.
- Alter placement of components using drawing blocks to create a use-able layout.
- Generate Chassis around the layout that incorporates space for all components.
- Place connections and fastener points, e.g. slotting/push fit points, screw holes, and nut traps.

6.3.1 Concept 1: planetary spherical parallel axis

The spherical design presented in 6.2 is based on layout 42 in Table 6.2, a planetary parallel axis system. The motors are placed in a parallel layout and drive the two main wheels through a planetary gear. The planetary gears contain two idle passive gears which define the rotational axis of the wheels as the centre of the robot. Either side also contains a shield to place hold the wheels in place laterally. Design space for the magnetic wheels is reduced due to limited possible wheel space caused by motor placement and the planetary gear system. The steel flux plates would need a large internal diameter to account for the inner planetary gear, thus reducing the room for the magnetic array placement. This would result in a reduced magnetic force at the wheels vs the standard wheel design in 4.

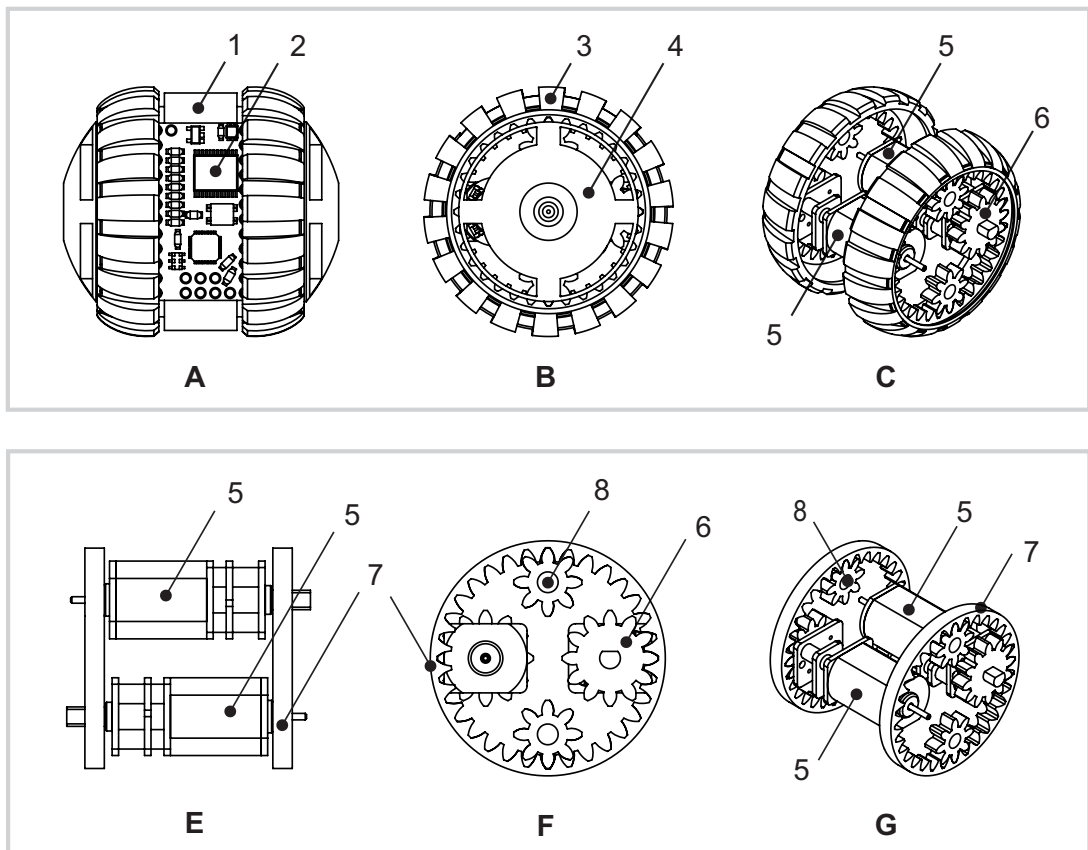


Figure 6.2: Robotic Concept 1: Spherical planetary design based on layout 42 in Table 6.2.

Table 6.5: Key design features in the spherical concept in Figure 6.2.

Part No.	Description
1	Battery storage area, including motor drivers.
2	Micro-controller unit for control with over Bluetooth.
3	Planetary wheel tread to increase friction on steel contact.
4	Planetary wheel guard stops lateral movement in wheel assembly.
5	DC motors in parallel configuration.
6	Planetary wheel drive pinion connected on to each DC motor.
7	Planetary outer wheel and magnetic array flux plate assembly.
8	Planetary wheel idle gears hold the main wheels stable in place.

Concept design 1 needs to be stabilised in the order to stop the chassis from rolling instead of the of the motors turning the wheels, there are a few ways to do this including gyroscopes, magnets, rear wheel [128]. An advantage of a completely spherical design is that it will fit in any pipe obstacle in a pipe diameter less than the diameter of the robot. This design would be suitable for both convex and concave step negotiation, however it would require a central magnet to keep the body in place or a small chassis extension to prevent the rotation of the motors simply rotating the chassis about the planetary gear. Steering would be performed using a tank style drive system, rotating one wheel to turn, or drive in opposite direction to rotate on the spot. The motor placement is in the y-axis of the pipeline which limits the accessible pipe width. The assembly is so large due to this that the robot is 49mm in diameter making it almost full bore in a 50.8mm (2-inch) diameter pipeline. This coupled with the need for magnetic wheel assemblies along the same axis in such a limited amount of space makes this design inefficient.

6.3.2 Concept 2: co-axial coupled drive and steering

The second robot concept design presented in Figure 6.3, is based on design 11 in Table 6.2. The robot is a co-axial bevel system with active motorised steering, the main issue with design 11 was its lack of steering capability. The key feature of this design is the inclusion of another set motors to enable coupled steering, the four motor system

6.3 Concept designs for a 2-inch pipeline

is shown in detail in 6.3. This concept investigates the increase in motor complexity to achieve driving and steering in a single shaft axis and essentially incorporates two model 11's stacked on top of each other. Because the two steering columns can be rotated independently they can be driven at the same time in opposite directions. As each motor turns the steering column a counter torque is applied to the robot, however if both motors turn in opposite directions the counter torques are cancelled and the body remains parallel in the pipeline.

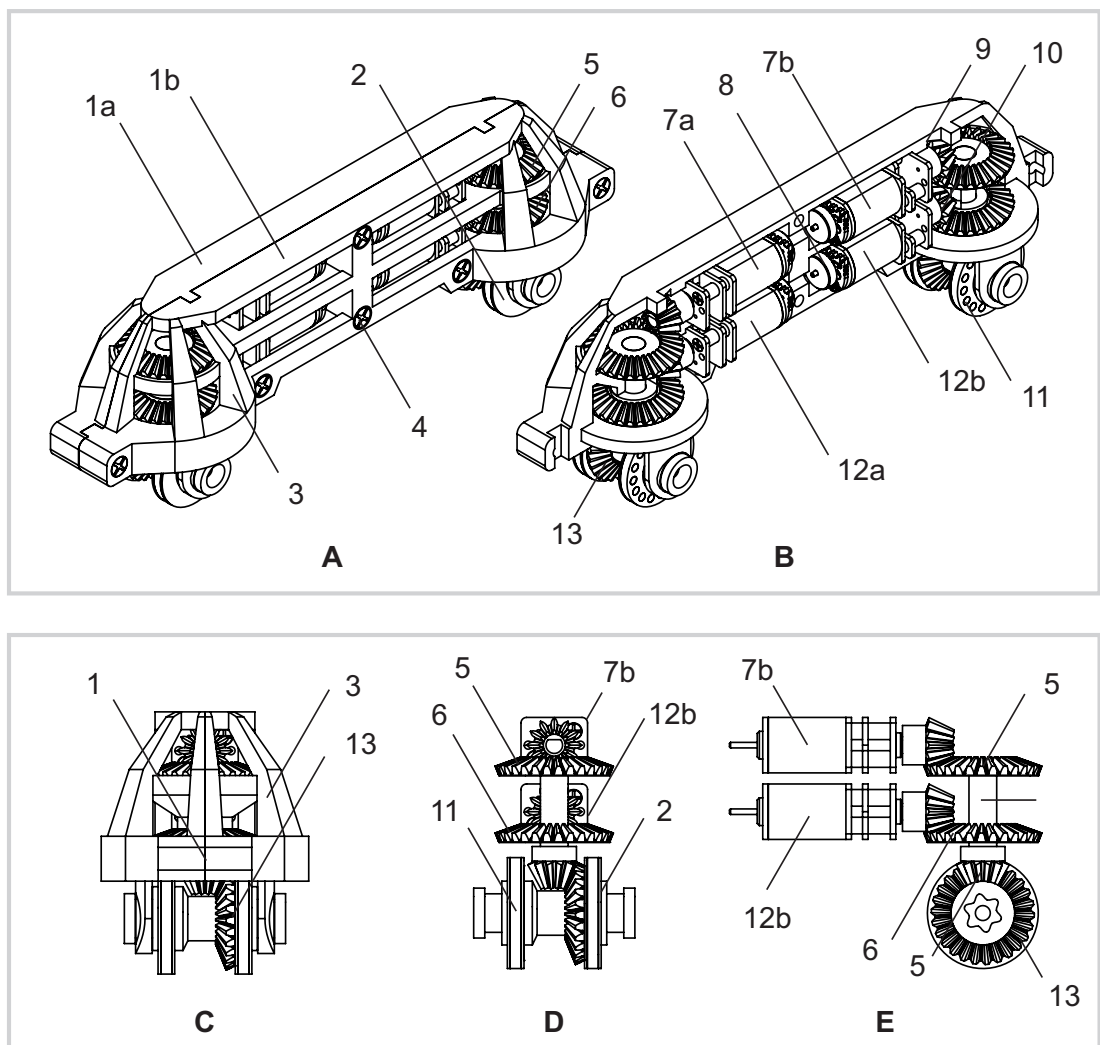


Figure 6.3: Robotic Concept 2: Based on layout 12 in Table 6.2, where the drive and steering are linked and then mirrored.

6.3 Concept designs for a 2-inch pipeline

Table 6.6: Key design features in the coupled drive and steering design in Figure 6.6.

Part No.	Description.
1a	Chassis 3D printed left half.
1b	Chassis 3D printed right half.
2	Early magnetic flux plate design (20mm diameter).
3	3D printed struts for support in the bevel housing.
4	Screws, six used in total to hold the design together.
5	Wheel drive bevel gear for the rear drive shaft.
6	Steering drive bevel gear for the rear steering column.
7a	Front wheel drive motor for the front column.
7b	Rear wheel drive motor for the rear column.
8	Encoder shaft and magnet reading pair.
9	Motor drive pinion for rear wheel drive bevel.
10	Motor steering pinion for rear steering bevel.
11	Magnet array in early wheel design.
12a	Front wheel steering motor for the front column.
12b	Rear wheel steering motor for the rear column.
13	Wheel drive transmission bevel.

This robots unique drive method requires the drive shaft to be mounted through the steering column in order to connect with the drive bevel of the wheel, shown in Figure 6.3.E. When manufacturing this part, it was 3D printed using non-assembly techniques to avoid any assemble of this tricky part. The steering column rotates the entire drive wheel around the drive shaft. This is made possible because the interaction between the drive transmission bevel and the shaft bevel are at 90° to each other. The 90° bevel connection allows rotation of one bevel around the other whilst maintaining constant gear mesh and putting no strain on the system. This robot was partially completed as a drive test model and as such does not contain any of the electronic stack design in the assembly. This robot would be driven using direct tether control, the addition of a wireless control package would be added at a later stage in the prototype development.

The concept presented some disadvantages in pipe negotiation. Turning was unstable when completely at a 90° angle for both motors because at this angle the body of the chassis was free to rotate about the now shared rotation axis for both wheels. This problem could be overcome by the installation of stabilisers in the form of either struts off the main 3D printed bodies 1a and 1b in 6.3, or through extra magnetic base points for stability. The magnet wheels themselves were early prototypes of the magnet wheels developed and refined in Chapter 4, larger magnets would be required in order for this design to be viable, and hence more space would be required for the wheels. The robot is 152mm long, roughly three times the specified diameter of the pipe. This is due to the addition of two more motors to allow steering, this extra length reduces the maximum in-pipe radius that can be completed by the robot. However the steering method does allow travel around a pipe without rotation of the robots body, this allows the robot to tackle corners by following the easiest path. This robot would not be capable of completing either a convex or a concave step case due to it's geometry. The wheels of the robot can only directly contact a wall case when turned at a complete right angle and hence only in a pipe larger than roughly 200mm in order for it to turn side-on.

6.3.3 Concept 3: bevel spur gear parallel axis

This concept design is based upon layout 12 in Table 6.2 and contains a bevel drive spur shaft gearbox in a vertical parallel configuration. Due to the size constraints when designing the robot for a 2-inch diameter pipe, the motors were mounted perpendicular

6.3 Concept designs for a 2-inch pipeline

to drive-shaft and the wheels vs the standard configuration in layout 12. The change from horizontal to vertical alignment allowed for the design of smaller transmission shafts to the main wheels, however it also meant the wheels rotation axes were no longer in the same plane as the drive motors. In order to rectify this problem the torque is transferred to the bevel drive shafts and then from a spur gear to the main wheel axle seen in Figure 6.4.D and 6.4.E. Each drive-shaft transmits power through the spur gear on the opposite side to drive the wheel with a transmission ratio of 1.2:1. These sections are 3D printed, they are assembled with 5mm I.D. 8mm O.D. bearings which are push fit into the chassis during assembly. These allow smooth rotation and locating the centres for transmission assembly, keeping meshing distance of the gears constant. Although the motors are interchangeable depending on the desired gear ratio the current 250:1 motors used in this concept allow a max wheel speed of 80 RPM. Dimensions of the robot concept can be found in Table 6.9.

The main body of the robot is printed as two separate halves (Figure 6.4, 11a and 11b) and screwed together after the addition of motors, electronics and battery. The prototype was formed using Objet material VeroWhite (60g) and Tango+ (4g) as well as breakaway support (186g) to form a complete model. The total build time for one robot is three hours:45 and requires an hour of support cleaning from surrounding material due to the delicacy and small size of the robot parts. Shown in the Table 2 is the bill of materials required to assemble the robot. The price is quoted as £171 to produce one unit, however the printing costs for the chassis account for 66% of this price. This price is based on the production of one robot, charged at a £25 hourly rate for use of the Objet 1000 printer and a printing time of 3 hours. These costs could be reduced if the robot were to be printed in batches.

The wheel design is presented in Figure 6.5, this was the second magnetic wheel design created for use in a concept pipe robot, the first being in concept 2's. Changes were made to this wheel including a 3D printed soft material sleeve built into the wheel array (2), and an endcap piece to clamp the assembly. This end-cap also has a rubber like 3D printed coating to increase traction at the pipeline when in magnetic contact. The wheel in the exploded view is screwed together to fully define movement laterally, the screw holes line up because of the wheel to drive spur gear meshing point (9). This meshing point is simply a 2D spline that is matched on each subsequent part of the assembly when drawn in CAD, but when 3D printed ensures the assembly is built in the

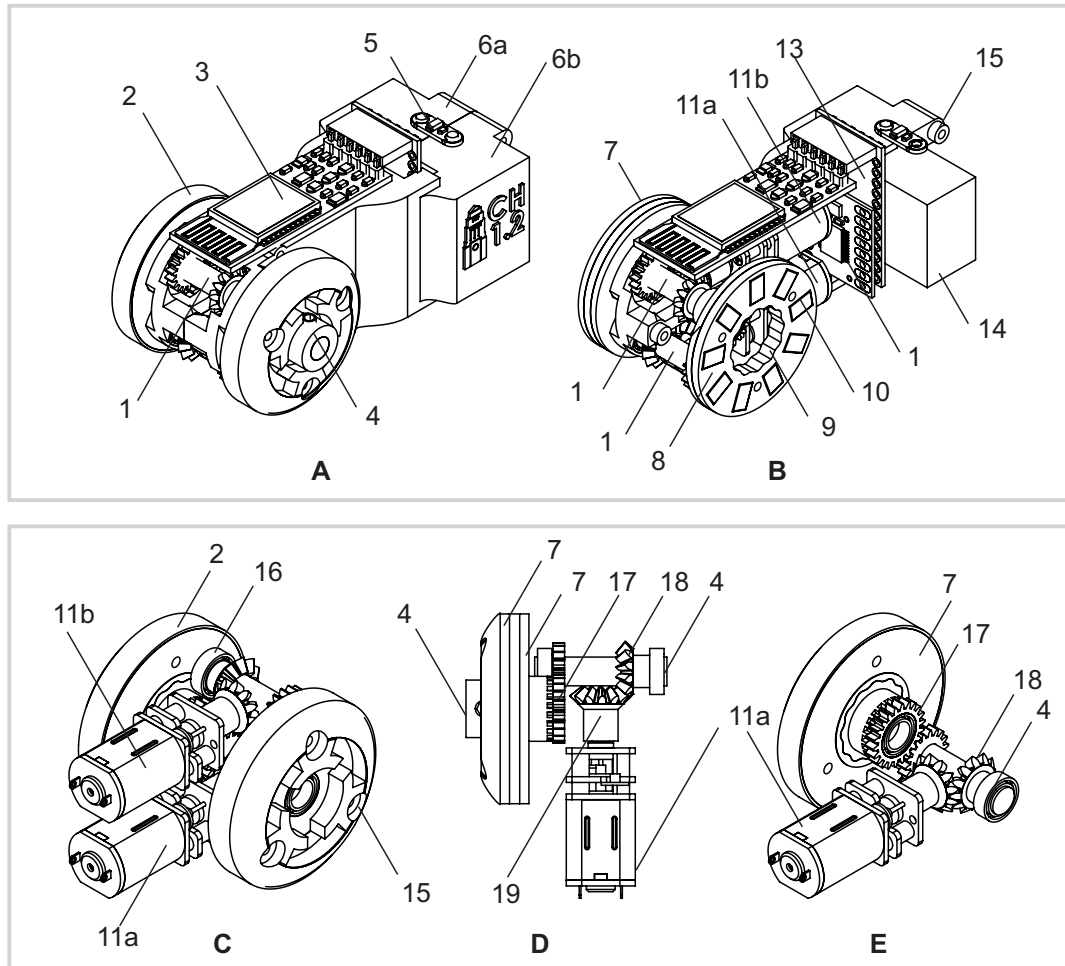


Figure 6.4: Robotic Concept 2: Based on layout 12 in Table 6.2, with an combined spur gear transmission axle.

correct orientation. The array of 9 magnets was used to fit a much magnetic surface area as possible within the plates, but was limited by the addition of the clamping screws. The 3D printed magnetic array holder and spacer (8) ensures the distance between the magnets is equally spaced and remains shielded between the flux plates in accordance with the specification set out in chapter 4.

6.3.4 Prototype development

Once the three 2-inch magnetic pipe robot prototypes had been designed, one of the concepts was selected to move on to the prototyping stage. It was important to select

6.3 Concept designs for a 2-inch pipeline

Table 6.7: Key features in concept 3, bevel spur gear parallel axis design in Figures 6.4 and 6.5

Part No.	Description.
1	Transmission shaft with bevel and spur gears
2	Rubber wheel coating to increase friction
3	Bluetooth Smirf module for wireless coms
4	Shaft collar 5mm I.D
5	Status Lilypad LED
6a	3D printed chassis left half
6b	3D printed chassis right half
7	Steel flux plate
8	3D printed magnetic array holder and spacer
9	Wheel to drive spur gear meshing point
10	Sparkfun motor driver breakout board 1.2A peak
11a	6x4x2mm magnet (0.75kg pull each)
11b	Left wheel drive motor
12	Right wheel drive motor
13	Arduino pro mini 3.3V
14	Turnigy nano-tech 7.4V 260mah battery
15	Screw connection point, 6 in total
16	8mm O.D 5mm I.D shielded bearing
17	Drive spur gear for transmission to the left wheel
18	Transmission bevel from bevel pinion to shaft
19	Bevel pinion from left wheel drive motor

the most promising robot to build into the physical model. To determine the robot with the most potential the robots in their concept CAD model stage were compared with using the criteria presented in Table 6.8.

All concepts would be capable of the basic manoeuvres of driving in a 2-inch pipeline and completing multi-directional steering however space available for magnetic wheel space design varied greatly. Concept 1 (Figure 6.2) due to its planetary design would

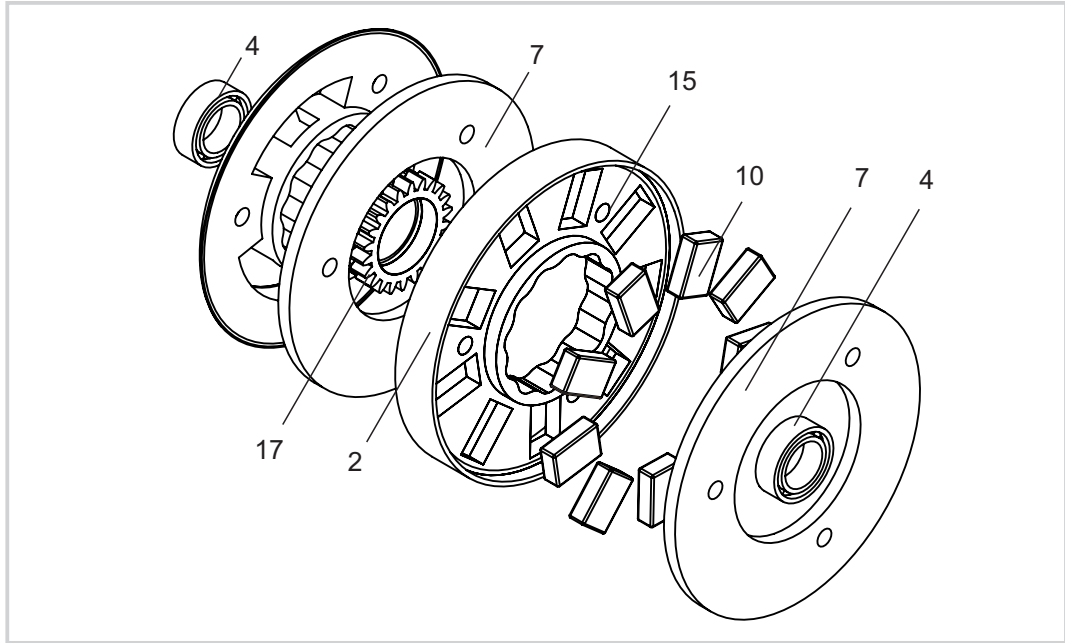


Figure 6.5: Exploded view of concept 3 early wheel design.

have room for large outer diameter flux plates (32mm), however the inner diameter would be greatly reduced to avoid hitting the chassis and idle gears. Concept 2 (Figure 6.3) has room for only 20mm wheels, and with greatly reduced flux plate and magnet thickness due to the complex bevel transmission design. Concept 3 (Figure 6.4) has wheels placed outside the width of the robot chassis and contains no internal mechanisms hence has the highest workspace volume for wheel design. Stability is poor in concept one due to its lack of a rear wheel, the robot relies on a magnetic chassis to keep it from moving in relation to the wheels. The magnetic force would have to be very large to keep the chassis from rotating due to the counter torque applied at the wheels. Stability of concept 2 is also poor due to the turning mechanism, as the robot approached 90° at the wheel the chassis is free to rotate around the turned wheel axis, stability modifications would need to be made to make this viable. Concept 3 has average stability, it is stable only in certain situations such as horizontal driving, verticals when the body is facing upwards. This is because the design has no rear magnetic wheel and as such the body is free to rotate about the wheel axis when in an unbalanced position.

Concept 1 does not have sufficient space for a battery due to the volume needed for

6.3 Concept designs for a 2-inch pipeline

Table 6.8: Selection criteria to choose concept to carry to prototype development

Criteria	Concept 1	Concept 2	Concept 3
Fits in 2-inch pipe	✓	✓	✓
Multi-directional steering	✓	✓	✓
Magnetic wheel space	Average	Low	High
Potential chassis and wheel stability	Poor	Poor	Average
Sufficient space for components	Low	Average	Good
Potential to complete concave (2-inch)	✓	✓	✓
Potential to complete convex (2-inch)	✓	✗	✗
Advance to prototype development?	✗	✗	✓

the parallel axis motor design and the spherical limitation. The limit for battery size has already been reached for a 2s lipo (40mm x 19mm x 15mm), a potential solution to this would be to place two 1s batteries in series however this would make charging impractical. This concept may show promise at a larger scale or with a modified and extended body for more space but when the design is extended there are better choices for transmission. Concept 2 also has poor component space, the four motors take up the majority of the robots volume. Components would be place on the sides of the robot, this would be enough for the electronic stack however the battery would prove difficult just as in concept 1. Concept 3 space at the rear of the robot for components, however increasing the length of the robot decreases the lowest possible radius bend it can complete. Concept 2 is the only robot incapable of completing a concave step case in a 2-inch pipeline, this is because there is no wheel clearance from the chassis and thus would never be able to touch the concave wall with the magnetic wheels. Concept 1 is the only robot with the potential to overcome a convex case in a 2-inch pipeline as it has no rear end or second wheel with the possibility to crash into the curve.

The result of the comparison is that concept 3, the bevel and spur gear parallel axis design should be taken forward to prototyping. The design of the concept robot to fit inside a 2-inch pipeline is pushing the limits of the volume available as shown in Figure 6.6. The gap between the wheel and the pipe (1) is just 1mm, and the gap between the beneath of the robot and the pipe (2) is 8mm. It is shown at 6.6-3 how the wheel end-cap interacts with the pipe to increase wheel contact surface area to reduce

6.3 Concept designs for a 2-inch pipeline

Table 6.9: Dimensions of the CH12 approximate volume.

Length (mm)	Width (mm)	Height (mm)
85.10	46.88	38.65

slippage of the robot. This contact is specific to 2-inch pipelines and is used to make up for the single point of contact at the main magnet wheel on each side of the pipe. This contact is not present in pipes larger than a 2-inch diameter but is moderated by the increased contact of the magnet wheels, e.g. in a large 1m diameter pipe flux plates will be in contact and the wheel will have full force range through the rubber Tango material. The full maximum dimensions of the robot are presented in Table 6.9. In Figure 6.7, images of the completed robot prototype are presented fully assembled with all components present in isometric view (A) and frontal view (B).

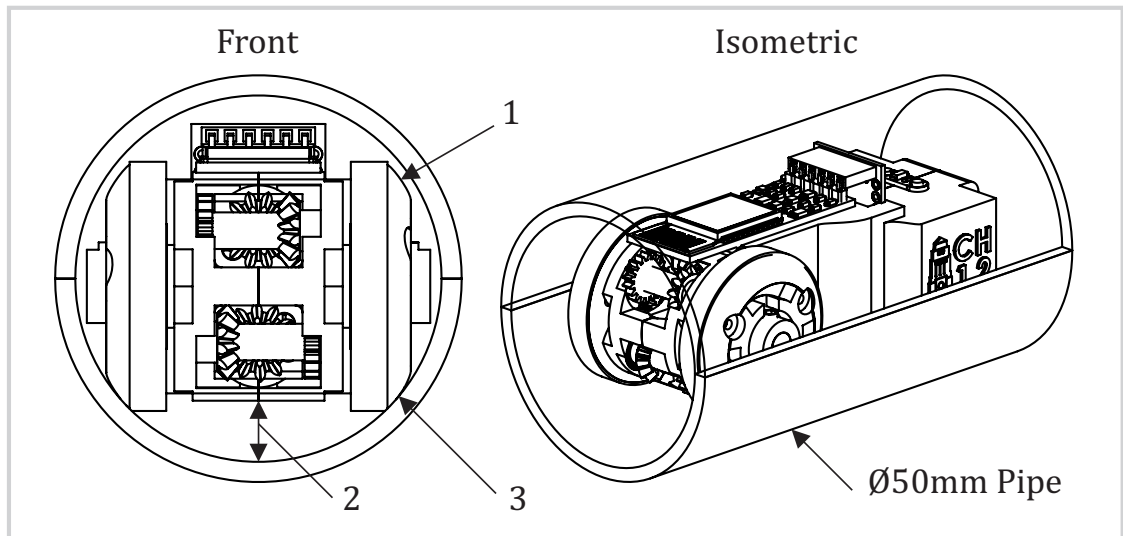


Figure 6.6: In-pipe design of the 2-inch concept, avoiding double wheel contact with both walls.

The components used to build the magnetic in-pipe robot are listed in full in 6.10. Components which were design and manufactured in house consist of all 3D printed parts, and the steel magnetic flux plates which were discussed in 4.

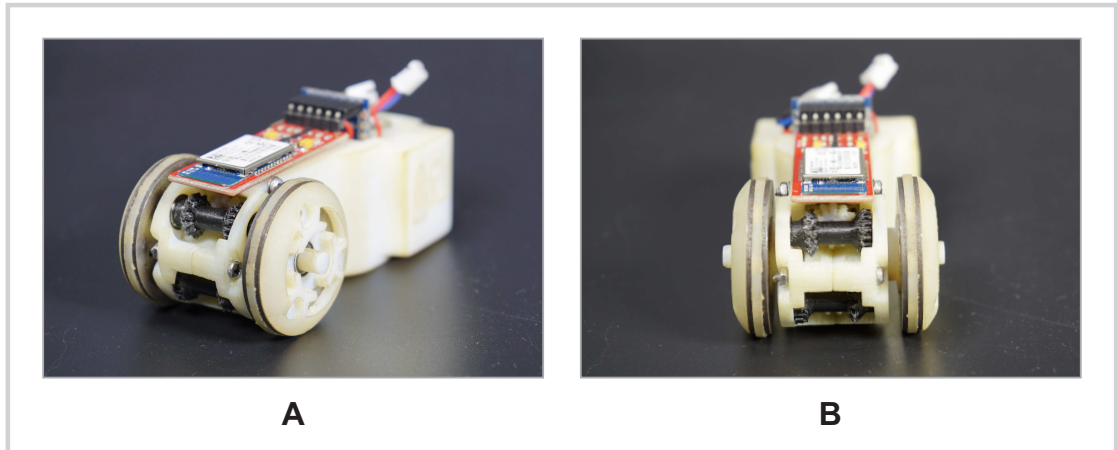


Figure 6.7: In-pipe design of the 2-inch concept, avoiding double wheel contact with both walls.

6.4 Concept and prototype for step case obstacles

Concept 3 was selected for a 2-inch pipeline, however it was still unable to complete the convex step case. The robot must be able to complete the convex case to perform inspection and exploration of all in-pipe geometry. Because concept 3 is at its limit for space in a 2-inch pipeline (Figure 6.6) this design must now be modified with the removal of the 2-inch constraint. Removing the space constraint will allow for the design of a system capable of both concave and convex cases. In order to access a concave case a front portion of the wheels must be left open to wall contact at the edge of the design. This is a necessity for wall-climbing, if direct wheel contact cannot be made with the target wall due to chassis interference than this requirement will not be fulfilled. As well as this, in order to remain stable the robot must maintain contact with the pipe at the rear of the chassis to halt rotation of the body around the wheel axis. Maintaining constant magnetic contact whilst moving around a convex corner poses a problem which is shown in Figure 6.8-A. This section will first look at how we can overcome curved convex step case problems without crashing the robot or losing wheel contact in attempt to rectify the problems faced by concept 3 in this regard. The robot will be simplified to a 2D model with open wheel contact at the front and rear wheels for step case movement and no presumed boundary on the space required for electronic components.

6.4 Concept and prototype for step case obstacles

Table 6.10: Final Concept: Bill of Materials

Part No	Component	Quantity	Mass (g)	Price
1	Pololu MicroMetalGear Motor 250:1	2	20	25.8
2	Arduino Pro Mini 328 - 3.3V/8MHz	1	2	8.0
3	Bluetooth Smirf Mate Silver	1	12	20.0
4	Motor Drive TB6612FNG	1	2	7.2
5	Arduino LilyPad LED	1	0.25	1.1
6	Turnigy 260mah 2S 35~70C Lipo	1	14	4.1
7	3D Printed Left Chassis	1	12	23.1
8	3D Printed Right Chassis	1	12	23.1
9	3D Printed Motor Shaft Gear	2	1	1.9
10	3D Printed Drive-Shaft	2	2	3.8
11	3D Printed Wheel Hub	2	9	17.3
12	3D Printed Wheel Magnet Array	2	3	5.8
13	N42 Grade Magnets 6 x 4 x 2mm	18	8.1	5.0
14	Steel Magnetic Flux Plates	4	30	20.0
15	Steel Bearings MR85zz 5x8x2.5mm	8	3.2	3.8
16	Shaft Collars 5mm	2	6	0.8
17	Screws/Nuts/Washers	72	7.2	0.1
	TOTAL	121	143.75	170.9

6.4.1 Optimal curvature

The simplification of in-pipe geometry problems to step cases was earlier 4.1. It showed how the issue of complex in-pipe geometry can be simplified to concave and convex step cases as a worst case scenario. The chapter discussed the issues of overcoming the two cases and the problems faced when using magnetic traction methods and defined wheeled locomotion as the primary suitable method for the in-pipe robot. During the conceptual design phase the mechanical considerations of the robot must be considered when travelling around these two obstacles. The layout and transmission design of the robot will have a significant effect on the way these problems are tackled so the design limitations in each case should be considered.

6.4 Concept and prototype for step case obstacles

Now that the robot has been developed further it must be tested against these step-cases. For safe completion of all step cases in any possible in-pipe orientation, the next version of the robot should have a magnetic wheelbase in constant contact with the pipe. The robot is unstable in the transition from upside-down orientation to 90 degree and cannot drive forwards facing down due to its lack of a rear magnet. To avoid this in the future a rear magnet must be attached to stop unstable chassis rotation about the front wheel in this transition case.

The initial concept designs presented in section 6.3 do contain appropriate geometry for convex step case negotiation. It is not possible for the two-inch concept robots to complete a convex case as they encounter interference shown in Figure 6.8: A. For the robots to complete this case they must force contact loss at W_2 .

For the completion of this obstacle it was necessary to modify the future designs with ground clearance between the wheelbase to avoid contact with step-case when moving around the corner as in Figure 6.8, (A). This could be done with a simple gap (6.8, B), but in order to maximise the space available for the robot the optimal curve for convex movement can be found as in (6.8, C). This modification to the chassis and wheelbase frame does require that the two-inch specification limit must be broken. The next robot will be designed two solve all of these cases whilst keeping the robot as compact as possible.

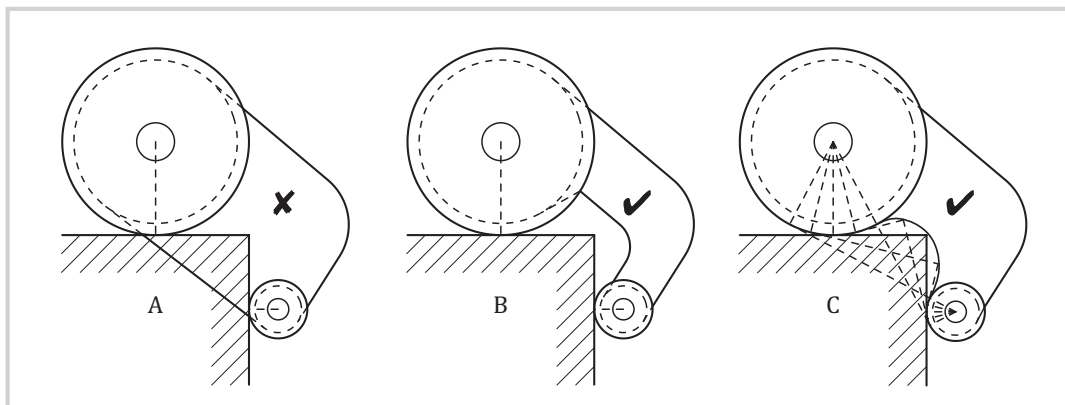


Figure 6.8: Chassis interaction with a convex curve case. Robot A: standard chassis design. Robot B: estimated clearance design. Robot C: optimally generated clearance curve.

Figure 6.9 presents a diagram of a two wheel simplified robot model, with the

6.4 Concept and prototype for step case obstacles

geometry required to build an ideal curve spline. The method to create the spline begins with choosing the two wheel radius r_{w1} and r_{w2} , and the length of the wheelbase of the model L_{wb} . Because this is the absolute minimum curve, a safety factor S_f is necessary to apply to r_{w1} to allow a gap between the corner and the underside of the robot chassis. The curve is generated between these two smaller wheels, a line is drawn from C_{w1} to $w2$ that is tangent to the rear wheel. Another tangent line is drawn from C_{w2} to W_1 , the points where these lines intersect the wheel on W_1 : p_{11}, p_{51} and on W_2 : p_{12}, p_{52} mark the range of points that the wheel comes into contact with through its rotation of 90° about the convex corner. To define points on the spline tangent lines are drawn from W_1 to the opposite tangent point on W_2 , this can be done for any number of points to further define the spline, five points are used to generate the curve in Figure 6.10.

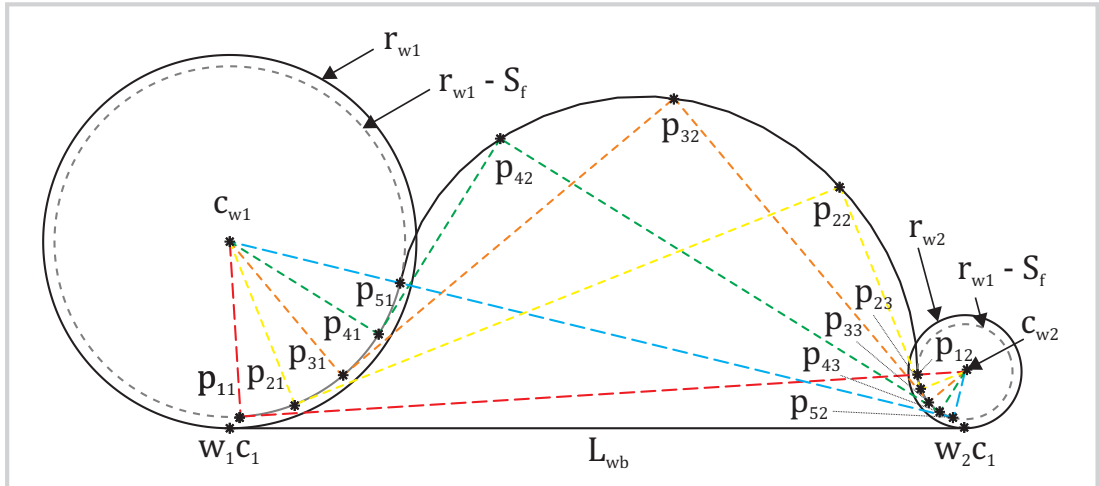


Figure 6.9: Minimal contact curve generation for convex step-case, example using a 32mm front wheel, 10mm rear, and 65mm wheelbase.

The parameters used in the generation of the optimal curve in 6.10 are presented in Table 6.4.1. Once the geometry has been created it is used in SOLIDWORKS as a basis to build a chassis for the robot. It also shows how an increase in the wheelbase of the robot can drastically increase the required ride height of the chassis during normal operation.

This curve is generated specifically for the convex case, however there are specific cases where a curve must also be used on the top section of the robot. Specifically in

6.4 Concept and prototype for step case obstacles

Robot Curve Generation Parameters	Value (mm)
r_{w1}	32
r_{w2}	10
S_f	1
$L_w b$	65

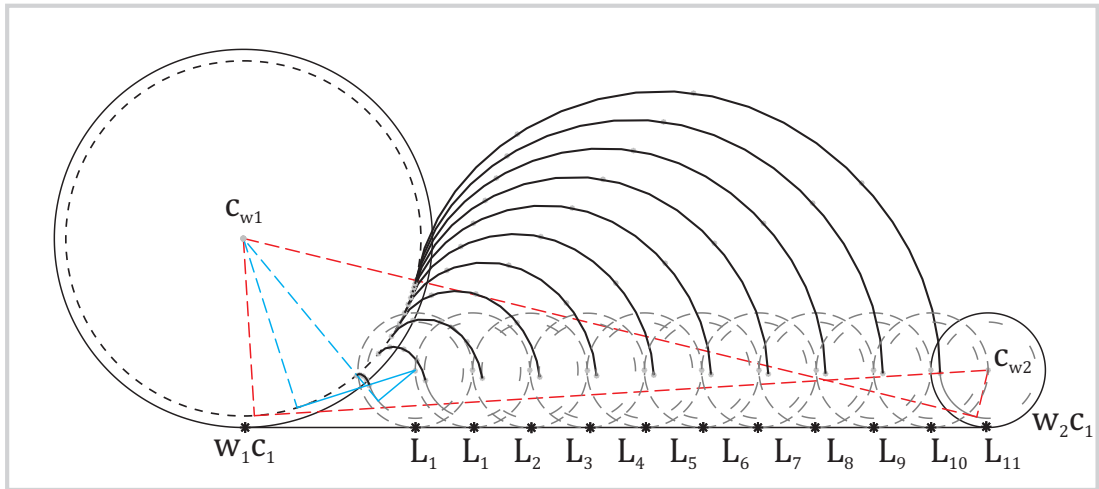


Figure 6.10: Change in curve generation with an increase in the wheelbase of the robot.

Wheelbase	L_1	L_2	L_3	L_4	L_5	L_6	L_7	L_8	L_9	L_{10}	L_{11}
Length (mm)	15	20	25	30	35	40	45	50	55	60	65

the case of a large robot moving through a small relative diameter pipeline and coming to a concave case. In this concave case the outer convex corner partnered with the concave case causes need for a curve to avoid collision. In a relatively large pipeline this does not matter as the body is always clear.

The curve generation method was created using SOLIDWORKS, this has since been replicated mathematically in MATLAB, the script works out many tangents to create a spline defined on a number of points defined by the user, this removes the need to draw many tangent lines by hand.

6.4.2 Concept 4: bevel with rear wheelbase

The concept 4 robot presented in Figure 6.11, and the part description for each label is given in Table 6.11. The robot is based upon concept 3 (6.3.3) and has been modified with the added information learned from studying the curvature for convex cases required in section 6.4.1. The robot maintains the dual bevel drive transmission design in an identical layout configuration to 6.2.

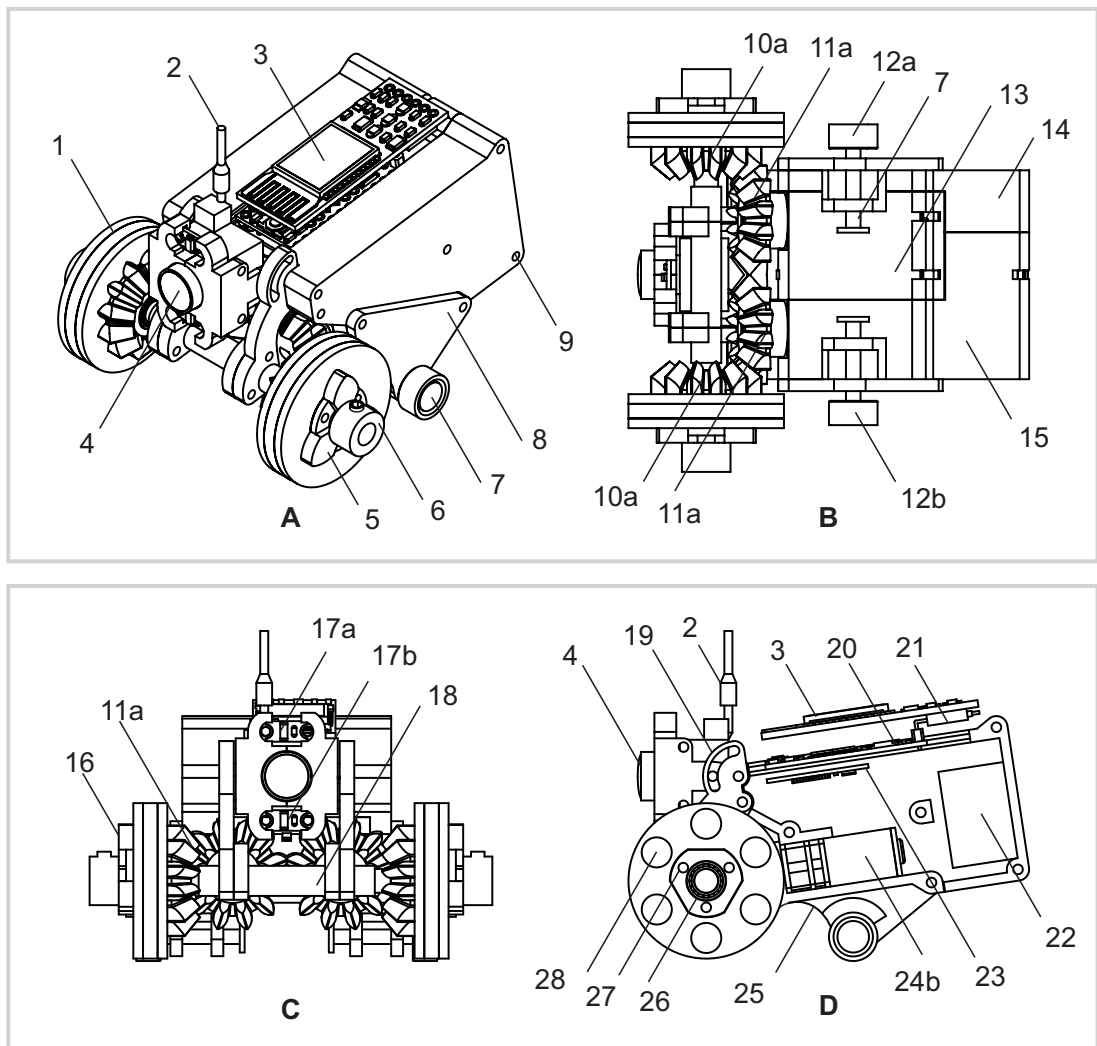


Figure 6.11: Schematic diagram of the robot dual bevel robot with rear magnetic wheel.

The space constraint of a 2-inch pipe has been lifted so a simple layout is all that was needed, the gearbox transfer in concept 3 is no longer required. This also removes the

6.4 Concept and prototype for step case obstacles

need to print small 1mm module spur gears to transfer to the main wheel drives. The torque from the motors can be transferred through the bevel gears at a 1:1 transmission ratio. The circuit stack used is the same, as well as the motor choice and ratio, and the battery is the same model 260mah LiPo. A 3.3V FPV camera has been added for visual inspection and feedback during operator driving, this will allow the operator to square up to a concave or convex step case and ensure the robot is perpendicular before driving forwards. This is necessary for remote operations where the robots position relative to the in-pipe geometry problem cannot be determined through line of sight. To assist in dark conditions, two LED headlights have been fitted to the custom camera mount in Figure 6.11 at parts 17a, and 17b. The camera is attached at the head of the chassis body and has an adjustable mount that uses a slider design (part 19) a screw through the slider secures the camera at the required angle. The FPV camera is not integrated into the main robot circuit and is powered from a separate 1S LiPo which is not shown in Figure 6.11, this will battery will be placed above the motors (24b) and beneath the motor driver (23).

6.4 Concept and prototype for step case obstacles

Table 6.11: Design of concept 4: a dual bevel connection robot with a rear magnetic wheelbase and curve for convex case locomotion.

Part No.	Description.	Part No.	Description.
1	Magnetic flux plate	15	Right chassis section
2	FPV camera antennae	16	Bearing mount
3	Bluetooth Smirf COM	17a/b	Camera LED's
4	FPV camera 3.3V	18	Wheel shaft connector
5	Wheel clamp	19	Camera tilt adjustment
6	Shaft collar 5mm I.D	20	Arduino pro mini 3.3V
7	Rear magnet shaft	21	Connection pins
8	Rear shaft chassis mount	22	Battery 2S LiPo 260mah
9	Screw holes	23	Motor driver
10a/b	Wheel drive bevels	24b	Left micrometal motor
11a/b	Motor pinion bevels	25	Convex curvature
12a/b	Rear magnets 10mm	26	Bearing 5mm I.D
13	Motor chassis section	27	Wheel flux plate shaft
14	Left chassis section	28	Magnet array 6mm

The magnetic wheel design on concept 3 uses the latest wheel model, the triangular hole in the centre allows the 3D printed shafts to be fitted and stops turning of the wheel without the need for screws required in concept 3 wheel design shown in Figure 6.5. Because of the lack of screws the magnetic wheels are clamped using part 5, and screw into the ends of the wheel shafts (part 27). The overall dimensions (x,y,z) of concept 4 are 84mm x 54mm x 84mm, this allows the robot to fit within a 4-inch (101.6mm) pipeline. The main modification to this design is the addition of rear wheel magnetic base in accordance with the optimal curvature generated in 6.4.1. This will allow this robot to move around convex obstacles without interruption. The rear wheel chassis housing (part 8) is removable and can be swapped out for different designs with different wheelbase lengths. Within this chassis is a free to spin rear axle (part 7), and on the end of this shaft is a 10x5mm N42 neodymium magnet (axially magnetised) that keeps the chassis from rotating in orientations where gravity is not in favour (upside-down). Like concept design 3 this robot will be taken forward to a full prototype build

in order to test the performance of the system on in the real word. The prototype robot has been 3D printed in PLA using a BCN3D Sigmax 3D printer, it is presented in Figure 6.12 with a front view (A) and isometric view (B).



Figure 6.12: Schematic diagram of the robot dual bevel robot with rear magnetic wheel.

6.5 Discussion and conclusion

In this chapter the mechanical design and overall layout of the in-pipe robots was considered. The most important criteria as defined in chapter 3 in terms of concept design of concepts were used to determine the focus of the robots. Initially this was deemed to be the overall volume of the robot in keeping with the original aim to develop an in-pipe robot capable of entering a 2-inch pipeline. Designing a robot to drive inside a 2-inch (50.8mm) diameter places many constraints on the design which make it inefficient to use standard four wheel configurations. The transmission methods were found to have the biggest impact on the layout of the robot and so three different concepts using three different transmission layouts were designed in CAD software. The designs were compared against criteria to assess their feasibility as potential prototypes and the most promising (concept 3) in section 6.3.3, was chosen. This was the most suitable of the 2-inch robot designs, however concept 3 would still be unable to complete convex pipe sections. The necessary geometry to move around convex corners whilst maintaining magnetic contact with the pipe is difficult in small diameter pipelines. It is impossible for a robot like concept 3 to complete a case convex step-case due as its chassis crashes with the corner case and does not allow the magnetic wheels to get

any purchase. A gap must be present between the wheel and the rear contact point of the chassis in order to allow the wheels over the edge. The geometry necessary to complete this case was investigated and an ideal curve to avoid convex contact was proposed. This ideal curve cannot be applied to the 2-inch concepts without breaking the size constraint set by the pipe as the concepts already use the bulk of the pipe with electronics and mechanical transmission systems. In order to apply the curve and design a robot that could possibly complete both concave and convex obstacles the 2-inch constraint was lifted and replaced with the criteria of "complete all obstacle cases". This lead to the conceptual design and then prototype development of concept 4 in Figure 6.11. Concept 4 is taken forward into chapter 7 to undergo experimental testing to determine performance when tackling these obstacles.

CHAPTER 7

Robot Obstacle Statics, Experimentation and
Evaluation

This chapter brings together the work from preceding chapters and combines the knowledge gained into one functional prototype. This final prototype is mathematically analysed in static and dynamic conditions attempting step-case problems. The robot is tested experimentally to determine the limits of its functionality when moving around concave or convex cases in different orientations. After assessment the robot is deployed into real world in-pipe environments.

7.1 Introduction

This section will bring together the work done in the previous chapters to experimentally test the final prototype version of the robot. The presented final prototype is a mobile platform for magnetic locomotion of any standard ferrous structure both in-pipe and out-pipe. In this chapter the effect of changes in vehicle parameters on the static and dynamic models will be investigated to determine the optimal solution for obstacle negotiation in the cases of concave and convex bends.

The magnetic robot consists of two sets of wheels with reaction forces, the rear wheels are free to spin and assumed frictionless, the front larger wheels are driven by a single DC motor each. The robot is stable and at rest when placed in any orientation on a steel plate it is even capable of hanging upside-down (inverted). Static friction from the motor's gearbox coupled with the frictional force at the wheel contacts prevents movement of the robot on a any plane. The robot never enters sliding friction in practice as the weight of the assembled robot is 0.12kg and the wheels are operate at forces of well over this 1.56N limit. Because the vehicle is magnetic, there a constant force at the contact point of the wheels acting perpendicular to the surface, assuming the material is ferrous.

7.2 Overcoming step-case obstacles

In this section the mechanics of the robot climbing both a concave and a convex step case will be explored. In these cases a right angle step will be used in the most challenging orientation. For the case of the concave step this will be from $0^\circ - 90^\circ$, and for the convex case it will be $90^\circ - 0^\circ$. In a real world environment these step cases can exist in any orientation in-pipe, the variables that change in these other cases are the direction of gravity, and a change in weight distribution. These cases are assumed to

be performed in large diameter pipes (>1m) such that the pipe is so large it can be assumed the wheel contact points share the same in-pipe height. Maximum torque at the motor is based on a 250:1 MicroMetal Motor [27] from the motor torque table selected in 5.5.

Cases will be considered statically at most points around the obstacles to determine forces present in the robot at each stage of movement. When taking moments about a point on the robot it is important to note that every magnetic force is balanced by its own reaction force at the point where it acts in contact with the wall. The only forces that are considered in the calculation of the system are the weight of the robot and the force of the torque from the motor. The magnetic forces are re-applied later. Moments in the y-axis are taken around the robots centre of gravity, (CG). All cases have been solved using the planar static equilibrium equations as a basis in equations 7.1, 7.2, and 7.3. Standard equations used in this chapter are also completed from equation 7.4, to 7.11.

$$\sum F_x = 0 \quad (7.1)$$

$$\sum F_z = 0 \quad (7.2)$$

$$\sum M_y = 0 \quad (7.3)$$

$$RPS = \frac{RPM}{60} = 120/60 = 2 \quad (7.4)$$

$$Tm_{max} = 0.33N - m \quad (7.5)$$

$$G_{ratio} = \frac{r_p}{r_g} = \frac{0.008}{0.008} = 1 \quad (7.6)$$

$$F_{axle_max} = G_{ratio} \cdot (Tm_{max}/r_p) = 0.33/0.008 = 41.2N \quad (7.7)$$

$$F_{w1_max} = \frac{F_{a_max} \cdot r_g}{r_{w1}} = \frac{20 \cdot 0.008}{0.016} = 20.6N \quad (7.8)$$

$$F_{f_max} = u_{w1} \cdot (F_{mag1}) = 0.71 \cdot (9.5) = 6.7N \quad (7.9)$$

$$W1_{circ} = pi \cdot (r_{w1} \cdot 2) = 0.05m \quad (7.10)$$

$$V_{max} = RPS \cdot W1_{circ} = 0.1ms^{-1} \quad (7.11)$$

Table 7.1: Description of parameters used within the free body diagrams in the concave and convex cases.

Parameter	Description
w_1c_1	Wheel one, pipe contact point one
w_1c_2	Wheel one, pipe contact point two
w_2c_1	Wheel two, pipe contact point one
w_2c_2	Wheel two, pipe contact point two
$c.g.$	Location of the centre of gravity
mg	Force of the weight of the robot
θ_R	Angle of the robot from the normal orientation
c_{w1}	Location of centre of wheel one
c_{w2}	Location of centre of wheel two
F_f	Force of friction
F_N	Force of the normal at the wheel contact point
F_{Tm}	Force of the torque at the motor
F_{mag1}	Force provided by magnetic wheel 1
F_{mag2}	Force provided by magnetic wheel 2

7.2.1 Concave case

The concave case is present in pipe bends as either high or low radius bends, the most extreme case is the mitred bend which forms a right angle. It can also be present as a valve flange in-pipe which acts as a sharp change in diameter.

Concave: section 1

Section 1 begins with the robot approaching a concave step case corner arrangement. The free body diagram of this case is displayed in Figure 7.1. Section one is a simple split of the weight components between the two points of contact to find the reaction. To solve this case forces are resolved in terms of the normal force direction of the robot which is the same for both F_{N-w1c1} and F_{N-w2c1} . By taking moments around c_{w1} and ignoring the magnetic forces for now:

$$M_{cw1} = mg * Lx_{cw1cg} \quad (7.12)$$

Solve for the reaction force by taking the sum of moments around any point as equal to zero from equation 7.3.

$$F_{N_w2c1} = \frac{M_{cw1}}{Lx_{cw1_w2c1}} \quad (7.13)$$

$$F_{N_w1c1} = mg - F_{N_w2c1} \quad (7.14)$$

Where: Lx_{cw1_w2c1} = Length in x - axis from c_w1 to $w2c1$

Now the magnetic forces can be re-applied. These forces are always applied directly perpendicular to the tangent point of wheel contact (the floor), and are therefore always coincident with the centre of the wheel. These forces are always collinear with the normal contact force and hence can be applied after the weight distribution of the robot has been calculated.

$$F_{N_w2c1} = F_{N_w2c1} + F_{mag1} \quad (7.15)$$

$$F_{N_w1c1} = F_{N_w1c1} + F_{mag2} \quad (7.16)$$

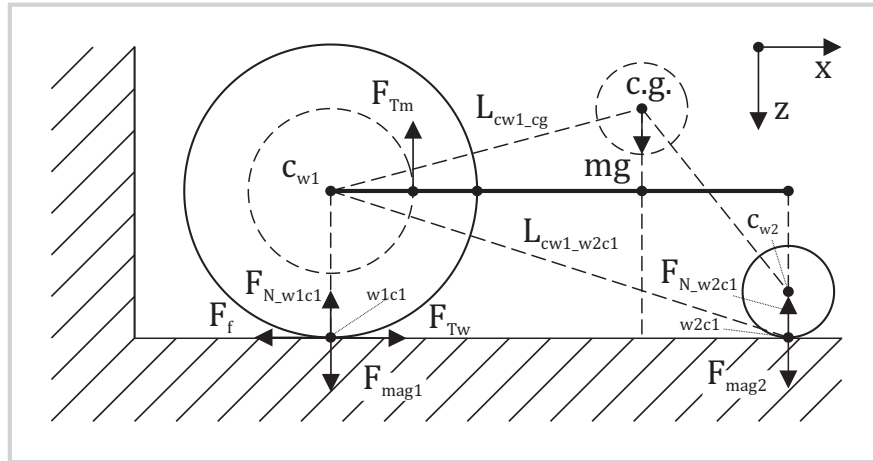


Figure 7.1: Concave case section one: robot approaches the wall.

The variance found in this section is that the start angle of the pipe can be anything from $0^\circ - 360^\circ$. This affects the direction of the weights force vector and can cause an

increase or a decrease in the normal force on each wheel depending on the orientation. The minimum normal force caused by the weight of the robot is found when the centre of gravity (*c.g.*) is vertically below the wheel contact points. Section 1 is assumed to end at the point that magnetic wheel 1 is just about to come into contact with the gradient attachment point of the step case.

Concave: section 2

For section 2 the vehicle starts with magnetic wheel 1 touching the pipe at two contact points. At this point the magnetic force of the wheel is now split between the two points of contact in the main wheel w_1c_1 and w_1c_2 . From Section 4.5.1 it is known that a double contact case causes the normal force of the each contact to drop from 100 to 67%. The requirements for the completion of this section are that the motor torque and applied force at the wanted contact point overcomes the unwanted attractive force of the wheel in double contact; F_{mag1} at w_1c_1 . It is important to note that during this section magnetic force does not change because the robot never actually moves. The magnetic force only alters (shifting force to w_1c_2) once wheel begins to come off the plate. It is assumed for simplicity of calculations that during double contact cases that the weight is now split between the two outer contact points, in this case: w_1c_2 and w_2c_1 . The beam simplification of the problem is represented in the free body diagram in Figure 7.2. The concave step-case is where the robot experiences it's torque peak, higher than any other movement.

During section 2 the motors ramp up to overcome the magnetic holding force $F_{mag1.w1c1}$ at w_1c_1 , which is keeping the wheel locked in the double contact position. This is the most important part of the concave problem as the robot must have both enough torque to overcome the total strength of the magnet. By resolving forces in z and taking moments around w_2c_1 the force required at w_1c_2 to overcome the force of the magnet $F_{mag1.w1c1}$ at w_1c_1 can be found. The force required is related to the wheelbase length, presented in equation 7.17.

$$F_{f.w1c2} = F_{mag1.w1c1} \cdot \frac{Lx_{cw1.w2c1} + r_{w1}}{Lx_{cw1.w2c1}} \quad (7.17)$$

This relationship shows that a wheelbase equal to the radius of wheel one r_{w1} would require half the force of w_1c_1 at w_1c_2 in order to bring the normal reaction force of $F_{mag1.w1c1}$ to zero. As the wheelbase increases (keeping constant radius at wheel

one) the force required by F_{f_w1c2} needed tends to the force of F_{mag1_w1c1} .

The maximum torque from the motor relates to the torque at the wheel by equation 7.8. In this double contact case it can be assumed that the torque is split equally at both contact points whilst there remains sufficient normal force to transfer traction at the contact point. The limit for sufficient traction at $w1c1$ is given by equation 7.20.

$$F_{f_w1c2} = F_{mag1_w1c1} - F_{f_w1c2} \cdot \frac{(Lx_{cw1_w2c1} + r_{w1})}{Lx_{cw1_w2c1}} \quad (7.18)$$

$$F_{f_w1c2} \cdot \left(1 + \frac{(Lx_{cw1_w2c1} + r_{w1})}{Lx_{cw1_w2c1}}\right) = F_{mag1_w1c1} \quad (7.19)$$

$$F_{f_w1c2} = \frac{F_{mag1_w1c1}}{\left(1 + \frac{(Lx_{cw1_w2c1} + r_{w1})}{Lx_{cw1_w2c1}}\right)} \quad (7.20)$$

After this limit is reached the frictional force will no longer be equal. More force is transferred into $w1c2$ as the maximum traction force at $w1c1$ falls to zero and the normal force F_{N_w1c1} is negated. This causes the F_{f_w1c2} to increase exponentially as more of the wheel torque becomes available. During this section the F_{f_w1c1} actually acts into the wall, increasing the normal force F_{N_w1c2} . This force is not useful to the movement however. It may initially stop slip due to the larger normal force, however when the $w1c1$ limit is reached this increased normal force is also reduced with the reduction in traction.

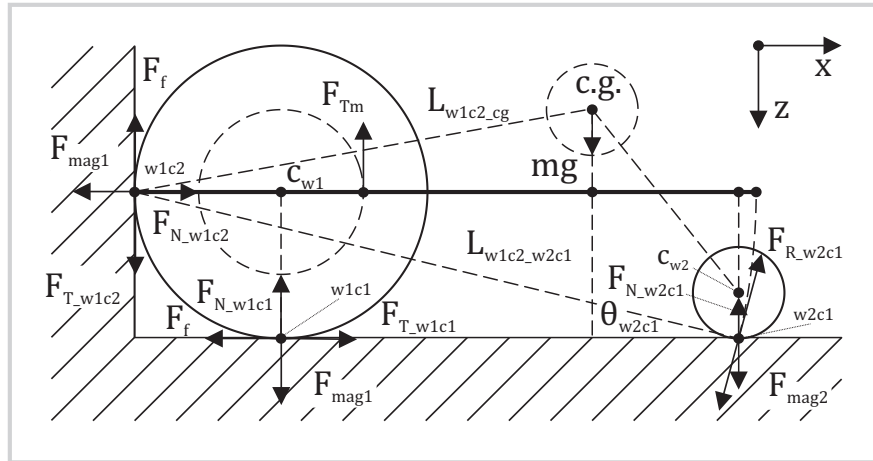


Figure 7.2: Concave case section two: robot is in double contact case with the step at wheel one.

At the end of this section the reaction force at w_1c_1 has reduced to zero and the robot is now ready to climb the step case in section 3.

Concave: section 3

In section 3 the robot has just moved off from unwanted contact force and the robot is now rotating around the corner case and moving up the wall. As the front wheel moves up the back wheel is swung into the corner case whilst maintaining magnetic contact at the point w_2c_1 . During this section the entire body of the robot is rotating around the corner case, this changes the weight distribution throughout the movement and is dependent on the original orientation of the robot and the total angle of the case. This section ends when wheel 2 is just about to make contact with the wall whilst maintaining contact with the lower portion of the step case. It is assumed in this model that the robot's second magnetic wheel lies beyond its chassis such that double contact can be made (a perfect two wheel system). The free body diagram for this case is presented in 7.3.

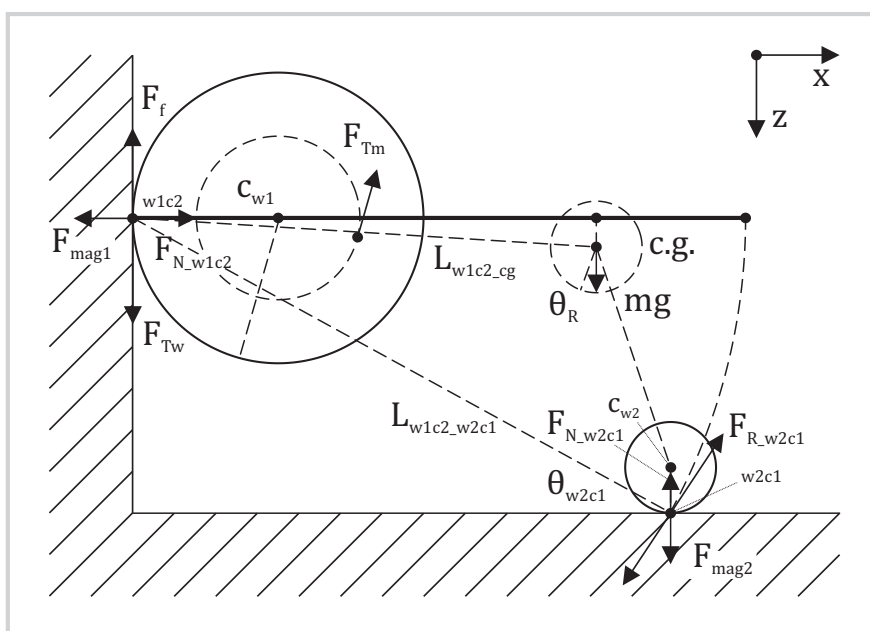


Figure 7.3: Concave case section three: robot has overcome double contact and rotation about the corner has begun.

Concave: section 4

In section 4 the robot has completed its rotation about the step case and has now made contact with the wall at w_2c_2 . The motor power must now increase to generate enough wheel traction to bring the reaction force of w_2c_1 to zero ready to pull off from the start of the step case. This section ends when the reaction force w_2c_1 is reduced to zero and is completed providing 7.21 is achieved.

$$F_{f_w1c2} > F_{N_w2c1} \tag{7.21}$$

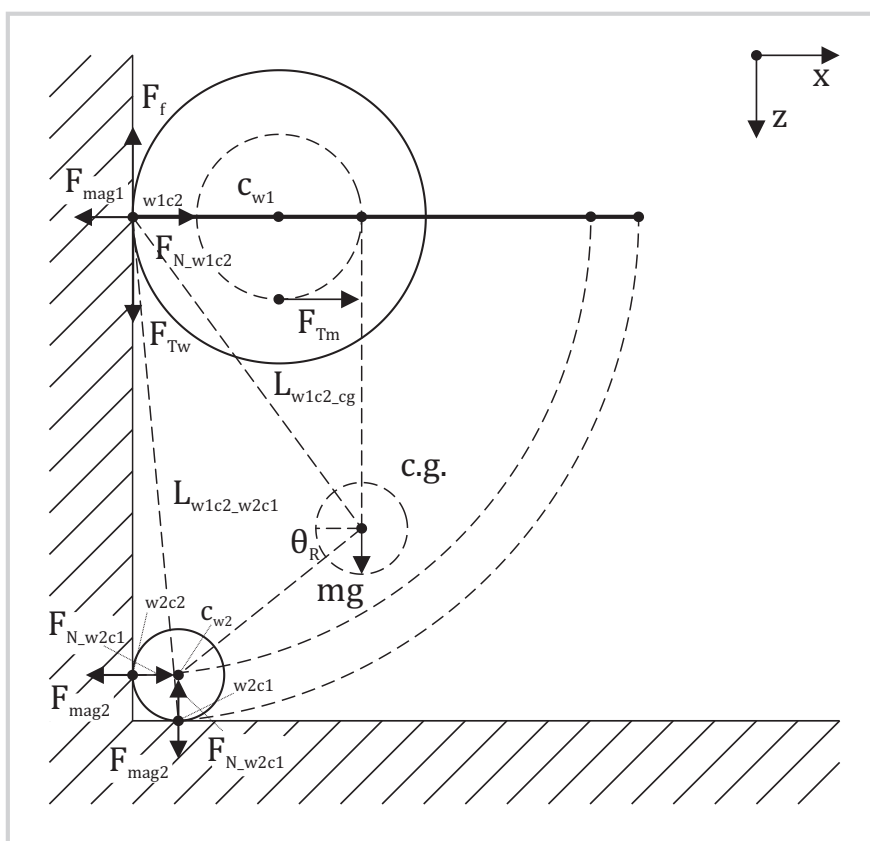


Figure 7.4: Concave case section four: robot is in double contact case with the step at wheel two.

After section 4 the robot moves off from the step case after disconnecting w_2c_1 from the pipe. The step-case has been completed and the robot is now in its new pipe orientation and can move on to its next obstacle.

7.2.2 Convex case

The convex geometry step case is present at every connection from a small diameter riser into a larger diameter pipeline. Getting around this obstacle is unavoidable if the larger diameter pipes are to be entered from the smaller connected bores. The convex step case is the harder of the two cases as there are some orientations which the robot cannot complete.

Convex: section 1

Section 1 begins with on a vertical wall with a robot angle of 90° . The robot drives to the corner of the step case, this section ends just as the robot is about to begin its rotation around the corner. When driving up to the corner the robots frictional co-efficient and the torque at the wheel provided by the drive motors must be greater than the robots weight.

$$(F_{Tw} > \frac{mg}{2}) \tag{7.22}$$

$$F_f > \frac{mg}{2} \tag{7.23}$$

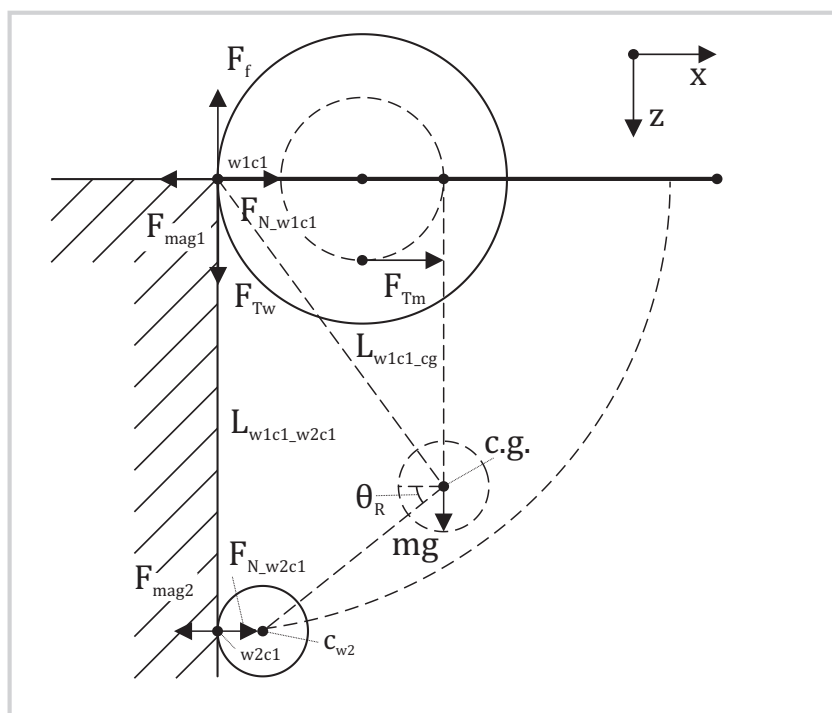


Figure 7.5: Convex case section one: robot angle is at 90° , ready to start rotation about the corner.

Convex: section 2

During section two the first wheel of the robot begins to rotate about the corner. This case is the opposite of the concave case section 2 at double wheel contact in that the robot is required to have a large wheel force to hold the weight of the robot during the contact of w_{1c1} with the corner. From chapter 4 it was discovered that F_{mag1} at this case is reduced to almost 10% of it's maximum pull force. Therefore to complete this section the robot must fulfil equation 7.24.

$$F_{mag1} * 0.1 > \frac{mg}{2} \tag{7.24}$$

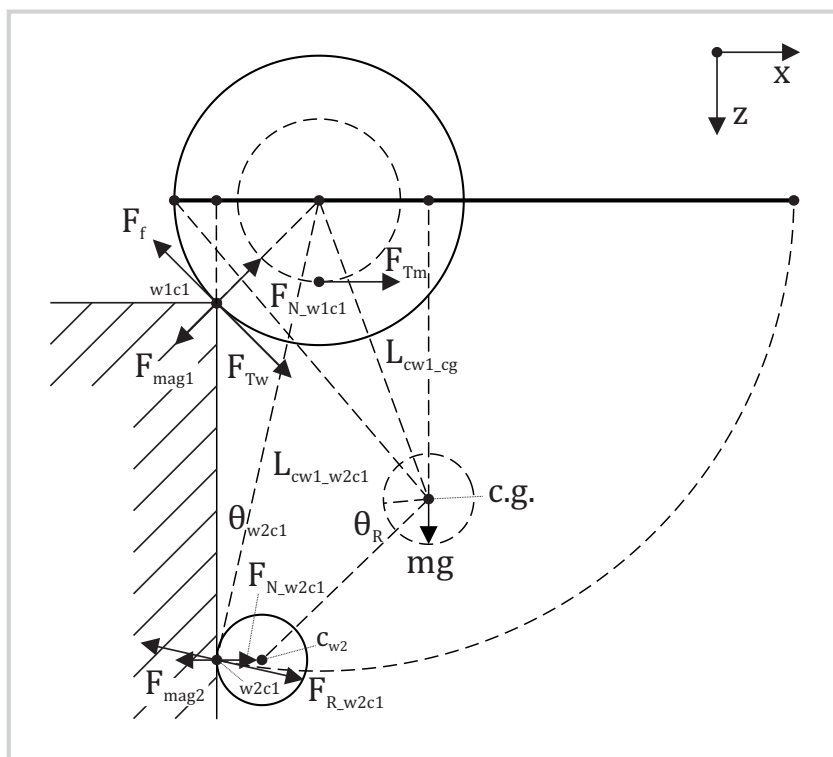


Figure 7.6: Convex case section two: robot has begun rotation around the corner and is the weakest magnetic contact case for wheel one.

Convex: section 3

In section 3, shown in Figure 7.7 the robot has rotated both drive wheels around the corner and it begins to drive off. The robot is still rotating and the rear wheel is coming closer to the corner case as it is dragged around by the main wheels.

It's at this point that a huge force begins to be placed on the rear wheel due to the counter torque on the body produced by the front wheel. The force is large and into the wall at F_{R_w2c1} , and due to the rotation of the robot the main driving force is parallel to the floor at F_f and the component in the Z - plane at w_2c_1 has reduced to a minimum. This lack of vertical force component, the weight of the robot acting against the wanted force, combined with the counter torque from the wheel, and the resistance from the magnet to move into the corner position means that there are three elements causing a negative force in the Z - plane about the chassis that keeps the robot trapped in this position. This case is only possible where mg acts away from the

convex corner.

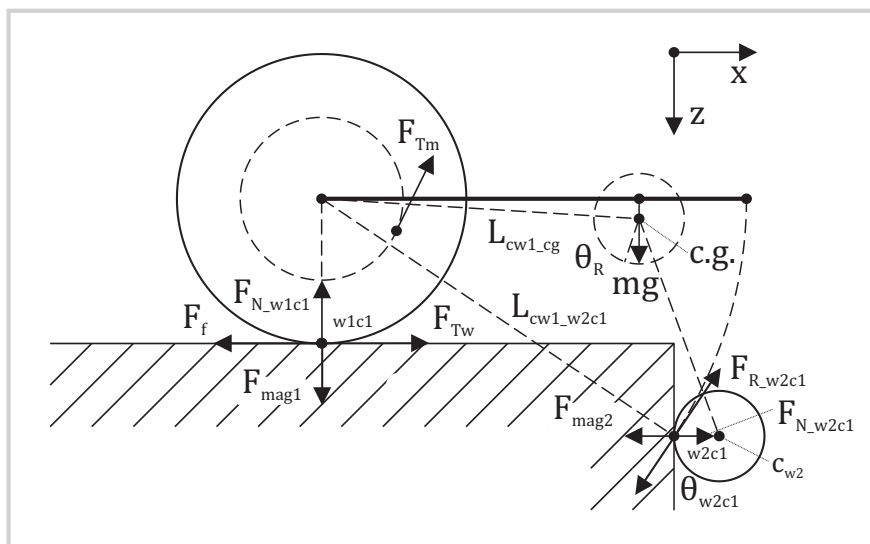


Figure 7.7: Convex case section three: wheel one has passed the corner and is now attempting to pull the rear passive wheel around the corner.

Convex: section 4

This case is especially significant when moving around the corner in the opposite direction, because the rear wheel magnet is in the weakest case it's holding force is significantly reduced to 10% of its maximum. When the robot rotates round the corner the rear wheel at a reduced force must balance the moment caused by the robot weight and fulfil the condition in 7.25. Failing to do this causes a detachment of the rear wheel followed by a rotation around the front axle and the robot crashing into the wall. The reaction from the crash can cause a complete detachment of the main wheel and the robot to fall off the pipe.

$$F_{mag2} * 0.1 * \cos(45) > mg * L_{w2c1_{mgx}} \quad (7.25)$$

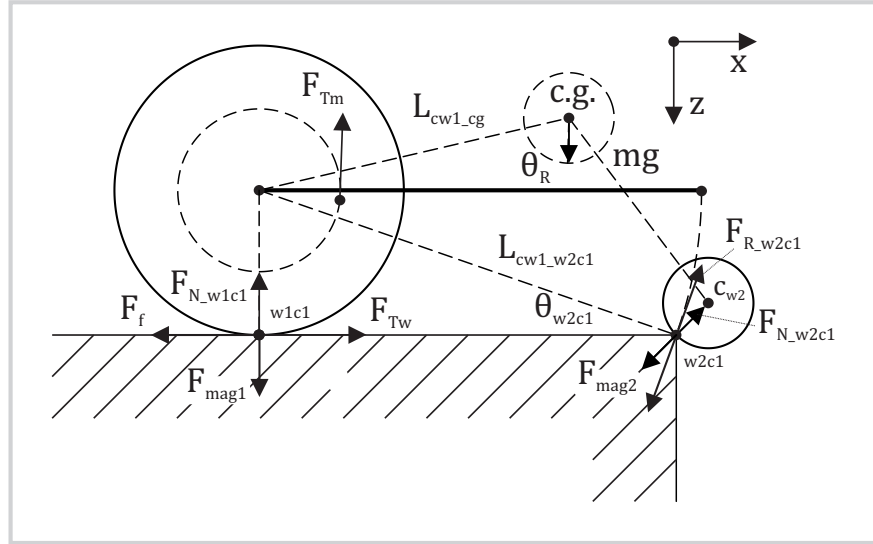


Figure 7.8: Convex case section four: wheel two is in the weakest magnetic case.

After section 4 the robot moves off from the step case after successfully completing its rotation around the convex. The step-case has been completed and the robot is now in its new pipe orientation and can move on to its next obstacle.

7.3 Experimental testing

This section covers the rig based testing of the final robot in various orientations of concave and convex cases. The rig set-up, shown in 7.9 consists of two main steel plates mounted to a central bearing such that two edges of the plate are always touching. The secondary plate can be rotated around the first to alter the angle of the step case using the 360° protractor mounters centrally behind the plates. The bottom plate is fixed in place and the secondary plate is clamped in place to halt movement during testing. The clamp attaches to the Rexroth frame which is fixed mounted to a 14.3kg block of steel. The rig has been used to gather experimental data showing the robots ability to climb step cases.

7.3.1 Concave cases

The concave cases were tested from a 75° acute angle up to a 180° flat case. Reviewing the cases in the free body diagram, the most challenging aspect of the concave problem

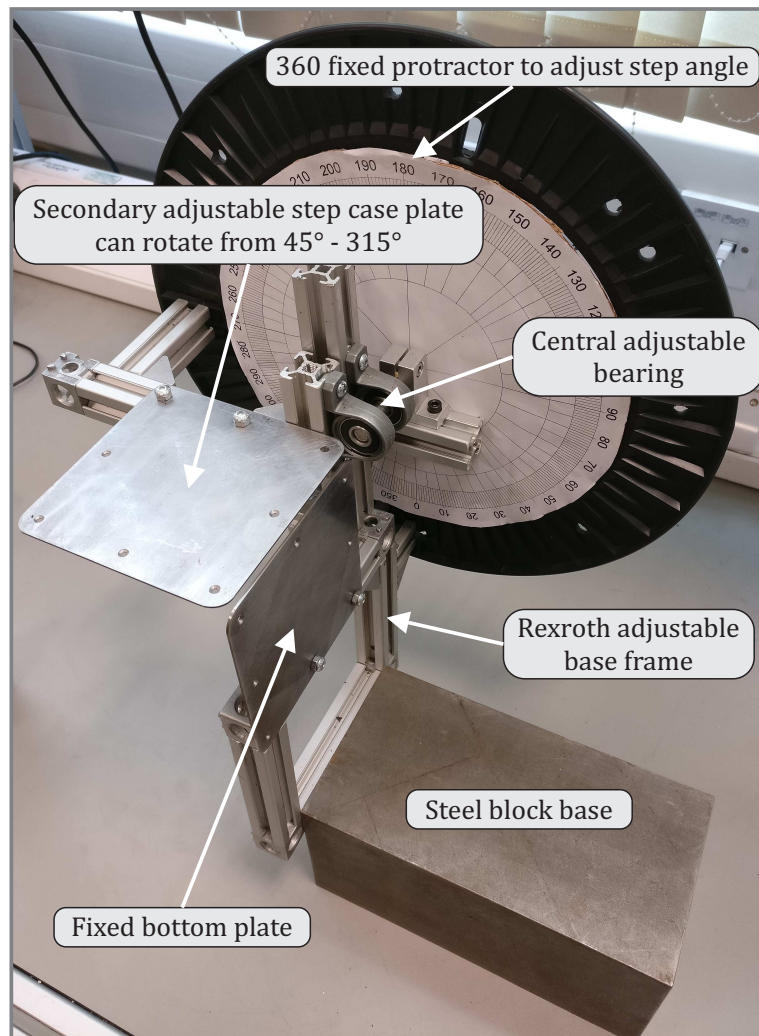


Figure 7.9: Test rig used to evaluate the robots performance on both concave and convex step cases at varying angles.

7.3 Experimental testing

is the double contact of main drive wheels in Concave: section 2 (Section 7.2.1). The experimental tests show that this is correct, the robot easily handles sections A, but becomes locked in double contact at Figure 7.10.B. At this point each of the 9.5N wheels hold 67% normal force in each contact point (6.4N). When the PWM value of both motors reaches high enough (240/255) the wheels are detached slightly from the unwanted contact point and the magnetic flux immediately transfers into the remaining contact point. The main contact point returns to 100% at 9.5N force and the robot leaves double contact section. After leaving double contact the robot is free and to rotate during around the corner until the rear magnets reach the corner case. Detaching the rear magnets at 100% requires 1.6N force each, a quarter of that needed to detach the main drive wheels. After detaching the rear magnets the robot is free to move in it's new inverted plane in Figure 7.10.

The concave cases tested are summarised in Table 7.2, including the PWM values reached as recorded on the LabVIEW input program. PWM values reached in this case relate to the load on the motor required to complete the manoeuvre, a PWM value of 255 represents the maximum possible power that can be applied to the motor, if a value of 255 is reached before completing the case the motors will have stalled and the robot will have failed the case. A value of 240 as shown in both the 90 degree and 75 degree concave cases confirms that the robot is close to its maximum power output as is expected in these cases which were predicted to be the hardest of the concave step angles to complete.

Table 7.2: Step-case rig: robot experimental results for concave testing at different angles.

Step-Case	Step Angle (°)	Forward Descending	Reverse Descending	Forward Ascending	Reverse Ascending	PWM
Flat	180	Y	Y	Y	Y	60
Concave	135	Y	Y	Y	Y	60
Concave	90	Y	Y	Y	Y	240
Concave	75	N	F	Y	Y	240

In a worst case where all the weight of the robot (0.12kg) acts on the wanted contact point and causes a 0.5N reduction in normal force of the main wheel contact (8%). The

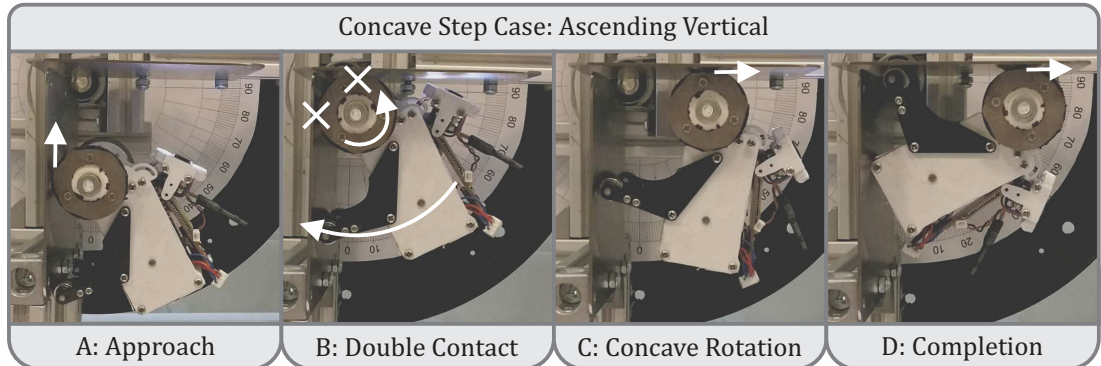


Figure 7.10: Concave case performed on the test rig. A: approaching the corner case. B: Double contact, the motor ramps up to overcome the unwanted contact force. C: The robot rotates around the concave corner after detachment. D: The completion of the concave corner case.

corner case presented in Figure 7.10 is closest to this worst concave situation. The robot can comfortably complete the concave case in this and any other orientation, the factor that affects this case the most is the wheel force and the wheel frictional co-efficient as shown in Figure 7.11. The graph shows the minimum required frictional co-efficient needed to overcome a concave step-case is between 0.6 and 0.65. The frictional co-efficient of the rubber coated wheels is 0.71 from Chapter 4, hence the robot is able to complete any concave step-case as long as the rubber coating is maintained. The wheels strength used to calculate these values was the 9.5N wheels used in the experiments. The relationships are exactly the same given a different wheel strength as they are independent of the force, changing the wheel strength only alters the Y-axis scaling.

7.3.2 Convex cases

The robot is shown approaching an ascending 90° convex case in Figure 7.12.A, and then reaching the weakest contact point at B. From Chapter 4, the weakest force on the step-case was calculated to be around 10% of the wheels maximum pull force (0.95N). The robot continues rotating around the corner with a tractive force of 0.67N at each wheel at 45° to the corner. As it rotates around the corner in section C the wheel force returns to maximum pull force and the robot attempts to pull itself around the step case. At section D, the rear wheel has become stuck close to the edge of the corner. This is a combined effect of the wheel torque increasing as the robot progresses around

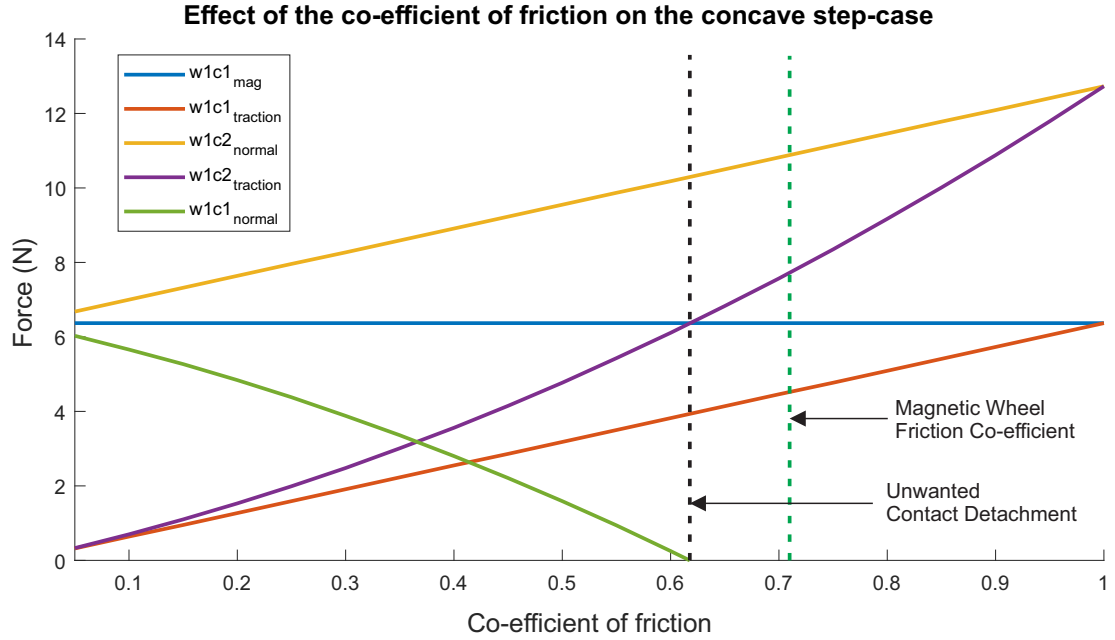


Figure 7.11: Graph showing the effect of an increase in wheel friction co-efficient on the contact forces at $w1c1$ and $w1c2$ for drive wheels with a pull strength of 9.5N.

the corner, and hence the counter torque of the body which resists rotation increasing. The result at this point is that the motors either stall or the wheels slip depending on the wheel pull force.

In the case of 7.13 the robot manages to complete the convex corner case because gravity is working in its favour instead of against it as in 7.12. The robot can fall in this case if the rear magnets are not strong enough. During convex rotation in part C when the rear wheels reach the corner and are at 10% pull force the chassis's rotation around the corner can cause detachment. This detachment is seen in another similar case example in 7.14. B, and causes the robot to crash. It should be noted that this crash position is recoverable with remote control as the main drive wheels have not been detached.

Table 7.3 shows the cases completed by the robot as well as the PWM values inputted from the control LabVIEW program to achieve the result. The robot completes 115° in its worst case ascending orientation as seen in Figure 7.12. Although the robot can make it around 90° corners in ideal cases, the minimum case for pipeline is from a 4-inch to a 12-inch pipeline as seen in Figures 7.15. Figure 7.16 shows a graph of the

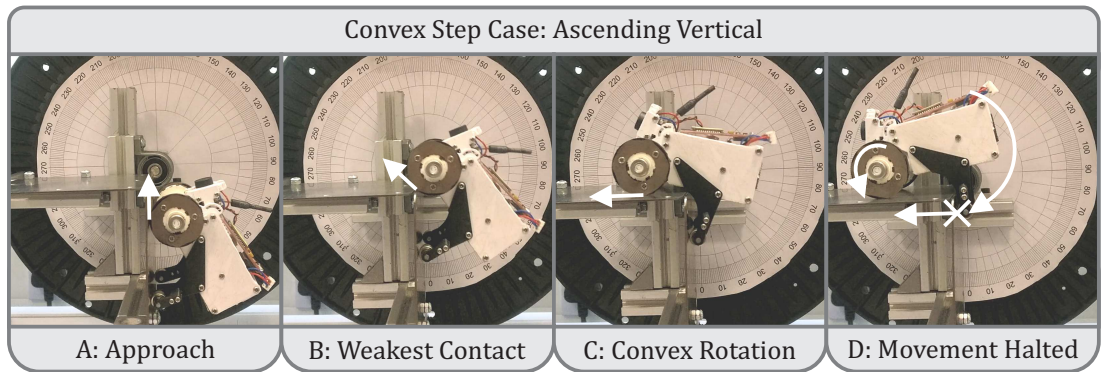


Figure 7.12: Robot attempting the convex corner case. A: Approaching the step case. B: The point of weakest contact for the magnetic wheel. C: Rotation of the robot around the convex corner. D: The robot can go no further as the passive rear wheel halts movement.

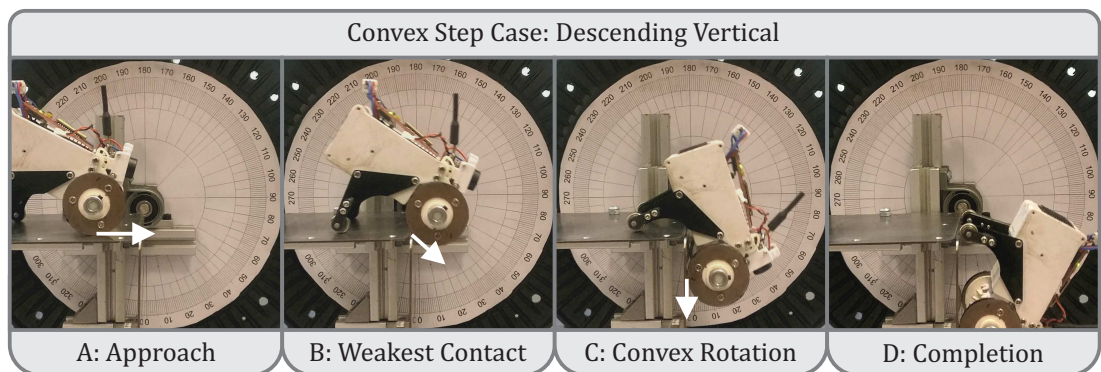


Figure 7.13: Robot completing the convex corner case. A: Approaching the step case. B: The point of weakest contact for the magnetic wheel. C: Rotation of the robot around the convex corner. D: The robot completes the case.

7.3 Experimental testing

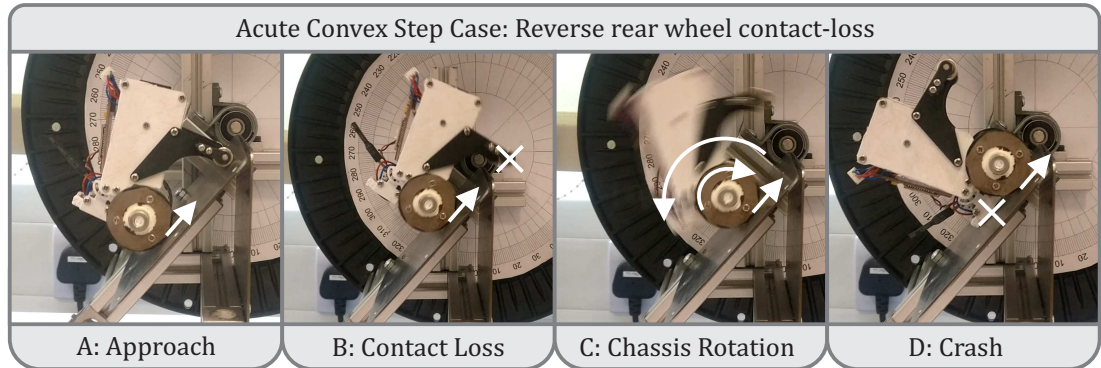


Figure 7.14: Robot completing the convex corner case. A: Approaching the step case in reverse. B: The back wheels lose contact at the convex weak corner point. C: The chassis rotates about the wheel axis. D: The robot crashes.

change in approach angle from 6-inch - 48-inch pipelines with both a 4-inch and 2-inch connection.

Table 7.3: Step-case rig: robot experimental results for convex testing at different angles.

Step-Case	Step Angle ($^{\circ}$)	Forward Descending	Reverse Descending	Forward Ascending	Reverse Ascending	PWM
Flat	0	\	\	\	\	\
Convex	45	N	N	N	F	60
Convex	90	Y	F	N	Y	60
Convex	100	Y	Y	N	Y	60
Convex	110	Y	Y	N	Y	60
Convex	115	Y	Y	Y*	Y	60, *120
Convex	120	Y	Y	Y	Y	60
Convex	135	Y	Y	Y	Y	60
Flat	180	Y	Y	Y	Y	60

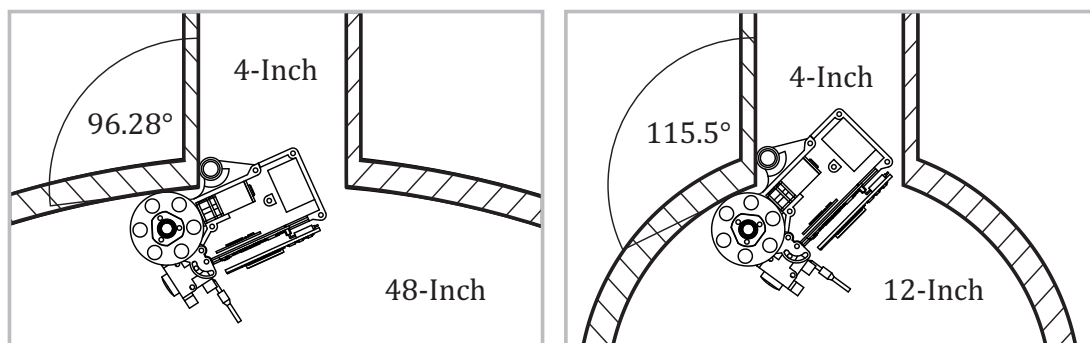


Figure 7.15: The difference in angle between a 4-inch pipe connection with a 48-inch pipe, and a 4-inch pipe with a 12-inch pipe.

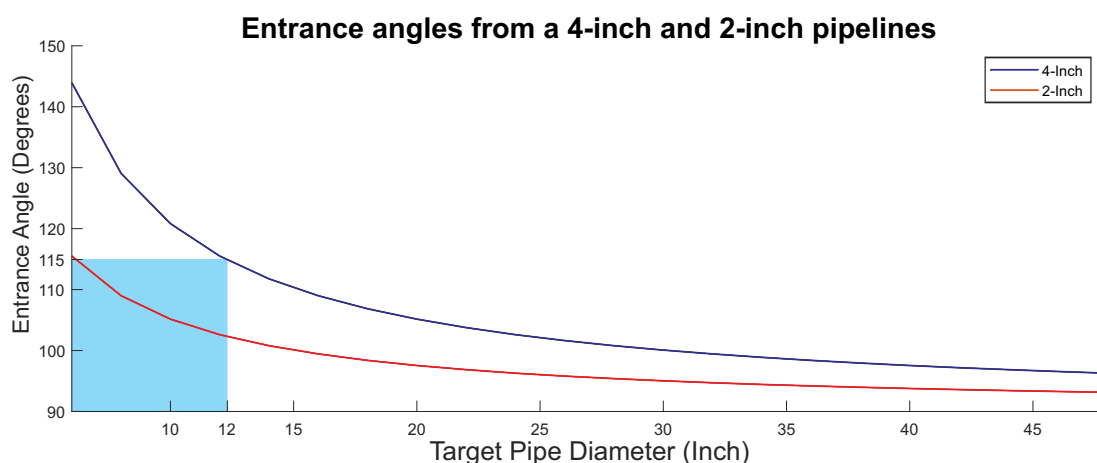


Figure 7.16: Graph of the change in approach angle with different size pipe connection fittings and different size target pipe inspection diameters.

7.4 Real in-pipe operation

Corrosion in gas pipelines can cause unstable ferritic scales in-pipe [129], that form part of the corrosion-erosion process that causes the failure of the pipe. To view how the robot might handle this type of problem the robot was tested in a real NTS 42-inch (1016mm) pipeline [26] provided by National Grid Gas Transmission to Synthotech's test site. The pipe was retrieved from a working AGI after replacement, the condition was that of an expected 40-year old underground pipeline. Figure 7.17 presents pictures of the robot exploring the pipeline, after operation the robot wheels were covered in

iron particles that reduced both the normal force and friction force provided by the wheels (D).

During tests on the real site the robot was found to function until the wheels became "clogged" by the scales of iron that had been broken from the pipe surface, or iron dust and powered sitting in the pipe that had been picked up by the magnets along the way. This dust is hard to remove as it is attracted to the wheels and . The build up of this material effectively reduces the magnetic force of the wheels as creates an iron casing around the magnet. Because the wheel is effectively encased in iron at this point the friction co-efficient drops drastically to that of iron on steel (0.27). With reduced magnetic force caused by the iron casing causes a drop in normal force at the wheel. When this point is reached movement is extremely difficult and will cause the robots wheels to slip, the robot will then be stuck in a state of wheel-spin. A secondary issue is the clogging of the bearings with iron deposits, this severely hinders movement is the particles are fine enough to enter the gaps in the shielding. This can potentially ruin the bearings and force them to require replacement.

7.4.1 Contact loss in-pipe

Robot crashes are caused by contact loss at the wheels, crashes where the robot completely detaches from the surface will generally fall onto hard steel surfaces beneath damaging the system. Some contact loss is recoverable, other cases require intervention to rescue the robot. A crash case is recoverable in most cases as long as the main wheels are in contact with the pipeline. The counter-rotation of the body due to the toque at the bevel gears will cause the detached rear wheels to re-connect with the pipeline. In the case of the robot not being able to make contact with ferrous material at the rear wheel it is capable of driving both forwards and in reverse in these conditions. Unrecoverable conditions include Contact loss due to reduced magnetic attraction. This can be caused by the wheels becoming coated in iron scales or particles during inspection. Contact loss of main drive wheels; loss of contact at the drive wheels renders the robot unmoveable by any command. The robot can also become stuck due to loss of frictional rubber wheel coating, this can wear during use and expose the flux plates underneath. This can cause the robot to constantly wheel-slip due to the reduced traction and could cause the robot to become irretrievable during operation.



Figure 7.17: Pictures from the real world tests on a decommissioned 1016mm natural gas pipeline. A: Driving vertically. B: Inverted. C: On the outer side of the pipe. D: Iron particles and scales that "clogged" the wheel flux. E: Full shot view of the pipe size versus the robot size.

7.5 Discussion and conclusions

This section looked at the problem of overcoming step-case problems using the prototype in-pipe robot. The robot was examined statically around four major sections of each step case to determine forces acting at various points. The robot was then tested in a lab environment to simulate step-cases in various orientations and view observed forces from the static analysis. The robot was then deployed in a real off-line natural gas pipeline which had been decommissioned from the National Transmission System.

The concave case defines the maximum required force of the robot. When the robot is in double contact with the wall a force equal to that of the normal force at the unwanted contact point must be generated at the wanted contact point. As found in Chapter 4 the force at each point is equal to 67% of the peak force on a flat plate. The torque needed at the motors to break contact can be reduced by shortening the wheelbase, however this also makes the robot more unstable in a convex case where rear wheels may detach, as seen in Figure 7.13. The friction co-efficient needed to break double contact was calculated in Figure 7.11 to be between 0.6 and 0.65 independent of the wheel force. The robot is able to fulfil this requirement reliably as it's rubber coated wheels have a co-efficient of friction of 0.71.

Overcoming the rear wheel problem in that of convex section 3 in an ascending convex case is the biggest challenge faced by the robot design. Without a driving force at the rear wheels it and with gravity working against the direction of intended travel the robot will become stuck as seen in Figure 7.12. However the robot is able to complete this worst case scenario at a minimum of 115° which would allow it to enter a connected pipeline of 12-inches maximum as shown by Figure 7.15. This problem will need to be solved to enter higher diameter pipelines.

In Table 7.3 the robot uses a lower PWM and hence a lower total power to move around these convex cases vs concave cases in Table 7.2. The PWM value to complete convex cases is 60 out of a total 255 PWM, which relates to around one quarter of the available power unlike the concave cases where near maximum is reached at 240/255. The reason for this difference is that a failure in the convex case results in wheel spin on the convex corner rather than a stall due to double contact at the concave corner. This results shows that the issue of convex case completion is related to the robot geometry, and cannot be solved with more power at the wheel drive.

In the real world testing the decommissioned pipeline had been left open to the

7.5 Discussion and conclusions

elements and as a result of its reaction with the oxygen in the atmosphere the pipe contained a lot of rust which was picked up by the robots wheels. In a real gas pipeline there is no oxygen present for safety reasons and hence rust will not be present. It is assumed that the "scales" and particles found in the real pipeline will behave in a similar vein.

CHAPTER 8

Conclusions and Future Work

This chapter details the conclusions that have been drawn from the work in previous chapters before summarising the research and its findings. The benefits of using the proposed systems are discussed and recommendations are made for further research.

8.1 Assessment of research objectives

1. ***Review current literature*** to better understand and critically assess existing literature surrounding state-of-the-art in-pipe robotics and to evaluate the performance of current locomotion methods used to negotiate complex pipe geometries.

The literature surrounding the field of in-pipe robotics has been collated and organised in Chapter 2. The limitations of full-bore robots and wall-press adaptation designs were discussed and a gap in knowledge was discovered. The miniature magnetic in-pipe robots in this work were developed as a result of this finding.

2. ***Understand the in-pipe environment*** by assessing the national grid gas network and developing a robotic specification and set of requirements to **choose the correct traction and locomotion methods**.

Information surrounding the history of the NTS and the likely problems and obstacles present was gathered in Section 2.4. The environment information was then analysed, once fully understood the robot requirements and specification in Section 3.3 were generated.

3. ***Design a detailed locomotion system for the robot*** and use this as a foundation to create a platform on which the robot can be built.

Multiple approaches to locomotion systems were investigated, however magnetic wheel designs were chosen for development in Section 4.2.1 as a result of the environment requirements. The magnetic wheel best suited for the robots environment was experimentally assessed in Section 4.5 and the behaviour of magnetic wheel adhesion force in step-case geometry was demonstrated.

4. ***Design and develop a software system*** to communicate with an embedded robot micro-controller.

A high level control program was developed using LabVIEW to take user input drive commands and communicate them over wireless Bluetooth transmission in Section 5.3.1. The robot communicates using a custom serial communication method to increase communication speed between the high level and low level controllers.

5. ***Generate detailed conceptual designs based upon the robot requirements and specification, the locomotion system, and the electronics package. Fabricate a working prototype using rapid techniques.***

In Section 6.3, many concept in-pipe robots designs were generated using different transmission methods and layouts. The concepts were assessed against the requirements and four high-ranking designs were developed further. A two-wheeled robot has been developed in Section 6.3 to investigate level of inspection achievable using restrictive design volume. The base geometric obstacles faced by magnetic in-pipe robots were highlighted and defined as concave and convex geometry problems. A method to overcome these problems was incorporated into a robotic solution 6.4.

6. ***Assess the performance of the robot in a range of step-cases simulating complex in-pipe geometry.***

The step-case simulation rig in Section 7.3 is used to assess the robots performance when traversing step-cases both concave and convex. Experimental studies have verified the robot's ability to overcome these obstacles and determined the ranges and orientations it is capable of.

8.2 Conclusions

8.2.1 Magnetic traction wheels

- When building a flux plate magnet array, the final configuration produces contact forces equal or greater than the sum of the magnet arrays combined provided the flux plate is thick enough not to become saturated. Under normal circumstances the wheel produced maximum pull forces of 82.9N whereas the manufacturers rated pull force of the 6x6mm N42 magnets produce 13.73N each, six of these should produce a pull force of 82.38N.

- A thin coating of 0.06mm rubber can cause the maximum force of the magnetic wheel to drop to half of the top rated pull force. This means that the rubber coating has a larger effect on the wheel contact uniformity than alignment of the interior magnet array, even minor thickness differences in the outer rubber coating will effect the wheel more than the 0.4 - 3.8% drop in force observed experimentally.
- The designed magnet wheels have a concentrated but shallow magnetic field around the contact area of the wheel. The larger reaching field of the disc magnet took over 10 times the displacement to reach 50% of it's maximum pull force. When coated in rubber sealant the wheels have around half the normal force but equal traction, this provides a great advantage during concave cases allowing simple detachment of the wheel in double contact without losing drive force.

8.2.2 Embedded system and software design

- The software requirements have been fulfilled with the development of a high level control program built in LabVIEW. The accompanying low level micro-controller program allows sending and receiving of wireless signals to move around its environment. The high level program communicates contains built in architecture to allow multiple Bluetooth robots to be connected at the same time. To fulfil the software requirement of low latency, the custom serial messages have been optimised to just minimise the length of the message that needs to be sent.
- The hardware requirements for the robotic platforms have been achieved. A small physical package or "stack" has been developed with small micro-controllers such as the Teensy 3.6 and the Arduino Pro Mini have been used. the number of motors was limited to two fulfil both the small physical package size requirement and the simple skid-steering requirement,
- The Bluetooth design choice greatly contributed the optimisation of the circuit for low power consumption. The secondary option of a Wi-Fi ESP8266 module is half the size, however it consumes over 5 times the power draw under constant communication with no increase in communication speed as both baud rates cap at 115200 BPS.

8.2.3 Magnetic in-pipe robot for step-case negotiation

- To overcome a convex corner case a gap must be present between the wheel and the rear contact point of a magnetic robot chassis in order to allow the wheels over the edge. The geometry necessary to complete this case was investigated and an ideal curve to avoid convex contact was generated. This ideal curve can be applied to other robotic systems given their wheelbase length and wheel diameter.
- The robot can overcome concave step-cases in all orientations. Chance of contact loss at the main drive wheels during these cases is minimal and requires a misjudgement on the wheel alignment when approaching the case such that the wheels are not perpendicular to the wall.
- The robot can complete all orientations of descending convex cases. When ascending the robot fails to proceed once the rear wheel reaches the top of the convex case. The robot can complete all angles past 115° corner cases in any orientation.

8.2.4 Conclusion summary

The developed robot uses magnetic wheels designed to increase the force at contact to greatly increase traction versus a regular open-air magnet. The shallow magnetic field allows the robot to easily break the double contact in a concave case once the unwanted force has been overcome. The software makes driving the device simple with easy to use control schemes on keyboard or gamepad. The optimised serial and high CPU clock rate message makes input response smooth with no lag. The curve geometry present between front and rear wheels allows the robot to move around a large portion of convex step cases. The front wheel torque is balanced with rubber coated magnet to ensure any concave obstacle can be completed no matter the orientation.

8.3 Future work

This section looks at future improvements that could benefit the design of the in-pipe robot in order to further the work carried out in this thesis.

8.3.1 Magnetic traction wheels

- The array magnetic traction wheel design should be applied to the passive rear wheel designs. The current rear wheels are simple countersunk axially magnetised magnets and could be upgraded to provide a higher contact force. A higher contact force at the rear wheel set would prevent contact loss over descending convex cases.
- Wheel coating methods could be improved to resist against wear during operation, this can cause constant wheel slip in a field test, making the robot irretrievable.

8.3.2 Embedded System and Software Design

- Swarm control could be implemented in the system to allow a group of robots to complete an inspection together. The framework for connecting many robots already exists within the developed LabVIEW high level controller, research must be conducted on the correct control algorithms for this system.
- Distance sensing between each magnetic-robot could be implemented to localise robots in swarm. This could be done using acoustic sensing in a network such that each can "hear" the position of the other systems in the pipe. Faster micro-controller processing speed would be needed to achieve the sample frequency to perform acoustic detection.
- It would be beneficial to have a form of NDT sensor integrated into the robot. The sensor could be a standard magnetic flux leakage system.
- The material the robot is driving onto is unknown in environments other than the national transmission system. The robot could come into contact with a wall that is not ferrous and crash. A magnetometer or an array of hall effect sensors might be used to check changes in the flux density inside the magnet wheel. This could determine a change in magnetic fields when the robots wheels come into contact with a ferrous wall.

8.3.3 Magnetic in-pipe robot for step-case negotiation

- The major obstacle for the in-pipe robot is the inability to clear some ascending convex corner cases. This problem could be solved with the addition of a force

component on the rear axle. This could be a servo which acts as a lever between the chassis and the pipe or another DC motor on the rear axles. A gear train or belt system from the main drive wheels to the rear may be the best option to keep the size and number of actuators on the robot low.

- It is important to make sure both wheels hit the corner case at the same time, this is called "squaring-up" the wheels and is necessary for moving around both concave and convex step cases. Without squaring-up in the case of concave problems the robot can end up at an awkward angle and require reversing to attempt again. In the convex case it can cause wheel contact loss in as the force required by each magnet is doubled when only one is in contact, this is especially troublesome for the weaker passive rear magnets. Using the FPV the operator of the robot can adjust the robot to be in line with the obstacle through vision however in the future this should be done autonomously. The robot can be fitted with two close range laser range finders to determine the distance from the robot to the wall or step. The sensors can be read to determine the distance from each wheel and alter the wheel speed accordingly to match the distance values.
- The FPV camera itself could be improved to switch on and off to conserve battery through the micro-controller logic and added to the LabVIEW program as a boot option. The FPV camera could be upgraded to higher resolution system with on-board recording. This would allow inspection data to be recorded and viewed after the mission to see defects in higher resolution, as well as record data without the need to transmit back to the controller constantly as this currently invokes a large current cost (300mAh) on the separate LiPo. The camera could also be upgraded with a pan and tilt servo attachment to allow control of the visual inspection area.
- For insertion of the robot into live gas mains, suitable ATEX rating is required. This will involve a lot of design work to create a use-able system that is leak proof and capable of being pressurised. This work will be required if the robot is to enter a real live gas main on the national grid.
- The main drive wheelbase could be reduced in assembly size. Machined non-ferrous metal gears as well as a metal seating shaft could allow for a thinner axle rod as

it is not bound by 3D printed material strength and accuracy. The bearing size and shaft collar could then also be reduced in size.

One of the two concave or convex cases can potentially be negated in small pipelines by rotating the entire body of the robot about the pipe axis. By doing this the robot could choose the path with the convex obstacle or the opposite concave. To achieve this work could be done on improving the robot steering, such as the inclusion of omni wheels so that the robot may turn whilst keeping parallel to the pipes central axis.

REFERENCES

- [1] S.-g. Roh, J.-S. Lee, H. Moon, H. R. Choi, *et al.*, “Modularized in-pipe robot capable of selective navigation inside of pipelines,” in *Intelligent Robots and Systems, 2008. IROS 2008. IEEE/RSJ International Conference on*, pp. 1724–1729, IEEE, 2008.
- [2] Z. Hu and E. Appleton, “Dynamic characteristics of a novel self-drive pipeline pig,” *IEEE Transactions on Robotics*, vol. 21, no. 5, pp. 781–789, 2005.
- [3] L. Paletta, E. Rome, and A. Pinz, “Visual object detection for autonomous sewer robots,” in *Intelligent Robots and Systems, 1999. IROS’99. Proceedings. 1999 IEEE/RSJ International Conference on*, vol. 2, pp. 1087–1093, IEEE, 1999.
- [4] S. U. Yang, H. M. Kim, J. S. Suh, Y. S. Choi, H. M. Mun, C. M. Park, H. Moon, and H. R. Choi, “Novel robot mechanism capable of 3d differential driving inside pipelines,” in *Intelligent Robots and Systems (IROS 2014), 2014 IEEE/RSJ International Conference on*, pp. 1944–1949, IEEE, 2014.
- [5] D. Lee, J. Park, D. Hyun, G. Yook, and H.-s. Yang, “Novel mechanisms and simple locomotion strategies for an in-pipe robot that can inspect various pipe types,” *Mechanism and Machine Theory*, vol. 56, pp. 52–68, 2012.
- [6] Y.-S. Kwon, B. Lee, I.-C. Whang, W.-k. Kim, and B.-J. Yi, “A flat pipeline inspection robot with two wheel chains,” in *Robotics and Automation (ICRA), 2011 IEEE International Conference on*, pp. 5141–5146, IEEE, 2011.
- [7] Y. Kawaguchi, I. Yoshida, H. Kurumatani, T. Kikuta, and Y. Yamada, “Internal pipe inspection robot,” in *Robotics and Automation, 1995. Proceedings., 1995 IEEE International Conference on*, vol. 1, pp. 857–862, IEEE, 1995.

-
- [8] F. Tâche, W. Fischer, G. Caprari, R. Siegwart, R. Moser, and F. Mondada, “Magnebike: A magnetic wheeled robot with high mobility for inspecting complex-shaped structures,” *Journal of Field Robotics*, vol. 26, no. 5, pp. 453–476, 2009.
- [9] K. Tadakuma, R. Tadakuma, K. Nagatani, K. Yoshida, S. Peters, M. Udengaard, and K. Iagnemma, “Crawler vehicle with circular cross-section unit to realize sideways motion,” in *Intelligent Robots and Systems, 2008. IROS 2008. IEEE/RSJ International Conference on*, pp. 2422–2428, IEEE, 2008.
- [10] J.-H. Kim, G. Sharma, and S. S. Iyengar, “Famper: A fully autonomous mobile robot for pipeline exploration,” in *Industrial Technology (ICIT), 2010 IEEE International Conference on*, pp. 517–523, IEEE, 2010.
- [11] Y.-S. Kwon and B.-J. Yi, “Design and motion planning of a two-module collaborative indoor pipeline inspection robot,” *IEEE Transactions on Robotics*, vol. 28, no. 3, pp. 681–696, 2012.
- [12] J. Park, D. Hyun, W.-H. Cho, T.-H. Kim, and H.-S. Yang, “Normal-force control for an in-pipe robot according to the inclination of pipelines,” *IEEE transactions on Industrial Electronics*, vol. 58, no. 12, pp. 5304–5310, 2011.
- [13] M. HORODINĂ, A. PREUMONT, and I. BURDA, “The heli-pipe inspection robots architecture for curved pipes,” in *International Conference of Manufacturing Systems ICMS*, pp. 149–154, 2003.
- [14] T. Nishihara, K. Osuka, and I. Tamura, “Development of a simulation model for inner-gas-pipe inspection robot: Spring,” in *SICE Annual Conference 2010, Proceedings of*, pp. 902–904, IEEE, 2010.
- [15] H. Schempf, E. Mutschler, A. Gavaert, G. Skoptsov, and W. Crowley, “Visual and nondestructive evaluation inspection of live gas mains using the explorer family of pipe robots,” *Journal of Field Robotics*, vol. 27, no. 3, pp. 217–249, 2010.
- [16] K. Sato, T. Ohki, and H.-o. Lim, “Development of in-pipe robot capable of coping with various diameters,” in *Control, Automation and Systems (ICCAS), 2011 11th International Conference on*, pp. 1076–1081, IEEE, 2011.

-
- [17] E. Dertien, S. Stramigioli, and K. Pulles, “Development of an inspection robot for small diameter gas distribution mains,” in *Robotics and Automation (ICRA), 2011 IEEE International Conference on*, pp. 5044–5049, IEEE, 2011.
- [18] Y. Lu, J. Yu, C. Sui, and J. Han, “Design of in-pipe 3spr/3rps parallel manipulator and its kinestatics analysis,” in *Cyber Technology in Automation, Control, and Intelligent Systems (CYBER), 2015 IEEE International Conference on*, pp. 42–47, IEEE, 2015.
- [19] A. S. Boxerbaum, K. M. Shaw, H. J. Chiel, and R. D. Quinn, “Continuous wave peristaltic motion in a robot,” *The international journal of Robotics Research*, vol. 31, no. 3, pp. 302–318, 2012.
- [20] A. Zagler and F. Pfeiffer, “” moritz” a pipe crawler for tube junctions,” in *Robotics and Automation, 2003. Proceedings. ICRA’03. IEEE International Conference on*, vol. 3, pp. 2954–2959, IEEE, 2003.
- [21] M. Tavakoli, C. Viegas, L. Marques, J. N. Pires, and A. T. De Almeida, “Omni-climbers: Omni-directional magnetic wheeled climbing robots for inspection of ferromagnetic structures,” *Robotics and Autonomous Systems*, vol. 61, no. 9, pp. 997–1007, 2013.
- [22] J. W. Romanishin, K. Gilpin, and D. Rus, “M-blocks: Momentum-driven, magnetic modular robots,” in *2013 IEEE/RSJ International Conference on Intelligent Robots and Systems*, pp. 4288–4295, IEEE, 2013.
- [23] T. I. Williams, *A history of the British gas industry*. Oxford University Press, USA, 1981.
- [24] N. N. G. G. Transmission, “Project graid: Gas robotic agile inspection device. progress report,” tech. rep., Ofgem, Gas Network Innovation Competition (NIC), 2015.
- [25] G. H. Mills, A. E. Jackson, and R. C. Richardson, “Advances in the inspection of unpiggable pipelines,” *Robotics*, vol. 6, no. 4, p. 36, 2017.
- [26] N. N. G. G. Transmission, “Project graid: Gas robotic agile inspection device. progress report 5,” tech. rep., Ofgem, Gas Network Innovation Competition (NIC), 2017.

-
- [27] Pololu Robotics and Electronics, *Micro Metal Gearmotors*, 6 2019. Rev. 4.1.
- [28] M. Tan, F. Varela, K. Wang, *et al.*, “Field experiences of using electrochemically integrated electrode arrays as corrosion monitoring probes for visualizing buried pipeline corrosion,” in *CORROSION 2019*, NACE International, 2019.
- [29] M. R. Kandroodi, B. N. Araabi, M. N. Ahmadabadi, F. Shirani, and M. M. Bassiri, “Detection of natural gas pipeline defects using magnetic flux leakage measurements,” in *2013 21st Iranian Conference on Electrical Engineering (ICEE)*, pp. 1–6, IEEE, 2013.
- [30] T. T. Nguyen, H. R. Yoo, Y. W. Rho, and S. B. Kim, “Speed control of pig using bypass flow in natural gas pipeline,” in *ISIE 2001. 2001 IEEE International Symposium on Industrial Electronics Proceedings (Cat. No. 01TH8570)*, vol. 2, pp. 863–868, IEEE, 2001.
- [31] T. T. Nguyen, S. B. Kim, H. R. Yoo, and Y. W. Rho, “Modeling and simulation for pig flow control in natural gas pipeline,” *KSME International Journal*, vol. 15, no. 8, pp. 1165–1173, 2001.
- [32] H. S. Han, J. J. Yu, C. G. Park, and J. G. Lee, “Development of inspection gauge system for gas pipeline,” *KSME international Journal*, vol. 18, no. 3, pp. 370–378, 2004.
- [33] T. T. Nguyen, D. K. Kim, Y. W. Rho, and S. B. Kim, “Dynamic modeling and its analysis for pig flow through curved section in natural gas pipeline,” in *Proceedings 2001 IEEE International Symposium on Computational Intelligence in Robotics and Automation (Cat. No. 01EX515)*, pp. 492–497, IEEE, 2001.
- [34] F. Gan, Z.-W. Sun, G. Sabde, and D.-T. Chin, “Cathodic protection to mitigate external corrosion of underground steel pipe beneath disbonded coating,” *Corrosion*, vol. 50, no. 10, pp. 804–816, 1994.
- [35] G. Caprari, A. Breitenmoser, W. Fischer, C. Hürzeler, F. Tâche, R. Siegwart, O. Nguyen, R. Moser, P. Schoeneich, and F. Mondada, “Highly compact robots for inspection of power plants,” *Journal of Field Robotics*, vol. 29, no. 1, pp. 47–68, 2012.

-
- [36] J. M. M. Tur and W. Garthwaite, "Robotic devices for water main in-pipe inspection: A survey," *Journal of Field Robotics*, vol. 4, no. 27, pp. 491–508, 2010.
- [37] A. Nayak and S. Pradhan, "Investigations of design issues related to in-pipe inspection robots," *International Journal of Emerging Technology and Advanced Engineering*, vol. 4, no. 3, 2014.
- [38] N. S. Roslin, A. Anuar, M. F. A. Jalal, and K. S. M. Sahari, "A review: Hybrid locomotion of in-pipe inspection robot," *Procedia Engineering*, vol. 41, pp. 1456–1462, 2012.
- [39] N. A. B. H. Yahya, N. Ashrafi, and A. H. Humod, "Development and adaptability of in-pipe inspection robots," *IOSR Journal of Mechanical and Civil Engineering*, vol. 11, no. 4, pp. 1–8, 2014.
- [40] L. Shao, Y. Wang, B. Guo, and X. Chen, "A review over state of the art of in-pipe robot," in *2015 IEEE International Conference on Mechatronics and Automation (ICMA)*, pp. 2180–2185, IEEE, 2015.
- [41] C. Choi and K. Youcef-Toumi, "Robot design for high flow liquid pipe networks," in *2013 IEEE/RSJ International Conference on Intelligent Robots and Systems*, pp. 246–251, IEEE, 2013.
- [42] J. Ong, D. Kerr, and K. Bouazza-Marouf, "Design of a semi-autonomous modular robotic vehicle for gas pipeline inspection," *Proceedings of the Institution of Mechanical Engineers, Part I: Journal of Systems and Control Engineering*, vol. 217, no. 2, pp. 109–122, 2003.
- [43] T. Okada and T. Sanemori, "Mogrer: A vehicle study and realization for in-pipe inspection tasks," *IEEE Journal on Robotics and Automation*, vol. 3, no. 6, pp. 573–582, 1987.
- [44] T. Okada and T. Kanade, "A three-wheeled self-adjusting vehicle in a pipe, ferret-1," *The International journal of robotics research*, vol. 6, no. 4, pp. 60–75, 1987.
- [45] A. Gargade, D. Tambuskar, and G. Thokal, "Modelling and analysis of pipe inspection robot," *International Journal of Emerging Technology and Advanced Engineering*, vol. 3, no. 5, pp. 120–126, 2013.

-
- [46] H.-o. Lim and T. Ohki, "Development of pipe inspection robot," in *2009 ICCAS-SICE*, pp. 5717–5721, IEEE, 2009.
- [47] Y. Zhang and G. Yan, "In-pipe inspection robot with active pipe-diameter adaptability and automatic tractive force adjusting," *Mechanism and Machine Theory*, vol. 42, no. 12, pp. 1618–1631, 2007.
- [48] H. R. Choi and S.-g. Roh, "In-pipe robot with active steering capability for moving inside of pipelines," in *Bioinspiration and Robotics Walking and Climbing Robots*, IntechOpen, 2007.
- [49] S.-g. Roh and H. Choi, "Strategy for navigation inside pipelines with differential-drive inpipe robot," in *Proceedings 2002 IEEE International Conference on Robotics and Automation (Cat. No. 02CH37292)*, vol. 3, pp. 2575–2580, IEEE, 2002.
- [50] H. M. Kim, J. S. Suh, Y. S. Choi, T. D. Trong, H. Moon, J. Koo, S. Ryew, and H. R. Choi, "An in-pipe robot with multi-axial differential gear mechanism," in *2013 IEEE/RSJ international conference on intelligent robots and systems*, pp. 252–257, IEEE, 2013.
- [51] S.-g. Roh and H. R. Choi, "Differential-drive in-pipe robot for moving inside urban gas pipelines," *IEEE transactions on robotics*, vol. 21, no. 1, pp. 1–17, 2005.
- [52] D. Chatzigeorgiou, K. Youcef-Toumi, and R. Ben-Mansour, "Design of a novel in-pipe reliable leak detector," *IEEE/ASME Transactions on Mechatronics*, vol. 20, no. 2, pp. 824–833, 2014.
- [53] L. Mateos and M. Vincze, "In-pipe robot with capability of self stabilization and accurate pipe surface cleaning," in *Proceedings of the IEEE International Conference on Automation Science and Engineering*, vol. 2013, p. 7, 2013.
- [54] P. Li, S. Ma, B. Li, and Y. Wang, "Multifunctional mobile units with a same platform for in-pipe inspection robots," in *Intelligent Robots and Systems, 2008. IROS 2008. IEEE/RSJ International Conference on*, pp. 2643–2648, IEEE, 2008.
- [55] Y.-S. Kwon, H. Lim, E.-J. Jung, and B.-J. Yi, "Design and motion planning of a two-moduled indoor pipeline inspection robot," in *2008 IEEE International Conference on Robotics and Automation*, pp. 3998–4004, IEEE, 2008.

-
- [56] Y.-S. Kwon, B. Lee, I.-C. Whang, and B.-J. Yi, "A pipeline inspection robot with a linkage type mechanical clutch," in *2010 IEEE/RSJ International Conference on Intelligent Robots and Systems*, pp. 2850–2855, IEEE, 2010.
- [57] F. Tâche, W. Fischer, R. Siegwart, R. Moser, and F. Mondada, "Compact magnetic wheeled robot with high mobility for inspecting complex shaped pipe structures," in *2007 IEEE/RSJ International Conference on Intelligent Robots and Systems*, pp. 261–266, IEEE, 2007.
- [58] A. Breitenmoser, F. Tâche, G. Caprari, R. Siegwart, and R. Moser, "Magnebike: Toward multi climbing robots for power plant inspection," in *Proceedings of the 9th International Conference on Autonomous Agents and Multiagent Systems: Industry track*, pp. 1713–1720, International Foundation for Autonomous Agents and Multiagent Systems, 2010.
- [59] F. Tâche, F. Pomerleau, W. Fischer, G. Caprari, F. Mondada, R. Moser, and R. Siegwart, "Magnebike: Compact magnetic wheeled robot for power plant inspection," in *2010 1st International Conference on Applied Robotics for the Power Industry*, pp. 1–2.
- [60] F. Tâche, W. Fischer, R. Moser, F. Mondada, and R. Siegwart, "Adapted magnetic wheel unit for compact robots inspecting complex shaped pipe structures," in *2007 IEEE/ASME international conference on advanced intelligent mechatronics*, pp. 1–6, IEEE, 2007.
- [61] W. Fischer, G. Caprari, R. Siegwart, and R. Moser, "Very compact climbing robot rolling on magnetic hexagonal cam-discs, with high mobility on obstacles but minimal mechanical complexity," in *ISR 2010 (41st International Symposium on Robotics) and ROBOTIK 2010 (6th German Conference on Robotics)*, pp. 1–7, VDE, 2010.
- [62] F. Tâche, F. Pomerleau, G. Caprari, R. Siegwart, M. Bosse, and R. Moser, "Three-dimensional localization for the magnebike inspection robot," *Journal of Field Robotics*, vol. 28, no. 2, pp. 180–203, 2011.
- [63] M. R. A. M. Zin, K. S. M. Sahari, J. M. Saad, A. Anuar, and A. T. Zulkarnain, "Development of a low cost small sized in-pipe robot," *Procedia Engineering*, vol. 41, pp. 1469–1475, 2012.

-
- [64] A. A. Nassiraei, Y. Kawamura, A. Ahrary, Y. Mikuriya, and K. Ishii, “Concept and design of a fully autonomous sewer pipe inspection mobile robot” kantaro”, in *Robotics and Automation, 2007 IEEE International Conference on*, pp. 136–143, IEEE, 2007.
- [65] M. M. Moghaddam and A. Hadi, “Control and guidance of a pipe inspection crawler (pic),” in *International symposium on automation and robotics*, pp. 11–14, 2005.
- [66] M. M. Moghaddam and M. R. A. Tafti, “Design, modeling and prototyping of a pipe inspection robot,” in *22nd International Symposium on Automation and Robotics in Construction ISARC*, pp. 11–14, 2005.
- [67] N. Truong-Thanh, N. Ngoc-Phuong, and T. Phuoc-Tho, “A study of pipe-cleaning and inspection robot,” in *2011 IEEE International Conference on Robotics and Biomimetics*, pp. 2593–2598, IEEE, 2011.
- [68] K. Tadakuma, A. Ming, M. Shimojo, R. Tadakuma, K. Nagatani, K. Yoshida, and K. Iagnemma, “Basic running test of the cylindrical tracked vehicle with sideways mobility,” in *2009 IEEE/RSJ International Conference on Intelligent Robots and Systems*, pp. 1679–1684, IEEE, 2009.
- [69] M. Ciszewski, T. Buratowski, M. Giergiel, P. Małka, and K. Kurc, “Virtual prototyping, design and analysis of an in-pipe inspection mobile robot,” *Journal of Theoretical and Applied Mechanics*, vol. 52, no. 2, pp. 417–429, 2014.
- [70] J.-H. Kim, “Design of a fully autonomous mobile pipeline exploration robot (famper),” 2008.
- [71] M. M. Moghaddam, M. Arbabtafti, and A. Hadi, “In-pipe inspection crawler adaptable to the pipe interior diameter,” *International Journal of Robotics and Automation*, vol. 26, no. 2, p. 135, 2011.
- [72] T. Oya and T. Okada, “Development of a steerable, wheel-type, in-pipe robot and its path planning,” *Advanced Robotics*, vol. 19, no. 6, pp. 635–650, 2005.
- [73] M. Ciszewski, M. Waclawski, T. Buratowski, M. Giergiel, and K. Kurc, “Design, modelling and laboratory testing of a pipe inspection robot,” *Archive of Mechanical Engineering*, vol. 62, no. 3, pp. 395–408, 2015.

-
- [74] A. Kakogawa and S. Ma, "Speed analysis for three driving modules of an in-pipe inspection robots for passing through bent pipes," in *Robotics and Biomimetics (ROBIO), 2014 IEEE International Conference on*, pp. 1731–1736, IEEE, 2014.
- [75] A. Kakogawa, S. Ma, and S. Hirose, "An in-pipe robot with underactuated parallelogram crawler modules," in *2014 IEEE International Conference on Robotics and Automation (ICRA)*, pp. 1687–1692, IEEE, 2014.
- [76] J. Park, T. Kim, and H. Yang, "Development of an actively adaptable in-pipe robot," in *2009 IEEE International Conference on Mechatronics*, pp. 1–5, IEEE, 2009.
- [77] Y. Kang, J. Park, and H. Yang, "Analytical approach of the in-pipe robot on branched pipe navigation and its solution," *International Journal of Mechanical, Aerospace, Industrial, Mechatronic and Manufacturing Engineering*, vol. 7, no. 5, pp. 907–911, 2013.
- [78] J. W. Park, W. Jeon, Y. K. Kang, H. S. Yang, and H. Park, "Instantaneous kinematic analysis for a crawler type in-pipe robot," in *2011 IEEE International Conference on Mechatronics*, pp. 381–385, IEEE, 2011.
- [79] J. Min, Y. D. Setiawan, P. S. Pratama, S. B. Kim, and H. K. Kim, "Development and controller design of wheeled-type pipe inspection robot," in *Advances in Computing, Communications and Informatics (ICACCI, 2014 International Conference on*, pp. 789–795, IEEE, 2014.
- [80] K. Nagaya, T. Yoshino, M. Katayama, I. Murakami, and Y. Ando, "Wireless piping inspection vehicle using magnetic adsorption force," *IEEE/ASME Transactions on Mechatronics*, vol. 17, no. 3, pp. 472–479, 2012.
- [81] M. Kurata, T. Takayama, and T. Omata, "Helical rotation in-pipe mobile robot," in *2010 3rd IEEE RAS & EMBS International Conference on Biomedical Robotics and Biomechatronics*, pp. 313–318, IEEE, 2010.
- [82] T. Takayama, H. Takeshima, T. Hori, and T. Omata, "A twisted bundled tube locomotive device proposed for in-pipe mobile robot," *IEEE/ASME Transactions on Mechatronics*, vol. 20, no. 6, pp. 2915–2923, 2015.

-
- [83] P. Li, S. Ma, B. Li, Y. Wang, and Y. Liu, "Self-rescue mechanism for screw drive in-pipe robots," in *2010 IEEE/RSJ International Conference on Intelligent Robots and Systems*, pp. 2843–2849, IEEE, 2010.
- [84] C. Ye, L. Liu, X. Xu, and J. Chen, "Development of an in-pipe robot with two steerable driving wheels," in *Mechatronics and Automation (ICMA), 2015 IEEE International Conference on*, pp. 1955–1959, IEEE, 2015.
- [85] S. Guo, Q. Yang, L. Bai, and Y. Zhao, "Magnetic driven wireless multiple capsule robots with different structures," in *2018 IEEE International Conference on Mechatronics and Automation (ICMA)*, pp. 626–630, IEEE, 2018.
- [86] P. Debenest, M. Guarnieri, and S. Hirose, "Pipetron series-robots for pipe inspection," in *Applied Robotics for the Power Industry (CARPI), 2014 3rd International Conference on*, pp. 1–6, IEEE, 2014.
- [87] D. Dâ€™Zurko, N. G. Association, *et al.*, "Completion of development of robotics systems for inspecting unpiggable transmission pipelines," tech. rep., NYSEARCH/Northeast Gas Association, 2013.
- [88] D.-K. Kim, H.-R. Yoo, J.-S. Yoo, D.-K. Kim, S.-H. Cho, S.-J. Koo, R.-Y. Woo, and H.-K. Jung, "Development of mfl system for in-pipe robot for unpiggable natural gas pipelines," in *2013 10th International Conference on Ubiquitous Robots and Ambient Intelligence (URAI)*, pp. 51–54, IEEE, 2013.
- [89] H. Choi and S. Ryew, "Robotic system with active steering capability for internal inspection of urban gas pipelines," *Mechatronics*, vol. 12, no. 5, pp. 713–736, 2002.
- [90] G. C. Vradis and W. Leary, "Development of an inspection platform and a suite of sensors for assessing corrosion and mechanical damage on unpiggable transmission mains," tech. rep., Northeast Gas Association (US), 2004.
- [91] S. A. Fjerdings, P. Liljebäck, and A. A. Transeth, "A snake-like robot for internal inspection of complex pipe structures (piko)," in *2009 IEEE/RSJ International Conference on Intelligent Robots and Systems*, pp. 5665–5671, IEEE, 2009.
- [92] E. Prada, M. Valášek, I. Virgala, A. Gmitterko, M. Kelemen, M. Hagara, and T. Lipták, "New approach of fixation possibilities investigation for snake robot

- in the pipe,” in *Mechatronics and Automation (ICMA), 2015 IEEE International Conference on*, pp. 1204–1210, IEEE, 2015.
- [93] E. Dertien, M. M. Foumashi, K. Pulles, and S. Stramigioli, “Design of a robot for in-pipe inspection using omnidirectional wheels and active stabilization,” in *2014 IEEE International Conference on Robotics and Automation (ICRA)*, pp. 5121–5126, IEEE, 2014.
- [94] C. Wright, A. Buchan, B. Brown, J. Geist, M. Schwerin, D. Rollinson, M. Tesch, and H. Choset, “Design and architecture of the unified modular snake robot,” in *2012 IEEE International Conference on Robotics and Automation*, pp. 4347–4354, IEEE, 2012.
- [95] R. Buckingham, V. Chitrakaran, R. Conkie, G. Ferguson, A. Graham, A. Lazell, M. Lichon, N. Parry, F. Pollard, A. Kayani, *et al.*, “Snake-arm robots: a new approach to aircraft assembly,” tech. rep., SAE Technical Paper, 2007.
- [96] W. Jeon, J. Park, I. Kim, Y.-K. Kang, and H. Yang, “Development of high mobility in-pipe inspection robot,” in *System Integration (SII), 2011 IEEE/SICE International Symposium on*, pp. 479–484, IEEE, 2011.
- [97] J. Yang, Y. Xue, J. Shang, and Z. Luo, “Research on a new bilateral self-locking mechanism for an inchworm micro in-pipe robot with large traction,” *International Journal of Advanced Robotic Systems*, vol. 11, no. 10, p. 174, 2014.
- [98] Y. Zhang, M. Zhang, H. Sun, and Q. Jia, “Design and motion analysis of a flexible squirm pipe robot,” in *2010 International Conference on Intelligent System Design and Engineering Application*, vol. 1, pp. 527–531, IEEE, 2010.
- [99] Z. Wang and H. Gu, “A bristle-based pipeline robot for ill-constraint pipes,” *IEEE/ASME Transactions On Mechatronics*, vol. 13, no. 3, pp. 383–392, 2008.
- [100] Y. Wu, D. Chatzigeorgiou, K. Youcef-Toumi, and M. Zribi, “Modeling and parameter estimation for in-pipe swimming robots,” in *American Control Conference (ACC), 2015*, pp. 2007–2013, IEEE, 2015.
- [101] M. J. Doyle, X. Xu, Y. Gu, F. Perez-Diaz, C. Parrott, and R. Groß, “Modular hydraulic propulsion: A robot that moves by routing fluid through itself,”

-
- in *Robotics and Automation (ICRA), 2016 IEEE International Conference on*, pp. 5189–5196, IEEE, 2016.
- [102] N. Khirade, R. Sanghi, and D. Tidke, “Magnetic wall climbing devices—a review,” in *Proceedings of the International Conference on Advances in Engineering & Technology, Singapore*, pp. 29–30, 2014.
- [103] F. Rochat, P. Schoeneich, O. T.-D. Nguyen, and F. Mondada, “Tripillar: Miniature magnetic caterpillar climbing robot with plane transition ability,” in *Mobile Robotics: Solutions and Challenges*, pp. 343–350, World Scientific, 2010.
- [104] K. Liu, W. Zhang, and P. Zeng, “Symmetrically centralized magnetic-wheel unit for wall-climbing robots,” in *Proceedings of the 13th IASTED International Conference ROBOTICS AND APPLICATIONS, (August 29-31, 2007)*, 2007.
- [105] W. Song, H. Jiang, T. Wang, D. Ji, and S. Zhu, “Design of permanent magnetic wheel-type adhesion-locomotion system for water-jetting wall-climbing robot,” *Advances in Mechanical Engineering*, vol. 10, no. 7, p. 1687814018787378, 2018.
- [106] H. Yaguchi, “Magnetic actuator capable of inspection in a complex pipe by phase control of multiple electromagnetic vibration components,” *IEEE Transactions on Magnetics*, vol. 51, no. 11, pp. 1–4, 2015.
- [107] A. Peidr , M. Tavakoli, J. M. Mar n, and  . Reinoso, “Design of compact switchable magnetic grippers for the hyecro structure-climbing robot,” *Mechatronics*, vol. 59, pp. 199–212, 2019.
- [108] M. E. Falkus, *Always Under Pressure: A History of North Thames Gas Since 1949*. Springer, 1988.
- [109] J. McHugh, “The engineering of the national transmission system of the british gas corporation,” *Proceedings of the Institution of Mechanical Engineers, Part A: Power and Process Engineering*, vol. 197, no. 3, pp. 179–196, 1983.
- [110] W. F. Rush Jr, B. K. Campbell, K. C. Hardy, and L. A. Sweetwood, “Process and apparatus for insertion of robots in gas distribution systems,” Aug. 26 1997. US Patent 5,660,202.

-
- [111] N. H. Versloot, A. Klein, and M. De Maaijer, “The atex directives: Explosion safety and regulation, the european approach,” *Emerg. Plan. Prep. Prev. Response, Hoboken, NJ, USA: John Wiley & Sons, Inc*, pp. 389–404, 2010.
- [112] T. Sato, T. Kano, R. Kobayashi, and A. Ishiguro, “Snake-like robot driven by decentralized control scheme for scaffold-based locomotion,” in *2012 IEEE/RSJ International Conference on Intelligent Robots and Systems*, pp. 132–138, IEEE, 2012.
- [113] J. Xiao and A. Sadegh, “City-climber: a new generation wall-climbing robots,” in *Climbing and Walking Robots: towards New Applications*, IntechOpen, 2007.
- [114] K. Autumn, Y. A. Liang, S. T. Hsieh, W. Zesch, W. P. Chan, T. W. Kenny, R. Fearing, and R. J. Full, “Adhesive force of a single gecko foot-hair,” *Nature*, vol. 405, no. 6787, p. 681, 2000.
- [115] G. Pahl and W. Beitz, *Engineering design: a systematic approach*. Springer Science & Business Media, 2013.
- [116] J. H. Jung, N. Pan, and T. J. Kang, “Generalized capstan problem: Bending rigidity, nonlinear friction, and extensibility effect,” *Tribology International*, vol. 41, no. 6, pp. 524–534, 2008.
- [117] F. Rochat, V. Hirschmann, T. Barras, H. BLEUER, and F. Mondada, “Climbing robot with thermal glue,” in *Field Robotics*, pp. 415–420, World Scientific, 2012.
- [118] L. Briones, P. Bustamante, and M. A. Serna, “Wall-climbing robot for inspection in nuclear power plants,” in *Proceedings of the 1994 IEEE International Conference on Robotics and Automation*, pp. 1409–1414, IEEE, 1994.
- [119] M. Eich and T. Vögele, “Design and control of a lightweight magnetic climbing robot for vessel inspection,” in *2011 19th Mediterranean Conference on Control & Automation (MED)*, pp. 1200–1205, IEEE, 2011.
- [120] Y. Zhang, T. Dodd, K. Atallah, and I. Lyne, “Design and optimization of magnetic wheel for wall and ceiling climbing robot,” in *2010 IEEE International Conference on Mechatronics and Automation*, pp. 1393–1398, IEEE, 2010.

-
- [121] W. Fischer, F. Tâche, and R. Siegwart, "Inspection system for very thin and fragile surfaces, based on a pair of wall climbing robots with magnetic wheels," in *2007 IEEE/RSJ International Conference on Intelligent Robots and Systems*, pp. 1216–1221, IEEE, 2007.
- [122] S.-C. Han, J. Kim, and H.-C. Yi, "A novel design of permanent magnet wheel with induction pin for mobile robot," *International Journal of Precision Engineering and Manufacturing*, vol. 10, no. 4, pp. 143–146, 2009.
- [123] W. Li, A. Li, and H. Wang, "Anisotropic fracture behavior of sintered rare-earth permanent magnets," *IEEE transactions on magnetics*, vol. 41, no. 8, pp. 2339–2342, 2005.
- [124] J. Coey, "Permanent magnet applications," *Journal of Magnetism and Magnetic Materials*, vol. 248, no. 3, pp. 441–456, 2002.
- [125] "Magnet expert. 6mm neodymium magnet products: F362-25, d-f364, f644-25." <https://www.first4magnets.com/circular-disc-rod-c34/6mm-diameter-wide-magnets-t55>. Accessed: 2019-06-24.
- [126] Mecmesin, *MultiTest 5-i Technical Datasheet ref 431-343-09*, 4 2019. Rev. 4.1.
- [127] V. G. Cerf, "Ascii format for network interchange," tech. rep., 1969.
- [128] R. H. Armour and J. F. Vincent, "Rolling in nature and robotics: a review," *Journal of Bionic Engineering*, vol. 3, no. 4, pp. 195–208.
- [129] M. Hernandez-Rodriguez, D. Martinez-Delgado, R. Gonzalez, A. P. Unzueta, R. Mercado-Solís, and J. Rodriguez, "Corrosive wear failure analysis in a natural gas pipeline," *Wear*, vol. 263, no. 1-6, pp. 567–571, 2007.

8.4 Appendix A: Published Work "Advances in the Inspection of Unpiggable Pipelines"

This appendix presents the work from Chapter 2 which has been published in an academic journal:

- G. H. Mills, A. E. Jackson, and R. C. Richardson, Advances in the inspection of unpiggable pipelines, *Robotics*, vol. 6, no. 4, p. 36, 2017.



Review

Advances in the Inspection of Unpiggable Pipelines

George H. Mills *, Andrew E. Jackson and Robert C. Richardson

School of Mechanical Engineering, University of Leeds, Leeds LS2 9JT, UK; A.E.Jackson@Leeds.ac.uk (A.E.J.); R.C.Richardson@Leeds.ac.uk (R.C.R)

* Correspondence: G.H.Mills@leeds.ac.uk

Received: 2 October 2017; Accepted: 23 November 2017; Published: 29 November 2017

Abstract: The field of in-pipe robotics covers a vast and varied number of approaches to the inspection of pipelines with robots specialising in pipes ranging anywhere from 10 mm to 1200 mm in diameter. Many of these developed systems focus on overcoming in-pipe obstacles such as T-sections and elbows, as a result important aspects of exploration are treated as sub-systems, namely shape adaptability. One of the most prevalent methods of hybridised locomotion today is wall-pressing; generating traction using the encompassing pipe walls. A review of wall-pressing systems has been performed, covering the different approaches taken since their introduction. The advantages and disadvantages of these systems is discussed as well as their effectiveness in the inspection of networks with highly varying pipe diameters. When compared to unconventional in-pipe robotic techniques, traditional full-bore wall-pressing robots were found to be at a disadvantage.

Keywords: in-pipe; review; locomotion

1. Introduction

Pipeline networks transport fluids such as oil, gas, water, and sewage between key locations through an estimated total of 2.5 million km (2.2 million miles) of global infrastructure [1]. Failure to adequately inspect and replace pipes results in pipe failure and subsequent loss of fluid transport, environmental damage, large excavations resulting in transport delays and air pollution. Most of the worlds pipelines are relatively easily inspected using advanced Pipeline Inspection Gauges or 'PIGs'; passive devices placed into the pipe and driven by the flow of the transported fluid. However, PIGs are uncontrollable and unable to adapt to sharp changes in pipe direction and diameter, making complex pipe infrastructure impossible to inspect. It is estimated that just 0.5% of pipe networks are inaccessible to conventional 'PIGGING' technology, the remaining 99.5% generally consisting of large bore, straight piggable lines. Whilst this proportion may seem low, the remaining 12,500 km represents the most valuable pipes in the network; Above Ground Installations (AGI's). Many of these unpiggable networks are now reaching the end of their design lives and are due for replacement, however with the condition of their interior walls unknown it is impossible to tell which pipes should take replacement priority. It has been estimated that through the use of advanced inspection techniques, savings made from unnecessary pipeline replacement could be equivalent to £14,000 per km a year [2].

1.1. Pipe Bends and Joints

Unpiggable pipe networks vary in diameter range, material, and fluid type and can be joined in various methods and configurations. Categorized pipe joint configurations are shown in Figure 1. Horizontal sections (Figure 1A) are considered the baseline for in-pipe complexity, any in-pipe robot should be able to navigate these. Configurations B to F are more complex, passing through them requires advanced motion planning techniques.

8.4 Appendix A: Published Work "Advances in the Inspection of Unpiggable Pipelines"

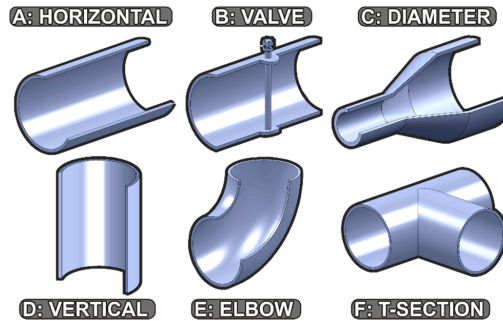


Figure 1. The most commonly encountered in-pipe bends and joints in networks.

Valves, are particularly difficult as designs such as plug valves (Figure 1B) can split the cross-section in two hindering full-bore robots. Changes in diameter (Figure 1C) are a common occurrence in unpiggable systems, many robots take measures to prepare for this obstacle specifically. Vertical sections (Figure 1D) require a traction method that must also overcome gravity. Elbows (Figure 1E) are very commonly encountered and are often described in terms of their bend radius; lower radius bends are tighter harder to navigate. T-Sections (Figure 1F) are extremely challenging obstacles due to their lack of wall support; only sophisticated robotic platforms can navigate these [3]. Each of these in-pipe obstacles can be found in any orientation and possibly even back-to-back e.g., encountering two consecutive bends. Developing a single robot to solve all of these problems in a wide range of diameters is currently unheard of and often requires a fleet of multiple systems in different class sizes [4]. In this review significant robots that have furthered the research field will be presented. Current state-of-the-art methods of in-pipe travel and inspection are discussed as well as the future abilities of in-pipe robots. By analysing the barriers facing current technology and the methods being employed to overcome them, breakthroughs can be made towards universal in-pipe inspection. This review addresses in particular the problems surrounding shape adaptability, fleets, and system classes and their role in universal pipe inspection.

1.2. Robotic in-Pipe Locomotion

In-pipe inspection robots have the potential to inspect the condition of these vital assets by manoeuvring through the network. This is no simple feat, and one of the first challenges faced is the generation of traction within the environment. Many potential robotic solutions have been proposed to inspect these ‘unpiggable’ pipelines, all of which utilised one of the in-pipe traction methods, presented in Figure 2. These traction methods are; Gravity (Figure 2A), reliance on gravity alone restricts vehicles to only horizontal and lightly inclined pipes. Wall-Pressing (Figure 2B), using the reaction force from the enclosed walls, usually in combination with diametric adaption mechanisms. Wall adhesion (Figure 2C), utilising ferrous pipelines to produce a reaction force. Fluid Flow (Figure 2D), utilising the transport medium to move usually in combination with a passive PIG or propeller device. Through the combination of these traction methods and the locomotion elements presented in Figure 2 specialised hybrid in-pipe systems can be created.

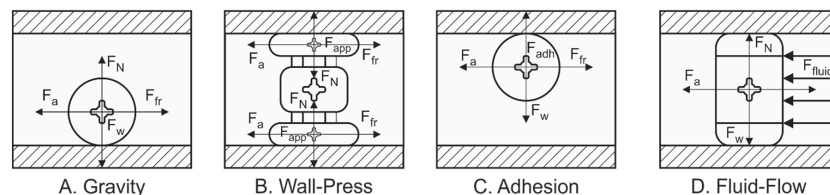


Figure 2. In-pipe traction method free body diagrams.

8.4 Appendix A: Published Work "Advances in the Inspection of Unpiggable Pipelines"

Initially when issues surrounding in-line inspection of unpiggable pipelines became apparent, traditional gravity based exploration robots were re-purposed for the task [5]. These robots were generally track or wheel based and built to handle rough terrain, they were not well suited to the pipeline environment and could explore only horizontal sections and gentle inclines. Although these systems performed adequately in large bore sewage and water based networks. It wasn't until robotic systems developed advanced methods of in-pipe traction such as wall-pressing, adhesion through magnetics, and fluid flow that the more complex pipeline configurations could be explored. Using the methods of traction in Figure 2 as a design basis, many variations of in-pipe locomotion have been created to solve in-pipe tasks. Figure 3 shows the different systems classified by their locomotion mechanism into the eight types labelled. PIGs (Figure 3A) are transport fluid driven devices, although very effective in horizontal pipes they cannot be controlled in complex networks. Wheeled robots (Figure 3B) are the simplest method of in-pipe locomotion and can be used in combination with many other element types. Tracked robots (Figure 3C), also known as caterpillars, are used as an alternative to wheeled systems, their large surface contact area generates high friction and reduce chances of losing wall contact. Screw robots (Figure 3D) use a spiral inspection path, they perform well in vertical sections and are resistant to slip due to their angled approach, even against an in-pipe flow. Snake robots (Figure 3E) take advantage of the length of the pipe, they are generally modular and adaptable to many in-pipe environments. Inchworm robots (Figure 3F) are slower than other types but can generally carry higher payloads due to their need for high wall-traction forces, useful in industrial transport tasks where speed is unimportant. Propeller based robots (Figure 3G) use transported fluid medium to navigate pipelines and have the advantage of not relying on walls for any movement, however they cannot move in offline systems without fluid. Walking robots (Figure 3H) use legs with multiple degrees of freedom (D.O.F) to move, their end effectors have low surface areas, useful in cutting through in-pipe wall contaminants.



Figure 3. The eight main elements of in-pipe robotic locomotion (A–H).

These basic locomotion elements are more often than not used in conjunction with another, forming a hybrid system. An example of a hybrid system would be an articulated snake robot that uses caterpillar tracks to move, or a screw robot that using wheels for rotation. Of the 234 systems reviewed only 18% were robots that used just one type, with the rest combining two or more. Wall-pressing is the most popular method of generating in-pipe traction, with 44% of robotic research systems applying it. These systems mostly consist of a chassis that is kept concentric with the pipe using some form of locomotion method or 'plane' of contact with the wall. These planes are normally tracks or wheel subsystems that are mounted perpendicular to the chassis. Wall-press designs using varying numbers of planes, each with set-up having their own advantages and disadvantages as shown in Figure 4.

8.4 Appendix A: Published Work "Advances in the Inspection of Unpigable Pipelines"

A great advantage of having a concentric chassis is the distance to each contact plane is constant and methods of pipe diameter adaptability can be centrally located. The parallelogram mechanism and pantograph scissor mechanisms are among the most commonly used in wall-pressing in-pipe robotics. These mechanisms perform well because the planes of contact remain parallel with the chassis of the robot and if centred properly, the inner wall of the pipe. Although they have many variations the most common use the rotation of a central lead screw in combination with a bar linkage design to achieve both traction, and size adaptability.

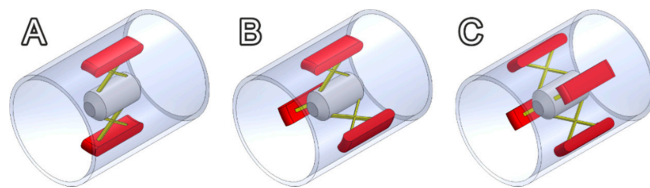


Figure 4. Examples of wall-pressing robots with; (A): 2, (B): 3, and (C): 4 plane designs.

2. Review of in-Pipe Locomotion Systems

An in-depth analysis of in-pipe robot publications over the last 30 years has been presented in Figure 5. Categorised by locomotion type and year published it gives a high level overview of the trends in the development of in-pipe inspection robots based on 234 published systems. The literature search was performed using the keywords; in-pipe, pipe, tube, system, robot, platform, in combination with locomotion and traction methods across multiple publishers. The volume of research robots being produced was found to steadily increase with time as the field has grown, this reflects on the necessity of pipe inspection as more networks become out-dated around the globe.

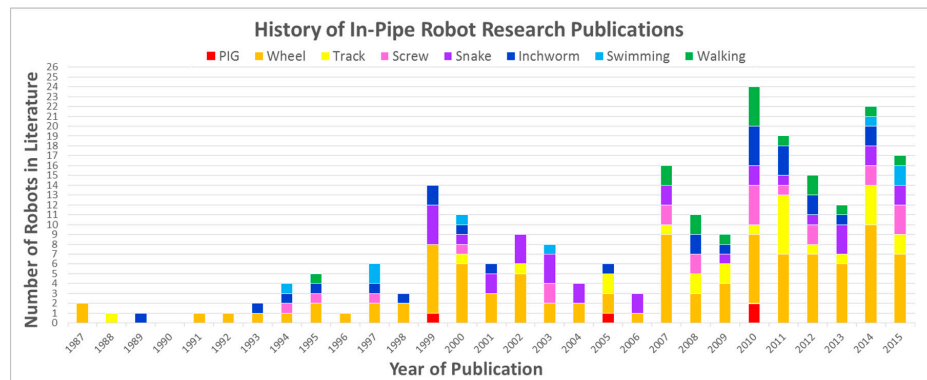


Figure 5. Locomotion types found in research based in-pipe robotic platforms.

Using the database of in-pipe research robots the key systems that have influenced the field have been selected and reviewed. These robotic platforms have been categorised in terms of their primary locomotion method, traction method, and their specified pipe diameter range. This section will look at robots from each of the eight in-pipe locomotion categories in detail. The strengths, weaknesses, and research direction of each type will be discussed later in Section 3.

2.1. Pipeline Inspection Gauges

PIGs may be simple devices but they are still the most efficient method of inspecting straight pipelines with a constant bore. New methods of pigging pipelines are still being developed, for example

8.4 Appendix A: Published Work "Advances in the Inspection of Unpiggable Pipelines"

Robotics 2017, 6, 36

5 of 13

in 2005 the University of Durham developed a new form of "PIG" [6] which incorporates a propeller, driven by the fluid flowing in the pipe as a mobile power source. Brushes embedded in the chassis will only allow movement in a single direction depending on the direction the brushes are facing, this results in a steady motion either upstream or downstream.

2.2. Wheeled Systems

Classified by the use of wheels as a main locomotion method, these systems can be combined with any of the four traction methods. When combined with wall-press and magnetic traction methods simple wheel based systems become efficient in-pipe robots. Shows wheeled systems (orange) are the most prevalent method of in-pipe locomotion, being used in 43% of all systems. This is due to their adaptability and ease of combination with other locomotion types excluding tracks to create hybrid in-pipe systems. Wheeled systems are predominantly used with wall press traction methods, with 49% of all wall pressing robots using wheel locomotion.

MOGRER, an in-pipe robot developed by Niigata University circa 1987 was one of the first wall-pressing systems [7]. It was created for the purpose of industrial pipe inspection tasks and set out to solve the biggest problem at the time; climbing angled pipes against gravity. MOGRER was an improvement on an even earlier wall-press design FERRET-1 which introduced a three wheeled adaptable robot with passive configuration using a spring system [8]. MOGRER further improved the spring system forming a scissor structure similar to a pantograph mechanism, a popular choice for diametric change methods in the future. Advanced wall-pressing systems have been in development for over a decade, MRINSPECT is a wheeled in-pipe robot series designed at Sungkyunkwan University [9]. The robot is capable of performing all types of geometry manoeuvres besides valves and has a 50 mm adaptability range from 130 to 180 mm. MRINSPECT uses a multi-axial differential gear system to control each of its four wheeled legs angles through active bevel drive connections.

Shenyang Institute of Automation have proposed a system which allows different robots to be created from the same platform. Although based around the same class size and pipe diameter of 200 mm three different systems were developed from one Multifunctional Mobile Unit, MMU [10]. These wheeled wall-pressing systems performed different functions; MMU1 could adapt to slight changes in pipe diameter, MMU2 was focused on detecting defects, MMU3 added a propeller function for fluid travel. The use of one common skeleton allowed these systems to be created from one design with relative ease compared a complete re-design. Advanced wheeled systems can adapt to almost all in-pipe obstacles, AQAM is a wheeled wall-pressing robot for 260–300 mm pipes, consisting of four arm mounted wheels in a single plane [11]. The robot has impressive manoeuvrability due to its four controllable arms and swivel mechanism to angle the wheels and hence rotate the robot in-pipe. This design allows the robot move through extremely complex in-pipe geometry such as T-Sections into a reduced vertical pipe section. AQAM shares its single plane design with Hanyang University's single-plane wheeled system [3]. These two systems have an advantage over multi-plane wall-pressing robots, by rotating in the pipe they can always maintains contact with the pipe walls in most complex obstacles. The problem faced with single plane contact is stability, any loss of wall contact in these designs will de-centralise the robot and make recovery extremely difficult. This is especially restrictive for Hanyangs system as the robot was capable of 80 mm–100 mm diameter pipes and hence only has a 20 mm adaptability range. Larger robots can also cover a wide range of diameters, Shanghai developed a large 3 planed wheeled system with a parallelogram mechanism that allowed adaption from 400 mm to 650 mm pipelines.

Wheeled in-pipe robots have capitalised on the ferrous properties of pipelines, magnetic robots allow the user to scale walls and maintain normal force without the need for wall-pressing functions. The first magnetic in-pipe robot was developed by the Osaka Gas Company in 1995, the system was a dual wheeled magnetic concept for the inspection 150–600 mm iron pipelines [12]. The concept was designed specifically to solve the T-section geometry problem without the need for a wall press robot, as these generally struggle with in-pipe valves and other sharp obstacle negotiation. MagneBike is

8.4 Appendix A: Published Work "Advances in the Inspection of Unpiggable Pipelines"

Robotics 2017, 6, 36

6 of 13

an advanced example of a wheeled in-pipe robot using magnetic traction that can steer in a large range of in-pipe diameters, not only this but in-pipe obstacles such as T-Sections become trivial [13]. MagneBike could inspect a maximum pipeline diameter of 300 mm and was designed for industrial applications inspecting power plants. MagneBike's use of wall adhesion in-pipe reduces all complex in-pipe obstacles to either convex or concave corners which it must overcome. This simplified problem is outlined in other wheeled mobile magnetic robots, such as the hexagonal climbing robot from ALSTOM systems [14]. Other magnetic traction systems have developed locomotion methods that could be adapted in-pipe, Omni-Climber is a multi-directional magnetic wheeled robot with built in chassis compliance, allowing it to adapt to a wide range of pipe diameters [15]. This could be adapted to in-pipe scenarios allowing a small robot to explore pipes which are respectively large in diameter.

Wheeled systems are even used in conjunction with PIG-like locomotion; using the fluid force to accelerate. Kantaro a wheeled wall-pressing in-pipe robot for sewage pipe applications developed at Kyushu Institute of Technology, Japan takes a different approach to wall-pressing by combining it with a fluid driven locomotion [16]. Relying simply on pipe geometry to 'sit' in the pipe, whilst it also has adaptability built in to move from 200 mm to 300 mm diameters. Fully autonomous with passive damping springs and no tether, the system was ambitious, boasting the ability to manoeuvre through pipe bends without the need for a controller.

2.3. Tracked Systems

Track, or caterpillar based locomotion can be used in the place of wheels, they hold the advantage when generating friction. The large contact surface area makes these systems more stable but also generally larger than their wheeled counterparts. Caterpillar tracks have been used in 11% of in-pipe systems and are growing in popularity in research robotics, Figure 5 Tracked systems are also predominantly wall-pressing with 75% of all caterpillar robots using the traction method, the remaining 25% relying on gravity alone.

Famper was developed as a fully autonomous mobile pipeline exploration robot at Seoul National University [17], it was a track/caterpillar robot using wall-pressing traction with four-planes. Designed for 6-inch sewage pipes; Famper uses a passive method of wall-pressing to attain normal force against the pipe using compression springs and coupled with a slider linkage mechanism. The four separate caterpillar tracks can be actuated independently allowing the robot to differentially drive through elbows and other obstacles where varied speed is required. Famper performs well in 6-inch pipes and claims to be capable of T-Sections but has only been proven to complete vertical T-sections from a horizontal down, utilising gravity in its favour during the contact-loss phase of the manoeuvre. The full-bore design of Famper leaves little room for shape adaptability, with a full range of just 127–157 mm, the purpose of which is mainly for obstacle negotiation. The lack of adaptability makes Famper unsuitable for any situation other than 6-Inch pipelines. This is a common occurrence with passive adaptability even in larger robots, systems such as AQAM which are exceptionally mobile and adaptable to changes in pipe geometry [11]. Caterpillar Wall-press systems are one of the most adaptive types of system in terms of shape adaptability. Tarbiat Modares University used active parallelogram adaption in a three-planed caterpillar wall-press system which could adapt from 250 mm to 350 mm, however this could be increased by altering the length of the linkages [18]. The lead screw used to alter the height of the tracks keeps all three planes extended at the same rate and hence keeps the chassis central in the pipe. Nigata University's tracked robot uses an adapted scissor mechanism can passively adapt from 140 mm to 210 mm [19]. Hanyang University developed a two module caterpillar wall-pressing robot using differential steering and a passive adaptability module using a four bar mechanism to produce the required normal force on the tracks. This system could handle 80–100 mm pipes and can tackle many difficult in-pipe obstacles using the two-module design [20]. The separate tracked modules were connected via a tension spring which would drag the rear or front module through an obstacle, removing the need for both modules to steer. AGH University have prototyped a large in-pipe robot for the inspection of 200 mm pipelines that uses caterpillar tracks on a

8.4 Appendix A: Published Work "Advances in the Inspection of Unpiggable Pipelines"

Robotics 2017, 6, 36

7 of 13

linkage which can alter their effective diameter [21]. This allows the robot to travel horizontally in a range of pipes from 201 mm to 235 mm. Although vertical travel is possible, this is only the case when the tracks are fully extended essentially making vertical travel possible only in a 235 mm pipe. AGH's systems low adaptability range is in stark contrast with Ritsumeikan University's parallelogram crawler; a caterpillar wall-press system with an impressive adaptive diameter of 136 mm to 226 mm almost double its own length [22].

Paroys-II uses an actively controlled pantograph mechanism with a partially passive spring mechanism, this allows large changes to be controlled and small obstacles to be ignored [23]. Its use of a second set of articulated caterpillar tracks allows a huge adaptive range of 400–700 mm. Similarly Pukyong National University's tracked in-pipe robot uses modules with both passive and active adaptability mechanisms [24]. The shape adaptability is controlled using a driven threaded shaft lead screw and allows for transitions between 300 mm to 500 mm effective diameter by altering the position of a four bar linkage. The second module replaces the lead screw with a compression spring allowing for both passive and active diametric adaptations.

2.4. Screw Systems

Screw systems are defined by the method of locomotion in-pipe, using a rotary motion to drive themselves forward using a spiral track, to move through the pipe in a pitched circle. These systems are always wall-pressing as they rely on the inner walls in order to thread through the pipes, this allows them to climb vertical pipelines with ease. Screw locomotion robots are generally very difficult to back-drive due to their angled wheels or tracks, making them effective in high flow networks. Screw systems have stayed relatively steady in terms of growth in Figure 5 although the element is only used in 9% of research systems.

Heli-Pipe a screw wall-press system has a diametric adaptive ability of just 10 mm, as a result four different prototypes were made, ranging from 170 mm to 40 mm. The largest of the systems having a range of 10 mm and the smallest 5 mm [25]. Emerging methods of in-pipe adaptability show the possibility of continuously deforming systems with many degrees of freedom. SPRING is a screw type wall-press robot developed at Osaka University, although it relies on full wall traction it is unlike traditional full-bore wall-press systems which keep their chassis centralised in the pipe [26]. The design consists of many connected modules which form a continuous tight spiral some of which contain wheels allowing the robot to move in a spiral motion. When faced with a sharp change in diameter the robot can stretch this spiral increasing its pitch and therefore decreasing its diameter to less than half its optimal width of 150 mm pipelines. This function is entirely possible because of the lack of a centralised chassis, making the robot very adaptable when faced with obstacles such as valves. Current issues include the complexity of the design, optimal redesign of the robot is very difficult due to the amount of parameters involved and so a simulation tool had been created to aid in this. Shenyang University created a wall-press robot based on helix movement in-pipe, capable of 250 mm to 300 mm pipeline exploration using a passively adaptive four bar linkage [27]. The robot can complete complex manoeuvres such as T-Sections using its active drive module to steer the course.

2.5. Snake Systems

In-pipe snake robots are typically feature articulated joints in a modular design paired with wheels or tracks for locomotion. The articulation allows many degrees of freedom within a single system making them very versatile in their approach to obstacles. In the last 15 years, in-pipe snake robots have become the preferred method of commercial pipeline inspection and account for 13% of in-pipe robotic research.

The PipeTron series developed by HiBot, Tokyo is a multitude of robotic in-pipe exploration snake robots. Predominantly designed for tight bend systems such as refineries and chemical plants, the system is tethered for instant retrieval and consists of passively articulated wheels connected in a series [28]. The passive torsion springs in each module joint allow the robot to bend and alter shape

8.4 Appendix A: Published Work "Advances in the Inspection of Unpiggable Pipelines"

Robotics 2017, 6, 36

8 of 13

depending on the problem encountered and the width of the pipe without requiring further actuators. Due to relatively low range of passive adaptability multiple platforms have been created for each commonly encountered pipe diameter: 75 mm, 100 mm and 150 mm. The Explorer series is a prime example of the amount of effort going into translation of robots for different size pipelines, initially developed at Carnegie Mellon University [4]. This large snake robot is designed for the inspection of live gas networks under operating conditions, however it requires a full bore to operate with little adaptability ranging from just 150–200 mm. Multiple systems have now been developed for operations in larger than specified networks.

Kanagawa University, presented an unusual and interesting method for coping with various pipe diameters. The robot is a hybrid of caterpillar and snake components, built from modular units each containing a driving caterpillar track [29]. Connecting three or more units allows the robot to drive in-pipe, should a larger diameter need to be traversed the number of driving units can be increased. Promising results were shown in experimental pipes of 100–300 mm, an exceptional range for a robot with modules of just 50 mm. Czech Technical University, Prague have developed a snake robot with the purpose of identifying new methods of generating pipe contact without relying on traditional wall-press mechanisms such as pantographs and parallelogram linkages [30]. The modular snake robot consists of many segments each of which contain both rotary and translational actuators, this allows the snake to form structures much more complex than full bore robots. The shape adaptability of 100 mm is already greater than twice the length of the body segments which measure just 50 mm, with greater numbers of segments this robot may even be able to handle a wider range of diameters. PIRATE was an in-pipe robot with the intended purpose of autonomous inspection of the gas distribution network in the Netherlands [31]. The robot is snake-like, and modular in nature featuring articulated clamping modules that can actively change the height of the robot to adapt to changes in pipe diameter. The design of the clamping modules was somewhat similar to the first proposal for a passively adaptive three wheeled inspection robot, [7]. However unlike passive systems the active articulated joints allow for an efficient change in pipe diameters, stretching to twice its original inspection diameter from 125 mm to 63 mm.

2.6. Walking Systems

Walking type in-pipe robots use multi D.O.F. legs to move around the pipe, these are generally complex and quite large due to the number of actuators involved. Walking types which incorporate wall-pressing functions sacrifice mobility for increased stability, these are generally slower in-pipe. As a trade-off, the application of active wall pressing mechanisms give them a great amount of control over the applied normal force in pipe and they can deliver heavier payloads. Walking systems are somewhat uncommon with only 7% of research robots using the technique although they have been appearing more often in recent years as seen in Figure 5. MORITZ, a pipe inspection robot built at the Technical University of Munich was one of the first walking style robots to be developed [32]. Using 2 modules with a total of eight legs with 2 actuators each, a bending joint, and a rotation joint this complex system had a large number of degrees of freedom for an in-pipe robot. MORITZ was capable of travelling through 600 mm to 700 mm diameter pipes thanks to the highly variable actuated legs, each with 2 degrees of freedom, extension of these legs allowed normal force to be controlled and frictional forces strong enough to hold up to 20 kg payloads. The high amounts of control and increased carrying capabilities compared to passive systems make robots such as MORITZ ideal for industrial inspection of power plants, where safety is a priority over speed of inspection and power requirements.

2.7. Inchworm Systems

In-pipe inchworms are currently only wall-pressing, they generate traction through large normal force applied at the front or back module whilst a central module contracts and extends in sequence. The high normal forces needed to support the robot during contraction makes these systems generally well suited for carrying high payloads. The use of point contact in inchworms and the removal of wheels or tracks makes them much more stable than other designs. Inchworms are also generally less

8.4 Appendix A: Published Work "Advances in the Inspection of Unpiggable Pipelines"

prone to slip due to contaminants in-pipe as they can “cut” through the grease. Use of inchworms is quite widespread in the field, 11% of systems were found to use this technique in the study.

A highly mobile inchworm inspection robot based on a parallel manipulator, developed at YonSei University. This wall-press inspection device can handle 205–305 mm pipes the large inspection range coupled with its ability to traverse T-Sections makes up for the slow inspection speed [33]. These platforms have shown promise in industrial networks and have inspired the further exploration of large inchworm systems such as the 3SPR parallel manipulator under development at Yanshan University. This is a large two-module in-pipe inchworm robot, although currently in a theoretical state is intended to have large load carrying capacity for industrial applications [34]. Industrial pipeline networks often contain large amounts of oil and grease traces; it is these applications where wall-pressing systems such as these excel due to their low contact area end effectors. Case Western Reserve University have developed a new method of in-pipe robotic locomotion using continuous-wave peristalsis, the same mechanism employed by earthworms [35]. The robot, named CMMWorm, is composed of many interlinked joints forming a mesh like structure that can deform in the presence of an environmental change. The braided mesh can currently smoothly expand and contract from 220 mm to 180 mm and although currently unable to steer through in-pipe obstacles the mechanism shows great promise in shape adaptability research. These robots can potentially alter their effective diameters in-pipe in any section of their body.

2.8. Propeller

Propeller based locomotion is quite unusual in pipe inspection, used in combination with mainly fluid flow in water pipes this niche application featured in only 3% of reviewed systems. These water pipe inspection robots have the opportunity to utilise the fluid and develop swimming robots for use in leak detection. The main advantage of propeller systems is removing the need for wall contact altogether. A swimming in pipe robot was developed at the Massachusetts Institute of Technology as a solution to the challenges faced by robots relying on wall contact in water transport networks. The robot, MIT-MRL contains a chassis with housed electronics and two propellers for propulsion, the swimming nature of the robot allows exploration of pipes 100 mm and above autonomously [36]. The University of Sheffield took a different approach to swimming, developing a modular robot which can manipulate the fluid in order to generate propulsion in a certain direction by combining their chassis to form complex shapes. Each of the modules in this system form a section of a hydraulic system which when connected to another module forms a flowing network [37]. The Multifunctional Mobile Unit, MMU3 [6] also utilised a propeller in a version specified for fluid travel.

2.9. Summary

Table 1 provides a summary of robots reviewed in this section, where in-pipe geometry obstacles have been simplified to X (horizontal), Y (vertical), L (elbow), T (T-section), V (valves). The capability of the robot to traverse these obstacles is denoted by (✓) when capable, (✗) when incapable, and (-) when a possibility in future versions of the system.

Table 1. Robot Type, Adaptability, and In-Pipe Capabilities.

REF No.	Information	Element		Adaptability			In-Pipe Geometry				
	Robot Name	Type 1	Type 2	Min	Max	Range	X	Y	L	T	V
[13]	MagneBike	Magnetic	Wheel	250	∞	U	✓	✓	✓	✓	-
[37]	Fluid Modules	Modular	Swimming	125	∞	U	✓	✓	✓	✓	✓
[36]	MIT-MRL	Swimming	Swimming	100	∞	U	✓	✓	✓	✓	✓
[12]	Osaka Robot	Magnetic	Wheel	150	600	450	✓	✓	✓	✓	-
[23]	PAROYS-II	Caterpillar	Wall-Press	400	700	300	✓	✓	✓	✓	✗
[7]	MOGRER	Wheel	Wall-Press	520	800	280	✓	✓	✓	✗	✗
[2]	Pukyong Robot	Wheel	Wall-Press	300	500	200	✓	✓	✓	-	✗

8.4 Appendix A: Published Work "Advances in the Inspection of Unpiggable Pipelines"

Table 1. Cont.

REF No.	Information	Element		Adaptability			In-Pipe Geometry				
	Robot Name	Type 1	Type 2	Min	Max	Range	X	Y	L	T	V
[29]	<i>Kangawa Robot</i>	Caterpillar	Snake	100	300	200	✓	✓	✓	✓	-
[25]	HELI-PIPE Series	Screw	Wheel	40	173	133	✓	✓	✓	✗	✗
[18]	<i>Tarbiat Robot</i>	Caterpillar	Wall-Press	250	350	100	✓	✓	✓	-	✗
[34]	<i>YonSei Robot</i>	Inchworm	Inchworm	205	305	100	✓	✓	✓	-	✗
[32]	MORITZ	Walking	Wall-Press	600	700	100	✓	✓	-	-	✗
[16]	KANTARO	Wheel	Wall-Press	200	300	100	✓	✗	✓	✓	✗
[31]	PIRATE	Wheel	Wall-Press	41	125	84	✓	✓	✓	-	✗
[28]	PIPETRON I-VII	Snake	Wheel	75	150	75	✓	✓	✓	✓	✗
[26]	SPRING	Screw	Wall-Press	75	150	75	✓	✓	✓	-	✗
[4]	EXPLORER II	Snake	Wall-Press	150	200	50	✓	✓	✓	✓	✓
[9]	MRINSPECT VI+	Wheel	Wall-Press	130	180	50	✓	✓	✓	✓	✗
[27]	<i>Shenyang Robot</i>	Wheel	Wall-Press	250	300	50	✓	✓	✓	-	✗
[11]	AQAM	Wheel	Wall-Press	259	305	46	✓	✓	✓	✓	✗
[35]	CMMWorm	Inchworm	Inchworm	180	220	40	✓	-	✓	-	✗
[17]	FAMPER	Caterpillar	Wall-Press	127	157	30	✓	✓	✓	✓	✗
[8]	FERRET-1	Wheel	Wall-Press	90	120	30	✓	✓	✓	✗	✗
[3]	<i>Two-Plane Robot</i>	Wheel	Wall-Press	80	100	20	✓	✗	✓	✓	✗
[21]	AGH Robot	Caterpillar	Wall-Press	210	210	0	✓	✗	✓	✗	✗
[30]	LOCOSNAKE	Snake	Snake	120	120	0	✓	✓	✓	✓	-

3. Discussion

Since the development of the first wall-pressing in-pipe robot in 1987 the technique has become the most popular method of generating traction in the field with over 23% of robots applying it in some way Figure 5. The popularity of wall-pressing systems stems from their ability to take advantage of the encompassing walls to generate traction. This feature is guaranteed in pipe networks and allows robots to easily move horizontally and even vertically thanks to the ability to generate friction in any orientation. Issues arise with wall-pressing robots when obstacles such as T-Sections present themselves and there is a possibility for contact loss. Systems were shown to have varying abilities depending on the number of points of contact with the wall varying between two, three or four planes of contact, examples of which are shown in Figure 4.

The field of in-pipe robotics research is heavily invested in the use of these classic wall-pressing systems, many of which have low diameter adaptability ranges. These systems are stable and efficient in their specified diameter range but none of the traditional systems reviewed showed the capability adapt to large changes. Systems such as AGH Universities 200 mm robot with only a 34 mm adaptability range would not be able to cope with even a 1.5× increase in pipe diameter and would lose the ability to climb angled pipe sections. In some cases, such as Hanyangs flat pipeline inspection robot a change over 20 mm would cause it to become completely unstable and unable to perform even basic locomotion tasks. Many of these robots would be deemed unsuitable for inspection of AGI networks. Some of these designs are simply too constrained by size due to their reliance on a chassis that is always concentric with the pipe. While the central mount provides a good base for adaptability mechanism control it does not benefit transformation range. This limitation means that pipe networks with large varying diameters cannot be inspected without an entire fleet of different class wall-press systems. Assuming a medium size wall-press robot with 100 mm adaptability range, a network with pipes ranging from 200 mm to 1000 mm diameters would require eight separate robots to inspect. Entering 8 different size systems into one network may require multiple access points on the pipe into the correct bore diameter and would need to be repeated across the AGI until the inspection is complete.

8.4 Appendix A: Published Work "Advances in the Inspection of Unpiggable Pipelines"

Robotics 2017, 6, 36

11 of 13

The use of snake wall-pressing robots overcomes the limitations of traditional wall-pressing systems with multiple planar contact. Snake robots with wall-pressing capabilities can utilise articulated limbs to increase their effective diameter well over the range of parallelogram and pantograph mechanisms. For instance Kangawa University's snake system has an adaptability range of 100–300 mm [29]. Snake systems hold a great advantage over full-bore designs as they can be entered into smaller pipes as an access point into larger networks. This non full-bore design also allows them to pass through tricky obstacles such as valves which would stop most traditional wall-press systems in their tracks.

4. Conclusions

This review has presented a historical overview of the field as well as displaying the current in-pipe technology trends, with a specific emphasis on locomotion methods and their prevalence in the field. In-pipe robots are incredibly diverse and many different hybrid systems have been developed, some of which have fulfilled specific niches of pipe inspection. However, the inspection of highly varying diameter networks is an area that has not been fully explored, this task requires a method that is not constrained by pipe size. This is a complex issue and one that cannot be solved using full bore wall-pressing robots due to the limitations inherent in their adaptability.

We are coming close to 100% inspection of unpiggable pipelines the last 0.5% of network which is un-inspect-able using PIGs is difficult to deal with. In the coming years in-pipe robotic solutions will become available to inspect all networks of any diameter. Robotic technology is advancing and the field of in-pipe robotics is only growing with the increasing age of valuable pipelines around the globe. Ultimately small robotics systems that do not rely on wall-pressing for traction will be the solution as they allow access to both the smallest and largest diameter pipes in a network. Until then developments in the next 5 years may lead to vehicles with multiple traction methods e.g., a wall-press swimming hybrid such that it could negotiate both pipes containing fluid as well as non-running dry pipes. In the next 10 years the miniaturisation of robotic components and power sources may allow the design of micro-scale in-pipe systems. In the distant future mesoscale robots that flow within the pipes transport fluid may become the answer to the 100% inspection rate.

Acknowledgments: This work has been funded by National Grid Gas Transmission (NGGT) as part of Project GRAID: Gas Robotic Agile Inspection Device [2]. Gas Transmission and its project partners Synthotech [38], Premtech [39], and Pipeline Integrity Engineers [40] have been awarded £5.7 million in funding by the 2014 Network Innovation Competition to design and build an agile robotic platform to inspect buried pipework on high pressure gas sites. The robot will be designed to negotiate its own route around the sites with the ability to withstand pressures of up to 100 Barg.

Author Contributions: R. C. Richardson and A. E. Jackson have provided extensive supervision of the direction and scope of this work, and have contributed greatly to writing the paper.

Conflicts of Interest: The authors declare no conflict of interest.

References

1. Central Intelligence Agency. Pipelines. Available online: <https://www.cia.gov/library/publications/the-world-factbook/fields/2117.html> (accessed on 18 June 2017).
2. National Grid 2017. Project GRAID. Available online: <http://projectgraid.com/> (accessed on 14 June 2017).
3. Kwon, Y.-S.; Lee, B.; Whang, I.-C.; Kim, W.-K.; Yi, B.-J. A Flat Pipeline Inspection Robot with Two Wheel Chains. In Proceedings of the IEEE International Conference on Robotics and Automation (ICRA), Shanghai, China, 9–13 May 2011; pp. 5141–5146.
4. Schempf, H.; Mutschler, E.; Gavaert, A.; Skoptsov, G.; Crowley, W. Visual and Nondestructive Evaluation Inspection of Live Gas Mains Using the Explorer Family of Pipe Robots. *J. Field Robot.* **2010**, *27*, 217–249. [CrossRef]
5. Hertzberg, J.; Kirchner, F. Landmark-based autonomous navigation in sewerage pipes. In Proceedings of the First Euromicro Workshop on Advanced Mobile Robot, Kaiserslautern, Germany, 9–11 October 1996; pp. 68–73.

8.4 Appendix A: Published Work "Advances in the Inspection of Unpiggable Pipelines"

Robotics 2017, 6, 36

12 of 13

6. Hu, Z.; Appleton, E. Dynamic Characteristics of a Novel Self-Drive Pipeline PIG. *Trans. Robot.* **2005**, *21*, 781–789.
7. Okada, T.; Sanemori, T. MOGRER: A Vehicle Study and Realization for In-Pipe Inspection Tasks. *J. Robot. Autom.* **1987**, *3*, 573–582. [[CrossRef](#)]
8. Okada, T.; Kanade, T. A Three-Wheeled Self-Adjusting Vehicle in a Pipe, FERRET-1. *Int. J. Robot. Res.* **1987**, *6*, 60–75. [[CrossRef](#)]
9. Yang, S.U.; Kim, H.M.; Suh, J.S.; Choi, Y.S.; Mun, H.M.; Park, C.M.; Moon, H.; Choi, H.R. Novel Robot Mechanism Capable of 3D Differential Driving Inside Pipelines. In Proceedings of the IEEE International Conference on Intelligent Robots and Systems, Chicago, IL, USA, 14–18 September 2014; pp. 1944–1949.
10. Li, P.; Ma, S.; Li, B.; Wang, Y. Multifunctional Mobile Units with a Same Platform for In-Pipe Inspection Robots. In Proceedings of the IEEE/RSJ International Conference on Intelligent Robots and Systems, Nice, France, 22–26 September 2008; pp. 2643–2648.
11. Lee, D.; Park, J.; Hyun, D.; Yook, G.; Yang, H.-S. Novel Mechanisms and Simple Locomotion Strategies for an In-Pipe Robot that can Inspect Various Pipe Types. *Mech. Mach. Theory* **2012**, *56*, 52–68. [[CrossRef](#)]
12. Kawaguchi, Y.; Yoshida, I.; Kikuta, T.; Yamada, Y. Internal Pipe Inspection Robot. In Proceedings of the IEEE International Conference on Robotics and Automation, Nagoya, Japan, 21–27 May 1995; pp. 857–862.
13. Tache, F.; Fischer, W.; Caprari, G.; Siegwart, R. MagneBike: A Magnetic Wheeled Robot with High Mobility for Inspecting Complex-Shaped Structures. *J. Field Robot.* **2009**, *26*, 453–476. [[CrossRef](#)]
14. Fischer, W.; Caprari, G.; Siegwart, R.; Moser, R. Very Compact Climbing Robot rolling on Magnetic Hexagonal Cam-Discs, with High Mobility on Obstacles but Minimal Mechanical Complexity. In Proceedings of the IEEE 6th German Conference on Robotics, Munich, Germany, 7–9 June 2010; pp. 1–7.
15. Tavakoli, M.; Viegas, C.; Marques, L.; Pires, J.N.; de Almeida, A.T. OmniClimbers: Omni-directional Magnetic Wheeled Climbing Robots for Inspection of Ferromagnetic Structures. *Robot. Auton. Syst.* **2013**, *61*, 997–1007. [[CrossRef](#)]
16. Nassiraei, A.A.F.; Kawamura, Y.; Ahrari, A.; Mikuriya, Y.; Ishii, K. Concept and Design of A Fully Autonomous Sewer Pipe Inspection Mobile Robot "KANTARO". In Proceedings of the IEEE International Conference on Robotics and Automation, Roma, Italy, 10–14 April 2007; pp. 136–143.
17. Kim, J.-H.; Sharma, G.; Iyengar, S.S. FAMPER: A Fully Autonomous Mobile Robot for Pipeline Exploration. In Proceedings of the IEEE International Conference on Industrial Technology, Vina del Mar, Chile, 14–17 March 2010; pp. 517–523.
18. Moghaddam, M.M.; Arbabtafti, M.; Hadi, A. In-Pipe Inspection Crawler Adaptable to the Pipe Interior Diameter. *Int. J. Robot. Autom.* **2011**, *26*, 135–145. [[CrossRef](#)]
19. Oya, T.; Okada, T. Development of a steerable, wheel-type, in-pipe robot and its path planning. *Adv. Robot.* **2005**, *19*, 635–650. [[CrossRef](#)]
20. Kwon, Y.-S.; Yi, B.-J. Design and Motion Planning of a Two-Module Collaborative Indoor Pipeline Inspection Robot. *Trans. Robot.* **2012**, *28*, 681–696. [[CrossRef](#)]
21. Ciszewski, M.; Wacławski, M.; Buratowski, T.; Giergiel, M.; Kurc, K. Design, Modelling and Laboratory Testing of a Pipe Inspection Robot. *Arch. Mech. Eng.* **2015**, *62*, 395–408. [[CrossRef](#)]
22. Kakogawa, A.; Ma, S. Speed Analysis for three Modules of an In-Pipe Inspection Robots for Passing through Bent Pipes. In Proceedings of the IEEE International Conference on Robotics and Biometrics, Bali, Indonesia, 5–10 December 2014; pp. 1731–1736.
23. Park, J.; Hyun, D.; Cho, W.-H.; Kim, T.-H.; Yang, H.-S. Normal-Force Control for an In-Pipe Robot According to the Inclination of Pipelines. *Trans. Ind. Electron.* **2011**, *58*, 5304–5310. [[CrossRef](#)]
24. Min, J.; Setiawan, Y.D.; Pratama, P.S.; Kim, S.B.; Kim, H.K. Development and Controller Design of Wheeled-Type Pipe Inspection Robot. In Proceedings of the IEEE International Conference on Advances in Computing, Communications and Informatics, New Delhi, India, 24–27 September 2014; pp. 789–795.
25. Horodonica, M.; Preumont, A.; Burda, I.; Mignon, E. The Heli-Pipe Inspection Robots Architecture for Curved Pipes. In Proceedings of the IEEE International Conference on Manufacturing Systems, Crystal City Hyatt Regency Washington, DC, USA, 5–8 October 2003.
26. Nishihara, T.; Osuka, K.; Tamura, I. Development of a Simulation Model for Inner-Gas-Pipe Inspection Robot: SPRING. In Proceedings of the Society of Instrument and Control Engineers of Japan, Taipei, Taiwan, 18–21 August 2010.

8.4 Appendix A: Published Work "Advances in the Inspection of Unpiggable Pipelines"

Robotics **2017**, *6*, 36

13 of 13

27. Ye, C.; Liu, L.; Xu, X.; Chen, J. Development of an In-Pipe Robot with Two Steerable Driving Wheels. In Proceedings of the IEEE International Conference on Mechatronics and Automation, Beijing, China, 2–5 August 2015.
28. Debenest, P.; Guarnieri, M.; Hirose, S. PipeTron Series—Robots for Pipe Inspection. In Proceedings of the IEEE 3rd International Conference on Applied Robotics for the Power Industry, Foz do Iguassu, Brazil, 14–16 October 2014; pp. 1–6.
29. Sato, K.; Ohki, T.; Lim, H.-O. Development of In-Pipe Robot Capable of Coping with Various Diameters. In Proceedings of the IEEE 11th International Conference on Control, Automation and Systems, Gyeonggi-do, Korea, 26–29 October 2011; pp. 1076–1081.
30. Prada, E.; Valasek, M.; Virgala, I.; Gmitterko, A.; Kelemen, M.; Hagara, M.; Liptak, T. New Approach of Fixation Possibilities Investigation for Snake Robot in the Pipe. In Proceedings of the IEEE International Conference on Mechanicals and Automation, Beijing, China, 2–5 August 2015.
31. Dertien, E.; Stramigioli, S.; Pulles, K. Development of an Inspection Robot for Small Diameter Gas Distribution Mains. In Proceedings of the IEEE International Conference on Robotics and Automation (ICRA), Shanghai, China, 9–13 May 2011; pp. 3447–3448.
32. Zagler, A.; Pfeiffer, F. "MORITZ" a Pipe Crawler for Tube Junctions. In Proceedings of the IEEE International Conference on Robotics and Automation, Taipei, Taiwan, 14–19 September 2003; pp. 2954–2959.
33. Jeon, W.; Park, J.; Kim, I.; Kang, Y.-K.; Yang, H. Development of High Mobility In-Pipe Inspection Robot. In Proceedings of the IEEE International Symposium on System Integration, Kyoto, Japan, 20–22 December 2011; pp. 479–484.
34. Lu, Y.; Yu, J.; Sui, C.; Han, J. Design of In-Pipe 3SPR/3RPS Parallel Manipulator and its Kinestatics Analysis. In Proceedings of the IEEE 5th Annual International Conference on Cyber Technology in Automation, Control and Intelligent Systems, Shenyang, China, 8–12 June 2015.
35. Boxerbaum, A.S.; Shaw, K.M.; Chiel, H.J.; Quinn, R.D. Continuous Wave Peristaltic Motion in a Robot. *Int. J. Robot. Res.* **2012**, *31*, 302–318. [[CrossRef](#)]
36. Wu, Y.; Chatzigeorgiou, D.; Youcef-Toumi, K.; Zribi, M. Modeling and Parameter Estimation for In-pipe Swimming Robots. In Proceedings of the IEEE American Control Conference, Chicago, IL, USA, 1–3 July 2015; pp. 2007–2013.
37. Doyle, M.J.; Xu, X.; Gu, Y.; Perez-Diaz, F.; Parrott, C.; Grob, R. Modular Hydraulic Propulsion: A Robot that Moves by Routing Fluid Through Itself. In Proceedings of the IEEE International Conference on Robotics and Automation, Stockholm, Sweden, 16–21 May 2016; pp. 5189–5196.
38. Synthotech Limited. Available online: <http://www.synthotech.com/> (accessed on 13 September 2017).
39. Premtech Limited. Available online: <http://www.premtechltd.com/> (accessed on 13 September 2017).
40. PIE—Pipeline Integrity Engineers. Available online: <http://www.pieuk.co.uk/> (accessed on 13 September 2017).



© 2017 by the authors. Licensee MDPI, Basel, Switzerland. This article is an open access article distributed under the terms and conditions of the Creative Commons Attribution (CC BY) license (<http://creativecommons.org/licenses/by/4.0/>).

8.5 Appendix B: Published Work "Miniature Magnetic Robots For In-Pipe Locomotion"

8.5 Appendix B: Published Work "Miniature Magnetic Robots For In-Pipe Locomotion"

This appendix presents the work from Chapter 6 which has been published in an academic journal:

- Mills, G. H., Liu, J. H., Kaddouh, B. Y., Jackson, A. E., & Richardson, R. C. (2018, September). Miniature Magnetic Robots For In-Pipe Locomotion. In *Memorias de Congresos UTP* (pp. 289-300).

MINIATURE MAGNETIC ROBOTS FOR IN-PIPE LOCOMOTION

GEORGE H MILLS[†]

*Department of Mechanical Engineering, University of Leeds,
Leeds, LS2 9JT, United Kingdom*

DR. JASON H W LIU, DR. BILAL Y KADDOUH, DR. ANDREW E JACKSON,
PROF. ROBERT C RICHARDSON

*Institute of Design Robotics and Optimisation, Lab G.54,
Leeds, LS2 9JT, United Kingdom*

Abstract— Inspection of both small and large diameter bore pipelines for pipe integrity and defect identification with a single system has previously been impractical; especially using wall-press locomotion methods with low adaptive range. A miniature magnetic wall-climbing robot has been developed as a robotic solution for the inspection of 50mm bore diameter pipelines which can scale in-pipe geometry obstacles to access larger connected pipelines. Using magnetic arrays directed through steel flux plates within the wheels, the robot uses magnetic forces to adhere to the pipe. The system is 3D printed and includes soft printed material rubber wheels. The robot prototype is wirelessly driven, controlled remotely through serial Bluetooth communication radio at 2.4 GHz rated up to 100m. The robot's unique compact geometry and magnetic design allows it to scale concave right-angle wall cases in just a 50mm diameter bore. By entering pipe networks through these small existing access points the robot removes the need for expensive drilling procedures required to fit launch vessels.

Index Terms—In-Pipe Robot; 3D Printed Robot; Magnetic Robot; Pipe Inspection

1. Introduction

The field of in-pipe robotics is rapidly growing as pipeline networks around the world begin to reach the end of their initial design lives. Maintenance and repair of these networks can be costly and damaging to the environment due to the unnecessary excavation of healthy pipelines. Inspection robots can be used to investigate sections of pipe flagged for replacement and can

This work was supported by National Grid Gas Transmission (NGGT) and its project partners Synthotech, Premtech, and Pipeline Integrity Engineers as part of Project GRAID: Gas Robotic Agile Inspection Device. ESPRC Grant Number: 1657711

8.5 Appendix B: Published Work "Miniature Magnetic Robots For In-Pipe Locomotion"

2

determine the true interior condition. Types of in-pipe robotic locomotion can be categorized using basic elements, the elements presented in Figure 1 expand on the types of locomotion discussed in previous in-pipe hybrid literature reviews [1]. Modern in-pipe robots combine basic locomotion elements to form hybrid in-pipe systems with the ability to traverse a wide range of pipe obstacles and diameters [2]. The simplest of these being wheeled and caterpillar type robots (B & D). Specialized in-pipe methods of movement include, screwing, wall-press, and inchworm systems (C, E, & F). These locomotion methods are often combined with the more advanced methods, snake, walking, and magnetic (G, H, & J). The most widely used hybrid is wheeled wall-press systems due to their ability to use the pipe walls for traction. Adaptable Quad Arm Mechanism (AQAM) is a hybrid wheeled wall-pressing robot for 260mm – 300mm pipes, consisting of four arm mounted wheels in a single plane. The robot has impressive maneuverability due to its four independently controllable arms and swivel mechanism [3]. Multifunction Robot for INSPECTION of pipeline (MRINSPECT) is a wheeled wall-press hybrid in-pipe robot series designed at Sungkyunkwan University. The robot can perform all types of in-pipe geometry problems shown in Figure 2. MRINSPECT uses a multi-axial differential gear system to control each of its four wheeled legs angles through active bevel drive connections [4].

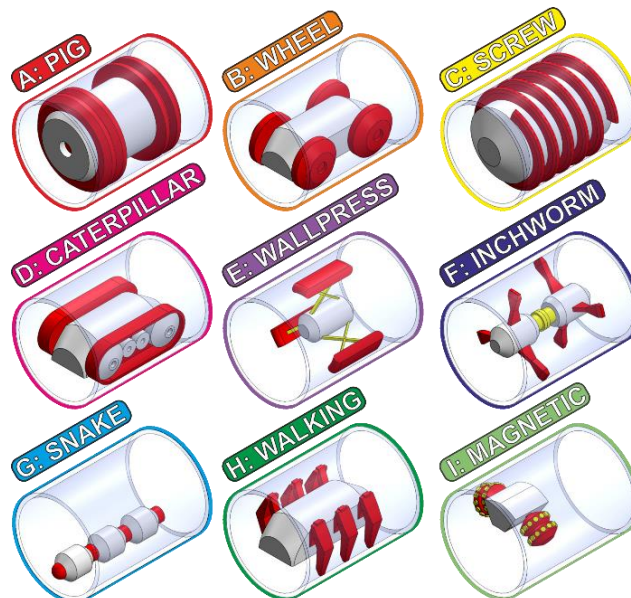


Figure 1: Basic in-pipe robotic locomotion types A – I.

Hanyang University developed a single-plane wheeled system. The problem faced with single plane contact is stability, any loss of wall contact in these designs will de-centralize the robot and make recovery extremely difficult [5]. Heli-Pipe is a series of wall-press systems that have a diametric adaptive ability of 10mm, as a result four different prototypes were made, ranging from 170mm to 40mm [6]. Caterpillar wall-press robots are also popular as a higher traction alternative to wheeled hybrid systems. Kanagawa University developed a hybrid of caterpillar and wall-press components, built from modular units each containing a driving caterpillar track. Connecting three or more units allows the robot to drive in-pipe, should a larger diameter need to be traversed the number of driving units can be increased [7]. Pipe Adaptive Robot of YonSei University (PAROYS-II) uses an actively controlled pantograph mechanism with a partially passive spring mechanism, this allows large changes to be controlled and small obstacles to be ignored. Its use of a second set of articulated caterpillar tracks allows a huge adaptive range of 400mm – 700mm [6]. SPRING is a screw type wall-press robot developed at Osaka University, although it relies on full wall traction it is unlike traditional full-bore wall-press systems which keep their chassis centralized in the pipe [9]. Snake robots are popular in industry pipe applications, they maximize space available and can be easily made to be modular in design allowing them to be flexibly suited to different tasks. PIRATE snake-like, and modular in nature featuring articulated clamping modules that can actively change the height of the robot to adapt to changes in pipe diameter [10]. The PipeTron series developed by HiBot, Tokyo is a multitude of robotic in-pipe exploration snake robots. Predominantly designed for tight bend systems such as refineries and chemical plants, the system is tethered for instant retrieval and consists of passively articulated wheels connected in a series [11]. The Explorer series is a multitude of industrial snake robots designed for the inspection of live gas networks under operating conditions, however it requires a full bore to operate with little adaptability ranging from just 150mm – 200mm [12].

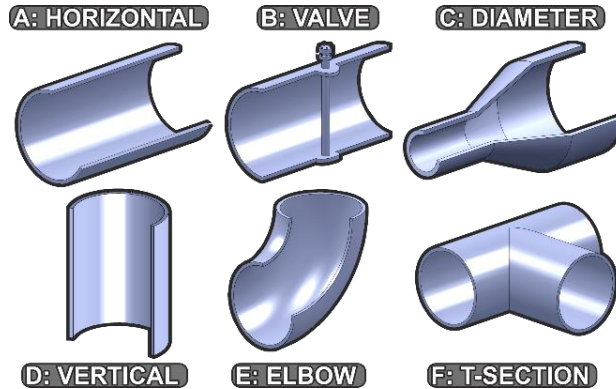


Figure 2: Common in-pipe obstacles A-F.

In ferrous pipelines, magnetic systems have all the locomotive advantages of wall-press without the need for adaptive diameter mechanisms. The first magnetic in-pipe robot was developed by the Osaka Gas Company in 1995, the system was a dual wheeled magnetic concept for the inspection 150mm - 600mm iron pipelines [13]. An advanced example of a magnetic wheeled in-pipe robot would be MagneBike. It can steer in a large range of in-pipe diameters, and can make obstacles such as T-Sections become trivial [14]. Synthotech [15] is making innovative progress towards complete pipe inspection with two robotic platforms targeting different challenges. The first; the Tier One Replacement System (TORS), a snake pipe robot focusing on lower diameter consumer pipeline replacement. Project Gas, Robotic Agile Inspection Device (GRAID) [16], will inspect the National Grid Gas Network under live operating conditions using a magnetically adhered caterpillar system. Magnetic robots are also used in out-pipe cases to traverse walls, ship hulls, and ferrous structures such as the boiler tube inspection prototype robot [17]. Omni-directional wheels used in conjunction with magnetics can lead to extremely maneuverable out-pipe robots such as Omni—Climber [18].

2. In-pipe robot design

The proposed in-pipe robot is intended to travel from small diameter pipelines to larger bores. The target inspection network consists of ferrous pipelines in the diameter range of 50mm – 1250mm. Magnetic adhesion is a suitable method in this case, performing the function of adhesion without the need for a full-bore wall-pressing system. As seen in other wall-pressing designs a full-bore adaption mechanism severely limits the range of pipelines that can be inspected by a single robot, even in the best case: the robot called PAROYS-II has a full adaption range

of 300mm [8]. The proposed robot will be specified to enter a 50mm inner diameter pipe and be able to overcome obstacles present in the network. For miniature wall-climbing robots, obstacles in Figure 2 can be simplified to distinct cases shown in Figure 3 in which a bend is either concave, or convex. Completion of both convex and concave geometries using magnetic systems is challenging without the use of articulated systems or many actuators allowing multiple degrees of freedom. Driving directly up to a convex case with magnetic wheels causes them to lock in place as the magnets act with equal force to each wall in contact.

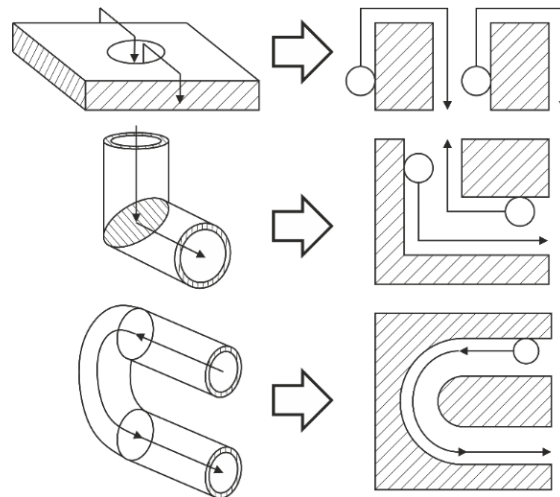


Figure 3: Simplified in-pipe geometry.

The concave case is equally challenging, as the wheels reach the right angle, magnetic force drops dramatically as the total potential magnetic flux transferred into the steel decreases causing slip at the wheels. The design challenge is to overcome these types of obstacle using a robot that stays within the tight space constraints of a 50mm pipeline. For this to be possible the robot profile must be below the given diameter with a clearance of the magnetic wheels such that they do not attract or lock with the top side of the inner pipe.

2.1. Robot Design Overview

The magnetic pipe robot, shown in Figure 5 was designed to enter 50mm internal diameter ferrous pipelines. The robot is equipped with magnetic wheels, a wireless control system, and two motors, it is 3D printed, including soft rubber wheels printed in-situ using soft printed material. Many basic vehicle designs were considered to save space within the pipe. The planar wheel (bike like)

8.5 Appendix B: Published Work "Miniature Magnetic Robots For In-Pipe Locomotion"

6

configuration as used in MagneBike [14] Figure 4 (a), allows for efficient placement of magnetic wheels however it requires stabilisers to remain laterally stable (b). In a 50mm pipe, space is paramount and so a two-wheel vehicle (d) has been designed which grants efficient motor placement along the length of the pipe, this reduces the length and complexity vs both a 4 wheeled magnetic vehicle (c), and caterpillar system (e).

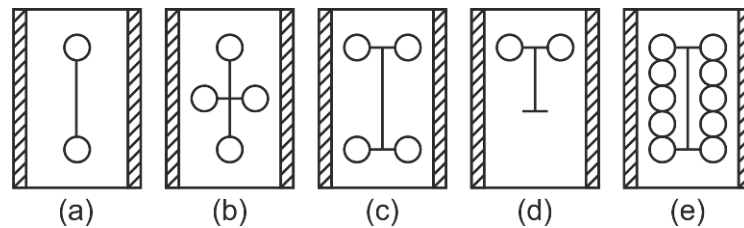


Figure 4: Magnetic robot skeleton base designs (a – e).

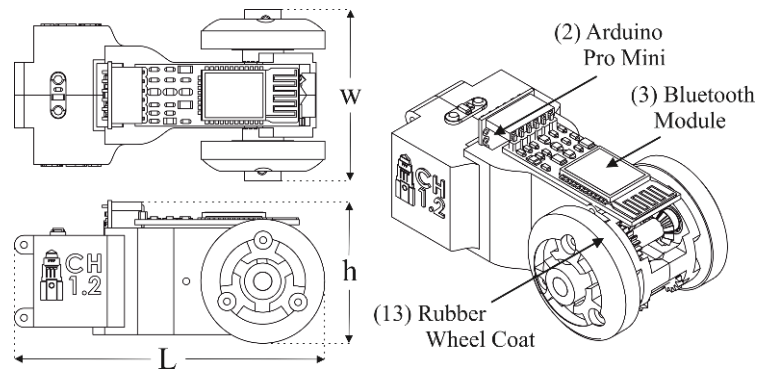


Figure 5: (a) Geometry of the magnetic robot.

$$L \times w \times h = 85.10\text{mm} \times 46.88\text{mm} \times 38.65\text{mm}$$

The main body of the robot is printed as two separate halves and screwed together after the addition of motors, electronics and battery. The wireless Bluetooth radio transceiver is mounted on top of the chassis directly with the Arduino FTDI. This allows reprogramming later by detaching the radio.

2.2. Transmission System

Due to the size constraints when designing a robot for a 50mm diameter pipe, the motors are mounted perpendicular to driveshaft and the wheels. The motors sit parallel one on top of the other, each drive one gear train with transmission through a bevel gear, shown in Figure 6. The driveshaft then transmits power through the spur gear on the opposite side to drive the wheel with a transmission

ratio of 1.2:1. These sections are 3D printed, they are assembled with 5mm I.D. 8mm O.D. bearings which are push fit into the chassis during assembly. These allow smooth rotation and locating the centers for transmission assembly, keeping meshing distance of the gears constant. Although the motors are interchangeable depending on the desired gear ratio the current 250:1 motors allow a max wheel speed of 80 RPM.

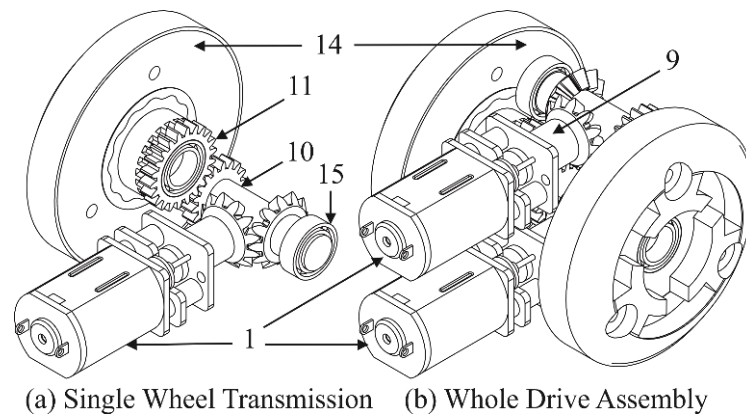


Figure 6: Transmission system, & Motor Layout, with part No. 1: Motor, 9: Gear, 10: Driving Shaft, 11: Wheel Gear, 14: Magnetic Wheels.

The prototype was formed using Objet material VeroWhite (60g) and Tango+ (4g) as well as breakaway support (186g) to form a complete model. The total build time for one robot is 2hrs:45min and requires an hour of support cleaning from surrounding material due to the delicacy and small size of the robot parts. Shown in the Table 1 is the bill of materials required to assemble the robot. The price is quoted as £171 to produce one unit, however the printing costs for the chassis account for 66% of this price. This price is based on the production of one robot, charged at a £25 hourly rate for use of the Objet 1000 printer and a printing time of 3 hours. These costs could be reduced if the robot were to be printed in batches.

2.3. Wireless Driving System

The robot is controlled using a 3.3V version of the Arduino Pro Mini which interfaces wirelessly over serial using the SparkFun Bluetooth Mate Silver. The 3.3V level logic voltage uses less power than 5V version of the pro mini at the cost of processing speed (8MHz vs 16MHz) however it is directly compatible with all secondary components and does not require a voltage regulator. Bluetooth radio was chosen for the same reason, when idle it draws much less current than

Wi-Fi options such as the ESP8266 (50mA vs 170mA during communication). As this robot is designed to operate in 50mm -1250mm diameter pipes, the Bluetooth 2.4 GHz module will only be effectively operational in 80mm - 1250mm diameter pipes. We are currently investigating the use of a 5.8GHz module for smaller diameter pipes (50mm - 80mm) in future versions. For the purpose of this proof of concept, the Bluetooth module achieves the desired outcomes. A SparkFun dual motor driver breakout board is used to control direction of the two motors and hence steering, and a 3.3V LED is used as a power indicator. The whole system runs on a 260mah 7.4V Lithium Polymer (LiPo) rechargeable battery which supplies logic voltage to the Arduino, and raw voltage to the dual motor driver board. Commands are given to the Pro Mini via serial sent from a master computer running LabVIEW. The additional circuitry required increases assembly time in terms of the time it takes to solder, estimated at half an hour. The circuit boards and LED's simply slide into the printed grooves and are held in place by frictional forces. A summary of the electronic materials used in the production of one unit, including price and weight can be found in Table 1.

2.4. *Magnetic Wheel System*

The magnetic wheels were designed to increase the strength of the magnets by redirecting the flux of the magnets to focus it into the tracks. Instead of having magnets directly in contact with the inner surface of the pipe, they are housed between two steel plates, Figure 7. This has two benefits; redirection of the magnetic flux into the steel plates, and protection of the neodymium magnets. Corrosion and shock impact can cause degradation and fracturing of the magnets, by encapsulating them rather than placing them in direct contact with the pipe wall they are significantly safer. The magnets used in the wheel assembly are N42 6x4x2mm rectangular magnets with a pull strength of 0.75kg. These magnets have their north and south faces on opposite sides of the 6mm x 4mm faces, which are in contact with the plates. The evenly spaced circular array of 9 magnets shown in Figure 7 is held within the wheel using a 3D printed spacing layer, this smooths out the flux dissipation to maintain an even distribution of tractive force as the wheel rotates.

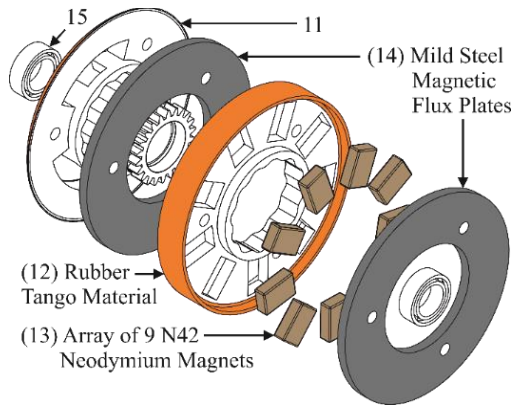


Figure 7: Exploded view of the 34mm diameter wheel assembly.

The wheel is connected using three screws which locate the entire assembly ensuring the wheel lines up optimally as intended in the CAD model. The through holes are seen in Figure 7. The flux lines run from one side the plate back, through the 1.5mm steel, into the pipe wall, and back through the second plate with the opposite face. By focusing the flux through the pipe wall in this way the magnetic absorption force increases, and a higher traction is generated at the wheel. Figure 8 presents a close up of a central wheel cross-section and shows the wheel in contact with a flat steel surface. The distance between the magnetic flux plates and the steel contact surface are seen to be offset by the rubber tango material. The distance between these two surfaces is 0.5mm on a flat plate and up to 3.5mm in a 50mm diameter pipe section.

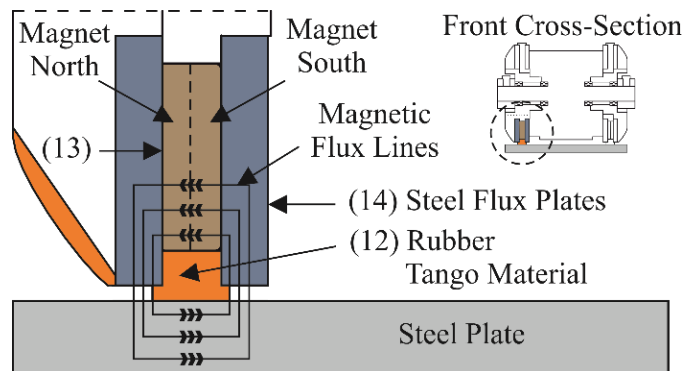


Figure 8: Magnetic wheel cross-section flux diagram.

3. Robot Performance

The robot was printed, wheel flux plates laser cut, and assembled. The complete system was then analyzed in terms of locomotive capabilities, magnetic force, and maneuverability, the finished robot is shown in a 50mm pipe Figure 9.

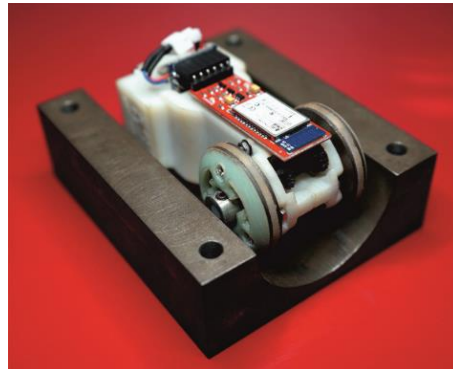


Figure 9: Assembled robot in a 50mm I.D. half-pipe.

The magnetic force generated by the wheels was tested on mild steel plates of varying diameter. The plates were fastened to a testing rig using 3D printed spacers, seen in orange, the robot was clamped to the 10 Newton load cell of the Emperor Force measurement device, Figure 10, and then pull force tests were undertaken. The tests followed the same method; initially the load cell was zeroed and the robot lowered down into contact with the plate until the load was at zero again. The robot was then pulled off the plate at a rate of 0.5mm/sec until a height was reached where the magnetic field no longer has influence (30mm). The experiment was repeated 5 times for each plate size. The setup for this experiment shown in Figure 10, the results; Figure 11. It should be noted that the robot was first placed in a compression pre-loaded state to reach equilibrium with the magnetic force. This pre-loaded state is highlighted before each peak force point in Figure 11.

Figure 11 shows that the pull force case for flat plate produces significantly stronger force (almost triple) when compared to the 50mm case. The uneven contact of the robot wheels in the 50mm diameter pipe case results in sub-optimal transfer of magnetic flux through the steel. The inner flux plates are a minimum of 3mm from the pipe walls making a complete flux flow through the two sides difficult.

8.5 Appendix B: Published Work "Miniature Magnetic Robots For In-Pipe Locomotion"

11



Figure 10: Single column linear force tester with a 10N load cell.

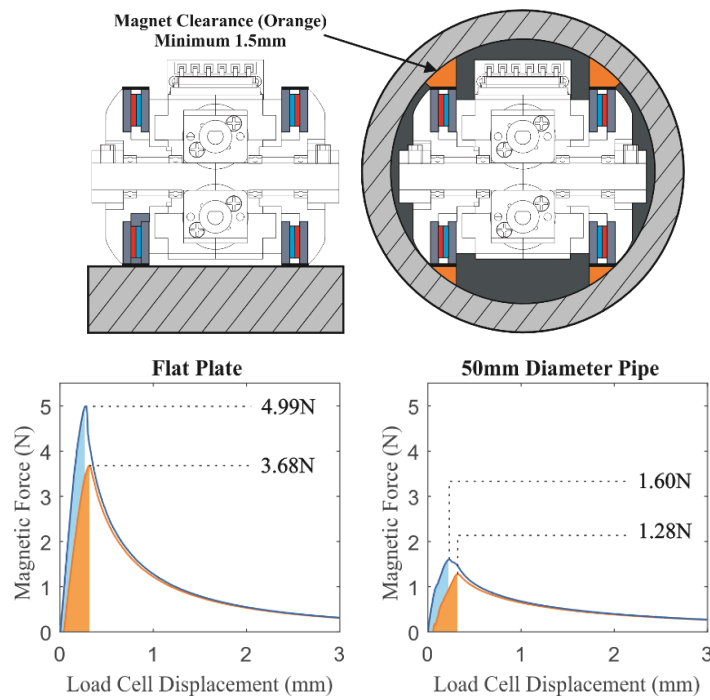


Figure 11: Magnetic pull force experiment result, pull force (blue), connection force (orange). In Figure 11, the peak pull force required to remove both wheel is highlighted in blue, whereas the re-attachment force is shown in orange. The shaded areas of the graphs indicate that the robot is in a compressed state.

Table 1: Standard deviation of 5 experiment samples.

	Flat Plate Pull	Flat Plate Push	50mm Pull	50mm Push
Standard Deviation	0.017	0.002	0.114	0.009

8.5 Appendix B: Published Work "Miniature Magnetic Robots For In-Pipe Locomotion"

12

Magnetic wheels can encounter problems in cases where one wheel has more than one point in contact with a ferrous surface. The wheel can become stuck as to move in either direction it first has to overcome the unwanted magnetic force produced. The forces involved in this situation are described in Figure 12, where the robot is driving up a wall at a 90-degree concave angle. The robot is capable of completing the case presented in Figure 12 in a pipe, where traction is minimum. The robot has been designed with this worst case scenario in mind; travelling vertically in-pipe in the lowest diameter where magnetic force is minimum. This scenario results in lowest traction case, designing to complete this ensures the robot can perform any other section with a wider inner diameter or preferable orientations where magnetic or traction force applied is higher.

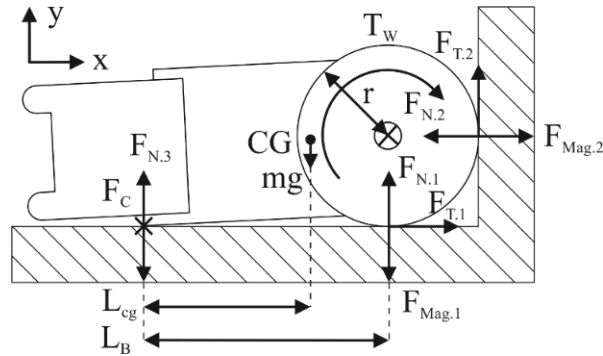


Figure 12: Forces acting at point of 90-degree wall contact.

For the wheel to drive up the wall from this position, the traction force $F_{T,2}$ must overcome the wheels magnetic pull $F_{Mag,1}$. In this scenario the weight of the vehicle must also be overcome making this the most difficult case in terms of tractive effort. Balancing the forces around the point of contact and assuming the wheel is at the point just before accelerating up the wall, traction $F_{T,2}$ will equal $F_{Mag,1}$ plus the weight component, equation (1).

$$F_{T,2} * (L_B + r)_c = F_{Mag,1} * (L_B) - mg(L_B - 2L_{cg}) \quad (1)$$

The magnetic forces required to allow this robot to provide enough traction to overcome weight means that the mg component is comparatively low (2).

$$-0.144 * 9.81 * (0.047 - 0.066) = 0.0276N \quad (2)$$

Balancing forces in terms of $F_{T,2}$ the total force that the wheel traction must overcome to climb the wall can be determined by equations (3), and (4).

$$F_{T,2} = \frac{F_{Mag,1} * (L_B)}{(L_B + r)} + 0.0276 \quad (3)$$

$$F_{T,2} = 2.89 + 0.0276 = 2.91N \quad (4)$$

8.5 Appendix B: Published Work "Miniature Magnetic Robots For In-Pipe Locomotion"

13

To accelerate up the wall at this equilibrium point the traction force must satisfy the equation (5). Maximum tractive force that can be applied at $F_{T.2.MAX}$ is governed by equation (6):

$$F_{T.2} > \frac{F_{Mag.1} * (L_B)}{(L_B + r)} + mg \sin(\emptyset) \quad (5)$$

$$F_{T.2.MAX} = \mu_s F_{N.2} \quad (6)$$

Where: μ_s = Static coefficient of friction of wheels

To satisfy the traction requirements, the static coefficient of friction, μ_s must be maximized. In the scenario outlined in Figure 12 $F_{N.2}$ is equal to the magnetic force from Figure 11; 4.99N (lowest recorded force), and $F_{T.2}$ is equal to 2.91N from equation (4). When entered into (7) the minimum required static friction coefficient can be obtained:

$$\mu_s > \frac{F_{T.2}}{F_{N.2}} \quad \mu_s > 0.58 \quad (7)$$

In Figure 13 the robot is shown driving on a steel floor directly up to a 90-degree steel wall in replica of the case outlined in Figure 12.

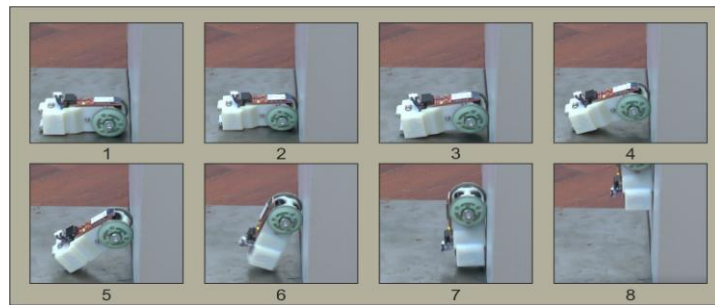


Figure 13: Magnetic robot climbing 90-degree from steel to steel.

The robot is optimized for high magnetic force on flat plate travel, this is due to the decreased risk in lower diameter pipelines. In large pipelines gas flow will likely be at the highest rate, hence a larger normal force will be required to maintain friction levels necessary to remove wheel slip. The robot can move at a top speed of 90mm/sec on a flat steel plate (Maximum magnetic attraction case) and can currently drive from any orientation. The robot is capable of completing a 180° pipe bend with minimum radius of 25mm within a 50mm pipeline. Driving straight around the inside of a pipeline is possible as when the robot reaches wall angles greater than 90 degree's the chassis simply hangs upside-down. This version requires that you turn around at the top of the pipe as the Bluetooth mate module blocks wheel contact. Removing additional actuators to climb step cases greatly reduced the size of the robot however currently the robot is incapable of

8.5 Appendix B: Published Work "Miniature Magnetic Robots For In-Pipe Locomotion"

14

convex right-angle cases due to the limited step space between the wheel and the chassis; currently 2.4mm.

4. Conclusion

A wheeled-magnetic in-pipe robot has been designed to enter small 50mm pipelines found within larger pipe networks. These small entrances of 50mm will allow the robot to enter the larger connected network pipes which range from 50mm – 1250mm. By using a magnetic robot that does not rely on wall-pressing for traction the obstacles usually encountered in-pipe can be simplified and focus can be narrowed to just two cases. The robot has proven effective at 90-degree wall climbing cases where two magnetic forces are active at once and can generate tractive forces necessary to overcome the unwanted magnetic force. Further work will be done on the optimization of the circular magnetic array, such as testing N52 neodymium and reducing the rubber thickness. Smaller magnetic wheels are to be added to stabilize the rear of the chassis, and the electronic component stack will be integrated within the frame of the robot to allow it to drive on either side of the chassis.

Acknowledgments

This work was supported by National Grid Gas Transmission (NGGT) and its project partners Synthotech, Premtech, and Pipeline Integrity Engineers as part of Project GRAID: Gas Robotic Agile Inspection Device. ESPRC Grant Number: 1657711

References

1. Roslin, N. S., Anuar, A., Jalal, M. F. A., & Sahari, K. S. M. (2012). A review: hybrid locomotion of in-pipe inspection robot. *Procedia Engineering*, 41, 1456-1462.
2. Mills, G. H., Jackson, A. E., & Richardson, R. C. (2017). Advances in the Inspection of Unpiggable Pipelines. *Robotics*, 6(4), 36.
3. Lee, D., Park, J., Hyun, D., Yook, G. and Yang, H.-s. Novel Mechanisms and Simple Locomotion Strategies for an In-Pipe Robot that can Inspect Various Pipe Types. *Mechanisms and Machine Theory*. 2012, 56, pp.52 - 68.
4. Yang, S.U., Kim, H.M., Suh, J.S., Choi, Y.S., Mun, H.M., Park, C.M., Moon, H. and Choi, H.R. Novel Robot Mechanism Capable of 3D Differential Driving Inside Pipelines. In: *International Conference on Intelligent Robots and Systems*, 14-18 Sept. 2014, Chicago, IL. IEEE, 2014, pp.1944-1949.
5. Kwon, Y.-S., lee, B., Whang, I.-C., Kim, W.-k. and Yi, B.-J. A Flat Pipeline Inspection Robot with Two Wheel Chains. In: *International Conference on Robotics and Automation (ICRA)*, 9-13 May 2011, Shanghai. IEEE, 2011, pp.5141-5146

8.5 Appendix B: Published Work "Miniature Magnetic Robots For In-Pipe Locomotion"

15

6. Horodonica, M., Preumont, A., Burda, I. and Mignon, E. The Heli-Pipe Inspection Robots Architecture for Curved Pipes. In: International Conference of Manufacturing Systems. 2003.
7. Sato, K., Ohki, T. and Lim, H.-o. Development of In-Pipe Robot Capable of Coping with Various Diameters. In: 11th International Conference on Control, Automation and Systems, 26-29 Oct. 2011, Gyeonggi-do, Korea. IEEE, 2011, pp.1076-1081
8. Park, J., Hyun, D., Cho, W.-H., Kim, T.-H. and Yang, H.-S. Normal-Force Control for an In-Pipe Robot According to the Inclination of Pipelines. In: Transactions on Industrial Electronics, Dec. 2011. IEEE, 2011, pp.5304 - 5310.
9. Nishihara, T., Osuka, K. and Tamura, I. Development of a Simulation Model for Inner-Gas-Pipe Inspection Robot: SPRING. In: Society of Instrument and Control Engineers of Japan, 18-21 Aug, Taiwan 2010.
10. Dertien, E., Stramigioli, S. and Pulles, K. Development of an Inspection Robot for Small Diameter Gas Distribution Mains. In: International Conference on Robotics and Automation (ICRA), 9-13 May 2011, Shanghai, China. IEEE, 2011, pp.3447-3448.
11. Debenest, P., Guarnieri, M. and Hirose, S. PipeTron Series - Robots for Pipe Inspection. In: 3rd International Conference on Applied Robotics for the Power Industry, 14-16 Oct, Foz do Iguassu. IEEE, 2014, pp.1-6.
12. Schempf, H., Mutschler, E., Gavaert, A., Skoptsov, G. and Crowley, W. Visual and Nondestructive Evaluation Inspection of Live Gas Mains Using the Explorer Family of Pipe Robots. *Journal of Field Robotics*. 2010, 27(3), pp.217-249.
13. Kawaguchi, Y., Yoshida, I., Kikuta, T. and Yamada, Y. Internal Pipe Inspection Robot. In: International Conference on Robotics and Automation, 21-27 May 1995, Nagoya. IEEE, 1995, pp.857-862.
14. Tache, F., Fischer, W., Caprari, G. and Siegwart, R. MagneBike: A Magnetic Wheeled Robot with High Mobility for Inspecting Complex-Shaped Structures. *Journal of Field Robotics*. 2009, 26(5), pp.453-476.
15. Synthotech Limited. [Online]. 2018. [Accessed: 16/04/2018.] Available from: <http://www.synthotech.com/>
16. National Grid 2018. Project GRAID. [Online]. 2018. [Accessed: 16/04/2018.]. Available from: <http://projectgraid.com/>
17. Boonyaprapasorn, A., Maneewarn, T., & Thung-Od, K. (2014, October). A prototype of inspection robot for water wall tubes in boiler. In *Applied Robotics for the Power Industry (CARPI), 2014 3rd International Conference on* (pp. 1-6). IEEE.
18. Tavakoli, M., Viegas, C., Marques, L., Pires, J. N., & De Almeida, A. T. (2013). Omniclimbers: Omni-directional magnetic wheeled climbing robots for inspection of ferromagnetic structures. *Robotics and Autonomous Systems*, 61(9), 997-1007.